



# **Experimental Investigation of Heat Transfer Characteristics from Arrays of Free Impinging Circular Jets and Hole Channels**

**Dissertation**

zur Erlangung des akademischen Grades

**Doktoringenieur**

**(Dr. –Ing.)**

vorgelegt von

**M. Sc. Eng. Mohamed Attia Mahmoud Attalla**

geb. am 28.12.1968 in Kena, Ägypten

genehmigt durch die

**Fakultät für Verfahrens- und Systemtechnik  
der Otto-von-Guericke-Universität Magdeburg, Deutschland**

Gutachter

**Prof. Dr.-Ing. Eckehard Specht  
Prof. Dr.-Ing. Ibrahim M. M. El-Moghazy**

**Promotionskolloquium am 21.12.2005**

# DEDICATION

*This work is dedicated to my father, my mother and my wife, my children, who supported me with their love, care and prayers*

*M. Attalla*

## Abstract

An experimental investigation of the convective heat transfer on a flat surface in a multiple-jet system and hole channel is described. The system consists of free jets with an undisturbed flow of the air. Principle arrays were considered as in-line as well as staggered with different spacing distance in X- and Y-directions.

For measuring the heat transfer, a metal sheet made of nickel alloy of size 200 mm  $\times$  170 mm was heated electrically with direct current supply up to 400 A and 7 V. The top side was cooled with air from the nozzle array. The temperature distribution on the black coated bottom side was recorded with an infrared thermo camera. Because of the sheet thickness was only 0.1 mm, the temperature on both sides can be assumed as equal. The resolution of the temperature difference is 0.15 mm/pixel, thus it is possible to determine the local heat transfer with a high accuracy. Varied parameters were the jet inner diameter with  $d$ , of 5.8 mm and 8 mm, the jet Reynolds number in the range from 1400 to 41400, the normalised distance nozzle to sheet  $H/d$  from 1.0 to 10.0, and the normalised nozzle spacing  $S/d$  from 2.0 to 10.0. The geometrical arrangement of nine jets arrays (3x3) was tested.

The profile of the local and average heat transfer coefficient for multiple free jets system were discussed and compared to those of a single free jet. The results have shown that the multiple jet system enhances the heat transfer over the entire range than those for the hole channel and a single nozzle. A maximum of the heat transfer was found for the normalised spacing  $S/d = 6.0$  for multiple jets system. This is because the interference between adjacent jets is reduced. But for the hole channel the normalised spacing  $S/d = 4$  provides the maximum heat transfer. The normalised distance  $H/d$  had nearly no effect on heat transfer in the range  $2 \leq H/d \leq 5$  for both multiple jets system and hole channel arrays. The Reynolds number exponent  $m$  for the multiple free jets arrays at optimum spacing distance of is found approximately 0.7. While for

the hole channel array the exponent of Reynolds number for maximum average Nusselt number is found 0.66. Because of the difference between exponents of Reynolds number for these two cases, the crossflow is limited for the multiple free jets system in comparison to the hole channel array.

In addition, the uniformity of the heat transfer is examined in this work. The experimental results show that the uniformity depends strongly on the type of the jet array. Therefore the heat transfer is more uniform over the impinging area for the staggered array than the other arrays.

## Kurzfassung

Der konvektive Wärmeübergang der Prallströmung von Düsensystemen und Lochkanälen wurde experimentell untersucht. Die Systeme bestanden aus freien Düsen mit einer unbeeinflussten Luftströmung. Prinzipielle Anordnungen wurden betrachtet wie fluchtend und versetzt mit verschiedenen Teilungen in X- und Y-Richtung.

Zur Messung des Wärmeübergangs wurde ein Metallblech aus einer Nickellegierung der Abmessung 200 mm x 170 mm elektrisch beheizt, mit einem Gleichstrom bis zu 400 A und 7 V. Die Oberseite des waagerechten Bleches wurde mit der Luftströmung gekühlt. Die Temperaturverteilung der mit Lack geschwärzten Unterseite wurde mit einer Infrarot-Thermokamera aufgenommen. Da die Blechdicke nur 0,1 mm betrug, kann die Temperatur auf beiden Seiten als gleich angenommen werden. Die Auflösung der Temperaturdifferenz war 0,15 mm/Pixel, wodurch der örtliche Wärmeübergang mit einer hohen Genauigkeit ermittelt werden kann. Als Parameter wurden variiert, der innere Düsendurchmesser mit 5,8 mm und 8 mm, die Reynoldszahl der Düse im Bereich von 1400 bis 41400, der bezogene Düsenabstand zum Blech  $H/d$  von 1 bis 10 und die Düsenteilung  $S/d$  von 2 bis 10. Die geometrische Anordnung bestand aus 3 x3 Düsen, so dass die mittlere Düse jeweils repräsentativ für ein großes Feld war.

Die Profile des örtlichen und mittleren Wärmeübergangskoeffizienten für die Düsensysteme werden diskutiert und mit denen der Einzeldüse verglichen. Die Ergebnisse haben gezeigt, dass die Düsensysteme den Wärmeübergang im ganzen Bereich verstärken im Vergleich zur Einzeldüse. Ein Maximum für den Wärmeübergang wurde für die Düsenteilung  $S/d = 6,0$  beim Düsensystem gefunden. Dagegen wurde für die Lochkanäle ein Maximum bei der Teilung von  $S/d = 4,0$  gefunden, dass allerdings nur geringfügig höher war als der Wärmeübergang bei der Teilung  $S/d = 6$ . Der Düsenabstand zum Blech übt keinen Einfluss im Bereich  $2 \leq H/d \leq 5$  aus sowohl für die Einzeldüsen als auch für die Lochkanäle. Der Exponent der Reynoldszahl des Düsensystems

kann für den maximalen Wärmeübergang bei der optimalen Teilung mit 0,7 angenähert werden. Bei dem Lochkanal passt dagegen der Exponent 0,66 besser zur Beschreibung des Einflusses der Reynoldszahl.

Schließlich wurde noch die Gleichmäßigkeit des Wärmeübergangs in Querrichtung eines unter dem Düsensystem transportierten Bleches untersucht. Hierbei ist der mittlere Wärmeübergang entlang von Längslinien von Bedeutung. Bei einer fluchtenden Anordnung der Düsen ist der Wärmeübergang entlang der Linien unter den Düsen erheblich höher als der zwischen den Düsen. Dagegen ist der Wärmeübergang in Querrichtung nahezu ausgeglichen bei einer versetzten Anordnung der Düsen.

## Acknowledgment

All gratitude is due to “ALLAH” who guides me to bring forth to light this thesis.

I wish to express my sincere thanks to my supervisor, **Prof. Dr.-Eng. Eckehard Specht**, who takes so much effort and patience in mentoring me to become a qualified researcher throughout this work.

I am also grateful to **Prof. Dr. –Eng. Ibrahim El-Moghazy**, University of El-Minia, Egypt, for kindly agreeing to be referees for this thesis in spite of their hectic schedules.

Also I am greatly indebted to my **parents**. I own all my achievement to my **wife**, who share all joy and bitterness every days and support as I completed my study.

Many thanks for all staff members of institute of Fluid Dynamics and Thermodynamics, **ISUT**, for their help in the experimental work.

Finally thanks to many other who have in a way or another helped me.

M. Attalla

# Contents

	Page
<b>1 Introduction and Review of Previous Work</b>	<b>1</b>
1-1 Introduction	1
1-2 Heat Transfer Between Jets and Surfaces	2
1-2-1 Single Jet	2
1-2-2 Multiple Impingement Jet	4
1-3 Problem Considered	9
1-4 The Main Objective of this Work	10
<b>2 Characteristics of Impinging Jet</b>	<b>19</b>
2-1 Introduction	19
2-2 Description of Flow Regions	19
2-3 Heat Transfer Definitions	21
<b>3 Experimental Work</b>	<b>26</b>
3-1 Experimental Set-Up	26
3-2 Location of Surface Temperature Measurement	28
3-3 The Infrared Thermography System	29
3-4 Determination of Emissivity	30
3-5 Determination of the Heat Transfer Coefficient	31
3-6 Distribution of Surface Temperature	36
3-7 Computation of Average Heat Transfer	37
<b>4 Heat Transfer for Multiple Jets Free System</b>	<b>48</b>
4-1 Introduction	48
4-2 Local Heat Transfer Distribution	48
4-2-1 Single Nozzle	48
4-2-2 Multiple jets Free System	50
4-2-3 Effect of Spacing Distance on Stagnation Point	51
4-3 Average Heat Transfer of Multiple Free jets	53

<b>5 Heat Transfer for Hole Channels</b>	<b>84</b>
5-1 Introduction	84
5-2 Local Nusselt Number Distribution	84
5-3 Influence of Spacing and Separation Distances	85
5-3-1 Stagnation Nusselt Number $Nu_{st}$	85
5-3-2 Average Nusselt Number $Nu_{av}$	86
<b>6 Uniformity of Heat Transfer for Multiple Free Jets</b>	<b>110</b>
6-1 Introduction	110
6-2 Uniformity of Heat Transfer	110
6-2-1 Uniformity of Heat Transfer for -line Array	110
6-2-2 Uniformity of Heat Transfer for Staggered Array	112
6-2-3 Uniformity of Heat Transfer for Hole Channels Array	113
6-4 Summary	114
<b>7 Conclusions and Further Work</b>	<b>133</b>
7-1 Conclusions	133
7-2 Recommendations for Further Work	135
<b>References</b>	<b>136</b>
<b>Appendices</b>	<b>147</b>
A- Distribution of Surface Temperature	147
A-1 In-line Array	147
A-2 Staggered Array	152
B- Local Nusselt Number Distribution for Staggered Array	157
C- Effect of Separation Distance at Stagnation Point	162
C-1 In-line Array	162
C-2 Staggered Array	165
<b>Nomenclature</b>	<b>168</b>

## **Introduction and Review of Previous Work**

### **1-1-Introduction:**

The jet impingement heat transfer has become well established as a high performance technique for heating, cooling and drying a surface. Applications of the impinging jets include drying of textiles and film; annealing of the glass; processing of some steel and glass industry; cooling of gas turbine components and the outer wall of combustors; cooling of electronic equipment; and freezing of tissue in cryosurgery. Interest in the topic from the standpoint of both empirical and theoretical applications continues unabated and may have even accelerated in recent years. The high heat transfer rates associated with impinging gaseous jet has been well recognized and documented for many years [1-7]. Besides the above applications, impinging jets are also adopted in paper industry to enhance drying of paper processes, and cooling of moving metal strip, [8, 9]. The majority of this chapter have been related to single jets and multiple impinging jets which considered for cooling or heating larger surface.

Direct impingement of turbulent jets onto a surface leads to high heat transfer rates. This method is often employed to achieve rapid heating or cooling and has been applied in the glass industry [10]. A major disadvantage of impinging isothermal jets is that the local heat flux can be highly non-uniform. Because of the importance of materials processing and other applications, the jet impingement heat transfer has been extensively studied to determine both the peak and the spatial heat transfer distribution for various configuration of jets and surfaces [11]. The impingement of unconfined axisymmetric (circular) jets on flat surface has received most of the research attention [12-15]. However, a wide variety of other unconfined and confined configuration-single round and slot, rows and arrays, obliquely inclined, and others have been studied [3].

## 1-2 Heat Transfer Between Jets and Surfaces:

### 1-2-1 Single Jets:

In the following it is focused on the single impinging jets. There are many different factors affect heat transfer between an isothermal jet and solid surface. The factors include turbulence, entrainment, exit jet velocity profile, nozzle geometry, separation distance ( $H/d$ ), surface form and external factors.

There is limited literature concerned with laminar jets. Sparrow and Lee [16] used a solution for the inviscid flow field as a boundary condition to determine the viscous flow along the impingement surface. They showed that with this method the Nusselt number is proportional to the Reynolds number to the 0.5 power. Saad et al. [17] solved the full Navier-Stokes equations using a finite difference approximation. They concluded that the Nusselt number was proportional to  $Re^{0.36}$  for a parabolic velocity profile and to  $Re^{0.5}$  for a flat velocity profile in the range of the Reynolds number from 900 to 1950. The numerical computations of Saad et al. show the importance of the velocity profile in the stagnation region and also in the wall jet region. The heat transfer from a parabolic impinging jet is higher than that from a uniform impinging jet in both stagnation and wall jet regions.

The Nusselt and Reynolds numbers for air at the stagnation point are usually expressed as  $Nu_{st} = c.Re^n$ . The Reynolds number exponent  $n$  from laminar boundary layer theory for a uniform exit velocity profile is 0.5. Polat et al. [18] compared the values of the exponent  $n$  that were determined by various numerical and experimental studies and found that there is considerable scatter. The value of  $n$  ranges from as low as 0.23 to as high as 0.67 and depends on whether the inlet velocity profile is flat or parabolic. The differences in the exit velocity profiles make a direct comparison of experimental and numerical results. The stagnation point heat transfer within the plate to jet (separation distance  $H/d \leq 5.0$ ) is in good agreement with laminar boundary layer for Reynolds number of 1050 and 1860 [19]. In the developed region  $H/d \geq 8$ ,

strong free jet turbulence effects were observed that augmented the convective heat transfer [20, 21].

The fact that a turbulent impinging jet yields a higher heat transfer than a laminar jet has been recognized for some time [22-28]. Donaldson et al. [28] examined free jet impingement and compared their measured heat transfer results to those predicted by laminar theory. At the stagnation point, they obtained the following relation for the Nusselt number  $Nu_{st} = (0.5c Pr)^{0.5} . Re^{0.5}$ . In this relation, both the Nusselt and Reynolds numbers are based on the local free jet half-radius and the value of  $c$  is 1.13 for fully developed free jets. A comparison between the predicted laminar heat transfer and the measured heat transfer revealed that the measured turbulent heat transfer rate is 1.4 - 2.2 times as high as the laminar rate.

In many aspects of materials processing and other applications of impinging jets, the gaseous jet is at a temperature other than of the surrounding air. When a temperature difference is present, the entrainment of the surrounding fluid affects the performance of the jet. The experimental work on heated single jets to study entrainment effects has been extensive [29-32]. Obot et al. [33] found that the effect of entrainment on the heat transfer to a turbulent jet is strongly dependent on nozzle configuration. Most of the published literature pertains to jets generated with well characterized nozzles. However, in many applications, the square nozzle configuration is preferred primarily because of ease of fabrication and installation, especially for multiple jet systems.

The experimental data of Hoogendoorn [25] clearly demonstrated that not only the stagnation point but also the local Nusselt number depend on the nozzle design and on the nozzle-to-plate ratio  $H/d$ .

The effects of nozzle-to-impingement surface spacing are now being understood [34, 35]. The local heat transfer coefficient depends on several factors, and the variation is complex [35]. For  $H/d > 4$  the maximum heat

transfer coefficient occurs at the stagnation point of the jet [11]. This optimum separation distance,  $H/d$ , apparently coincides with the length of the potential core. Beyond the potential core, the jet velocity decays and the heat transfer coefficient falls.

Depending on the jet Reynolds number and separation distance two radial peaks have been observed for circular air jets [34, 35]. The inner peak is located at approximately  $X/d = 0.5$ . For  $H/d < 0.25$ , global mass continuity requires that the fluid accelerate between the nozzle and the impingement surface. The resulting acceleration produces local thinning of the boundary layer, explaining the peak seen at  $r/d = 0.5$  Fig. 1.1 [36]. The experimental results of Adler [34] given in Fig. 1.2 shows that this peak occur at radial distance  $X/d$  equal to 2. But the result of Lytle and Webb [35] provided in Fig. 1.3 this peak becomes more pronounced at radial distance is 1.75 especially for high Reynolds number. The discussion of prior work by these authors suggests that the local maximum in the Nusselt number at  $X/d$  is strongly dependent on separation distance and Reynolds number.

The strong effect of the nozzle-to-impingement surface ratio,  $H/d$ , on the local heat transfer coefficient is illustrated in Fig. 1.4 for a wide range of separation distance. At a separation distance of 6 the maximum Nusselt number occurs at the stagnation point and then decreases monotonically. The variation of the Nusselt number is similar for the separation distance of 0.5 except for the appearance of a slight secondary local maximum at  $X/d = 1.75$ . However, as the separation distance is decreased below 0.5, the Nusselt number shows a significant increase at all radial locations, and two local maximum occur at  $X/d = 0.5$  and  $X/d = 1.3-1.75$  [35, 36].

### **1-2-2 Multiple Impingement Jet:**

The heating or cooling of large areas with impinging jets requires arrays; however, the flow and geometrical parameters have to be carefully selected to

provide both a sufficiently high average heat transfer coefficient and uniformity of the heat transfer over the impingement surface [37]. The need for uniformity is important in applications such as drying of textile and paper, annealing and tempering of glass, cooling of turbojet engine structure to avoid local hot spots, and spot cooling of electrical apparatus. These and other applications motivated the research. Because of this there are numerous studies dealing with isothermal multiple jets impingement systems, and some selected papers are summarized in Table 1.

The flow from arrays of impinging nozzle has the same three flow region-free jet, stagnation, and wall jet- as the single impinging jet [3, 5, 10, 44 and 57-59]. However, there are some basic differences in the fluid mechanics of single and multiple jets that complicate the use of single jet heat transfer results for the design of multiple jet systems. The individual jets that make up a multiple jet system may be influenced by two types of interactions that do not occur for single jets. First, there is possible interference between adjacent jets prior to their impingement on the surface. The likelihood of such interference effects is enhanced when the jets are closely spaced and when the separation distance between the jet orifice and the impingement surface is relatively large. Second, there is an interaction due to collision of surface flows associated with the adjacent impinged jets. These collisions are expected to be of increased importance when the jets are closely spaced, the jet orifice impingement plate separation is small, and the jet velocity is large [60, 61].

The multiple jets systems can be subdivided into three different kinds of arrays. (I) Round jets from free tube (e.g. In-line and staggered), (II) round or slot jets from perforated plate with or without spent air holes, and (III) rows from hole channels which can be considered as mixture of perforated plate and free jet. Many additional factors influence the heat transfer in multiple jets impingement systems. These factors include separation distance, jet-to-jet spacing distance, kind of array, geometry of jet, diameter of jet and impingement surface form [2, 3. and 60, 61].

For arrays perforated plate impingement jets, a cross flow is formed by the spent air from the impinging jets in a confined space, and the amount of cross flow increases as the flow moves downstream. Turbulent intensity of impinging jets is increased because the cross flow disturbs impinging jets at downstream region. Therefore, the local heat transfer rate around the stagnation region is enhanced [42, 47, and 62-63]. However, at the mid-way region, the heat/mass transfer is decreased because the spent fluid upstream jets in an array can sweep away the downstream jets and delay impingement. Also the thermal boundary layer is developed in the cross flow at this region. Therefore, the heat/mass transfer coefficient is non-uniform over the overall impingement surface [64]. Experiments on the influence of cross flow on impinging heat transfer have used both single row [15, 40, 58, 65] and multiple jet arrays [39, 42, 46, 66-70] both cases were used perforated plate. Most investigators found that crossflow reduced impingement heat transfer.

Convective heat transfer from a flat surface to a row of impinging, submerged air jets formed by square edged orifices having a length/diameter ratio of unity have been measured [63]. The local Nusselt numbers were averaged over the spanwise direction, and average Nusselt numbers were calculated and then correlated by the equation [63],

$$\overline{Nu} = \left( \frac{2.9 \exp \left[ -0.09 \left( \frac{X}{d} \right)^{1.4} \right]}{22.8 + \left( \frac{S}{d} \right) \left( \frac{H}{d} \right)^{0.5}} \right) Re^{0.7}. \quad (1-1)$$

Where X is streamwise coordinate. This correlation is appropriate for the range of parameters studies ( $2 \leq H/d \leq 6$ ,  $4 \leq S/d \leq 8$ , and  $10000 \leq Re \leq 40000$ ).

The heat transfer coefficient from a flat plate to a multiple jets system with perforated was examined by more investigators. For example, Dagan and Hollworth et al. [58, 66] found that, for arrays with staggered spent air exit

holes in the perforated plate, the heat transfer convection was 20-30% larger than for arrays with cross flow spent air exit geometry. Huber and Viskanta [49-50], studied the effect of spent air exit in the orifice plate on the local and average heat transfer for 3\*3 square array jet with 2\*2 square spent air exit using the liquid crystal technique. In addition, they examined the effects of the separation distances  $H/d = 0.25, 1.0, \text{ and } 6.0$  and Reynolds number  $Re = 3500, \text{ and } 20400$ . They found that the interaction of adjacent impinged jets is reduced by spent air and the heat transfer on target plate is more enhanced. Several investigators [13, 37, 39, and 62] have determined the average Nusselt numbers ( $Nu_{av}$ ) in the presence of crossflow. The results show that for  $Re < 5500$ , the average Nusselt number pass through a maximum about  $H/d = 4.0$ . For large value of Reynolds number, the average value of Nusselt number decreases with increasing spacing for any particular flow scheme. It can be established that  $\overline{Nu} \propto \left(\frac{H}{d}\right)^{-n}$ , where n depends on the exhaust scheme [3, 62].

Metzger et al. [71] investigated experimentally another importance difference between the heat from a single jet and an array of jets. They found that for a jet-to-jet spacing distance (S) of 1.67-6.67 nozzle diameters, a maximum in the average heat transfer coefficient was observed for a separation distance (H/d) of about one. A value of  $S/d = 4$  was recommended by Freidman and Mueller [72] to reduce adjacent jet interference and maximum heat transfer over the surface for large separation distance  $H/d \geq 8$ , while Martin [1] recommended an optimum value of roughly 7 diameter for  $H/d = 5.4$ .

Hrycak [13] also comments that a small separation distance appears to be characteristic for maximum heat transfer from multiple jets system. Ichimiya and Okuyama [73] studied a square array of four circular jets with a confining wall as the separation distance was varied from 0.5 to 8.0. They found that, the maximum average Nusselt number occurred between a separation distance H/d of 1.5 and 2.0 as the Reynolds number was varied from 3000 to 40000. Ichimiya and Okuyama [73] concluded that the effective dimensionless

distance between the nozzles and impingement surface (separation distance  $H/d$ ) does exist for a constant jet Reynolds number. For turbulent flow when three slot jet nozzle are located a small separation distance from the impingement surface ( $0.5 < H/d_h < 1$ ), two strong peaks in the local Nusselt number were observed behind the second nozzle [74]. This is attributed to a pair of vortices at the stagnation region. From their experiments in confined crossflow with a single slot jet, Chong et al. [68] concluded that jet-to-crossflow momentum flux ratio is a kinematic parameter of the flow that influences the ratio of the maximum Nusselt number to its crossflow counterpart.

The following paragraphs have been decreased the heat transfer coefficient from arrays of free jet (based on the first kind of arrays). Only a few investigators studied the heat/mass transfer coefficient from this array [2, 38, 51, 75]. Xiaojun Yan and Nader Saniei [48] investigated the effect of jet-to-jet spacing ( $S/d$ ) and jet-to-plate distance ( $H/d$ ) on local heat transfer for a constant Reynolds number ( $Re = 23000$ ) by using a pair of circular air jet impinged on a flat plate. The spacing and separation distances were in the range (1.75 to 7.0) and (2 to 10) respectively. The results of the investigation showed that the local Nusselt number at the center point between the two jets exceeds that one at the jet stagnation point when  $S/d < 3.5$ , and is less than one that at the stagnation point when  $S/d > 3.5$ . Also, in larger jet-to-jet spacing ( $S/d > 5.25$ ), the local heat transfer distribution in the region between the jets shows two maximum value, first one at  $r/d = 0.3$  and the other one at  $r/d = 1.3$ , for a closer jet-to-plate distance ( $H/d = 2.0$ ). But a pair of nozzles is not representative for the average heat transfer of an area for a whole array.

Slayzak et al. [75] investigated the local heat transfer coefficient on a surface with a constant heat flux. They used two jets also but water as fluid. The experiments were carried out for a slot nozzle and only for one nozzle-to-plate distance. They showed that there is a oscillating interaction zone midway between the impingement points. Within the stable interaction zone, there is a

local maximum in the heat transfer coefficient. Hilgeroth [38] defined the heat transfer coefficient on the basis of the logarithmic mean temperature difference between the wall and the air. So it is difficult to compare their results with other investigators. Gromoll [2] investigated the heat transfer on the target plate for arrays of impingement jets with different types of arrays (in-line and staggered array). He found that the local heat transfer of a staggered array is enhanced than of an in-line array. The results were summarized by the following correlation,

$$\text{Nu} = 0.863 \left(\frac{S}{d}\right)^{0.65} \left(\frac{S}{H}\right)^n \text{Re}^{0.6} \text{Pr}^{0.3} \quad (1-2)$$

where  $n = 0.6$  at  $S/H > 1$  and  $n = 0.53$  at  $S/H < 1$ . This is the only relation for Nusslet number in case of free tube jets, based on may knowledge.

### **1-3 Problem Considered:**

Based on the above, the exponent  $n$  of the jet Reynolds number in correlations for perforated plates had been reported [8, 11, and 44] to be 0.7 and 0.727, which is a much higher number than the 0.6. Adler [34] had reported for heat transfer for the single jet that the exponent depends on the radial distance from the center of jet. In a distance larger of two  $d$ , which is general the case for arrays, the exponent was greater than 0.6. The Nusselt number function in equation (1-2) gives no maximum value in the spacing distance ( $S$ ) as reported the other authors. A comparison of average Nusselt number calculated from the correlations proposed in five publications as shown in Fig. 1.5 reveals significant differences in the values as well as in the slope of the Reynolds number. One of the reasons the correlation of Hollworth and Berry [37] yields lower  $\overline{\text{Nu}}$  than the others is that it is for a spacing distance  $S/d = 10$  and not like the others. Their correlation is based on data for spacing distance  $S/d \geq 10.0$ . The correlation of Martin [1] is based on the data of several investigators and is appropriate for a wide range of parameters. The major difference in the average Nusselt number predicated by the correlation

of Gromoll [2] and those of others investigators is attributed to the others investigators used orifices made from perforated plates to produce their impinging air jets. While Gromoll's correlation is based on data obtained with free tube jets. Because the orifices and nozzles produce different exit velocity profiles and turbulent levels, which influence the boundary layer developed along the impingement surface and hence local and average heat transfer rates differently.

Many authors measured the convective heat transfer from impingement surface by using liquid crystals technique (LCT) [35, 74, 76] and laser induced fluorescence (LIV) [77]. Thereby the surface that has to be measured is lubricated with certain substances. These substances change their color according to different temperature (LC) or they fluorescence in various wavelength areas of visible light. With the application of a CCD-camera the color distribution over the surface can be recorded and converted into temperature distributions. A disadvantage of these methods is that the location of energy output and temperature difference is significant, and the temperature which, measured in a close region is imprecise [34]. The temperature distribution over the impingement surface is measured in the present study with a relatively new method using non-contact measurement system (infrared thermography) [34]. By applying this method, the distribution of the surface temperature can be measured in an almost arbitrarily large interval without tangency.

#### **1-4 The Main Objective of this Work:**

From the previous studying, there are so much contrary results. Therefore, the convective heat transfer coefficient was measured in this work for a multiple free tube jets system which impinging on the flat plate. These free tube jets allow a better comparison with the heat transfer for a single nozzle, which were researched very often.

The major objective of the study was to investigate the effect of the following experimental parameters on the local and average heat transfer coefficient:

- i)** Spacing distance between jets ( $2 \leq S/d \leq 10$ ),
- ii)** Separation distance between jets and impingement plate ( $1 \leq H/d \leq 10$ ),
- iii)** Exit jet velocity  $U$ , (3.5 m/sec to 108 m/sec), and
- iv)** Inner jet diameter  $d$ , (5.8 mm and 8 mm).

The comparison of the local and average heat transfer between two differences kinds of arrays (in-line and staggered) were presented in this work. The heat transfer coefficient for a single jet was measured at the different experimental parameters (separation distance, jet exit velocity and inner jet diameter). These results from a single jet were compared with the result from multiple jets system. This work examined also the heat transfer coefficient for the hole channels (based on the third type of arrays – sec. 1-2-2). The width of the channel was selected two times of the inner jet diameter.

The average heat transfer coefficient over the lines on the impingement area was calculated for the many types of jets arrays (in-line and staggered arrays, hole channel and in-line array with different spacing distance  $S_x \neq S_y$ ). In this case, it can be calculated at the degree of the heat transfer uniformity over the moving impingement plate (industrial application).

**Table 1 Some Investigations for Multiple Round Impinging Jet Systems**

Author	Kind of Arrays	Jet Diameter d mm	Reynolds number ( $Re_d$ )	Separation distance H/d	Jet-Jet Spacing S/d	Notes
Hilgeroth E. [38]	Cell & Equilateral Triangle	15 – 50	$1.5 \cdot 10^4 - 5 \cdot 10^4$	2 - 6	2.2 – 30.6	- Data cared out by thermocouple. - Jet from perforated pate.
Kercher D. M. & Tabakoff W. [39]	Square Array	0.5 - 2.0	$3 \cdot 10^2 - 3 \cdot 10^3$	1.0 - 4.8	3.1 - 12.5	- Data cared out by thermocouple. - Jet from perforated plate. - Including effect of spent air. - $Nu = k Re^m Pr^{0.33} (H/d_i)^{0.091}$ - $m = f(S/d, Re)$ (0.5 to 0.9) - $k = f(S/d, Re)$ ( $2 \cdot 10^{-2}$ to $1 \cdot 10^{-1}$ )
Koopman R. N. & Sparrow E. m. [40]	Single Row	6.35	2570 - 10000	2, 4, 7, 10	4, 6.67	- Data cared out by naphtha lens technique. - Jet from perforated plate
Gromoll B. [2]	Square Array	4, 5, 6, 7.5	$4 \cdot 10^3 - 2.4 \cdot 10^4$	2 – 37.5	25, 37.5, 50, 75, 150	- Jet from free tube. - $Nu = 0.77 Re^{0.6} Pr^{0.33} (S/d)^{-0.65} (S/H)^n$ - $n = 0.06$ at $S/H > 1.0$ and - $n = 0.53$ at $S/H < 1.0$
Florschuetz L. W. & et al., [41].	In-line & Staggered arrays	7.62 , 3.81, & 2.54	From $5 \cdot 10^3$ to $5 \cdot 10^4$	1, 2, & 3	4 - 15	- Data cared out by thermocouple. - Jet from perforated plate.
Dyban E. P. & et al. [42]	Staggered Arrays	1 - 5	$1.1 \cdot 10^3 - 17 \cdot 10^3$	1, 2.6, 3.6, 10, 16	2, 3, 4, 4.25, 4.75, 8	- Data cared out by thermocouple. - Jet from perforated plate.

Introduction and Review of Previous Work

Florschuetz L. W. & et at. [43]	In-line & Staggered arrays	.6, 2.54, 5.08, 7.6, & 7.6	$2.5 \cdot 10^3 - 7 \cdot 10^4$	1 - 3	4 - 15	-Data cared out by thermocouple. -Jet from perforated plate. - $Nu = 0/363 Re^{0.727} Pr^{0.33} (H/d)^{0.068} (S_x/d)^{-0.554} (S_y/d)^{-0.442}$ -Effect of cross flow.
Hrycak P. [13]	Single Row	3.18 , 6.35, 9.52	25000 - 66000	2, 5, 8	2, 4, 8	-Flow to curved surface, $d_c = 127\text{mm}$ -Jet from perforated plate. -Data cared out by thermocouple. - $Nu = 1.04 Re^{0.7} Pr^{0.33} (H/d)^{-0.42} (S/d)^{-0.16} (d/d_c)^{0.402}$
Golstein R. J. & Timmers J. F. [44]	3 jets in one row & 7 jets Staggered	10	Constant = 40000	2, 4	Constant = 4	-Jet from perforated plate. -Data cared out by Liquid-Crystal technique
Pan Y. & Webb B. W. [45]	In-line & Staggered arrays	1., 2, 3	5000 - 20000	2, 5	2, 4, 6, 8	-Used water. -Jet from perforated plate. -Data cared out by Infrared Radiometer.
Florschuetz L.W. & Lsoda Y. [46]	Staggered Arrays	3.2	$2.5 \cdot 10^3 - 5 \cdot 10^3$	1, 2, 3	4 - 8	-Effect of Velocity and pressure. -Jet from perforated plate
Florschuetz L. W. & et at. [47]	In-line & Staggered Arrays	2.5 & 1.25	$2.5 \cdot 10^3 - 7 \cdot 10^4$	1 - 3	4 -15	-Effect of initial cross flow. -Flow Distributions -Jet from perforated plate. -Data cared out by thermocouple.
R. J. Goldsten & W. S. Seol, [15]	Single Row	6.35	10000 - 40000	2, 4, 6	4, 8	-Jet from perforated plate. -Data cared out by Liquid-Crystal technique

Introduction and Review of Previous Work

Huber A. M. & Viskanta R. [48]	3*3 square arrays	6.35	3500 - 20400	0.25, 10, 6.0	4, 6, 8	-Data cared out by Liquid-Crystal technique -Effect of Center Jet. -Jet from perforated plate. - $\bar{Nu} = 0.285 Re^{0.71} Pr^{0.33} (H/d)^{-0.123} (S/d)^{-0.725}$
Huber A. M. & Viskanta R. [49]	3*3 square arrays	6.35	10200 - 17000	0.25, 10, 6.0	Constant = 6	-Data cared out by Liquid-Crystal technique. -Effect of perimeter jets. -Jet from perforated plate.
Huber A. M. & Viskanta R. [50]	3*3 square arrays	6.35	3500 - 20400	0.25, 1.0, 6.0	Constant = 6.0	-Data cared out by Liquid-Crystal technique -Jet from perforated plate. -Effect of spent air.
Xiaojun Y. & Saine N., [51]	Two jets	20.5	Constant = 230000	2, 4, 6, 8, 10	1.75, 3.5, 5.25, 7	-Jet from free tube. -Data cared out by Liquid-Crystal technique
Jung-yan S. & Mae.De L. [52]	5 jet Staggered arrays	3.0	10000 - 30000	2, 3, 4, 5	4, 6, 8, 12, 16, 24	-Data cared out by thermocouple. -Jet from perforated plate.
Brevet P. & et at. [53]	3 jets In-line & 3*3 arrays	6.35	3000 - 20000	1, 2, 3 10	2, 4, 6, 10	-Jet from perforated plate. -Data cared out by Infrared Camera.
May Su L. & Shyy W. C. [54]	In line arrays	3.0, 5.0	1000 - 4000	.01 - 8	Constant = 4	-Jet from perforated plate. -Effect of grooved surface.
Dong L.L. & et al. [55]	3 jets In-line	5.0	900.0 (Laminar flow)	2 - 8	2.6 - 7.0	-Jet from free tube. -Butane / Air flow.

Introduction and Review of Previous Work

---

Dong-Ho R. & et al. [56]	Square arrays	10	5000 - 10000	0.5 - 10	6	-Jet from perforated plate. -Effect of spent air. -Data cared out by thermocouple.
--------------------------	---------------	----	--------------	----------	---	--

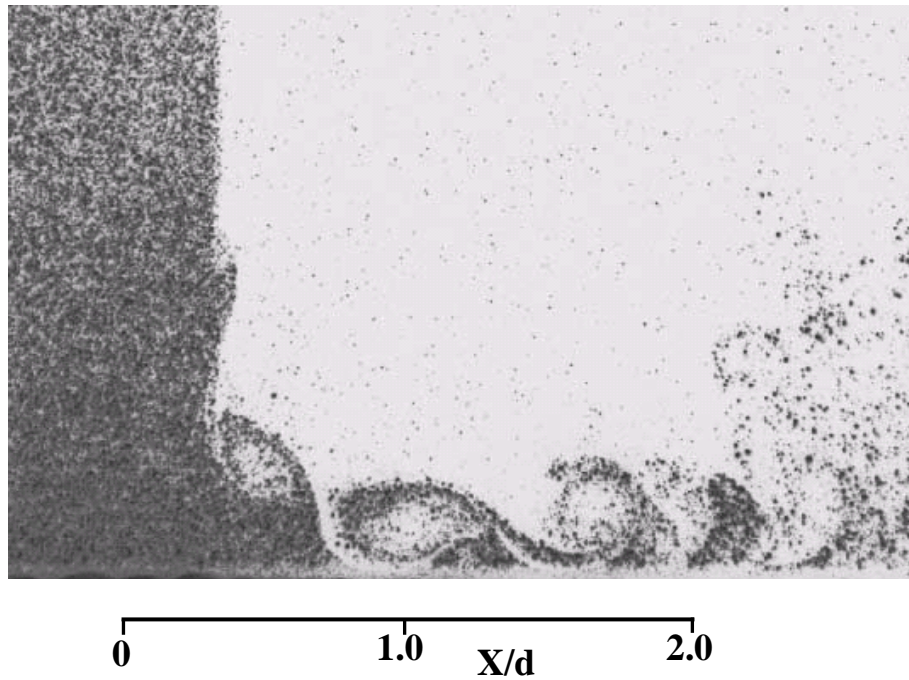


Fig. 1.1 Instantaneous Velocity Field in the Stagnation and Wall Jet Region by PIV for  $H/d = 2$ ,  $Re = 1000$ , [36]

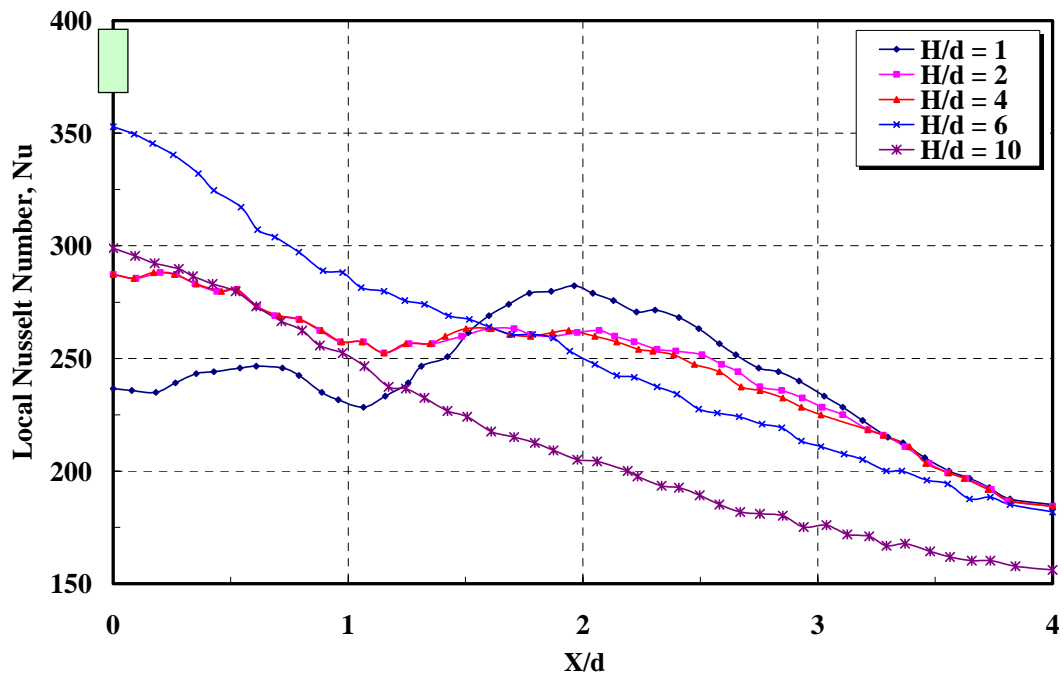


Fig. 1.2 Local Nusselt Number Distribution with Radial Distance for  $Re = 90000$ , [34]

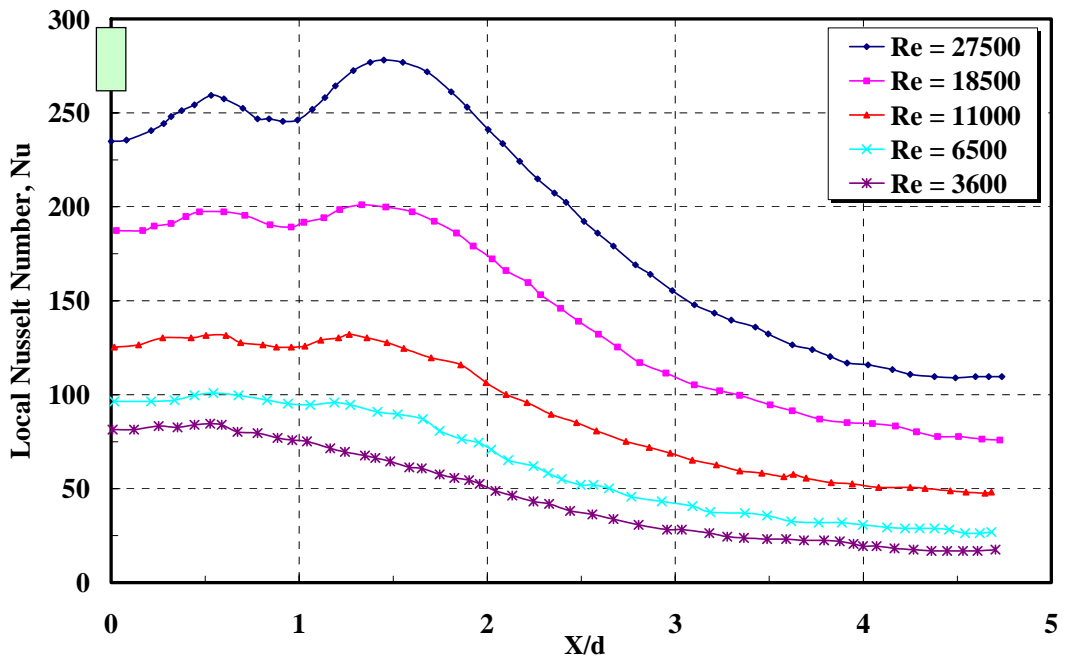


Fig. 1.3 Radial Variation of the Local Nusselt Number for  $H/d = 0.2$ , and  $d = 10.9$  mm, [35]

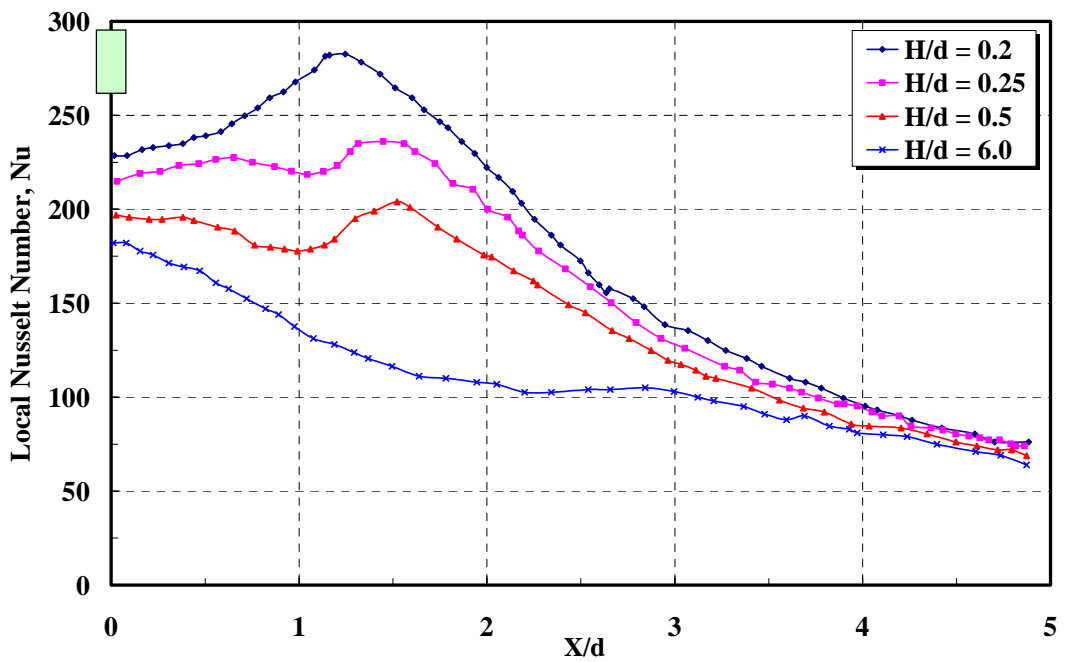


Fig. 1.4 Variation of Local Nusselt Number with Radial Position for  $Re = 23000$ ,  $d = 7.8$  mm, [35]

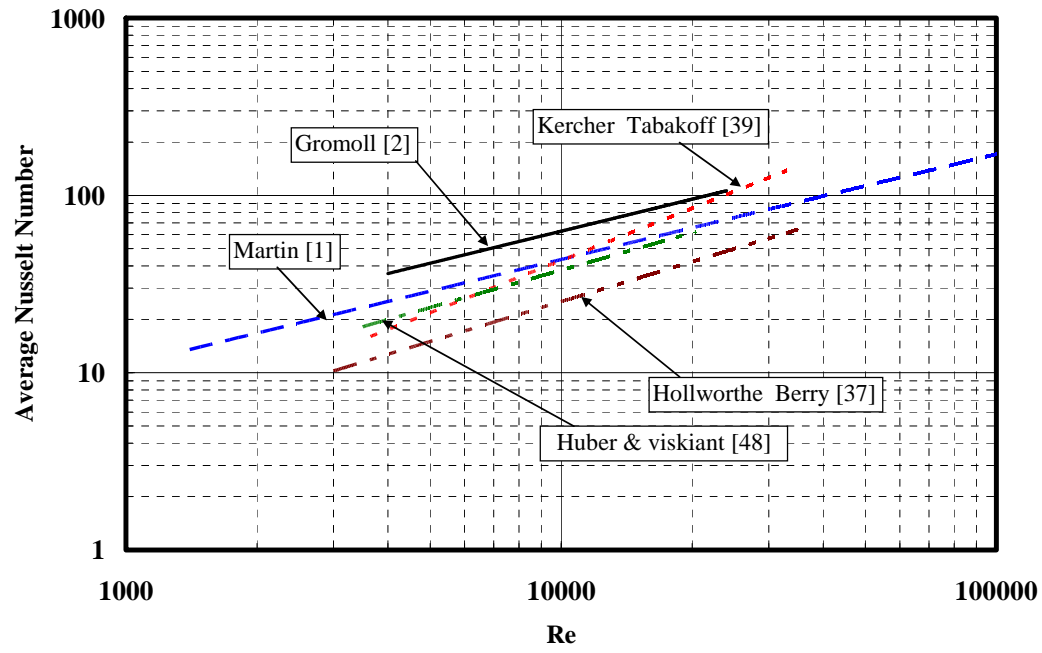


Fig. 1.5 Comparison of Different Average Nusselt Numbers Versus Re Correlations for Multiple Jet Systems,  $r/d = 4.5$ , and  $H/d = 5$

## Characteristics of Impinging Jet

### 2-1 Introduction:

This chapter includes two sections. The first section describes the aerodynamic of submerged jets, and explains the effect of geometrical parameters on the different zones of the impingement jet. The potential core length is described with more detail in this section. The parameters those measure the heat transfer of the impingement jet are explained in the next section.

### 2-2 Description of Flow Regions:

Detailed discussions of the aerodynamics of submerged jets can be found in textbooks [78-80], and reviews of impinging jets are also available in [3, 5]. Here, I introduce only some of the fundamental concepts and terminology for future reference. As a starting point of this section, we consider a single round jet shown schematically in Fig. 2.1. The geometric arrangement is characterized by the nozzle diameter,  $d$ , and the separation distance,  $H/d$ . It is assumed that, the jet fluid exit has a nearly uniform velocity,  $U$ , and temperature,  $T$ . The flow structures of impinging axisymmetric and slot jets have been characterized and can be subdivided into three characteristic regions [81, 82]: a) the free jet region, b) the impingement (stagnation) flow region and c) the wall jet region Fig. 2.1. In the free jet region, the shear-driven interaction of the exiting jet and the ambient produces entrainment of mass, momentum, and energy. The net effects include the development of a nonuniform radial velocity profile within the jet, expansion of the jet, an increase of the total mass flow rate, and modification of the jet temperature before it impinges upon the surface. The impingement zone is characterized by a stagnation region and the turning of the jet in the radial direction, which affects a transition for a wall jet further downstream. The thickness of the impingement zone boundary layer is approximately constant [1, 3]. The wall jet region is characterized by a bulk flow in the outward radial direction. The

velocity maximum occurs at approximately one jet diameter from the impingement zone for the range of the separation distance ( $0 < H/d < 12$ ) [78, 83, 84]. The level of the jet velocity, which is eventually advected into the near-wall region, has a strong effect on the heat transfer rate. The strong aerodynamic and thermal interaction that exists between the submerged gaseous jet and the impingement surface greatly affects the local heat transfer in the stagnation and wall jet regions as well as the average heat transfer over the surface.

The free jet region can be subdivided into three zones: the potential core zone, the developing zone, and the fully developed zone. These three zones are shown in Fig. 2.2. In the potential core the velocity remains constant and equal to the nozzle exit velocity [3, 6]. The length of the potential core is dependent on the turbulence intensity in the nozzle exit and the initial velocity profile. Livigood and Hrycak [11] found that the potential core length extends 6-7 diameters from the nozzle exit for round jets and 4.7 to 7.7 slot widths for slot jets.

The developing zone is characterized by the decay of the axial velocity profile caused by large shear stresses at the jet boundary. These large shear stresses generate turbulence and promote the entrainment of additional fluid. After the developing zone the velocity profile is fully developed. Reichardt [85] found that a Gaussian velocity distribution best fit his experimental measurements in this zone, and others have shown that in the fully developed zone the jet broadens linearly and the decay of the axial velocity is reciprocal linear [86].

An impinging jet is considered to be laminar up to a single jet Reynolds number of approximately 2500 [18]. This value is used although there is no direct evidence confirming a transition Reynolds number for impinging jets. More specifically, there are four characteristic regions for circular free jets:

- 1- The dissipated laminar jet,  $Re < 300$

- 2- A fully laminar jet,  $300 < Re < 1000$
- 3- A transition jet,  $1000 < Re < 3000$
- 4- A fully turbulent jet,  $Re > 3000$ .

Polat et al. [18] state that whether a laminar free jet is still laminar before impingement depends on many factors such as Reynolds number,  $Re$ , original velocity profile,  $U$ , and separation distance,  $H/d$ . These factors all affect the mixing at the outer jet boundaries that transforms a laminar into a turbulent jet.

The radial pressure distribution on the impingement surfaces for around impinging jet has been measured by many researchers [1, 2, 3, 4 and 87]. This is because one general form of correlations for the Nusselt number involves the radial velocity gradient  $\beta$ . The gradient can be determined from the pressure distribution by using Bernoulli's equation if viscous effects are negligible and the velocity just outside the boundary layer is assumed to be equal  $\beta(r)$  [3],

$$\beta = \left( \frac{d}{dr} \cdot \frac{\sqrt{2\{P_s - P_r\}}}{r} \right)_{r=0} \quad (2-1)$$

Thus, although many investigators have measured the pressure distribution, most heat transfer reports result for  $\beta$  and not  $P_r$  [88]. At small separation distance ( $H/d = 1.2$ ), the velocity of the jet has not had sufficient distance to develop and is essentially uniform. Thus, impingement occurs within the potential core of the jet and the pressure distribution agrees well with the inviscid solution. As the separation distance increases, the velocity profile of the jet becomes more non-uniform.

### **2-3 Heat Transfer Definitions:**

The heat transfer from the impingement surface is defined in this section. The local convective heat transfer is defined by

$$\alpha = \frac{\dot{q}_\alpha}{(T_o - T_{ad})} \quad (2-2)$$

where  $\dot{q}_\alpha$  is the convective heat flux,  $T_{ad}$  is the local adiabatic temperature and  $T_o$  is the wall temperature. The heat transfer coefficient,  $\alpha$ , and wall temperature,  $T_o$ , results are presented in terms of the Nusselt number

$$Nu = \frac{\alpha \cdot d}{k_a} \quad (2-3)$$

A effectiveness as dimensionless temperature

$$\theta = \frac{T_o - T_r}{T_j - T_\infty} \quad (2-4)$$

or recovery factor

$$RF = \frac{T_{ad} - T_j}{U^2 / 2c_p} \quad (2-5)$$

For low jet velocities the adiabatic wall temperature is equal to the jet temperature. The local Nusselt number distribution can be averaged to obtain the mean Nusselt number,

$$\overline{Nu} = \frac{\overline{\alpha \cdot d}}{k_a} = \frac{d}{k_a} \int_A \frac{\alpha \cdot (T_o - T_{ad}) \cdot dA}{A \cdot \overline{\Delta T}} \quad (2-9)$$

where the average temperature difference  $\overline{\Delta T}$  is defined as,

$$\overline{\Delta T} = \overline{(T_o - T_{ad})} = \int_A \frac{(T_o - T_{ad}) \cdot dA}{A} \quad (2-10)$$

These definitions are appropriate for both axisymmetric and slot jets. Note that the mean values of both  $\overline{Nu}$  and  $\overline{\Delta T}$  are expected to depend on the area,  $A$ , over which the quantities have been averaged. If the temperature different

$(T_o - T_{ad})$  is constant over the impingement surface and if the jet is axisymmetric, equation (2-9) for the mean Nusselt number reduces to

$$\overline{Nu} = \frac{2}{r^2} \int_0^r Nu(r).r.dr \quad (2-11)$$

If the heat flux,  $\dot{q}_a$ , is constant over the impingement surface  $\pi.r^2$ , the mean Nusselt number becomes

$$\overline{Nu} = \frac{\dot{q}_a \cdot d}{k_a \cdot \Delta T} \quad (2-12)$$

Where

$$\overline{\Delta T} = \overline{(T_o - T_{ad})} = \frac{2}{r^2} \int_0^r (T_o - T_{ad}).r.dr \quad (2-13)$$

The emphasis in the discussion that follows is on the phenomena, understanding of effects, and gaps in data and understanding and not on the comparison for design purposes. To a large extent this has already been accomplished by previous reviews [1, 3, 11, 89].

The aim of the investigation is to determine the convective heat transfer from the metal sheet due to the multiple jets system.

The Nusselt number in the flow direction ( $y = 0$ ) can be expressed as a function of parameters variables as follows:

$$Nu = f(Re, Pr) \quad (2-15)$$

The jet Reynolds number is defined as,

$$\text{Re} = \frac{U \cdot d}{\nu}, \quad (2-16)$$

where  $U$  is the mean exit jet velocity, and  $d$  is the inner jet diameter. The thermal conductivity  $k_a$ , and the kinematic viscosity  $\nu$  of the air were taken for the temperature of the jet exit.

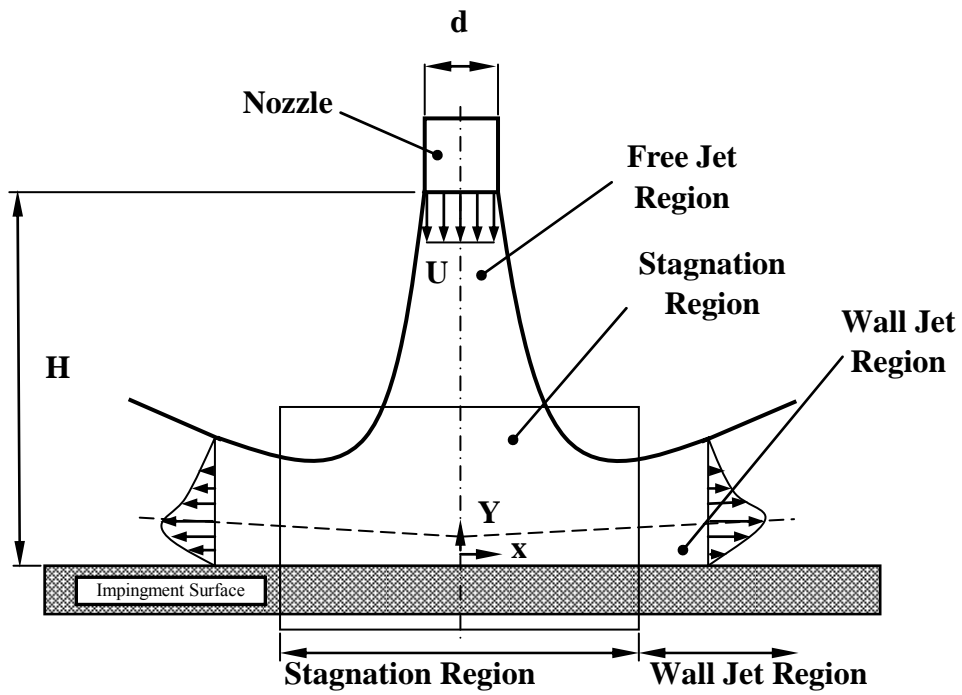


Fig. 2.1 Flow Region for an Impinging Jet

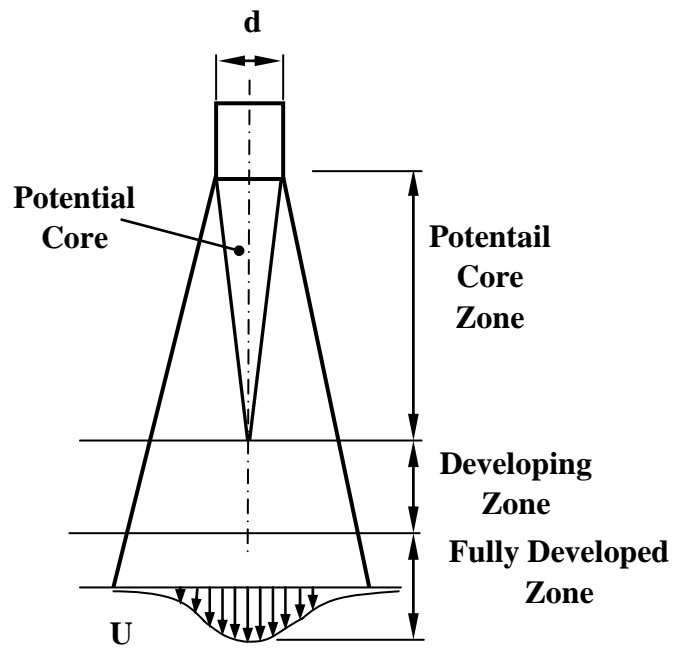


Fig. 2.2 Flow Zones of a Free Jet

## Experimental Work

### 3-1 Experimental Set-Up:

The experimental set-up sketched in Fig. 3.1 was constructed to determine the heat transfer from a flat plate sheet with multiple jets arrays. This includes the air supply section, heating section, distribution box, multiple jets system, impingement sheet and Infrared thermo camera.

The metal sheet was made up of the nickel basis alloy Inconel 600 of size 200 mm x 170 mm. It is being cooled on one side (top side) by the air multiple jets system, while on the other side (bottom side) the surface temperature was measured by an infrared thermo camera. Because of the small thickness of 0.1 mm, the temperature difference between both sides was always lower than 0.065 K, therefore the temperature of both sides could be assumed to be equal, as will be explained later.

The metal sheet was clamped lengthwise between two copper blocks. These copper blocks conduce to the fixation of the plate and in addition to the consistent conduction of electricity. To generate a constant electric transition, a conductive paste of copper basis was used between the copper blocks and the metal sheet. Bar electrodes were embedded in the copper blocks which run from the flexible copper cable to the power source. The power supply was made up of DC transformer (400 A, 7 V) which was controlled by a PC. The amperage was to be assumed and the voltage was adjusted according to the total drag of the current path.

If the metal sheet is flowed through by the electrical current, it warms up due to its ohmic resistance, and thus expands. Therefore one electrode was arranged flexibly and connected by a spring. Hence, the metal sheet was permanently stretched lengthwise. To facilitate a certain expansion a slopping

is provided for the clamping. The metal sheet was provided with uniform plackets which loom into the material for about 15 mm Fig. 3.2.

The air supply is produced from a reciprocating air compressor at a pressure of approximately 6 bar in the experiment hall. This air was filtered, dried and has the same temperature as the ambience and was controlled with valves. For the realization of variable air volume flows, two parallel connected rotameters are used. A pressure reducer is also connected to set overlapping measurement ranges for different flow rate. Each flow control unit has an adjustment range of about 1:10. The parallel connection permits a total control range of 1:1000. Depending on the diameter and the shape of the nozzle, an amount of only 1:500 is reached, which is mainly due to the limited capacity of compressed air supply.

To determine the actual value of volume flow rate, the respective temperature and pressure were recorded. The temperature was measured with the help of sensing devices of type PT100 and passed on a PC. The pressure is recorded via a pressure transducer (forwarding of the signal to a PC) and a conventional manometer with analog display. The temperature of the surrounding area and of the flow at jet exit was recorded using calibrated Hot Wire anemometer (Dantec 54N60).

The air flow then entered into the distribution box, passed through the perforated cylindrical and two perforated plates, as illustrated in Fig. 3.3. So, the amount of air entering into each nozzle was equally distributed.

An in-line and a staggered array of single nozzles were used as shown in Fig. 3.4. Each nozzle was formed by a free tube with a developing flow length exceeding fifty hydraulic diameters. The inner diameters for the nozzles were selected of 5.8 and 8 mm. The nozzle field could be moving in X-direction to obtain the different distances between the centres of neighbouring jets (spacing distance  $S$ ), which varied from  $2d$  to  $10d$ . The level of the nozzle field could

be regulated to adjust different spacing between it and impingement sheet (separation distance H). This distance varied between 1d to 10d. The nozzles field were conducted in an aluminium frame. The infrared thermo camera was arranged vertically at a distance of 800 mm under the metal sheet to measure the bottom surface temperature.

### 3-2 Location of Surface Temperature Measurement:

In the experimental test, a thin metal sheet heated was cooled on one side by a multiple jet system. The surface temperature was measured on the other side with the help of IR-measurement equipment. For the analysis of the heat transfer was assumed that the temperature is equal on both sides of the metal sheet. This is demonstrated in the following.

The Fourier's differential equation can be written for a plate Fig. 3.5 at steady state conditions with an internal heat source as following:

$$\dot{q}_1 = -k_a \frac{\partial^2 T}{\partial y^2}. \quad (3-1)$$

Where  $q_1$  is heat transfer flux due to the electrical power

$$\dot{q}_1 = \frac{P_{el}}{V} = \frac{I^2 \cdot R}{w \cdot t \cdot l} = \frac{I^2 \cdot \rho_{el} \cdot l}{w \cdot l \cdot t} = \left( \frac{I}{w \cdot t} \right)^2 \cdot \rho_{el} \quad (3-2)$$

The thermal conductivity  $k_a$  can be considered as a constant for the observed temperature. The following equation can be obtained from the above equations:

$$T = -\frac{\dot{q}_1}{k_a} \cdot \frac{1}{2} y^2 + C_1 y + C_2 \quad (3-3)$$

Both constant ( $C_1$  and  $C_2$ ) will be determined through two local boundary conditions. One surface temperature is directly known from the infrared thermograph. This boundary condition is;

$$T\Big|_{y=\frac{t}{2}} = T_{w2} \quad (3-4)$$

Furthermore, no heat was emitted at the same point. Consequently the temperature gradient takes the value zero. That is boundary condition 2:

$$\frac{\partial T}{\partial y}\Big|_{y=\frac{t}{2}} = 0 \quad (3-5)$$

By applying the two boundary conditions into equation (3-3), the integration constants  $C_1$  and  $C_2$  can be known and the temperature different  $\Delta T$  can be described by the following function:

$$\Delta T = T_{(x=-\frac{t}{2})} - T_{(x=\frac{t}{2})} = \frac{1}{2} \cdot \frac{\dot{q}_l}{k_a} \cdot t^2 \quad (3-6)$$

At an amperage up to 400 A and thickness,  $t$ , of the foil is 0.1 mm in the presented experiments, the temperature difference between both sheet sides amounts to 0.065 K. This value is less than the resolution of IR-thermography. Therefore, the temperature on both sides can be assumed to be equal.

### 3-3 The Infrared Thermography System:

The temperature field on the bottom side of the sample are recorded by means of infrared thermography thermoCAM® SC 3000 of the company FLIR. The hardware of the infrared system consists basically of two components, infrared camera and the calculation unit (PC).

An main part of the camera is CCD chip. The chip face has a matrix structure. The elements of the matrix are light sensitive sensors which transfer electromagnetic radiation of a certain wave length in the infrared spectrum into electric current.

The intensity of the approaching infrared radiation serves as quantum of the height of the temperature. To determine the actual surface temperature of the examined sample from this intensity, the emissivity  $\varepsilon$  of this area (sample) is required. The intensity is directly proportional to the emissivity. Thus, the emissivity of the surface must be known in advance in order to determine the temperature with IR-thermography. The emissivity depends on a variety of factors (e.g. roughness, shape, homogenous, corrosion, etc.) and therefore has to be measured experimentally.

In the present study the sheet is made of nickel basis alloy Inconel 600, which possess of a low emissivity about 0.2 to 0.3. Therefore, the bottom surface was coated with graphite layer. In this case the emissivity will be increased to (0.7 - 0.8). The surface emissivity was determined in a separate experiment. This experiment will explained in the next section.

Other important characteristics of the camera will be explained in this section. The objective necessary to carry out the experiment has a fixed focal length with acceptance angle of  $20^\circ$ . An excellent image quality can be taken within the long wave range (8  $\mu\text{m}$ -9  $\mu\text{m}$ ). This camera can measure in the following four temperature ranges;  $-20^\circ\text{C}$  to  $80^\circ\text{C}$ ,  $10^\circ\text{C}$  to  $150^\circ\text{C}$ ,  $100^\circ\text{C}$  to  $500^\circ\text{C}$  and  $350^\circ\text{C}$  to  $1500^\circ\text{C}$ . The resolution is  $136*272$  measurement values per pixel. The size of the measuring point depends on the objective and the distance, approximately 0.65 mm/pixel in the present study. The measured pictures can be evaluated with following analysis tools; Isotherm, Spot Tool, Surface and Line. The detailed analysis of the picture was taken place with the evaluation software ThermoCAM® Reseacher. That is a software packing for the admission and analysis of digital real time data.

### **3-4 Determination of Emissivity:**

To determine the surface temperature by means of infrared thermography requires a uniform and high surface emissivity. The observed metal sheet side

was coated with a special paint (graphite colour). The metal sheet was annealed in an furnace at a temperature approximately 350°C. The measurement set-up used to determine the temperature dependent emissivity of the coated surface ( $\varepsilon_1$ ) is illustrated in Fig. 3.6. It consists of two equal metal sheets of the same material as used for the heat transfer test. Both outer sides of the metal sheets were coated to ensure a symmetric heat loss. Between the sheets a thermocouple was arranged. Because of the enclosure of all sides it measured exactly the surface temperature. The metal sheets were connected by welding spots on their upper and lower edges. For the power supply, the sheets were clamped between two pairs of copper jaws. An electric current was conducted through the metal sheet. Because of the symmetric assembly of the test section, the same amperage flow through both sides of the metal sheet. By changing the electric current different temperature could be adjusted. These temperatures were measured using a calibrated thermocouple. The emissivity at the scanner of the camera was regulated until the shown temperature matched with that of the thermocouple. This emissivity is shown in Fig. 3.7. The emissivity depend on the surface temperature can be approximated with the following equation;

$$\varepsilon_1 = 1.08 * T_0^{-0.072} \quad (3-7)$$

The values are slightly lower than the value of 0.95, which is often given for graphite colours [34]. This is caused by the extreme thin layer to avoid a resistance for the heat conduction through it. In the same way, the emissivity of the bright metal side,  $\varepsilon_2$ , was determined. It was found to be approximately 0.3.

### **3-5 Determination of the Heat Transfer Coefficient:**

The metal sheet was heated electrically by a direct current up 400 A and 7 V to determine the heat transfer coefficient for a position regarded on the metal sheet at steady state condition. Due to Ohm's law the generated electrical power can be calculated by the following equation;

$$Q_I = R.I^2 \quad (3-8)$$

The mean current density is used for calculating the electrical power equation (3-8). To this end, the ratio of current flow and area flow is calculated. The temperature of the metal sheet is not equal at every position and the specific electric resistance increases with increasing temperature. Consequently the distribution of electric power over the metal sheet is not uniform. Fig. 3.8 depicts the distribution of the specific electric resistance based on a radial temperature distribution with a minimum temperature at centre of the metal sheet and a maximum temperature at its border. The specific electric resistance is lowest at the centre of the metal sheet and greater at its border. The difference in specific electric resistance is about 4% for this extreme temperature difference [34, 90-92].

By applying the energy balance over the metal sheet at steady state condition as shown in Fig 3.9, the electrical power  $Q_I$  is transferred by the three known heat transfer mechanisms and can be written in the following form;

$$Q_I = Q_\alpha + Q_\epsilon + Q_k \quad (3-9)$$

Where  $Q_\alpha$  is the heat transfer by convection,  $Q_\epsilon$  is the radiation heat transfer from both metal sheet sides and  $Q_k$  is the conduction heat transfer through the metal sheet thickness,  $t$ . Because the heat source is uniformly distributed over the metal sheet as explained before, therefore the electrical power in equation (3-9) can be calculated by

$$Q_I = \dot{q}_I \cdot \Delta V = \left[ \left( \frac{I}{w \cdot t} \right)^2 \cdot \rho_{el} \right] \cdot w \cdot t \cdot \Delta X \quad (3-10)$$

With  $I$  as amperage,  $w$  and  $t$  as the width and thickness of the test metal sheet, respectively,  $\rho_{el}$  as specific electrical resistance of the metal sheet, its dependency on the metal temperature can be corrected by the following equation [92]

$$\rho_{el} = (1,0208 + 2 * 10^{-4} * T_o - 6,38 * 10^{-8} * T_o^2) * 10^{-6} \quad (3-11)$$

Radiation and conduction were considered as heat losses. The radiation heat from both sides of the metal sheet is given by

$$\begin{aligned} Q_e &= Q_{e1} + Q_{e2} \\ &= (\varepsilon_1 + \varepsilon_2) \cdot \Delta A \cdot \sigma (T_o^4 - T_a^4) \\ &= (\varepsilon_1 + \varepsilon_2) \cdot w \cdot \Delta X \cdot \sigma (T_o^4 - T_a^4) \end{aligned} \quad (3-12)$$

where  $\varepsilon_1$  and  $\varepsilon_2$  are the emissivities of the coated and bright surfaces, respectively,  $\sigma$  is the Stefan-Boltzmann constant,  $T_a$  is the ambient air temperature. Both emissivities were known from the measurement explained before.

Because of the radial temperature distribution with the minimum temperature in the center of the jet, as shown in Fig. 3.10, heat is conducted in the metal foil plane from outer regions of the jet to its center. This conduction heat  $Q_k$  can be calculate with Fourier's differential equation for cylinder coordinates, because the temperature gradient is known from the measurements,

$$\begin{aligned} Q_{km} &= q_{km} \cdot \Delta V \\ &= -t \cdot k_m \cdot \frac{1}{r} \cdot \frac{\partial}{\partial r} \left( r \cdot \frac{\partial T_o}{\partial r} \right) \cdot \Delta V \\ &= -t \cdot k_m \cdot \frac{1}{r} \cdot \frac{\partial}{\partial r} \left( r \cdot \frac{\partial T_o}{\partial r} \right) \cdot w \cdot t \cdot \Delta X \end{aligned} \quad (3-13)$$

For all experimental conditions, this conduction heat flux was estimated lower than 2% of the total input heat.

The total heat losses (radiation and conduction heat transfer) amount up to 10% of the electrical heat flux for laminar flow. For turbulent flows, the heat losses were reduced to value down to 2%.

The heat by forced convection was caused by the flow impinging against metal sheet and was defined by;

$$\begin{aligned} Q_{\alpha} &= \alpha \cdot \Delta A \cdot (T_o - T_{ad}) \\ Q_{\alpha} &= \alpha \cdot w \cdot \Delta X (T_o - T_{ad}) \end{aligned} \quad (3-14)$$

where  $\alpha$  is the convective heat transfer coefficient. The temperature different  $(T_o - T_{ad})$  consists of the bottom side sheet temperature  $T_o$  was recorded by IR-thermography and the reference temperature which can be defined as the adiabatic wall temperature  $T_{ad}$ . This temperature can be measured from the local temperature distribution over the metal sheet area. In the present study the exit jet velocity lower than 108 m/sec, the difference between the adiabatic wall temperature and the exit air jet temperature is less than 2 K. Thus, the adiabatic wall temperature in the last equations can be replaced by the exit air jet temperature  $T_j$ .

The heat transfer by convection can be differentiated between free and forced convective heat transfer. Free convective results at the sheet surface from the density variation in the surrounding air. This leads to air movements, which cause again a convective heat transfer. The forced heat transfers by convective caused by the impingement between the airflow come out of the multiple jets system with metal sheet area. In this work the heat transfer by this forced convective heat transfer is to be examined.

As known, if the exit jet velocity is very small and the temperature difference between the surrounding air and metal sheet is large, then the heat transfer by free convective is significant. In case of vertical plate, the adiabatic wall

temperature is not constant over the surface of the metal sheet. Therefore, the free convection is difficult to be determined. Horizontal plate is usually applied in the most of industrial applications. In addition, the heat transfer by free convection was measured in case of zero velocity of jet to be about  $5 \text{ W/m}^2\cdot\text{K}$  [34]. Thus, the metal sheet was arranged horizontally to ensure a low and a nearly equal adiabatic wall temperature. Considering that the minimum jet velocity was  $3.5 \text{ m/sec}$  in the present study, the heat transfer by free convection was negligible.

Applying the equations from (3-10) to (3-14) in equation (3-9) and eliminating the factor  $(w, \Delta X)$ , which is contained in each term, then computing the energy balance of a regarded pixel in the metal sheet area, this equation can be written as follows:

$$\left(\frac{I}{w}\right)^2 \cdot \frac{\rho_{el}}{t} = \alpha \cdot (T_o - T_j) + (\varepsilon_1 + \varepsilon_2) \cdot \sigma (T_o^4 - T_a^4) + \left[ -k_m \cdot \frac{1}{r} \cdot \frac{\partial}{\partial r} \left( r \cdot \frac{\partial T_o}{\partial r} \right) \right] \cdot t \quad (3-15)$$

Firstly, the emissivity of the surface was assumed to be used in the software of camera. From this emissivity, the surface temperature recorded by the camera can be determined. As it is known, the radiation intensity depends on the emissivity and on the fourth power of the surface temperature. The surface temperature which be computed with this assumed emissivity is not accrued. Then the correct emissivity can be determined. In this way the correct surface temperature was calculated  $T_{co}$ . By using the following equation,

$$\varepsilon_c \cdot \sigma \cdot A \cdot (T_c^4 - T_a^4) = \varepsilon_{co} \cdot \sigma \cdot A \cdot (T_{co}^4 - T_a^4) \quad (3-16)$$

and by the emissivity given by the equation (3-7), the correct surface temperature becomes as follows;

$$T_{co} = \sqrt[4]{\frac{\varepsilon_c}{1.08 \cdot T_{co}^{-0.072}} \cdot (T_c^4 - T_a^4) + T_a^4} - 273.15 \quad (3-17)$$

Then correct surface temperature  $T_{co}$ , is used to determine the convection heat transfer in equation (3-15).

### 3-6 Distribution of Surface Temperature:

The convection heat transfer caused by the multiple jets system is based on the surface temperature measured with infrared thermography. Fig.3.11 and Fig. 3.12 show photos of the temperature field for an in-line and a staggered array respectively for difference velocity. A relative symmetric temperature distribution is obvious. This symmetry will be shown in more detail in Fig. 3.13. This figure illustrates the sheet temperature distribution for the two lines X and Y. The X axis is through the stagnation points in spanwise direction and the other axis Y is perpendicular to it. The right ordinate corresponds to the temperature distribution for the high ( $Re = 41400$ ) and the left ordinate for the low ( $Re = 1400$ ) Reynolds number. In this example the spacing of jets is  $S/d = 6$  for in-line array and separation distance is  $H/d = 2$ . In both cases, the distribution of the temperature is approximately the same in X and Y directions. For the case of the high Reynolds number ( $Re = 41400$ ), the temperature distribution has two minimum values, the first at the stagnation point, and the second at the radial distance  $X/d = 1.8$ . This second minimum temperature is caused by the flow transition from laminar to turbulent. This effect is well known from the heat transfer of a single jet [1, 3, 34, 93-97]. For the case of the low Reynolds number ( $Re = 1400$ ), the temperature has only one minimum value. The second minimum value does not exist, because the flow is completely laminar.

This paragraph demonstrates the surface temperature distribution which was computed in section 3-5. The uncertainty of the temperature measurements is about 5%, mainly influenced by the uncertainty in determining the emissivity

of the surface. The metal sheet was heat by constant direct current up to 400 A and 7 V is led through it. After the metal sheet temperature reached to a steady state condition, the multiple jets systems is cooled from the top side. The local surface temperature is recorded by an infrared scanner from the bottom side.

Figures 3.14 to 3.18 illustrate the temperature distribution on impingement plate for in-line array ( $S/d = 2, 4, 6, 8,$  and  $10$ ) and the separation distance ( $1 \leq H/d \leq 10$ ) are parameters. They are based on two Reynolds numbers ( $Re = 41400, 19000$ ) for example. The working conditions of the electrical power do not change for all tests (400 A, and 7 V). From these figures, it can be seen that the range of temperature is from 40 to 120 °C for high Reynolds number of 41400 while this range increases for low Reynolds number of 19000 to be from 100 to 270 °C. This is because the turbulent intensity is high with increase of the Reynolds number and the energy remove from the metal sheet is high. The temperature is low value at stagnation point for each nozzles and it is high at the middle point between adjacent jets. This temperature is increased at the border of the sheet without limit. Therefore the temperature distribution is waving form over the metal sheet surface in the distance between jets for both high and low Reynolds numbers.

The temperature distribution for in-line array ( $S/d = 2, 4, 6, 8,$  and  $10$ ) in the large range of the Reynolds number ( $30700 \leq Re \leq 1400$ ) is show in appendix A-1. The temperature distribution for staggered array is shown in appendix A-2 at the same conditions that for the in-line array. They have the same trend for the in-line array as explained before under the same conditions.

### **3-7 Computation of Average Heat Transfer:**

The temperature field in two dimensions was measured by the IR-thermography. The geometrical of this field is a rectangle form as shown in Fig. 3.19. The temperature value was measured at the centre of rectangular measuring surface (pixel). This temperature is assumed as constant over the

surface of pixel. The size of pixel is depended on some factors, these factors include the array of element on the chip of the IR scanner, the type of the optics, and the distances from the chip to the optics, as well as from the optics to the measuring surface.

The form of the chip matrix with the assigned technology rectangular gives the pixel size. The edge lengths of this pixel represent the local dissolution of the system in the respective attempt. The basic parameters in the present work are not change. Therefore, the length of pixel,  $\Delta X_p$ , is constant and equal to approximately 0.65 mm.

The average Nusselt number over unit cell was calculated in the present work as shown in Fig. 3.19. Each unit cell has a particular number of pixels depend on the spacing distance between jets  $S/d$ . Therefore, the average Nusselt number over the each unit cell can be calculated by the following equation,

$$\overline{Nu} = \frac{\sum NU_p}{n_p} \quad (3-18)$$

where  $Nu_p$  is the local Nusselt number in each pixel and which can be calculate with equation (2-3) and  $n_p$  is the number of pixels over each unit cell. By the same way, the average Nusselt number over line can be calculated. This Nusselt number will be used to explain the uniformity of the heat transfer over impinging surface in chapter six.

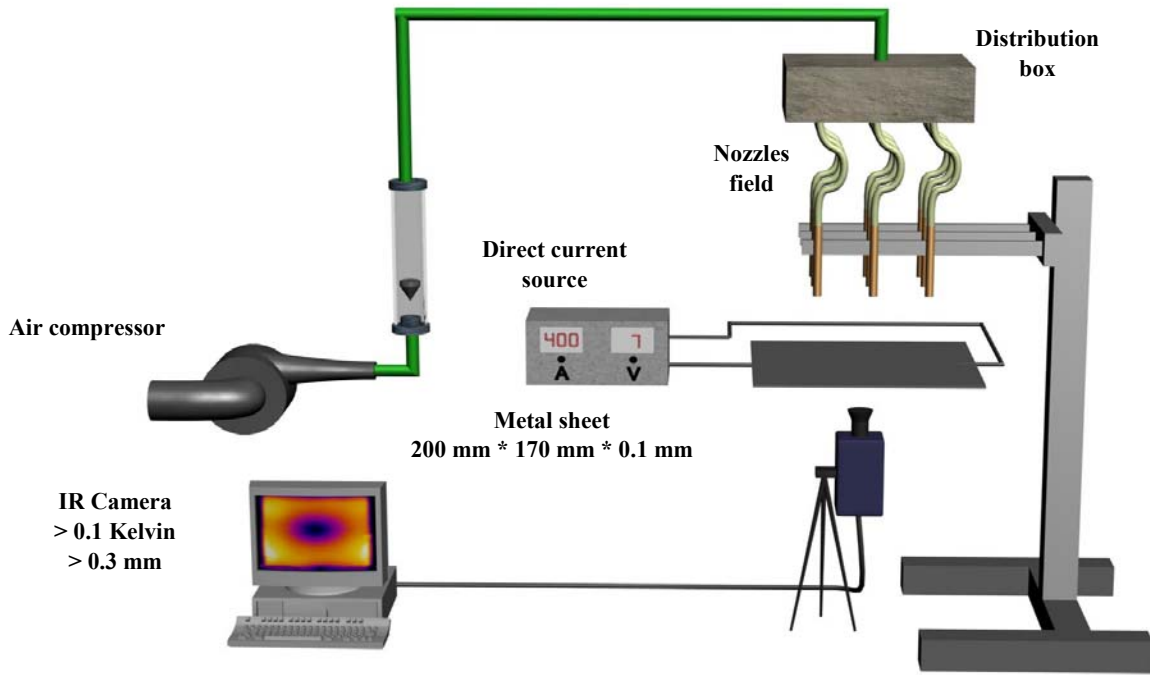


Fig. 3.1 Experimental Set-Up

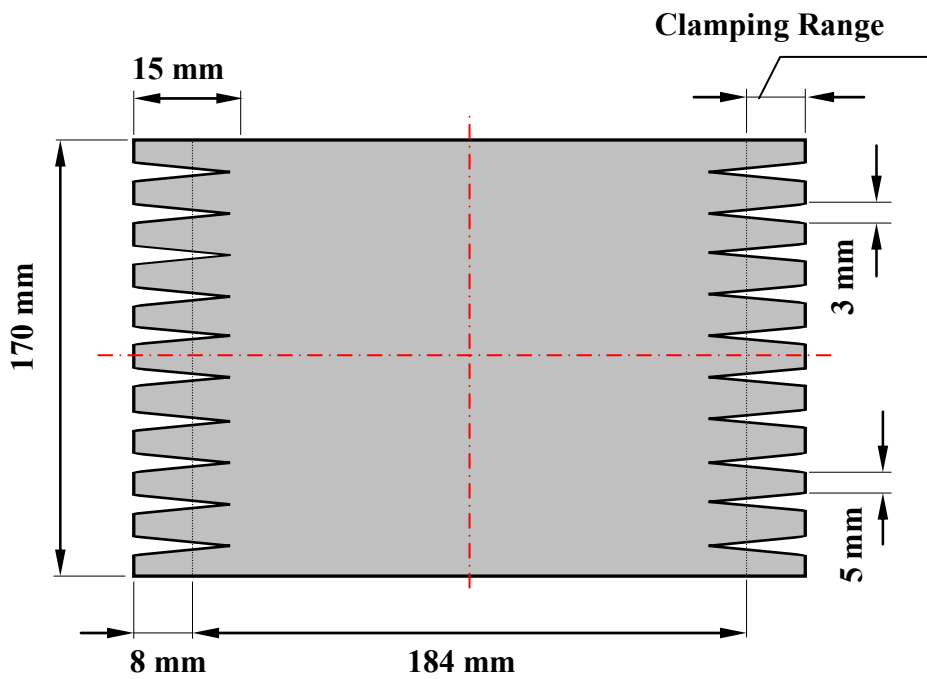


Fig. 3.2 Tested Metal Sheet

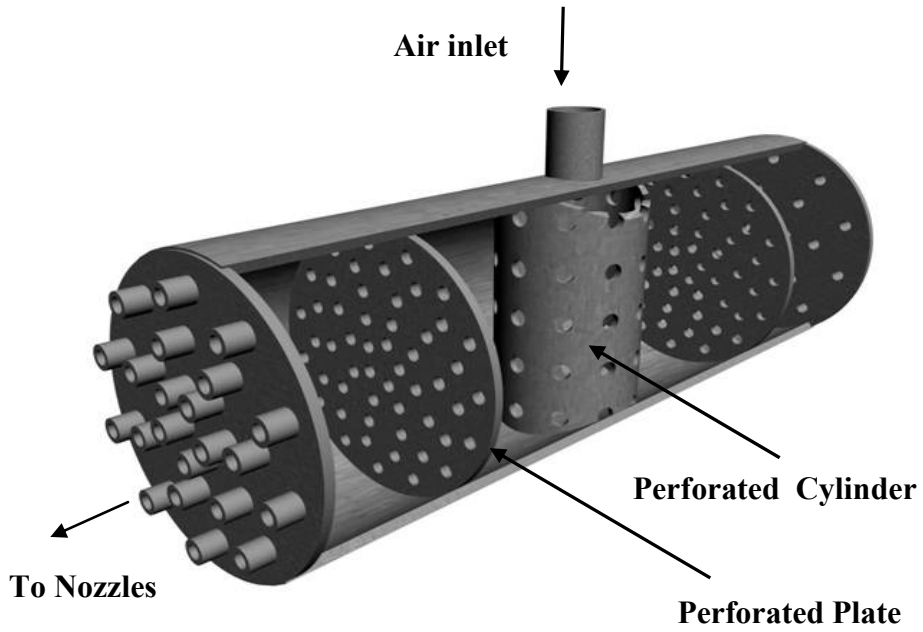
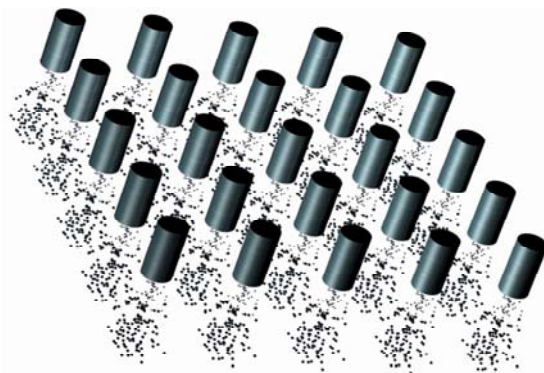


Fig. 3.3 Distribution Box



(a) In-line Array



(b) Staggered Array

Fig. 3.4 Single Nozzles Arrays

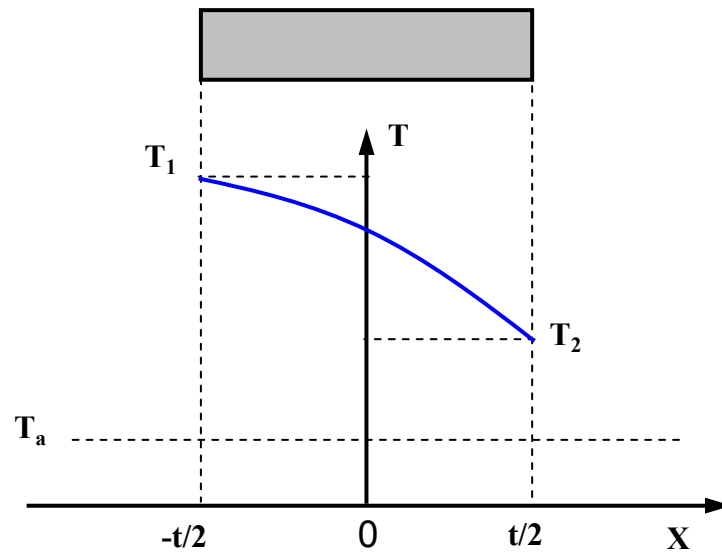


Fig. 3.5 Temperature Distribution in a Axisymmetrically Cooled Sample Element

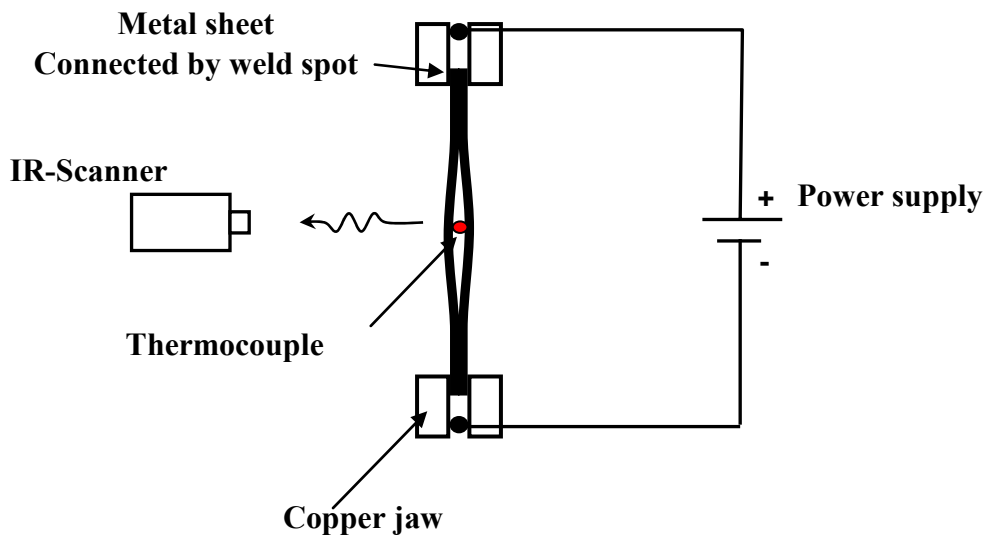


Fig. 3.6 Measurement Set-Up for Determining Emissivity of the Coating Surface

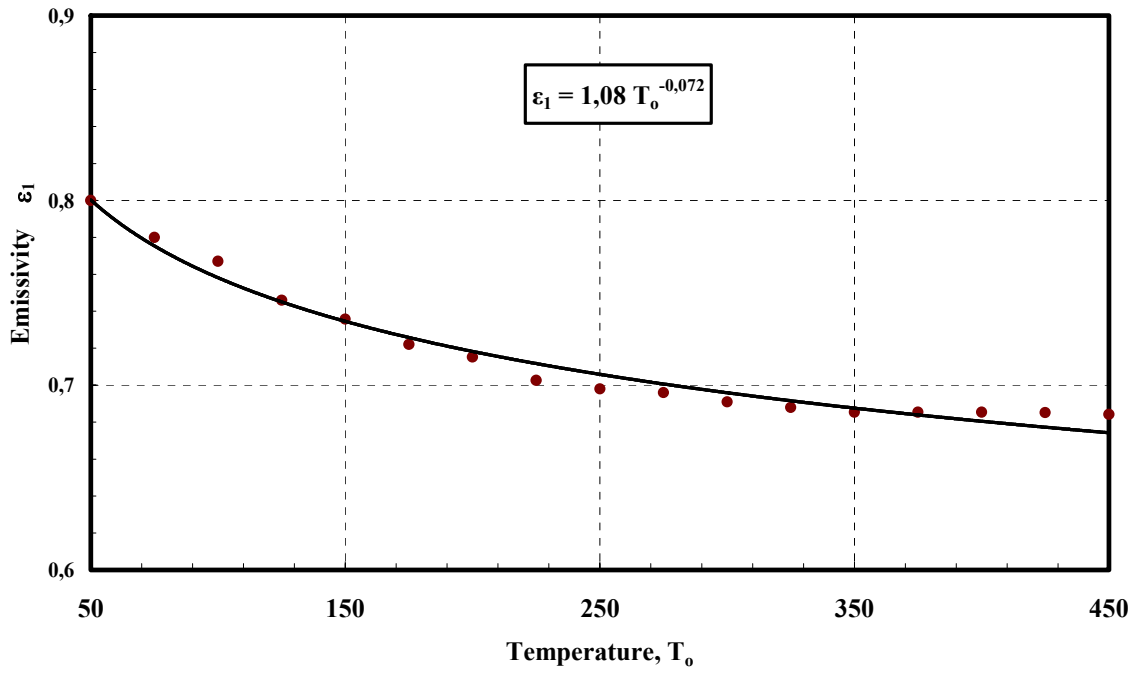


Fig. 3.7 The Variation of Emissivity of the Sample Surface Provided with Coating with Surface Temperature

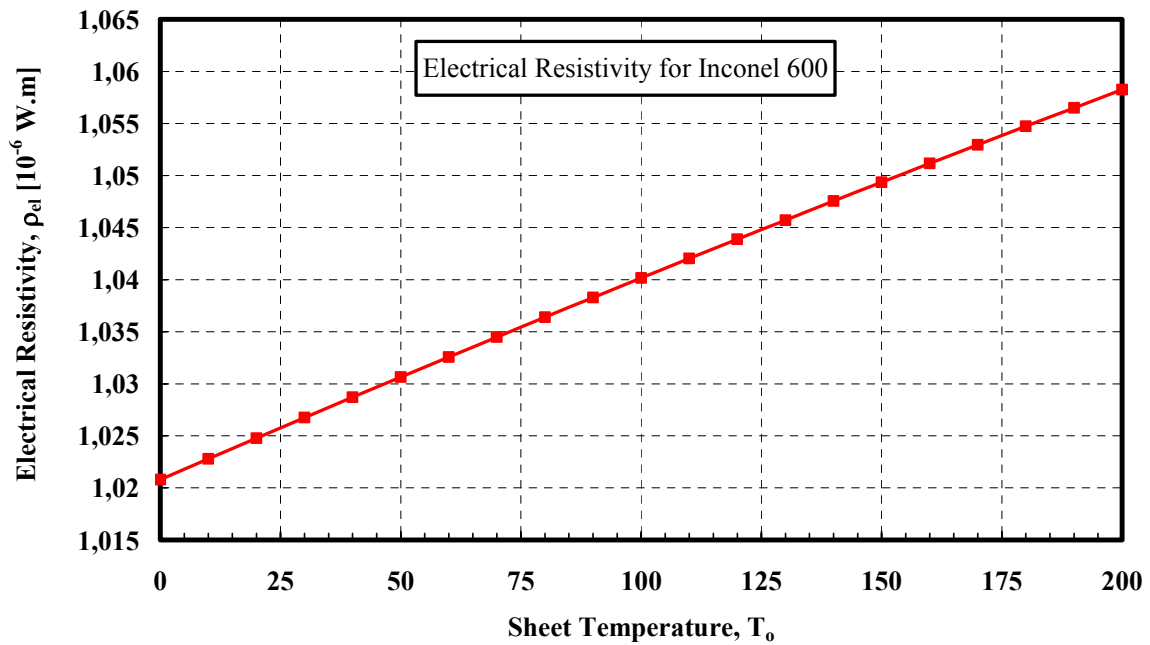


Fig. 3.8 Electrical Resistivity of INCONEL 600 as Function of Temperature

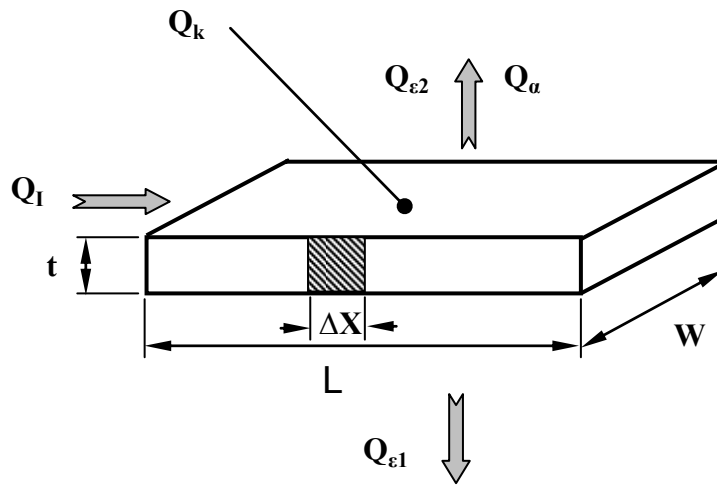


Fig. 3.9 Sketch of the Metal Plate

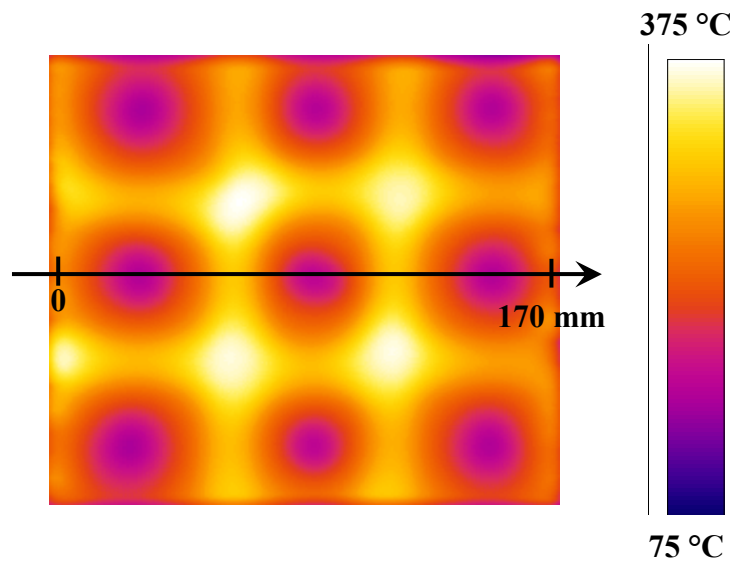


Fig. 3.10 Infrared Picture

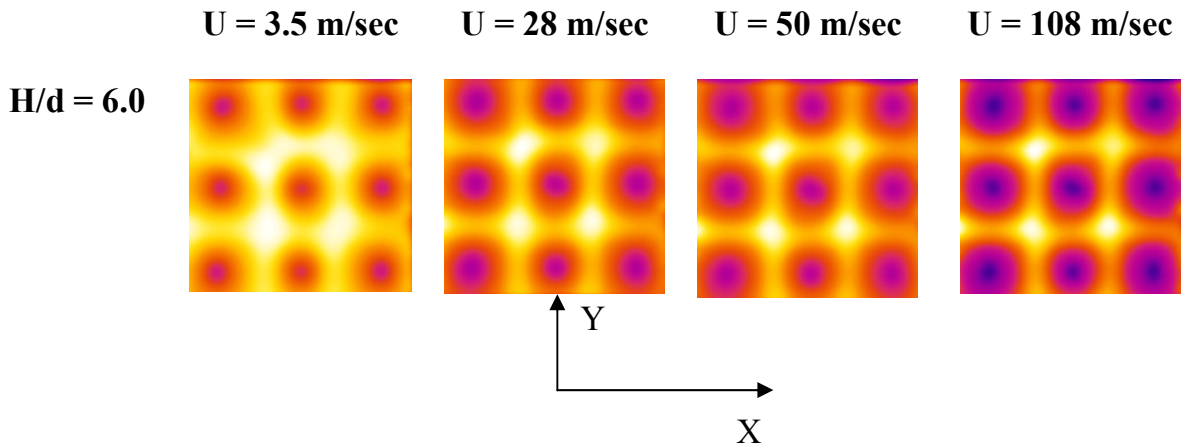


Fig. 3.11 Infrared Image, In-line Arrays,  $S/d = 10.0$

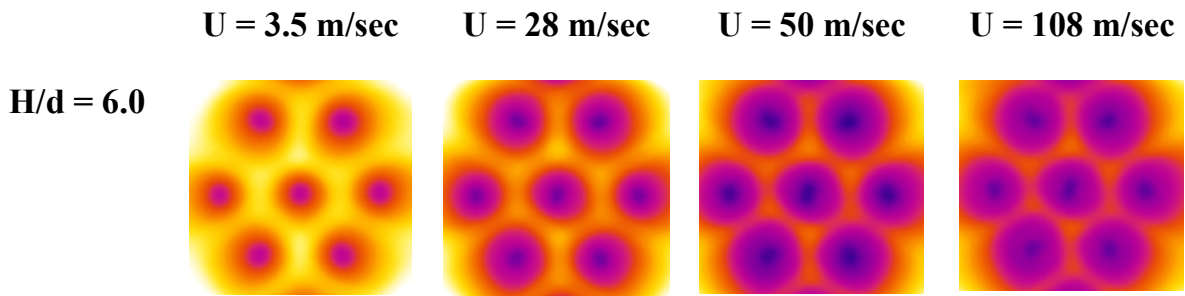


Fig. 3.12 Infrared Image, Staggered Arrays,  $S/d = 10.0$

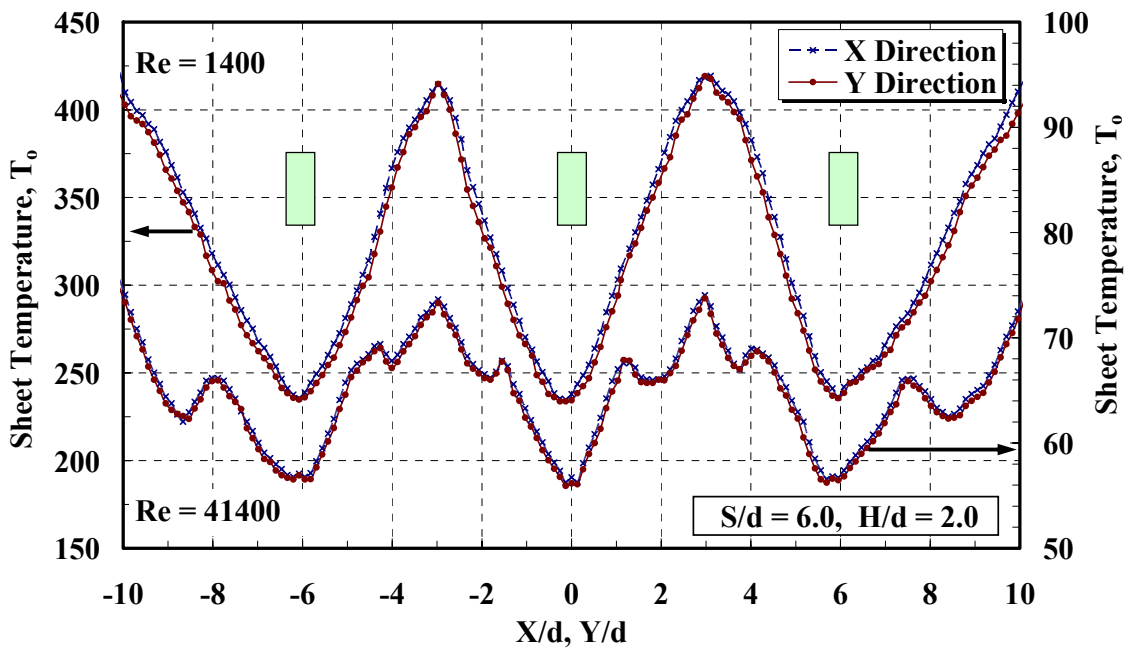


Fig. 3.13 Local Sheet Temperature Distribution for two Reynolds Numbers

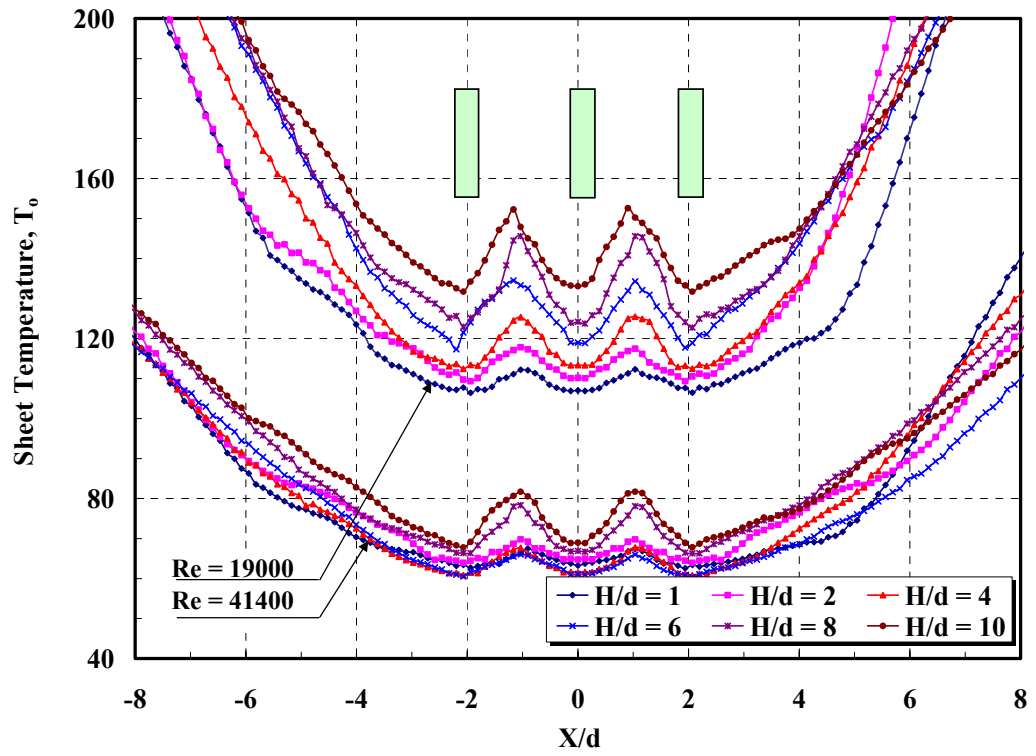


Fig. 3.14 Local Sheet Temperature Distribution at different  $H/d$  ratio for  $S/d = 2$

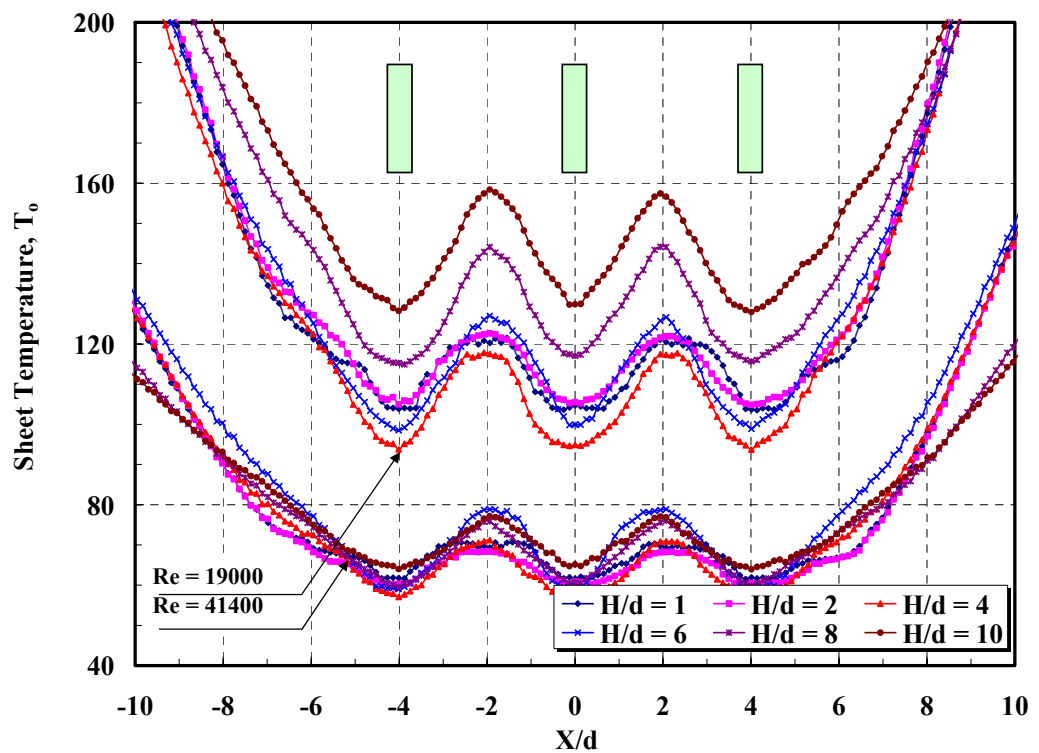


Fig. 3.15 Local Sheet Temperature Distribution at different  $H/d$  ratio for  $S/d = 4$

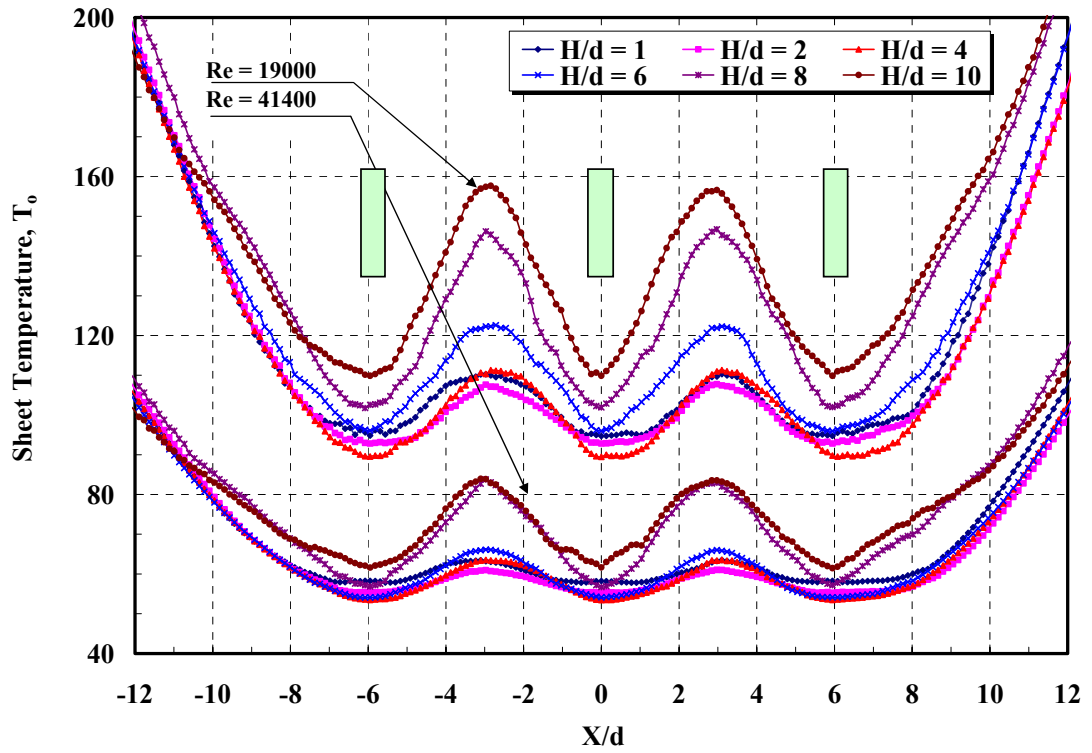


Fig. 3.16 Local Sheet Temperature Distribution at different  $H/d$  ratio for  $S/d = 6$

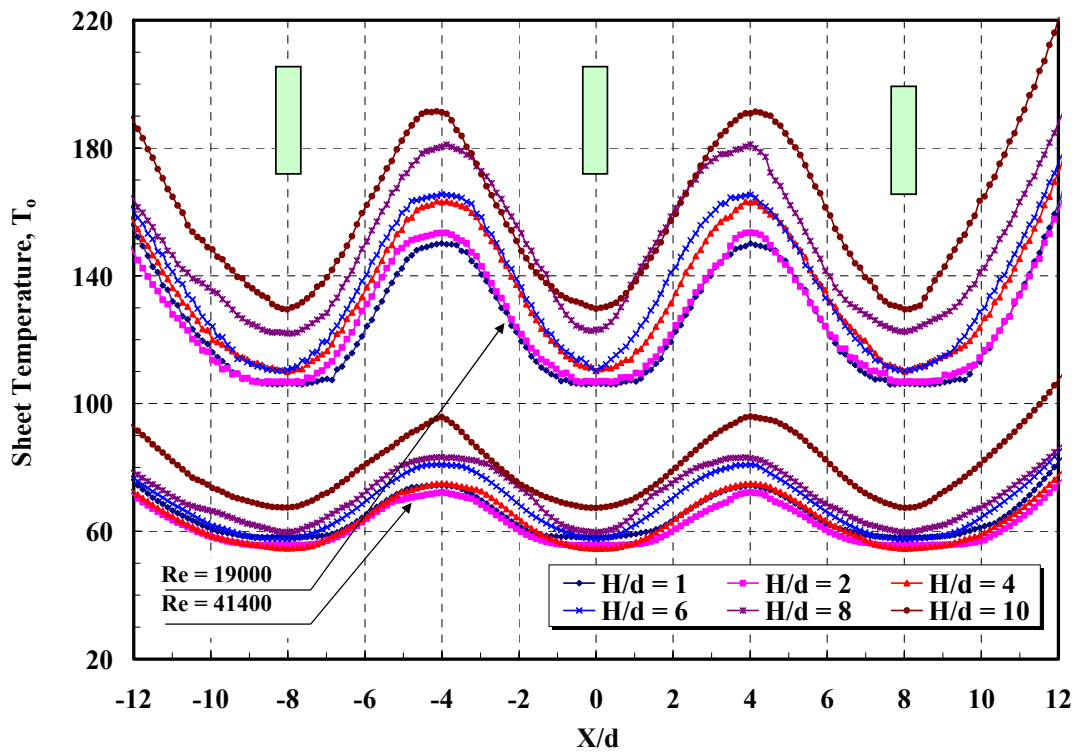


Fig. 3.17 Local Sheet Temperature Distribution at different  $H/d$  ratio for  $S/d = 8$

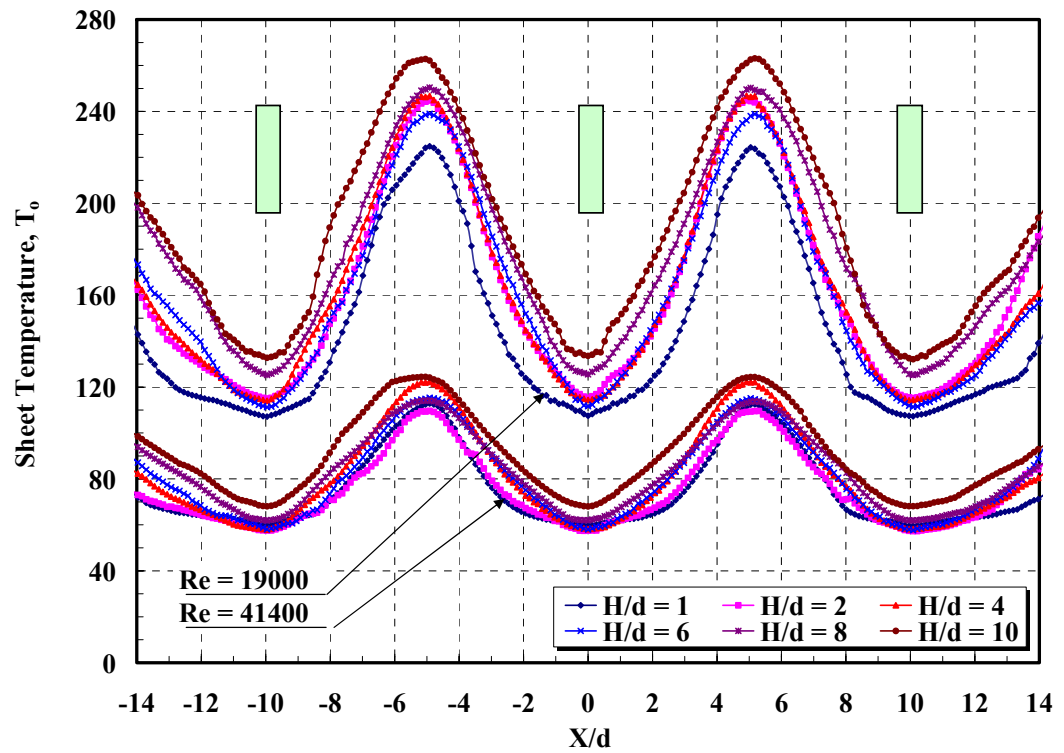


Fig. 3.18 Local Sheet Temperature Distribution at different H/d ratio for S/d = 10

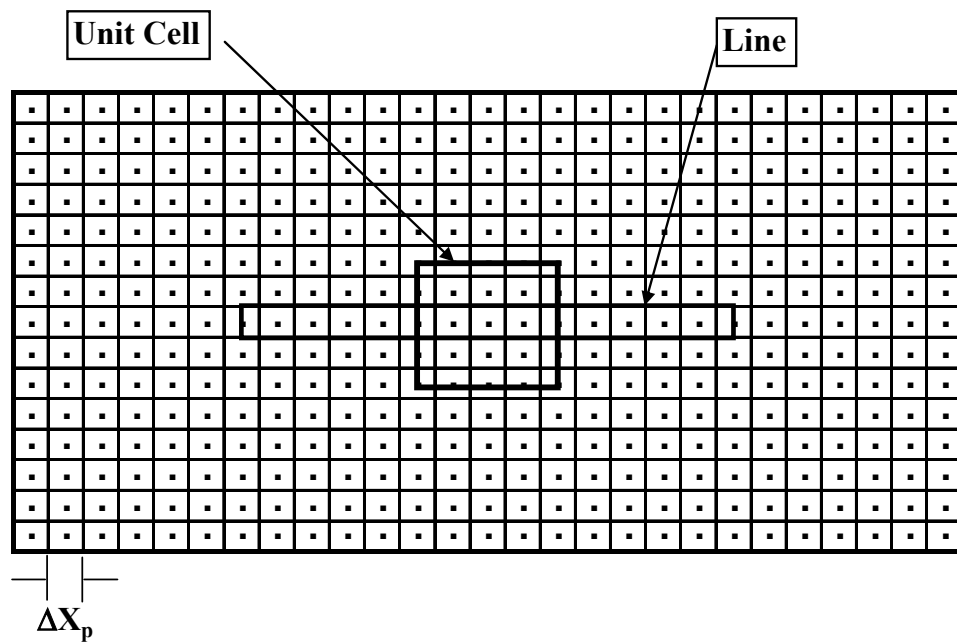


Fig. 3.19 Matrix Structure of the Measuring Surface for IR-system,  $\Delta X_p$  is Local dissolution

## Heat Transfer for Multiple Free Jets System

### 4-1 Introduction

In-line and staggered arrays are the baseline cases to study the multiple jets impingement heat transfer. For this study, nine isothermal jets (3x3 in-line and staggered arrays) were used with difference of the spacing distance ( $S/d$ ) varying from 2 to 10. Nine jets were chosen because the centre jet is completely surrounded by adjacent jets, similar to an individual jet in a large array which is not located on the perimeter. Also, the use of only nine jets resulted in a smaller required impingement area and larger Reynolds number range. A value of  $S/d = 4$  was recommended by Freidman and Mueller [72] to reduce adjacent jet interference and maximum heat transfer over the surface for large separation distance  $H/d \geq 8$ , while Martin [1] recommended an optimum value of roughly 7 diameter for  $H/d = 5.4$ . Thus, spacing distance values of 2 to 10 were chosen to provide understanding of the Nusselt number trends. The separation distance ( $H/d$ ) varying from 1 to 10 was chosen. The effect of jet Reynolds number (1400, 6000, 16000, 19000, 23000, 30700, and 41400) is studied for all configurations. This study provides details (stagnation, local, and average) of the heat transfer distribution for effect of spacing and separation distances, and array of configurations. The characteristic of the heat transfer carried out for two inner jet diameters (5.8 mm, and 8 mm). The average Nusselt number which was calculated from in-line array is compared with that from a single nozzle. In the following section, the local and average Nusselt number distribution over the impingement plate in spanwise direction was provided for single nozzle.

### 4-2 Local Heat Transfer Distribution:

#### 4-2-1 Single Nozzle:

The experimental results will focus firstly on the local heat transfer of a single nozzle. These results were measured with one jet of inner diameter of 5.8 mm and in the range of Reynolds number from 1400 to 41400. In addition, the

separation distance  $H/d$  was chosen in the range from 1 to 8. Fig. 4.1 depicts the radial distributions of the local Nusselt number for two Reynolds numbers ( $Re = 23000$  and  $11100$ ) for example. The parameter is the separation distance ( $1 \leq H/d \leq 8$ ). For the high Reynolds number ( $Re = 23000$ ) and the low separation distance ( $H/d \leq 2$ ), the impingement plate is within the potential core length of the free jet region. Thus, the heat transfer characteristics are very complicated due to the complex interaction between the impinging jet and the impingement plate [2, 3, 94, 97-98]. As shown in this figure, the local Nusselt number decreases rapidly from the stagnation point to a minimum value at  $X/d = 1.2$  and then increases, giving the peak value at  $X/d = 2$ . Moving outward from the peak value, the heat transfer rate decreases monotonically. Similar profiles with the positions  $X/d = 1.2$  and  $X/d = 2$  for the minimum and maximum peak, respectively, were reported by other authors [94, 98-100], as already mentioned in chapter 1. For the case of the separation distances ( $H/d = 4$ ) a minimum and maximum does not occur any more. At the two positions of peak only the gradient changes.

At high separation distances ( $H/d \geq 6$ ) the local Nusselt number decreases monotonically upon going outward along the impingement plate and do not show the peak value. For jet at plate separation distance larger than  $H/d = 6$ , the turbulence intensity of the impinging free jet zone has a maximum heat transfer at the stagnation point.

The average Nusselt number,  $Nu_{av}$  distribution depend on the radial distance  $X/d$  is plotted for the two different Reynolds numbers of 23000 and 11100 in Fig. 4.2. The separation distance is varied from  $H/d = 1$  to  $H/d = 8$ . This figure shows that the average Nusselt number decreases with the increase of the radial distance,  $X/d$ . For high Reynolds number ( $Re = 23000$ ) there are to peaks at  $X/d = 0.5$  and  $2.5$  for small values of values of separation distance. These peaks disappeared with increase of  $H/d$  and for low Reynolds number (11100). These results are similar to those reported by many other authors, e.g. [25, 54, 101-102].

#### 4-2-2 Multiple Free jets System:

The radial distribution of local Nusselt number for the in-line array is presented in Figs. 4.3a-d to Figs. 4.7a-d for four Reynolds numbers (41400, 23000, 16000 and 6000). The separation distance  $H/d$  was chosen in the range from 1 to 10. The distributions of the heat transfer for  $S/d = 10$  and 8 are shown in Figs. 4.3a-d and, Figs. 4.4a-d. Examination of the Nusselt number values of Figs. 4.3a-d clearly shows the presence of secondary region or peak. This is because the spacing distance between adjacent jets is large and can consider each jet as single nozzle. In this case, the maximum Nusselt number occurs at the stagnation point as observed with larger separation distances. The secondary peak is ring around the stagnation point. This ring occurs at  $X/d \approx 0.5$  and  $X/d \approx 1.8$ . The peaks which occurred at  $X/d \approx 1.8$ , is attributed to both the fluid accelerating out of the stagnation region which thins the local boundary layer and the influence of the shear layer generated turbulence around the circumference of the jet. This peak also caused by the transition to turbulent flow in the boundary layer [48-49, 102]. Thus, as Reynolds number increases, the peak in the local Nusselt number becomes more pronounced. This peak becomes less pronounced as the Reynolds number is reduced and the separation distance is increased. A decrease in Reynolds number and an increase or the separation distance appears to promote an earlier boundary layer transition from laminar to turbulent flow, because the location of this peak moves toward the stagnation point when either of these two parameters are varied appropriately [48].

Figures 4.5a-d illustrate the local Nusselt number distribution for spacing distance,  $S/d = 6$ . In this case, the spacing distance between jets is decreased. Therefore, the effect of the other jets is increased and the interference between jets has a more effect on heat transfer rate. So it can be seen the secondary peak at high Reynolds number. The local Nusselt number distributions for  $S/d = 4$  are present in Figs. 4.6a-d with different separation distances. From these figures it can't be observed clearly the secondary peak for high Reynolds

number in the distance between jet as like the other spacing distance,  $S/d = 6$ , 8, and 10. This is due to the interference between jets before the flow hit impinging plate.

The local Nusselt number distribution for in-line array at  $S/d = 2$  is shown in Figs. 4.7a-d. They illustrate that the Nusselt number decreases monotonically from the stagnation point to midway between adjacent jets. The transition region in this case is not appeared and the maximum heat transfer rate occurs at the stagnation region, regardless of the jet Reynolds number. At the spacing distance  $S/d = 2$ , (smaller value of spacing distance), the interactions between jets occur before impingement. These interactions increase the decay of the exit jet velocity, increase entrainment of surrounding air and influence the ring vortices located around the jet circumference that affect the turbulent mixing associated with the shear layer [1, 3].

The radial distribution of the local Nusselt number for staggered array at the spacing distance ( $2 \leq S/d \leq 10$ ), Reynolds number ( $1400 \leq Re \leq 41400$ ), and separation distance ( $1 \leq H/d \leq 4$ ) have the same trend for in-line array. These distributions can be shown in Appendix B. The heat transfer at stagnation point for in-line and staggered arrays will be plotted versus thus spacing distance. The next section explain with more details the effect of spacing and separation distances on the heat transfer at stagnation point for in-line and staggered arrays

#### **4-2-3 Effect of Spacing Distance at Stagnation Point:**

In this section, the stagnation Nusselt numbers  $Nu_{st}$  are plotted in dependence on the spacing distance  $S/d$  for multiple jets system (in-line and staggered arrays) with separation distance  $H/d$  as parameters. Figs. 4.8a-h exhibit the effect spacing distance on the stagnation Nusselt number for in-line array. From these figures, it can be seen that, the stagnation Nusselt number distribution for spacing distance equal to 6 is higher than the other spacing distance for all Reynolds numbers. In addition, the spacing distance equal to 2

has lowest values of the stagnation Nusselt number distribution for all values of the Reynolds number.

The stagnation Nusselt numbers for staggered arrays are presented in the Figs. 4.9a-h. In these figures, the stagnation Nusselt number is depended on the spacing distance  $S/d$  for different Reynolds numbers. The separation distances ( $1 \leq H/d \leq 10$ ) are parameters. In these figures, there exists a maximum  $Nu_{st}$  for every curve. To the left of the maximum, the jets interference is strong. Thus, as expected as the spacing distance,  $S/d$ , increases, the interference effect rapidly diminishes. This results in an increase of the stagnation Nusselt number with the spacing distance increases. To the right of the maximum point, due to an increase of the heated area under the jet array, the stagnation Nusselt number  $Nu_{st}$  begins to decrease with increasing of spacing distance. These figures indicate that the optimum spacing distance  $S/d$ , corresponding to the maximum stagnation Nusselt number is 6 for all considered cases. This implies that the Reynolds number has no effect on the optimum spacing distance  $S/d$ . This trend is a similar as the in-line array.

The effect of the separation distance on the stagnation Nusselt number for in-line and staggered arrays, is presented in appendix-C. In both cases, it could be noted that the stagnation Nusselt number in the range of the separation distance of ( $1 \leq H/d \leq 5$ ) is nearly constant.

The influence of the jet Reynolds number  $Re$  on the stagnation Nusselt number  $Nu_{st}$  is presented in Fig. 4.10 for three cases, the single nozzle, and nozzle array with spacing distance 6 and 4. All measured values are indicated for the range  $2 \leq H/d \leq 6$ . For all cases, the stagnation Nusselt number is proportional to Reynolds number exponent of 0.5 ( $Nu_{st} \propto Re^{0.5}$ ), which agrees closely with the laminar boundary layer flow case, [1]. It can be noted that the heat transfer is enhanced in the array of nozzles at spacing distance  $S/d = 6$ .

### 4-3 Average Heat Transfer of Multiple Free jets:

In the following section, the average Nusselt number will be considered. The average heat transfer coefficient is greatly dependent on the integration area as explained before in chapter three. The local Nusselt numbers were averaged over the square unit cell area Fig. 4.11. The average Nusselt number for this unit cell is representative for the whole array. Figs. 4.12a-h illustrates the average Nusselt number for various spacing distances,  $S/d$  at different separation distance  $H/d$ . Every figure is presented for one Reynolds number. From these figures it can be seen that the average Nusselt number is nearly constant in the range of spacing distance  $2 \leq S/d \leq 4$  for all Reynolds numbers. The total impingement area in the spacing distance equal to 6 is sufficient to remain the interference between adjacent jet in the wall region is minimized. Therefore, the average Nusselt number has a maximum value again at  $S/d = 6$  for all values of separation distance ( $1 \leq H/d \leq 10$ ). With increase of spacing distance  $S/d > 6$  the average Nusselt number is decreased and the values are nearly equivalent, specially with low Reynolds number.

For a constant Reynolds number, the average Nusselt number has nearly the same value in the range of separation distance  $1 \leq H/d \leq 5$ . For increasing  $H/d \geq 6$ , the average Nusselt number is decrease. At the low Reynolds number of 6000 and 1400 and optimum spacing distance ( $S/d = 6$ ) in Fig. 4.12g and Fig. 4.12h the difference between the average Nusselt number for the  $H/d = 10$  and constant value in the range of  $1 \leq H/d \leq 5$  is approximately 35%. This due to the peak are virtually nonexistent at this value ( $H/d = 10$ ). But, as the Reynolds number is increased, the peak appear and become more pronounced. Thus, the average Nusselt number  $Nu_{av}$  becomes significantly highest value.

The average Nusselt number is plotting in dependence on the spacing distance  $S/d$  in Figs. 4.13a-d. The inner jet diameter is parameter of 5,8mm and 8mm. Every figure is presented for one separation distance and two different Reynolds number. It can be seen that the inner jet diameter has no effect on the

average Nusselt number for both Reynolds numbers. The average Nusselt number is maximum value again at spacing distance equal to 6 for all values of the separation distance.

Now comparisons are made for the average heat transfer of the in-line with the staggered array. The representative unit cell of the staggered array is also shown in Fig. 4.11. The average Nusselt number for these arrays is depicted in Figs. 4.14a-h in dependence on the separation distance  $H/d$  for the Reynolds numbers ( $1400 \leq Re \leq 41400$ ) and the spacing distance ( $4 \leq S/d \leq 10$ ). No effect of the array pattern can be seen for all parameters. For a constant Reynolds number, the average Nusselt number has nearly the same value in the range of separation distance  $1 \leq H/d \leq 5$ . For increasing  $H/d > 6$ , the average Nusselt number is decrease again.

The average Nusselt number is examined over the impingement surface for in in-line array with un-equal spacing distances  $S_x \neq S_y$ . In this case, the nine jets was arranged in in-line array with fixed spacing distance in Y-direction is  $S_y/d = 6$ , and the another spacing distance in X-direction is varied,  $S_x/d = 3, 4$ , and 4.5. The average Nusselt number in this case are plotted with the separation distance,  $H/d$ , in Figs. 4.15a-h. The parameter is the ratio between the spacing distance in X and Y direction  $S_x/S_y$ . Every figure is based on one jet exit Reynolds number. They show that, the value of average Nusselt number is nearly constant for all three difference spacing distances in the range of separation distance is  $2 \leq H/d \leq 4$ . Figs. 4.15a-h also shows the value of average Nusselt number at optimum spacing distance,  $S/d = 6$  or  $S_x/S_y = 1.0$ . We can be seen that the values of average Nusselt number at  $S_x/S_y = 1.0$  is highest value and the spacing distance  $S_x/S_y = 0.5$  is showed to the lowest value for all Reynolds number. In addition, for low Reynolds number as in Figs. 4.15f-h the values of the average Nusselt conveyed as the separation distance,  $H/d$ , increases

At last, the influence of the Reynolds number will be discussed. Fig. 4.16 shows the maximum value of the average Nusselt number at spacing distance  $S/d = 6$  in dependence on the Reynolds number. Parameter is the separation distance  $H/d$ . As mentioned before the separation distance has no influence in the range  $2 \geq H/d \geq 6$ . The measured point can be well approximated with a line. The least-square curve fitting has the following correlation:

$$\text{Nu}_{\text{av,max}} = 0.104 \text{Re}^{0.7}. \quad (4-1)$$

For a constant Prandtl number  $\text{Pr}$ , (air), the average Nusselt number in equation (4-1) can be represented by the following equation,

$$\text{Nu}_{\text{av,max}} = 0.117 \text{Re}^{0.7} \text{Pr}^{0.42}. \quad (4-2)$$

This equation is valid in the range of parameters for the experimental data, which are:  $1400 \leq \text{Re} \leq 41400$ ,  $S/d = 6$ , and  $2 \leq H/d \leq 6$ .

Fig. 4.16 also shows the presented measurements for a single nozzle. The area for averaged of the heat transfer in the square area around the single nozzle with radial length of three diameter. The average Nusselt number for the both cases, nozzle array at  $S/d = 6$  and single nozzle had the same gradient approximately 0.7. This average Nusselt number for the nozzle array is 75% higher than for the single nozzle.

The values of average Nusselt number based on the present correlation at optimum spacing distance ( $S/d = 6.0$ ) are compared with the other previous correlations presented by Martin [1] and Huber [48] in Fig. 4.17. Because the present experimental data was obtained with free tube impinging jet and the interference between adjacent jet is minimized. The present results are enhanced than Martin [1] and Huber [48], which the correlating exponent  $n$  on Reynolds number reported for the perforated plate. The Martin correlation has a Reynolds number exponent of 0.667, while the present experimental data has an exponent of about 0.7.

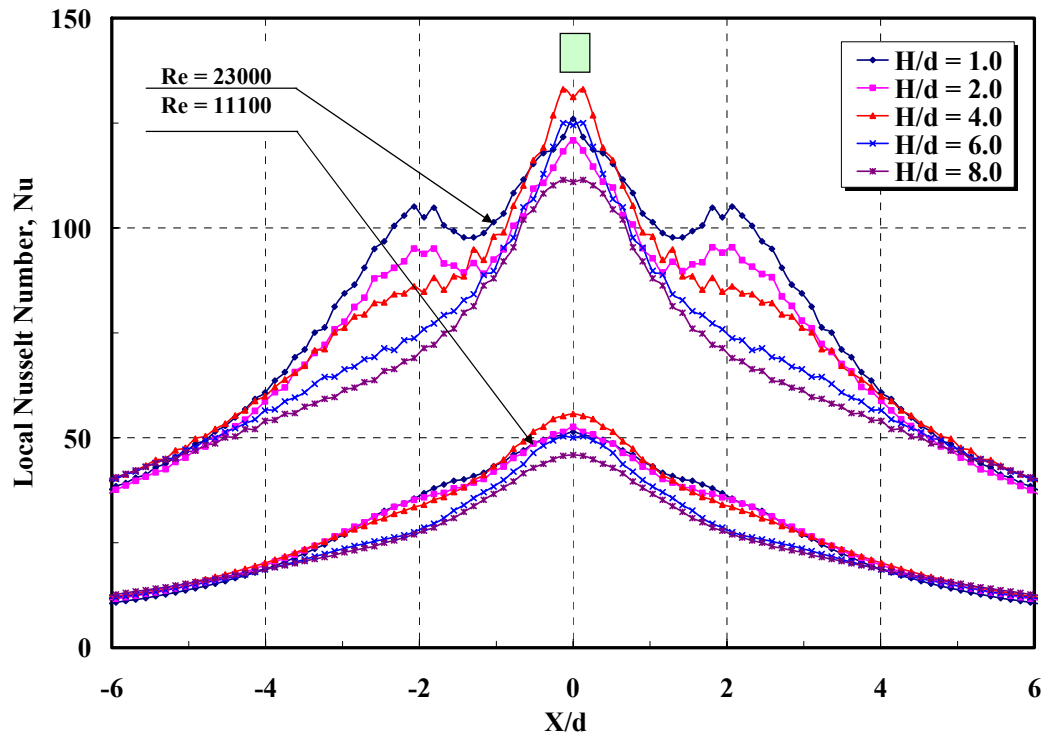


Fig. 4.1 Local Nusselt Number Distribution Versus with Radial Distance in Single Nozzle

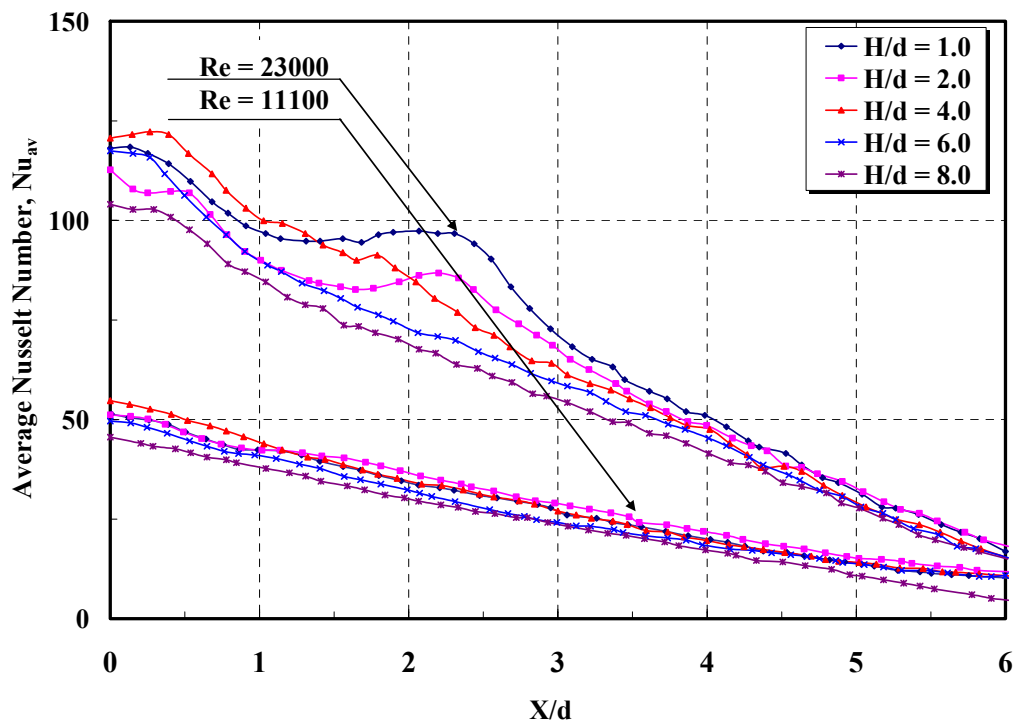


Fig. 4.2 Average Nusselt Number Distribution Versus with Radial Distance in a Single Nozzle

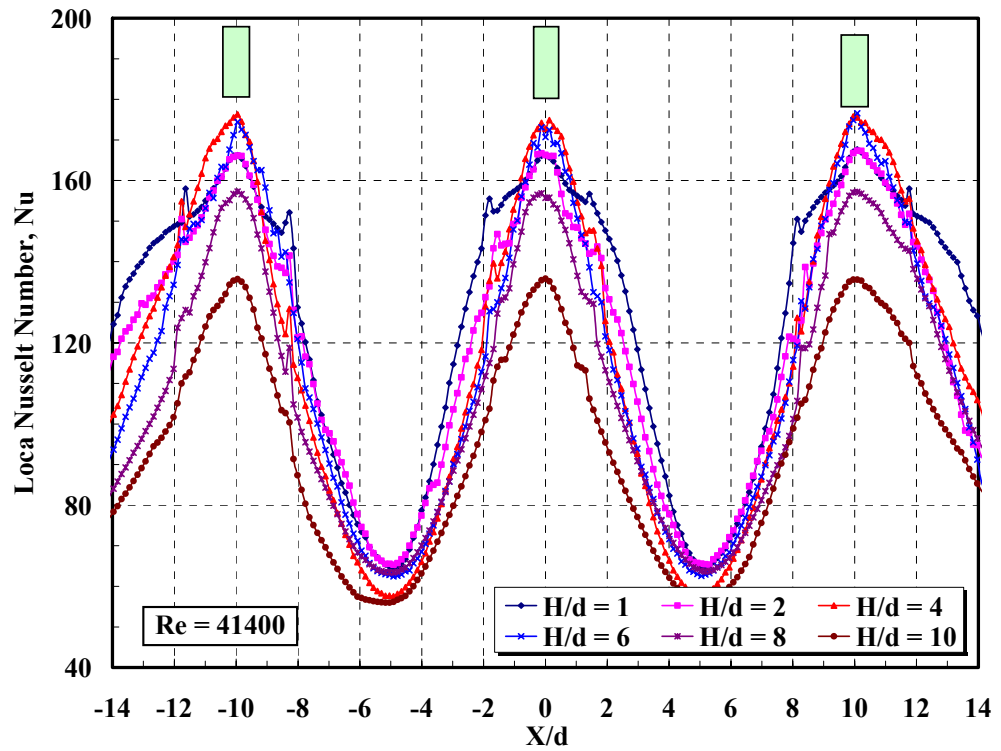


Fig. 4.3a Local Nusselt Number Distribution in Nozzle Field,  
 $S/d = 10$ ,  $Re = 41400$

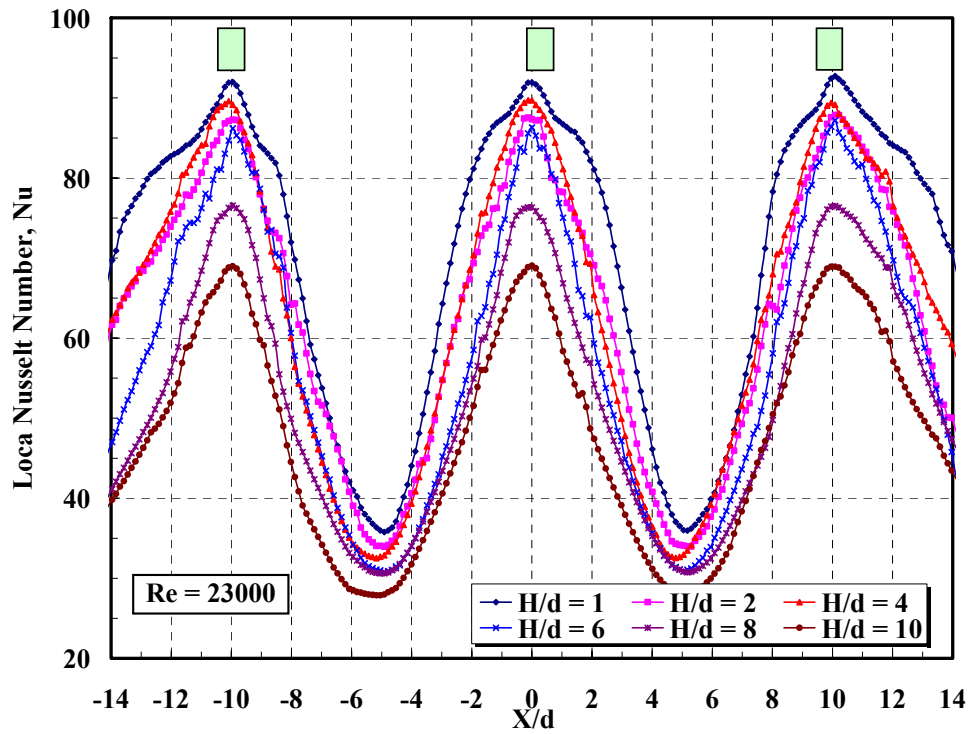


Fig. 4.3b Local Nusselt Number Distribution in Nozzle Field,  
 $S/d = 10$ ,  $Re = 23000$

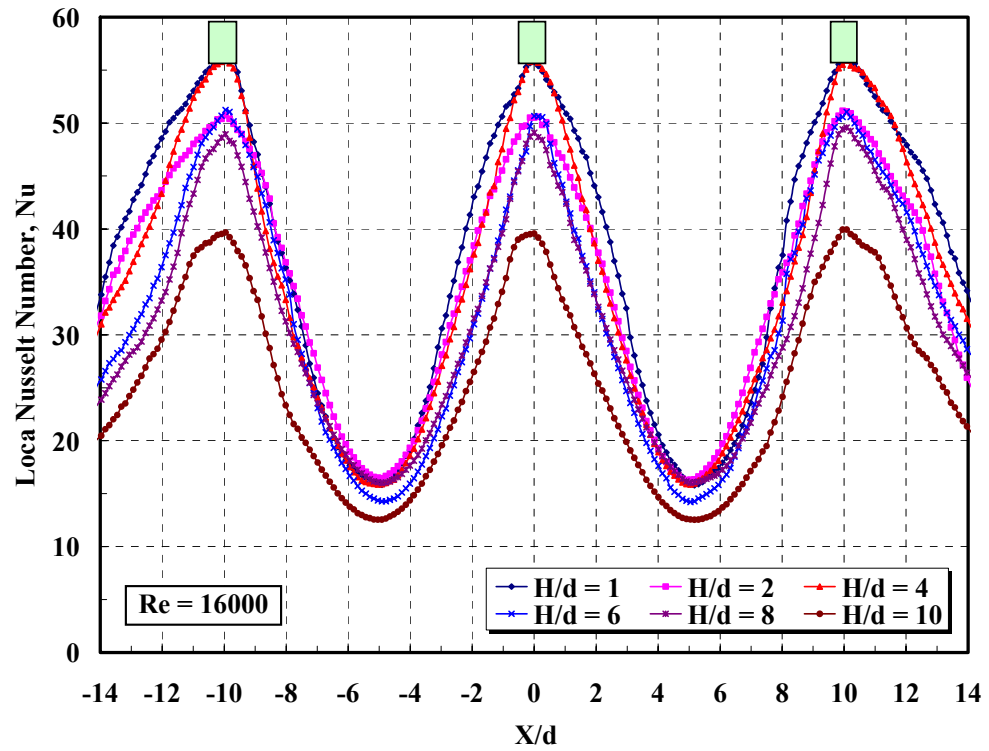


Fig. 4.3c Local Nusselt Number Distribution in Nozzle Field,  
 $S/d = 10$ ,  $Re = 16000$

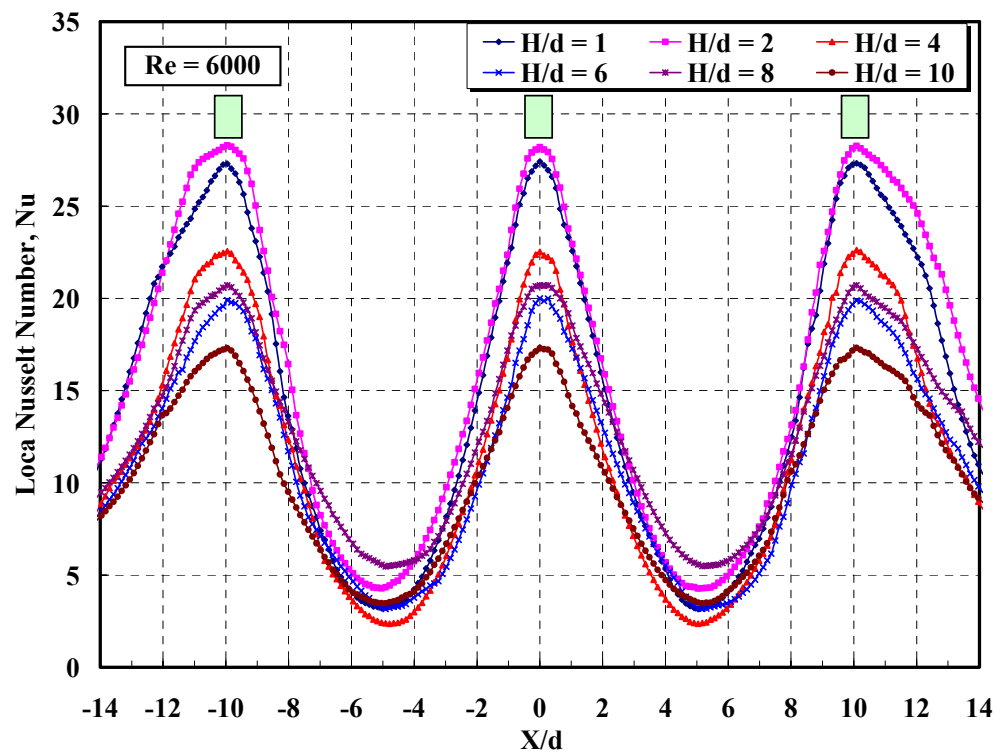


Fig. 4.3d Local Nusselt Number Distribution in Nozzle Field,  
 $S/d = 10$ ,  $Re = 6000$

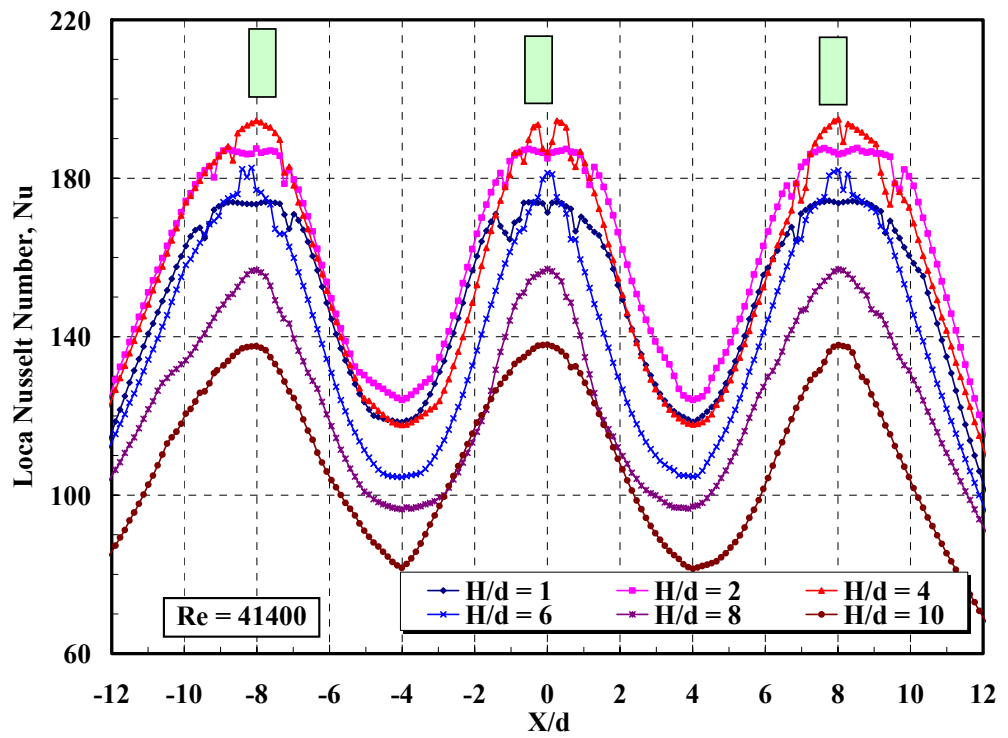


Fig. 4.4a Local Nusselt number Distribution in Nozzle Field,  
 $S/d = 8$ ,  $Re = 41400$

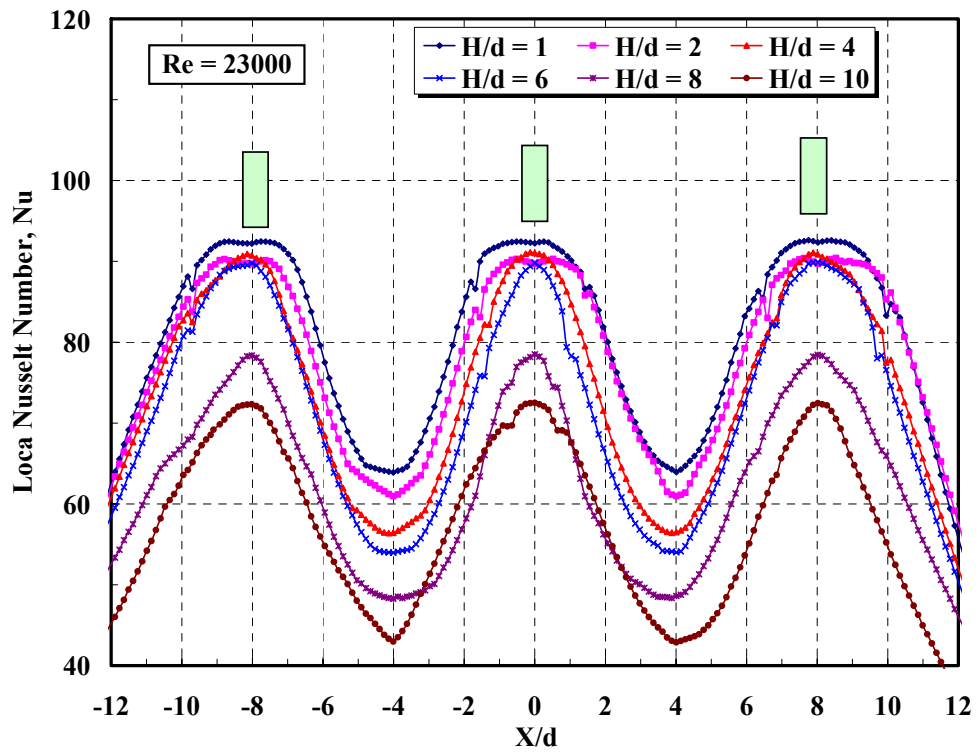


Fig. 4.4b Local Nusselt Number Distribution in Nozzle Field,  
 $S/d = 8$ ,  $Re = 23000$

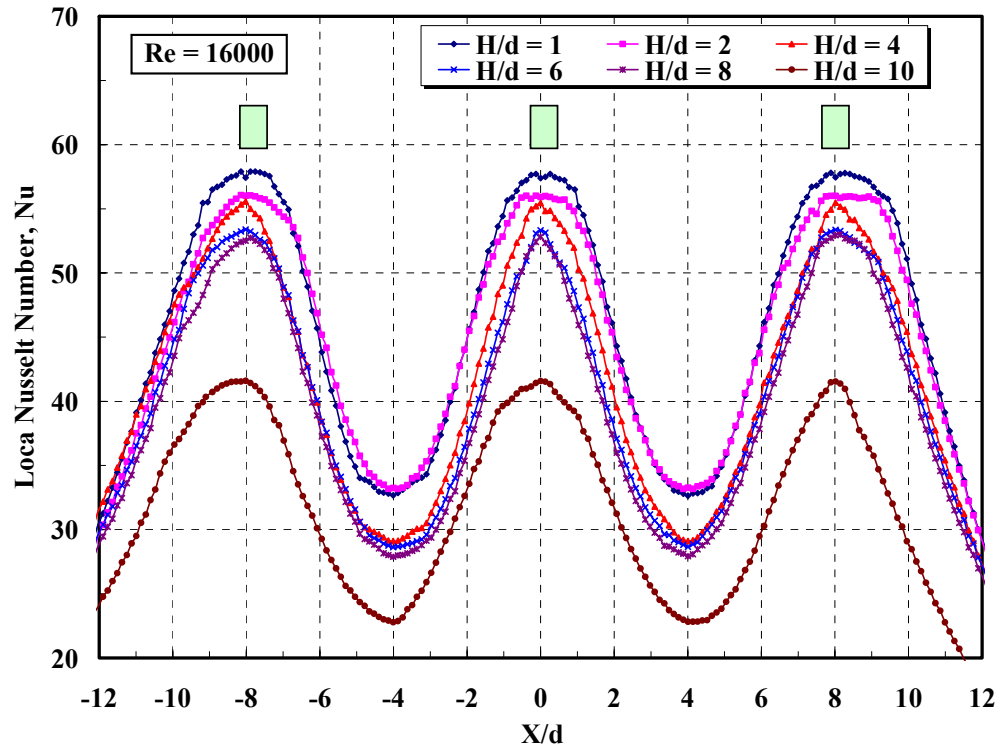


Fig. 4.4c Local Nusselt Number Distribution in Nozzle Field,  $S/d = 8$ ,  $Re = 16000$

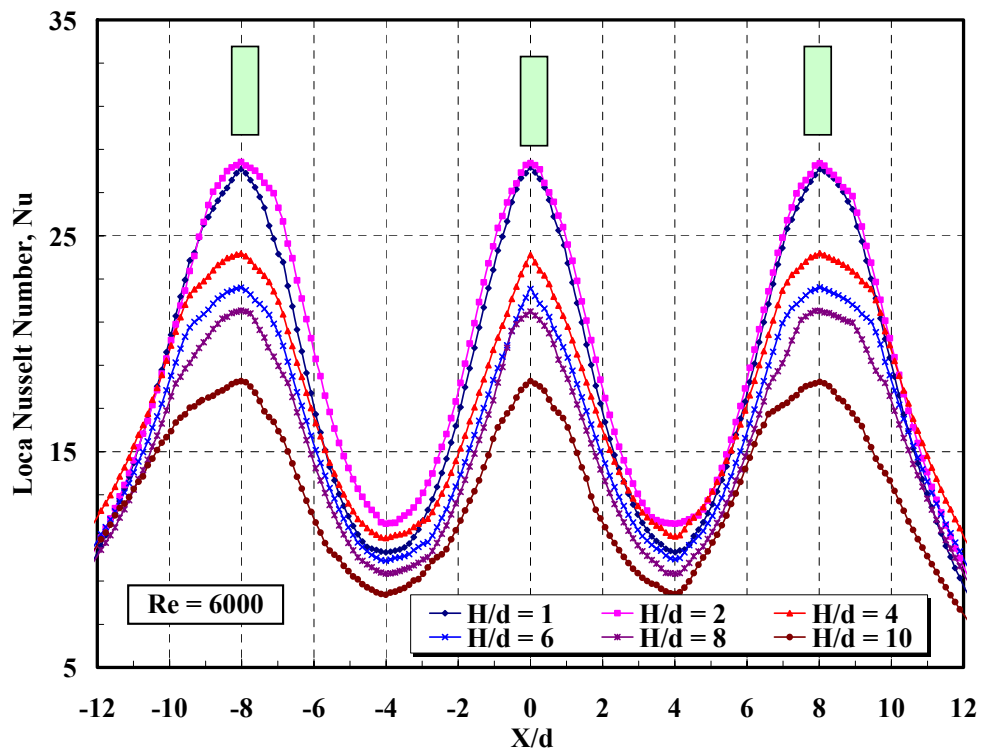


Fig. 4.4d Local Nusselt Number Distribution in Nozzle Field,  $S/d = 8$ ,  $Re = 6000$

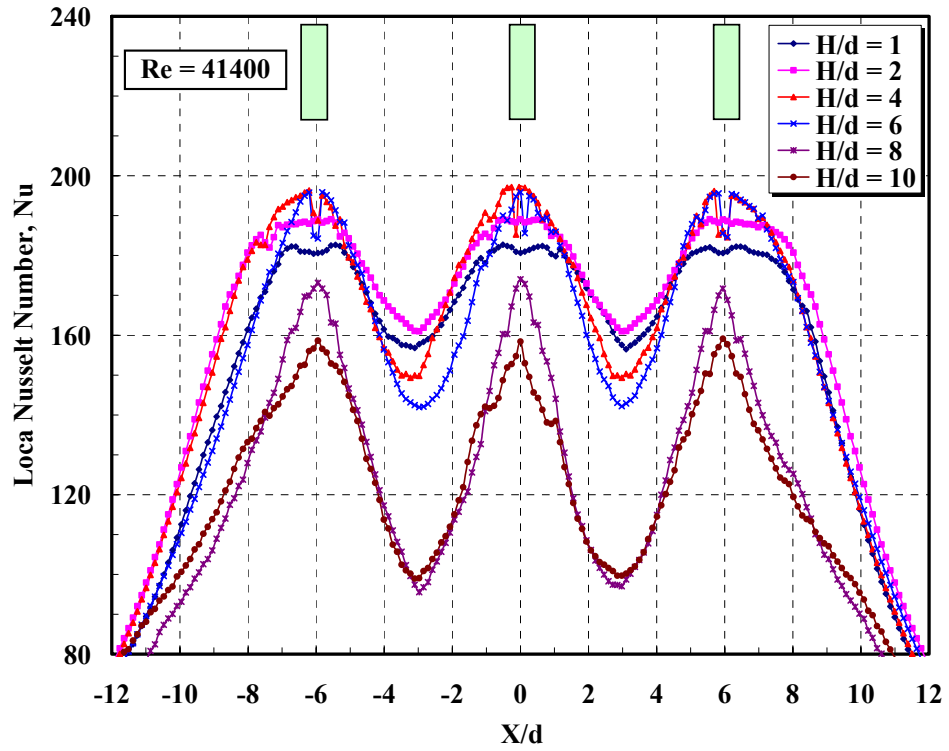


Fig. 4.5a Local Nusselt Number Distribution in Nozzle Field,  
S/d = 6, Re = 41400

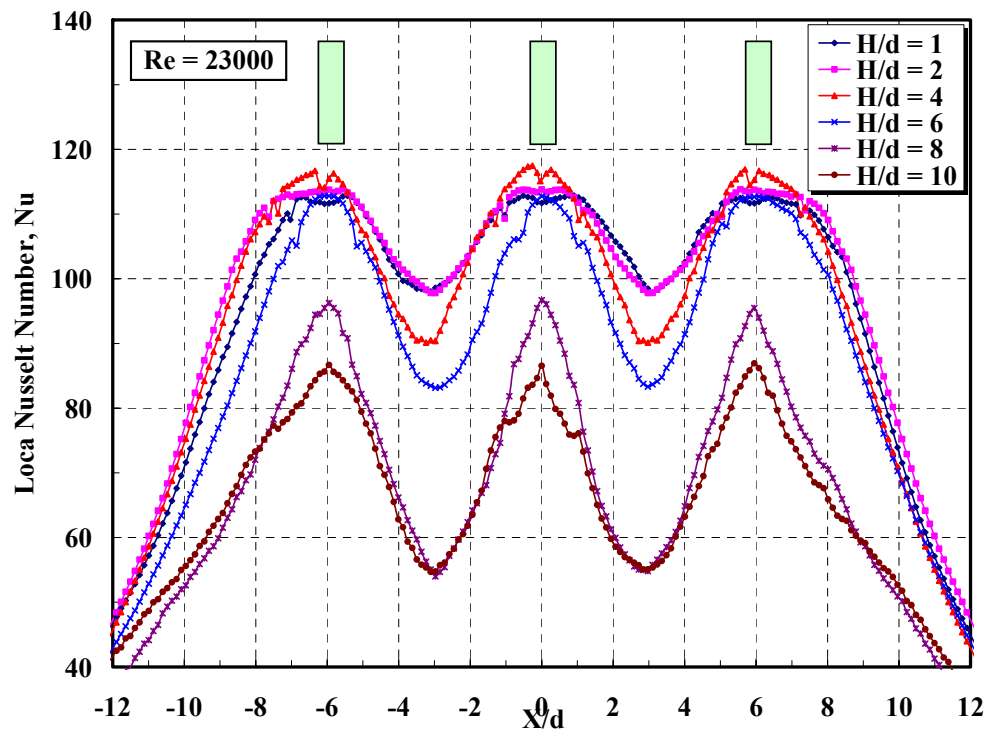


Fig. 4.5b Local Nusselt Number Distribution in Nozzle Field,  
S/d = 6, Re = 23000

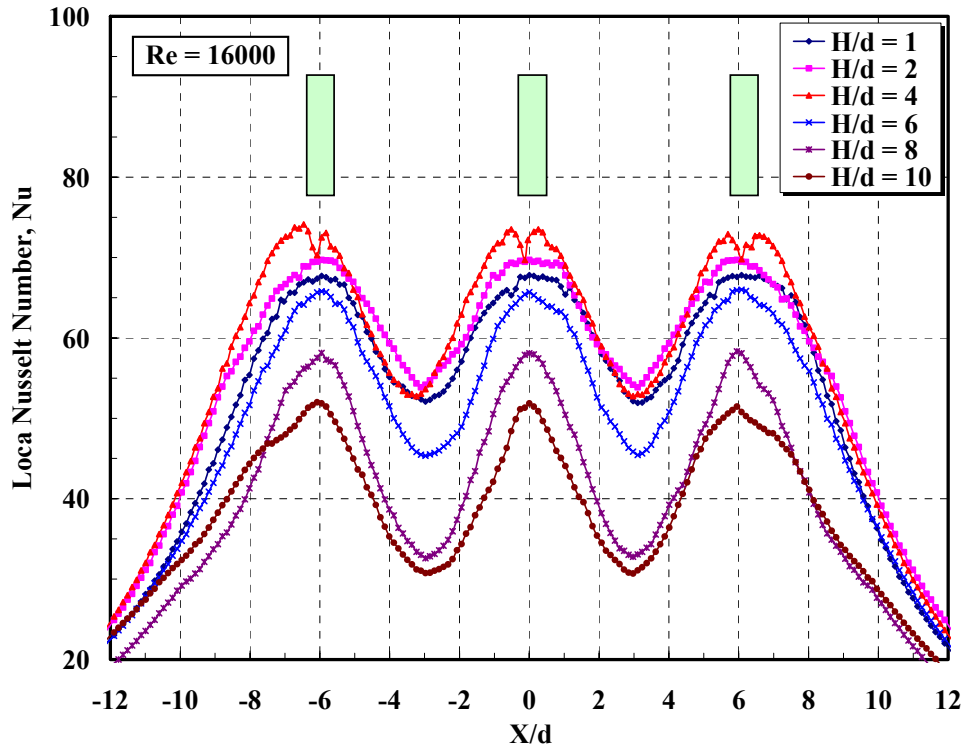


Fig. 4.5c Local Nusselt Number Distribution in Nozzle Field,  
S/d = 6, Re = 16000

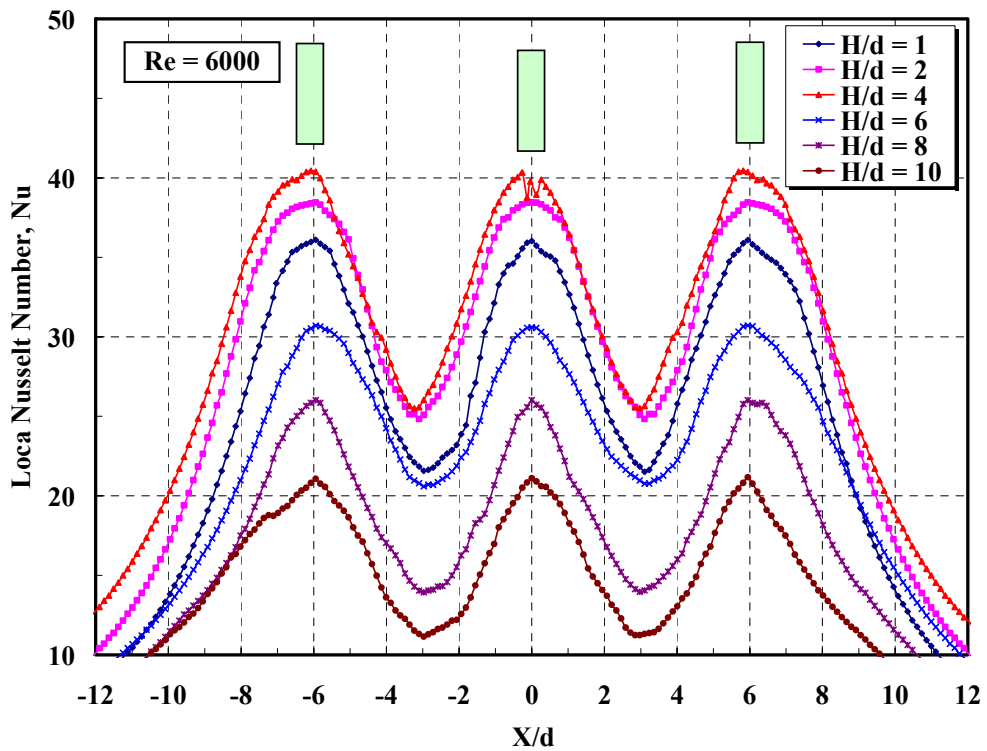


Fig. 4.5d Local Nusselt number Distribution in Nozzle Field,  
S/d = 6, Re = 6000

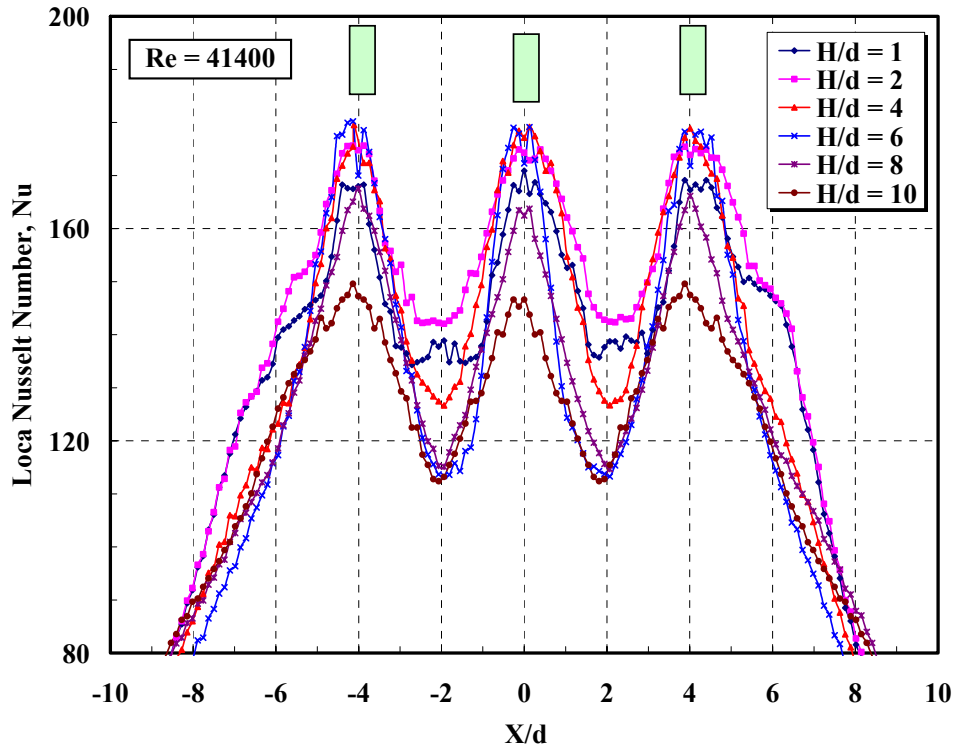


Fig. 4.6a Local Nusselt Number Distribution in Nozzle Field,  
 $S/d = 4$ ,  $Re = 41400$

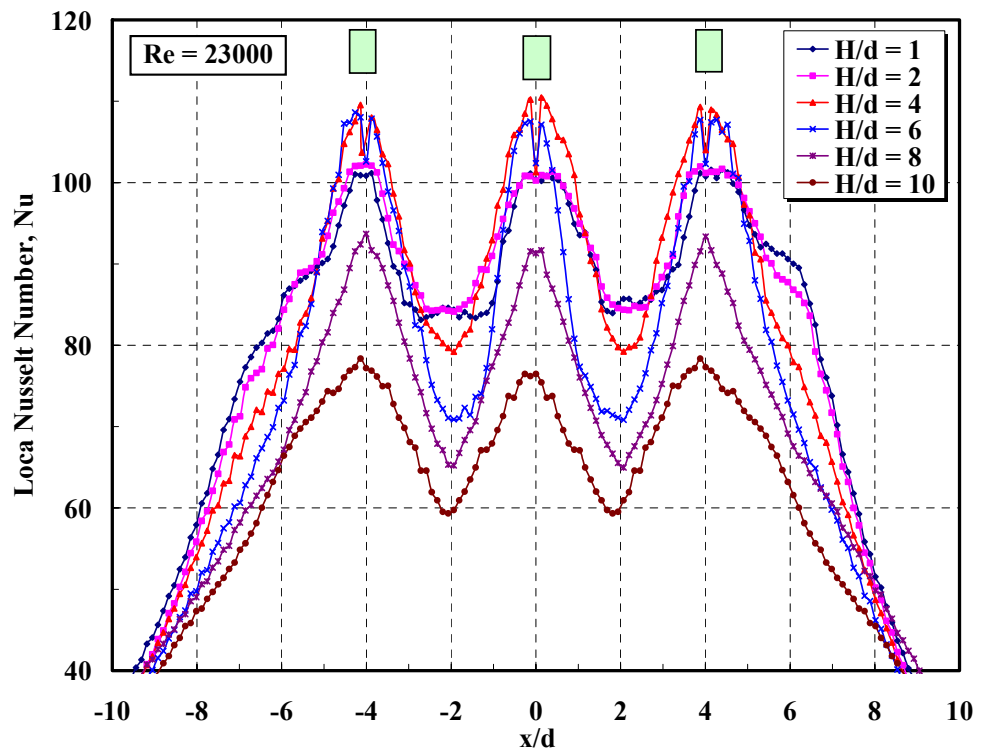


Fig. 4.6b Local Nusselt Number Distribution in Nozzle Field,  
 $S/d = 4$ ,  $Re = 23000$

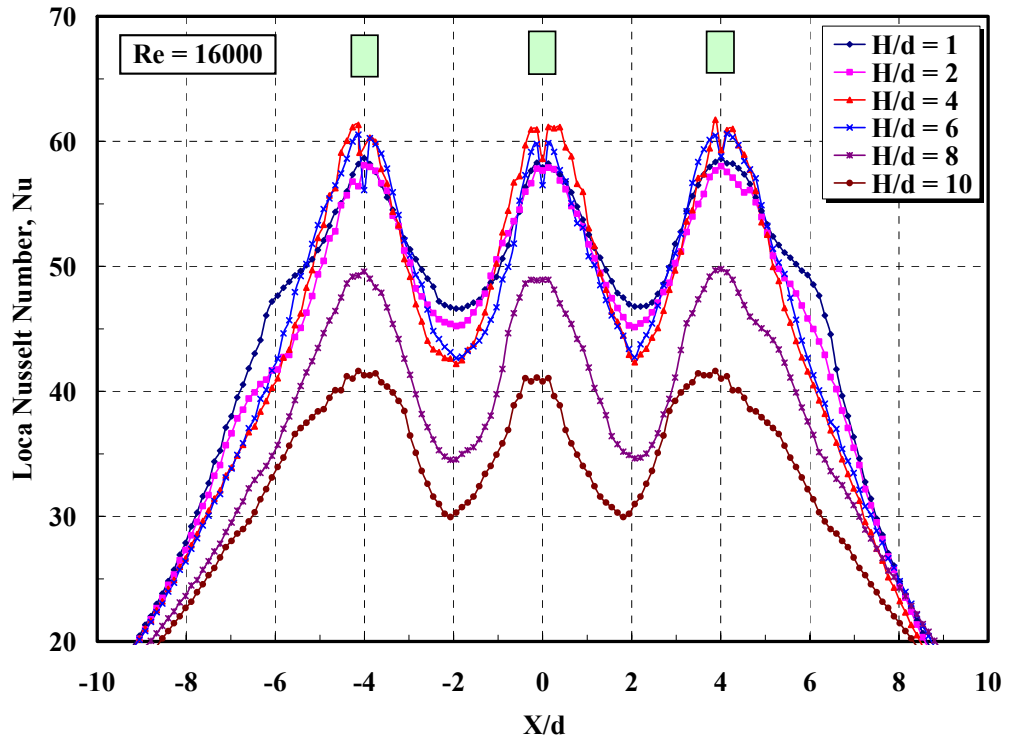


Fig. 4.6c Local Nusselt Number Distribution in Nozzle Field,  $S/d = 4$ ,  $Re = 16000$

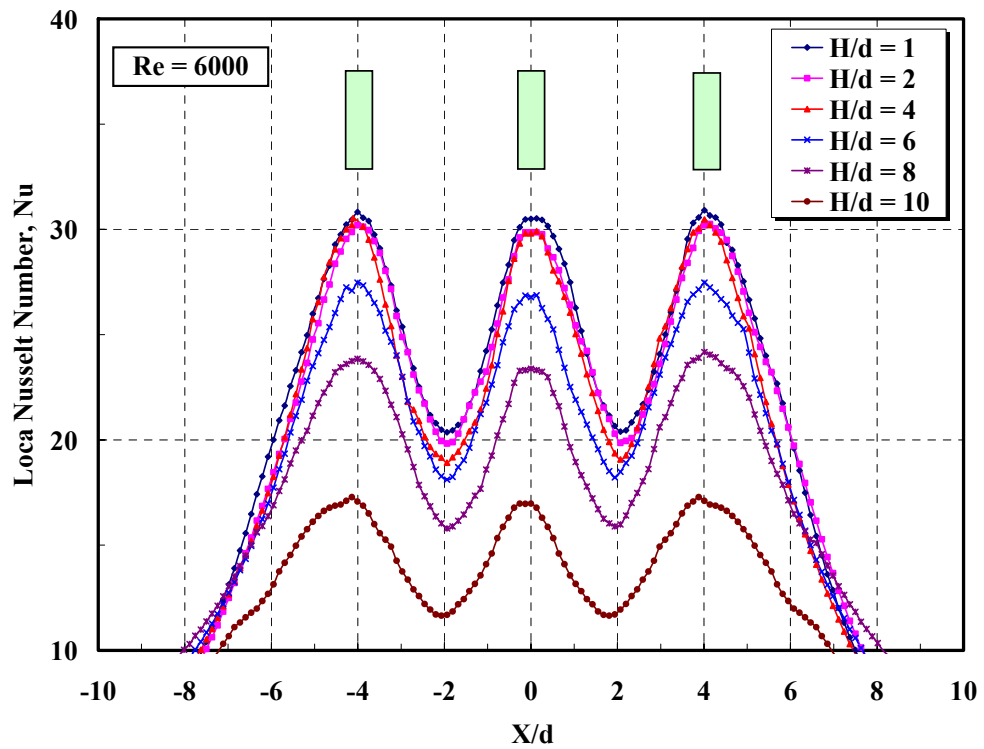


Fig. 4.6d Local Nusselt Number Distribution in Nozzle field  $S/d = 4$ ,  $Re = 6000$

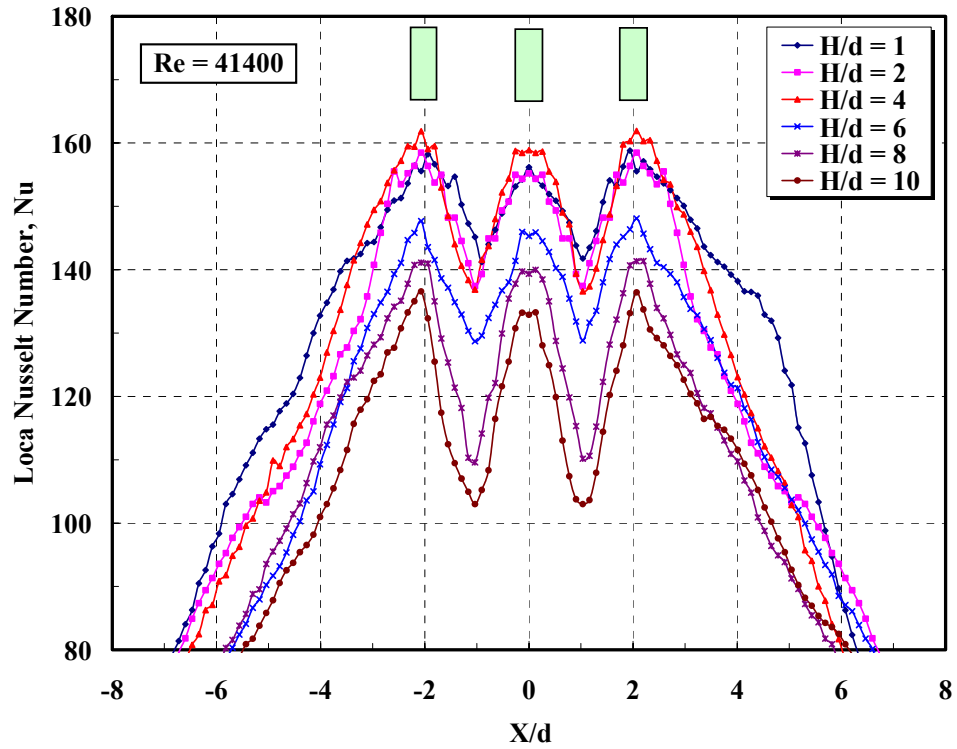


Fig. 4.7a Local Nusselt Number Distribution in Nozzle Field,  $S/d = 2$ ,  $Re = 41400$

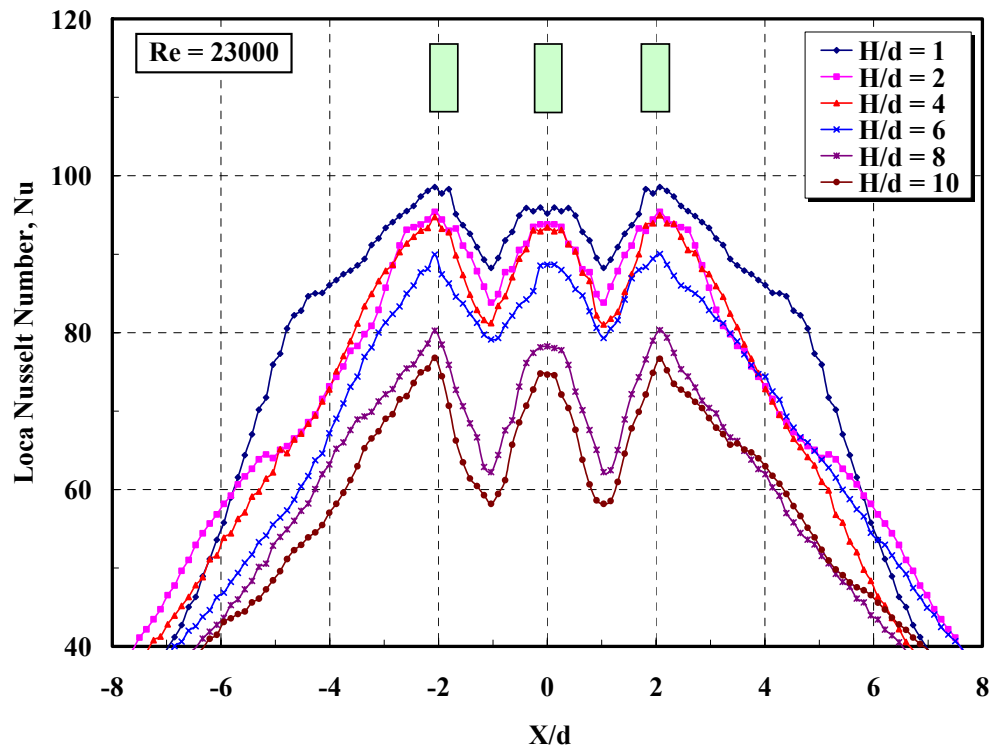


Fig. 4.7b Local Nusselt Number Distribution in Nozzle Filed,  $S/d = 2$ ,  $Re = 23000$

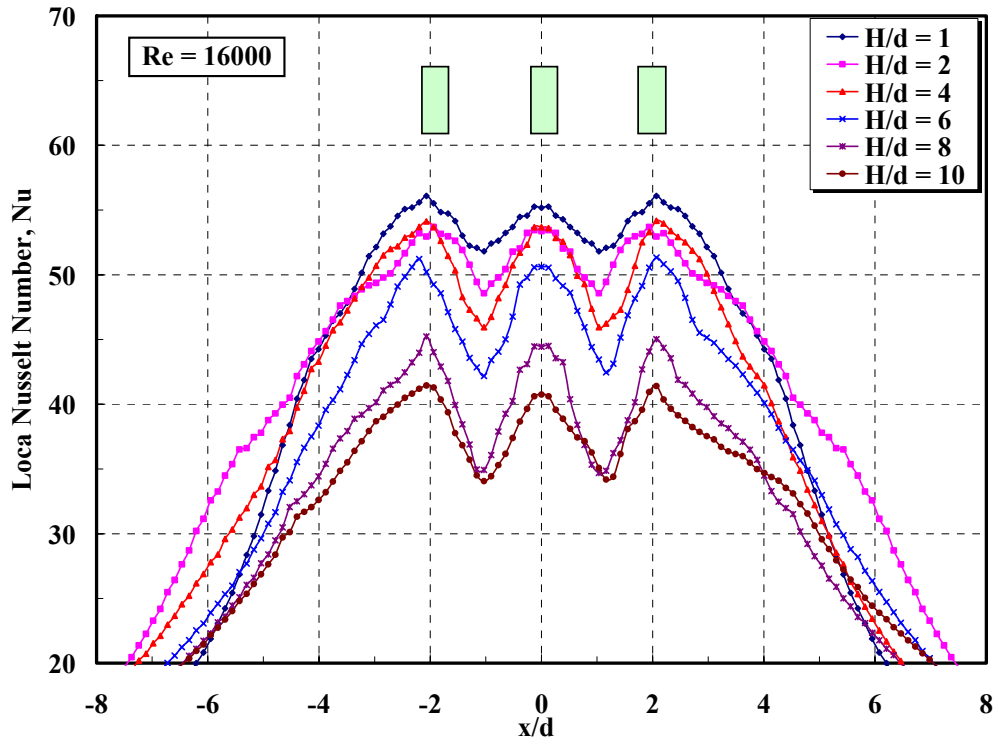


Fig. 4.7c Local Nusselt Number Distribution in Nozzle Field,  $S/d = 2$ ,  $Re = 16000$

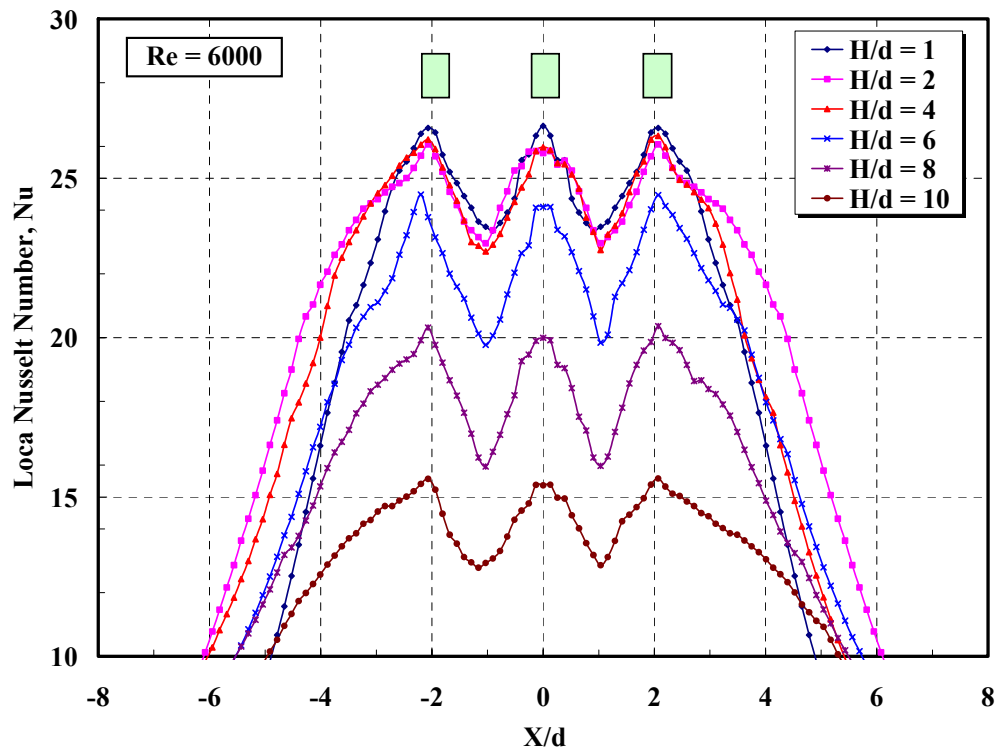


Fig. 4.7d Local Nusselt Number Distribution in Nozzle Field,  $S/d = 2$ ,  $Re = 6000$

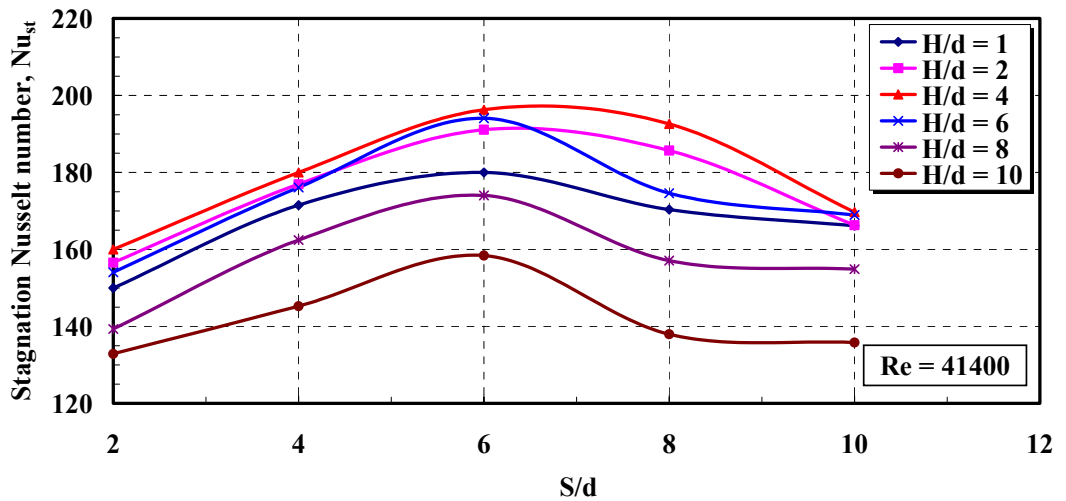


Fig. 4.8a Stagnation Nusselt Number Distribution for In-line Array,  $Re = 41400$

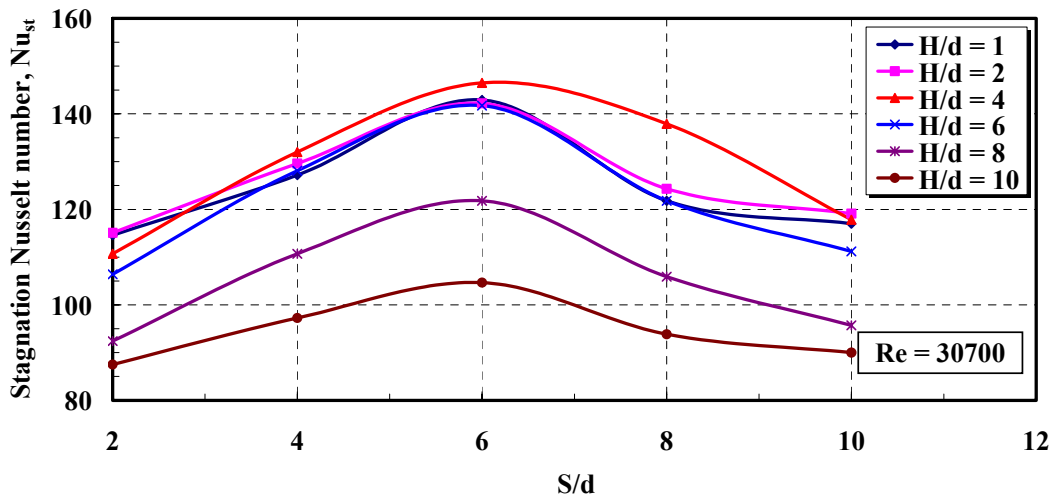


Fig. 4.8b Stagnation Nusselt Number Distribution for In-line Array,  $Re = 30700$

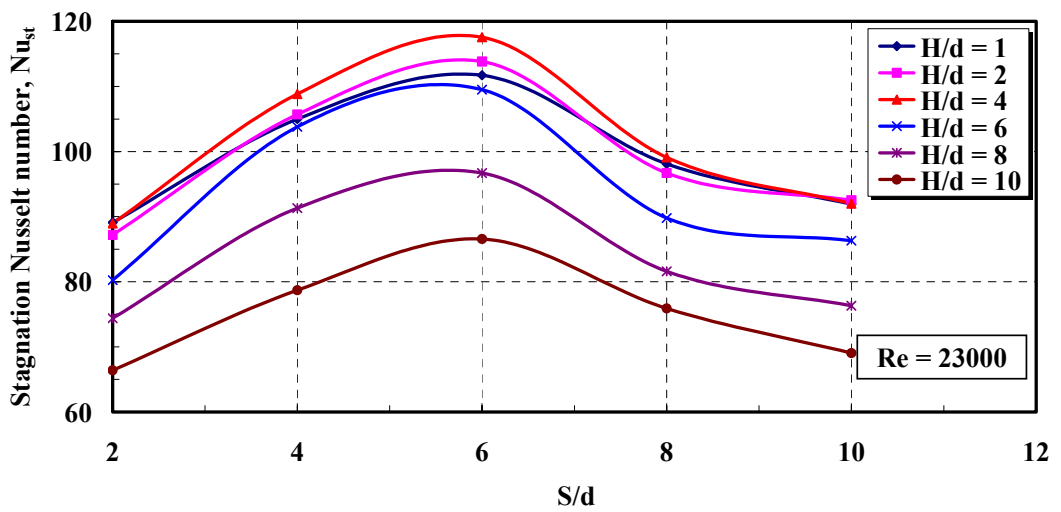


Fig. 4.8c Stagnation Nusselt Number Distribution for In-line Array,  $Re = 23000$

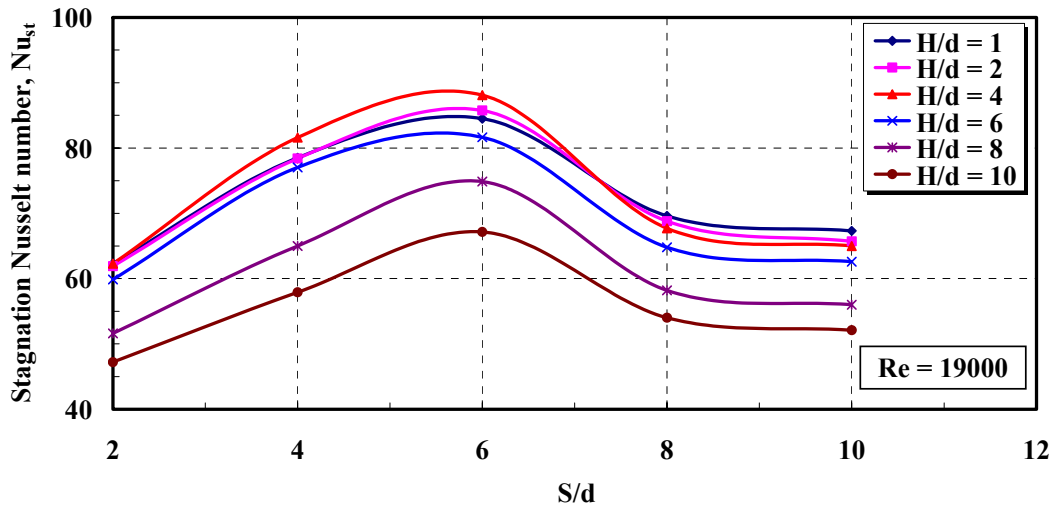


Fig. 4.8d Stagnation Nusselt Number Distribution for In-line Array, Re = 19000

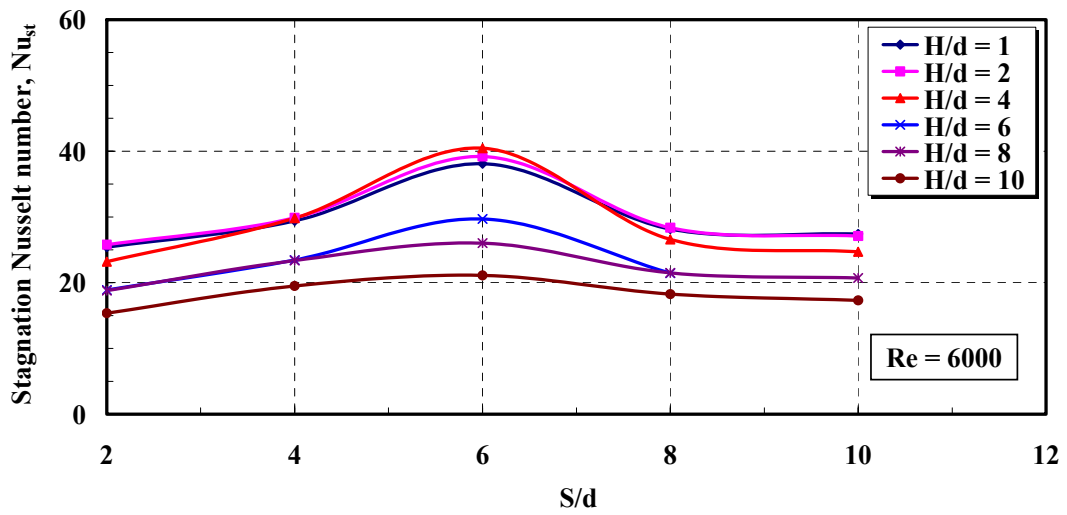


Fig. 4.8e Stagnation Nusselt Number Distribution for In-line Array, Re = 16000

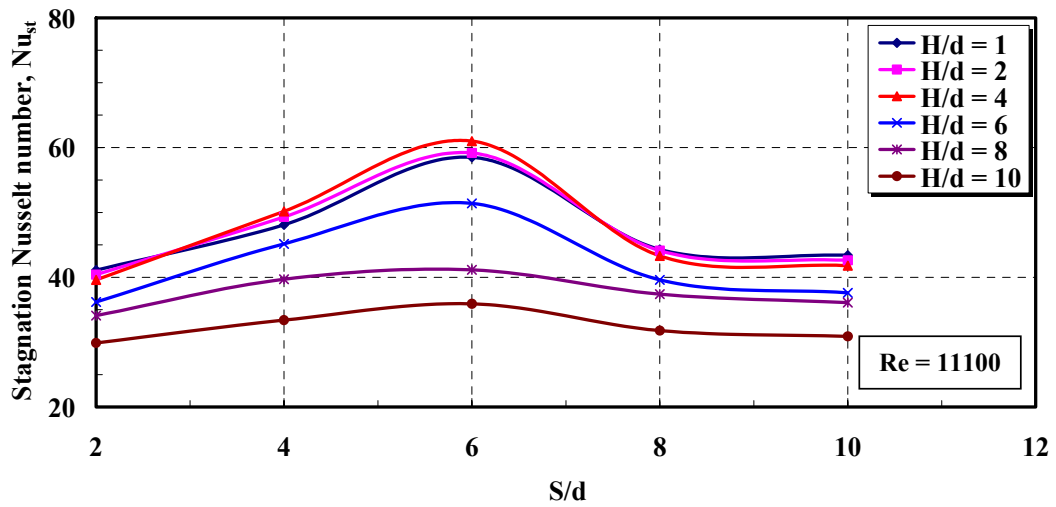


Fig. 4.8f Stagnation Nusselt Number Distribution for In-line Array, Re = 11100

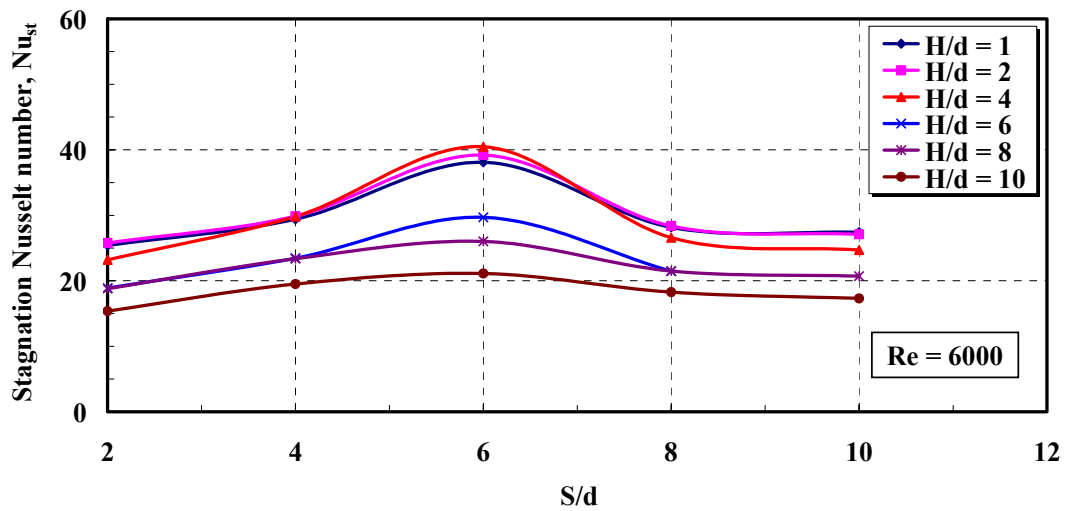


Fig. 4.8g Stagnation Nusselt Number Distribution for In-line Array, Re = 6000

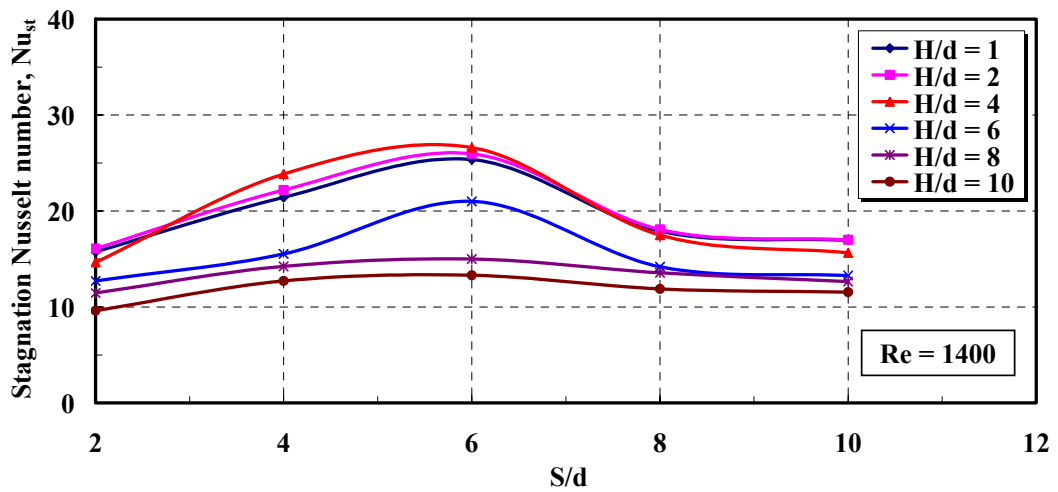


Fig. 4.8h Stagnation Nusselt Number Distribution for In-line Array, Re = 1400

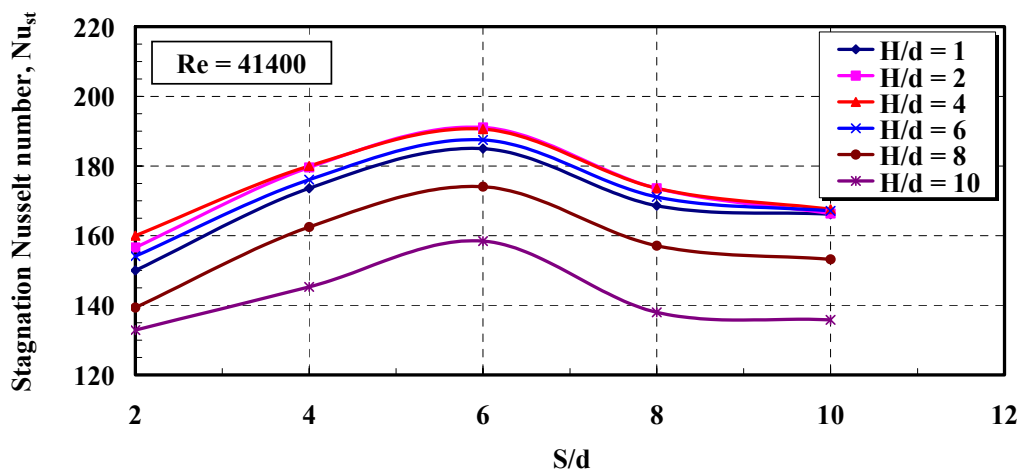


Fig. 4.9a Stagnation Nusselt Number Distribution for Staggered Array, Re = 41400

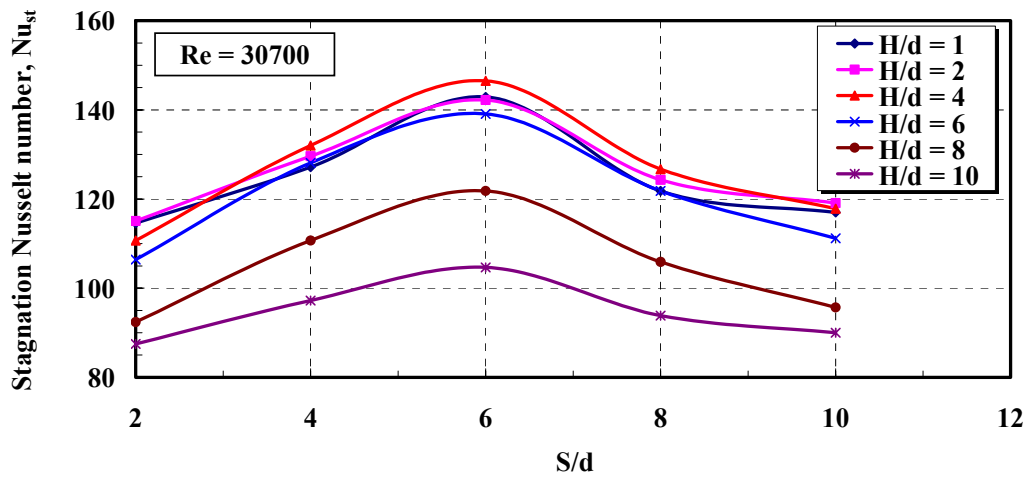


Fig. 4.9b Stagnation Nusselt Number Distribution for Staggered Array, Re = 30700

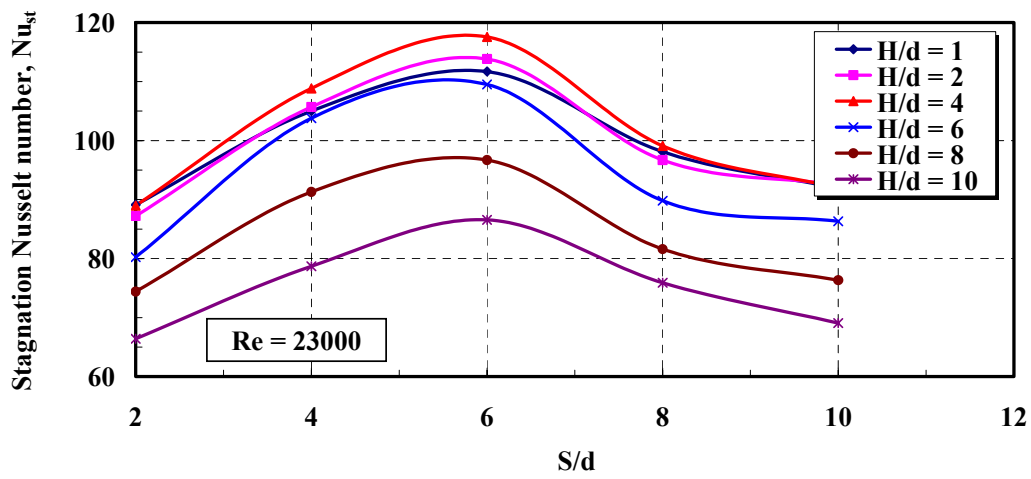


Fig. 4.9c Stagnation Nusselt Number Distribution for Staggered Array, Re = 23000

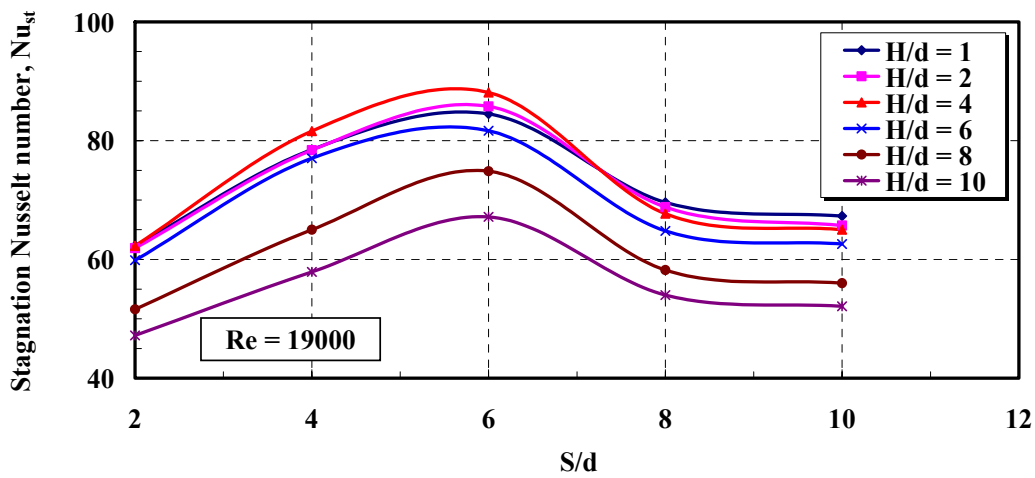


Fig. 4.9d Stagnation Nusselt Number Distribution for Staggered Array, Re = 19000

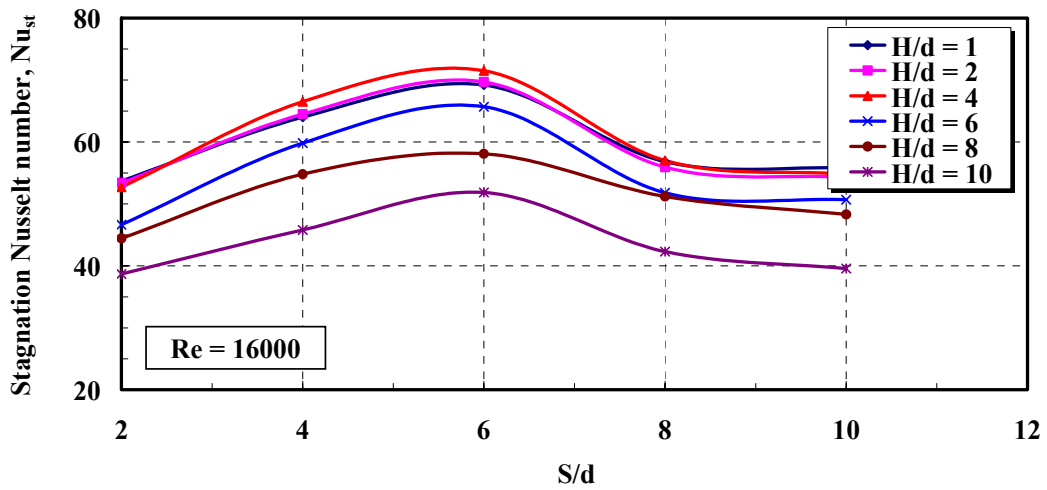


Fig. 4.9e Stagnation Nusselt Number Distribution for Staggered Array, Re = 16000

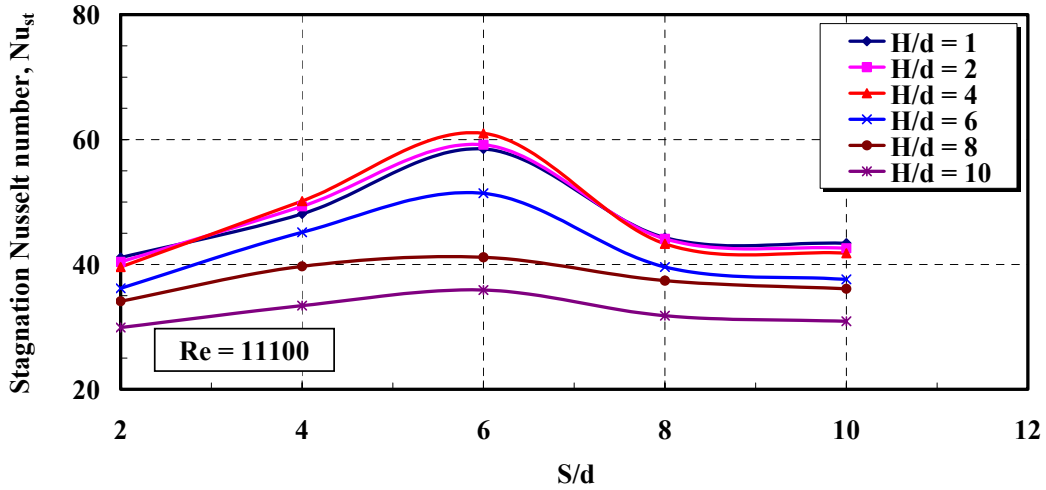


Fig. 4.9f Stagnation Nusselt Number Distribution for Staggered Array, Re = 11100

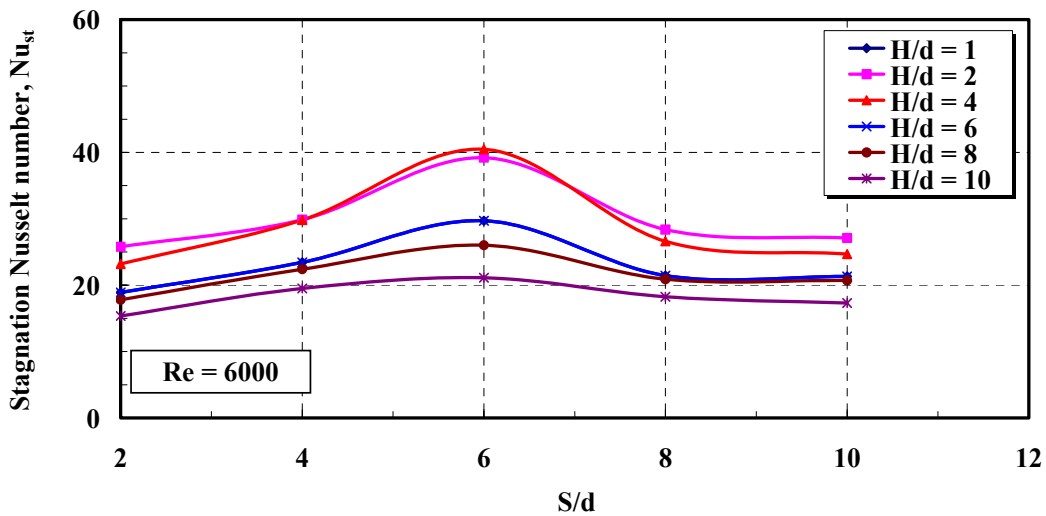


Fig. 4.9g Stagnation Nusselt Number Distribution for Staggered Array, Re = 6000

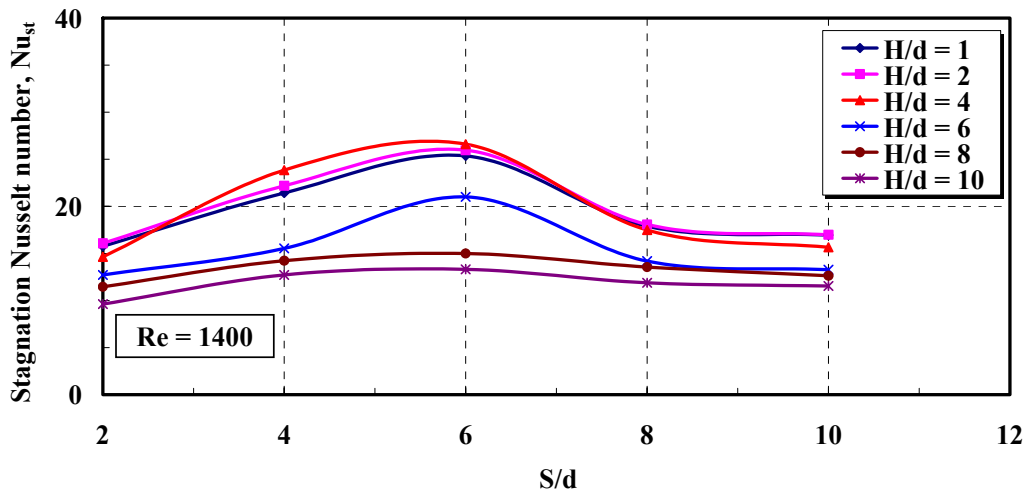


Fig. 4.9h Stagnation Nusselt Number Distribution for Staggered Array,  $Re = 1400$

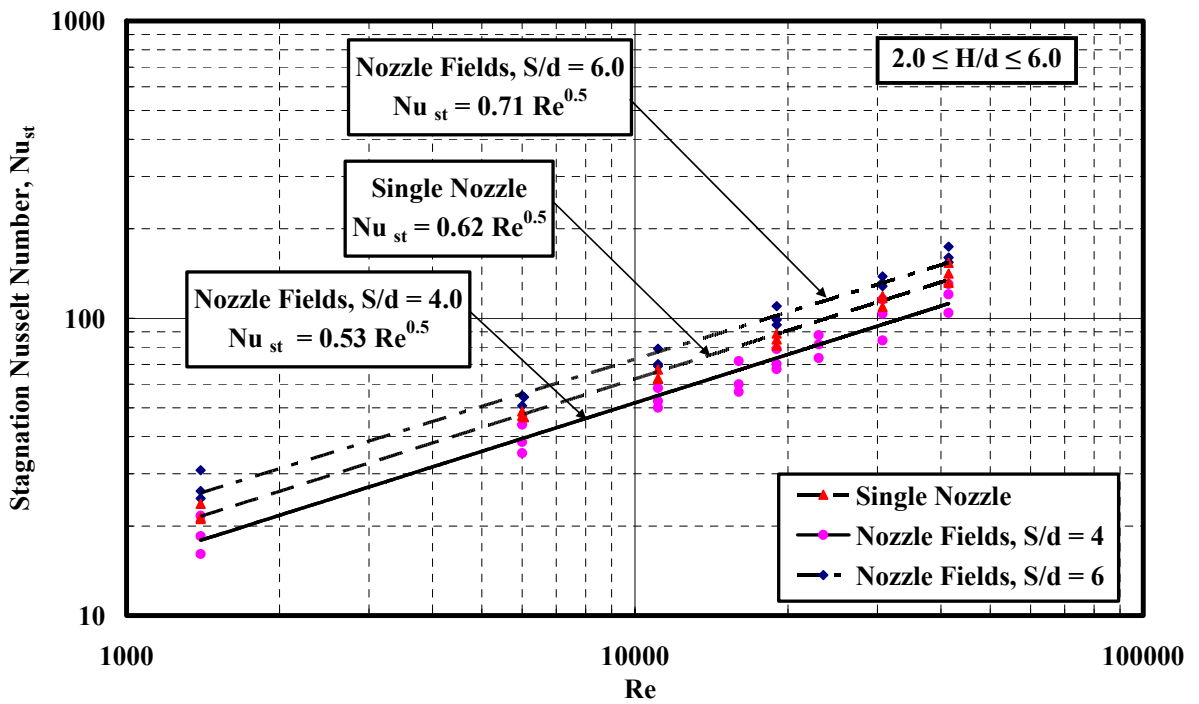


Fig. 4.10 Stagnation Nusselt Number Variation with Jet Reynolds Number

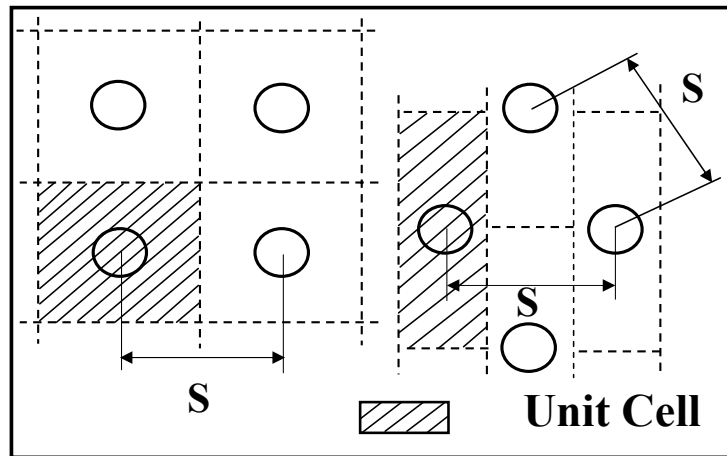


Fig. 4.11 Array Pattern Configurations Tested

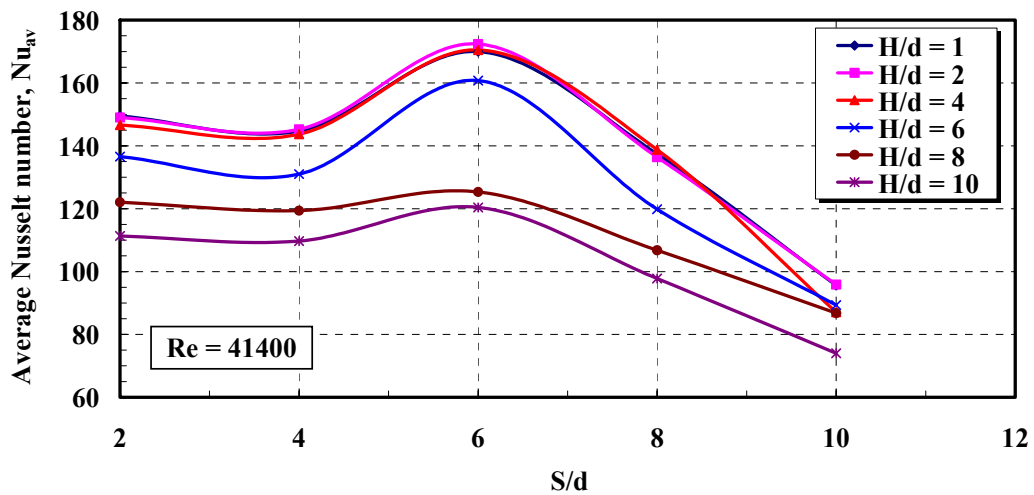


Fig. 4.12a Average Nusselt Number Distribution Versus with  $S/d$  at Different  $H/d$  for In-line Array,  $Re = 41400$

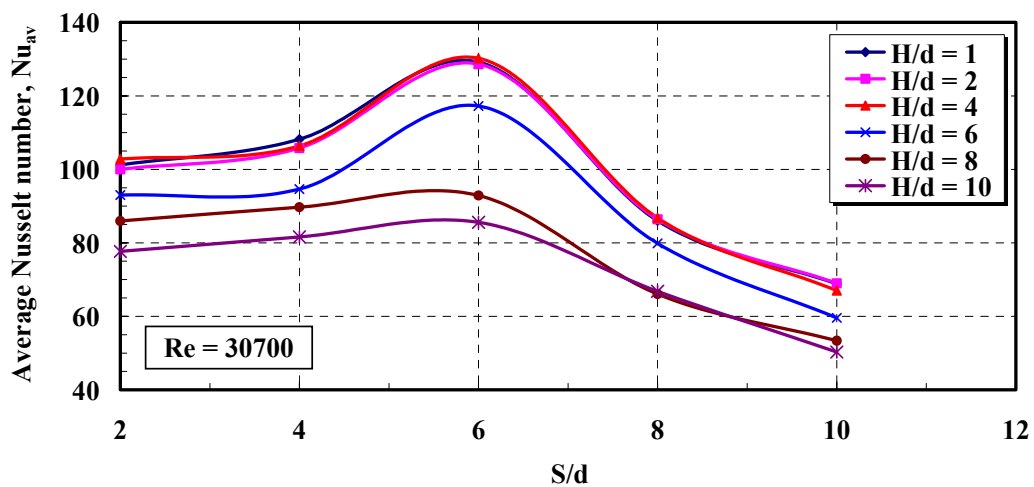


Fig. 4.12b Average Nusselt Number Distribution Versus with  $S/d$  at Different  $H/d$  for In-line Array,  $Re = 30700$

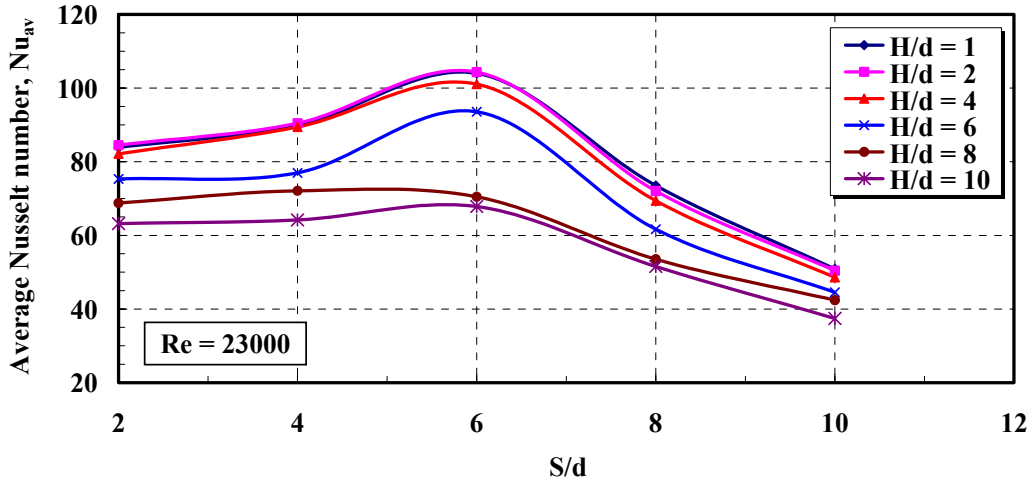


Fig. 4.12c Average Nusselt Number Distribution Versus with  $S/d$  at Different  $H/d$  for In-line Array,  $Re = 23000$

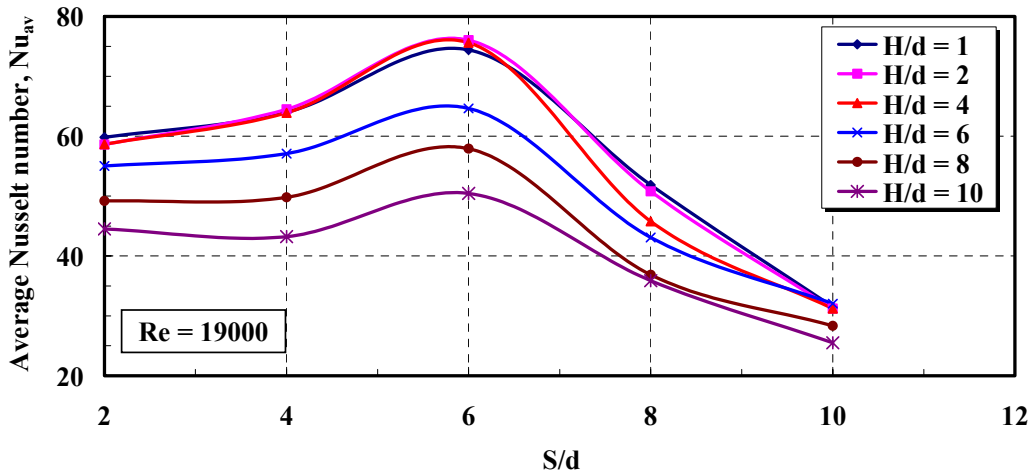


Fig. 4.12d Average Nusselt Number Distribution Versus with  $S/d$  at Different  $H/d$  for In-line Array,  $Re = 19000$

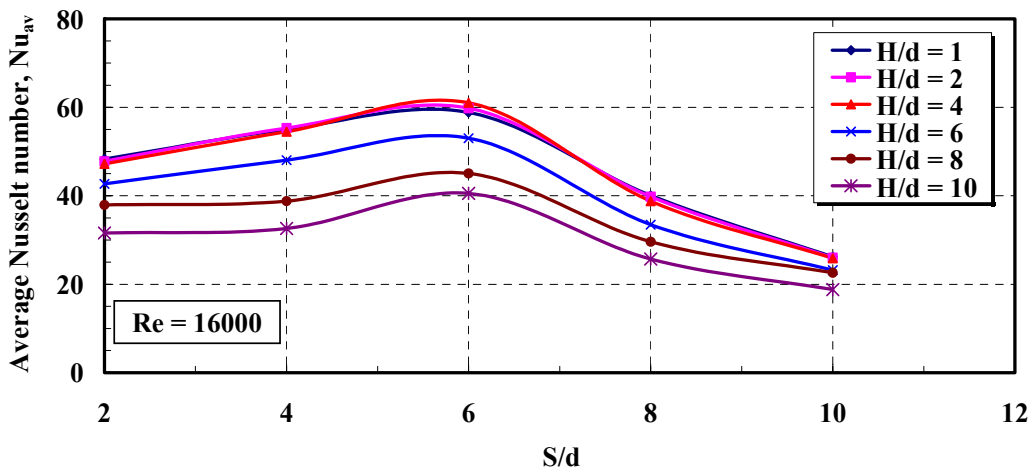


Fig. 4.12e Average Nusselt Number Distribution Versus with  $S/d$  at Different  $H/d$  for In-line Array,  $Re = 16000$

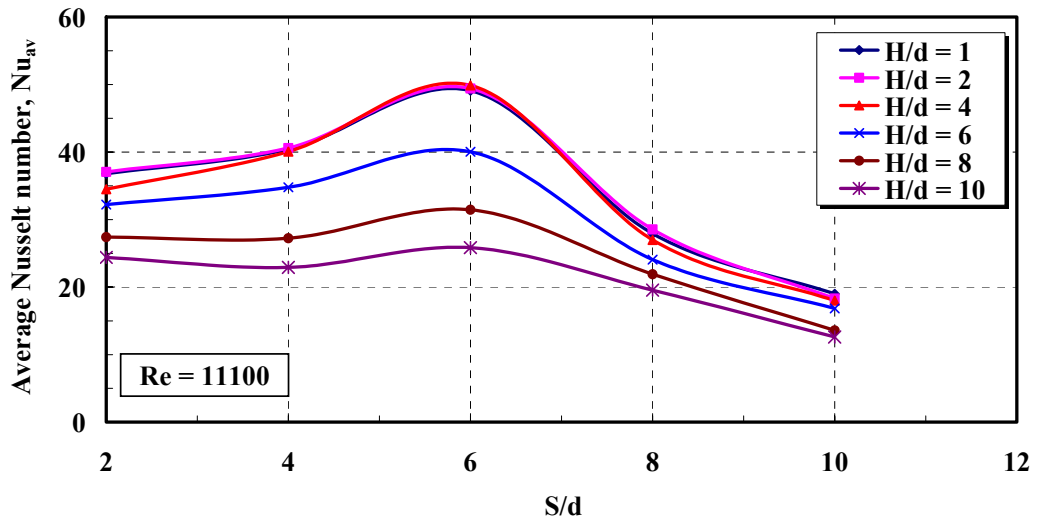


Fig. 4.12f Average Nusselt Number Distribution Versus with S/d at Different H/d for In-line Array, Re = 11100

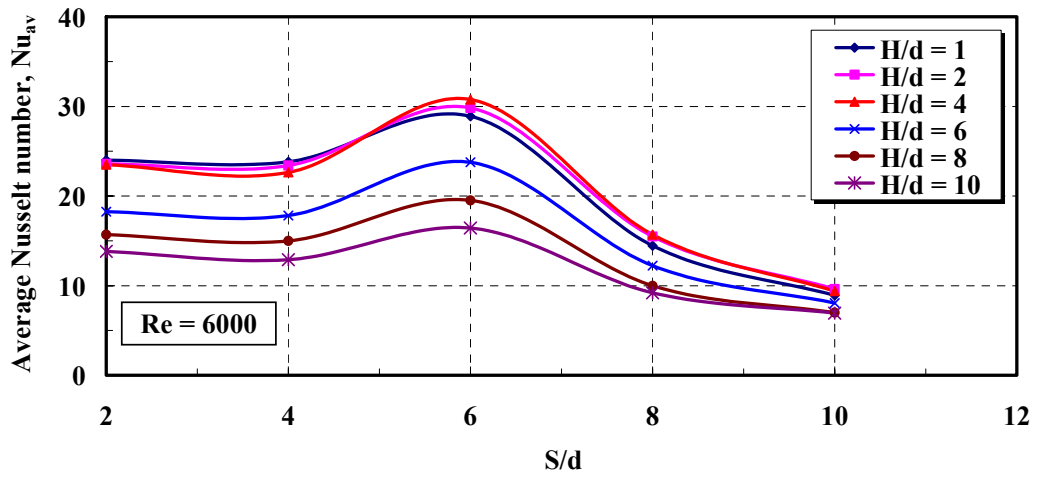


Fig. 4.12g Average Nusselt Number Distribution Versus with S/d at Different H/d for In-line Array, Re = 6000

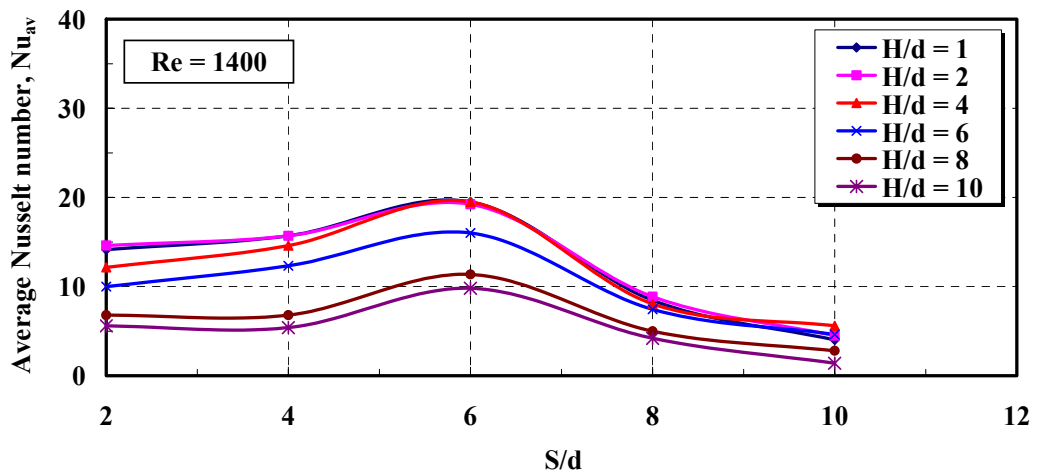


Fig. 4.12h Average Nusselt Number Distribution Versus with S/d at Different H/d for In-line Array, Re = 1400

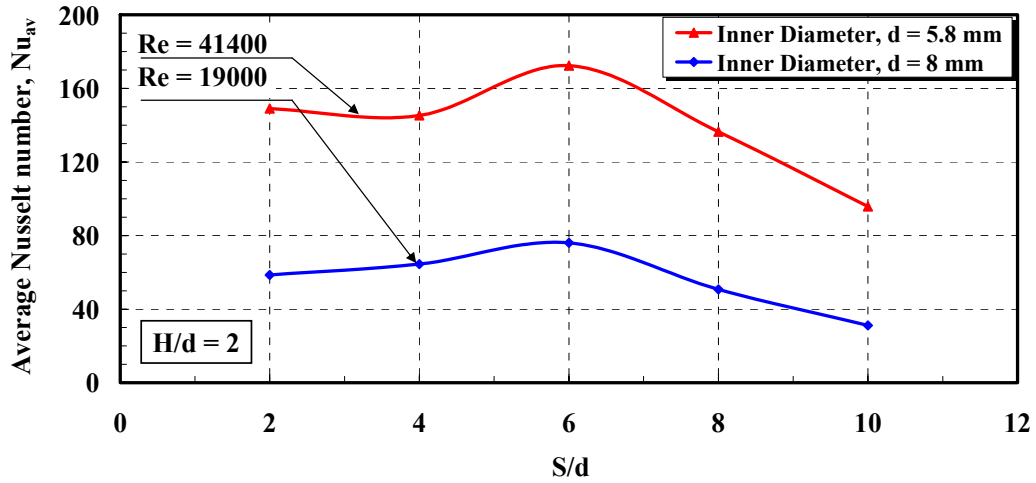


Fig. 4.13a Average Nusselt Number Vs Spacing Distance for two Inner Jet Diameter, H/d = 2

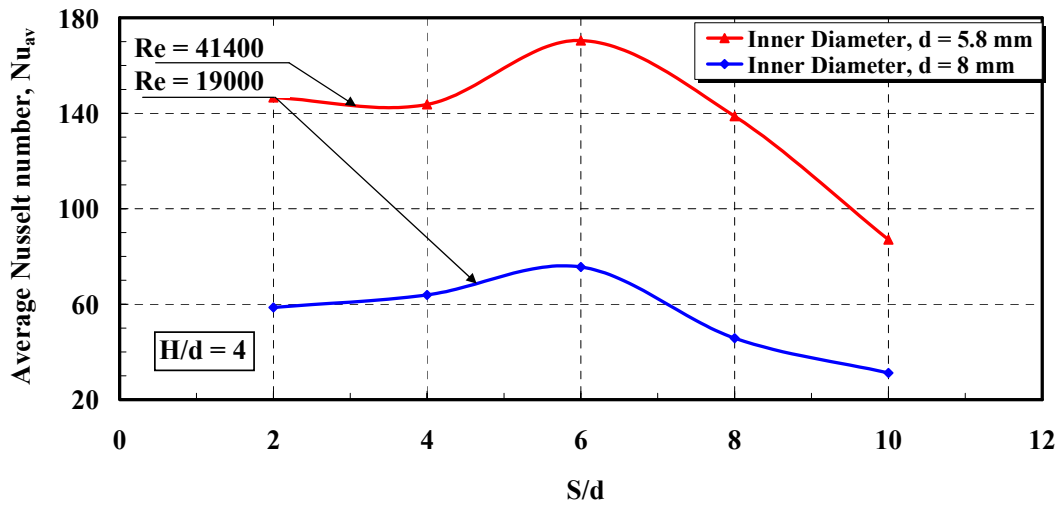


Fig. 4.13b Average Nusselt Number Vs Spacing Distance for two Inner Jet Diameter, H/d = 4

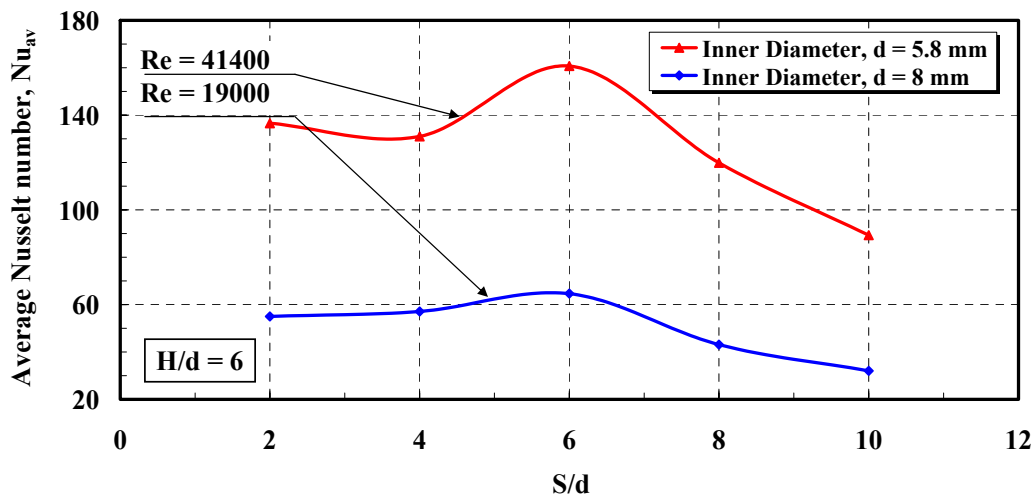


Fig. 4.13c Average Nusselt Number Vs Spacing Distance for two Inner Jet Diameter, H/d = 6

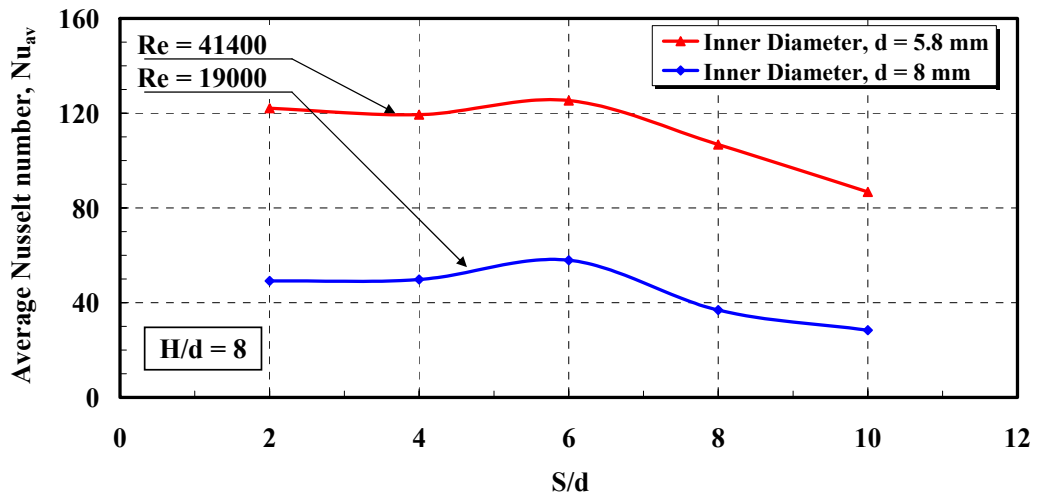


Fig. 4.13d Average Nusselt Number Vs Spacing Distance for two Inner Jet Diameter,  $H/d = 8$

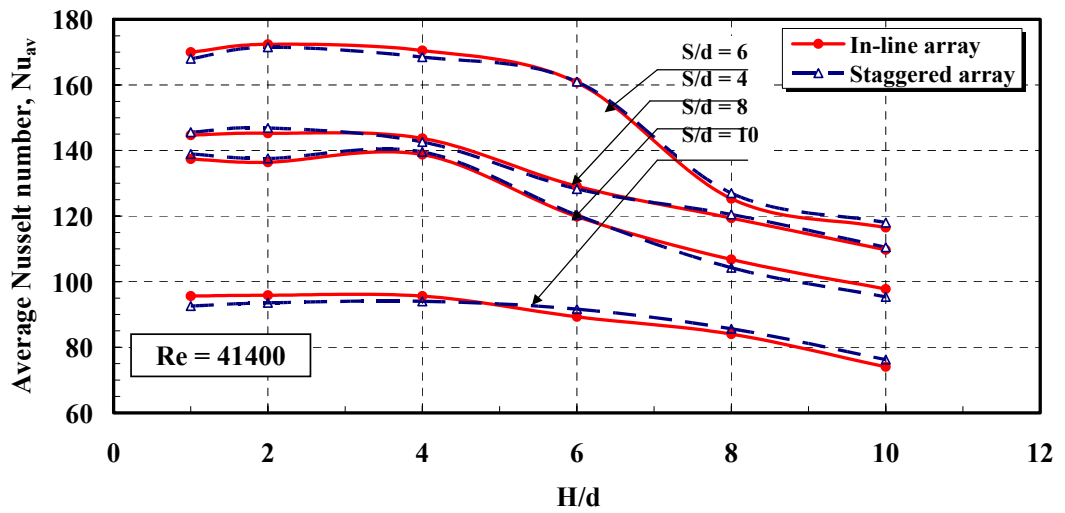


Fig. 4.14a Average Nusselt Number Versus  $H/d$  for the Staggered Array,  $Re = 414000$

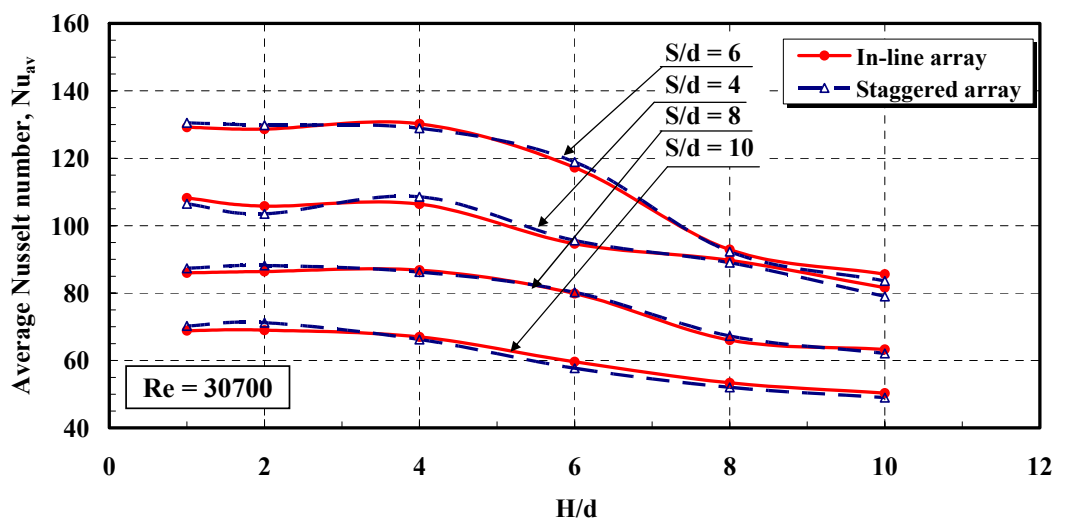


Fig. 4.14b Average Nusselt Number Versus  $H/d$  for the Staggered Array,  $Re = 30700$

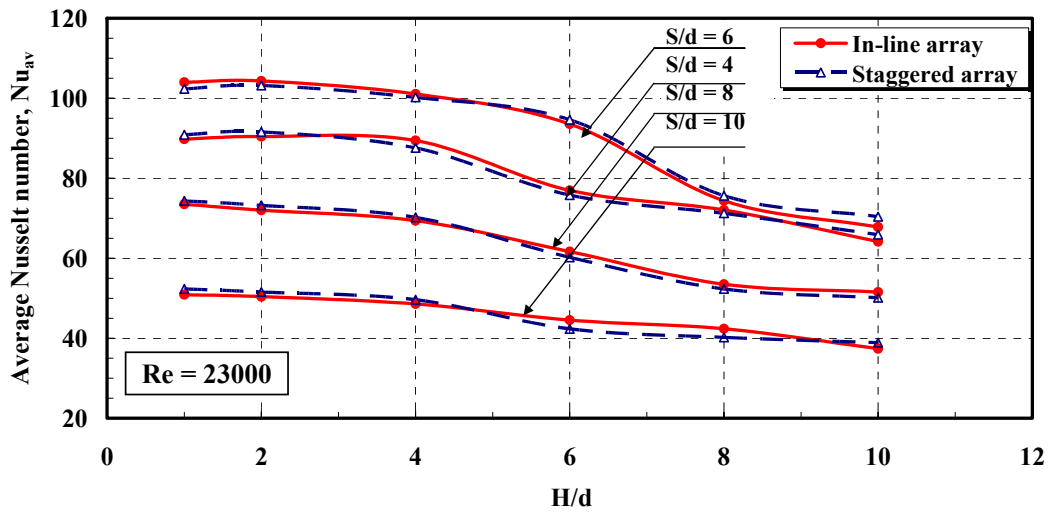


Fig. 4.14c Average Nusselt Number Versus H/d for the Staggered Array, Re = 23000

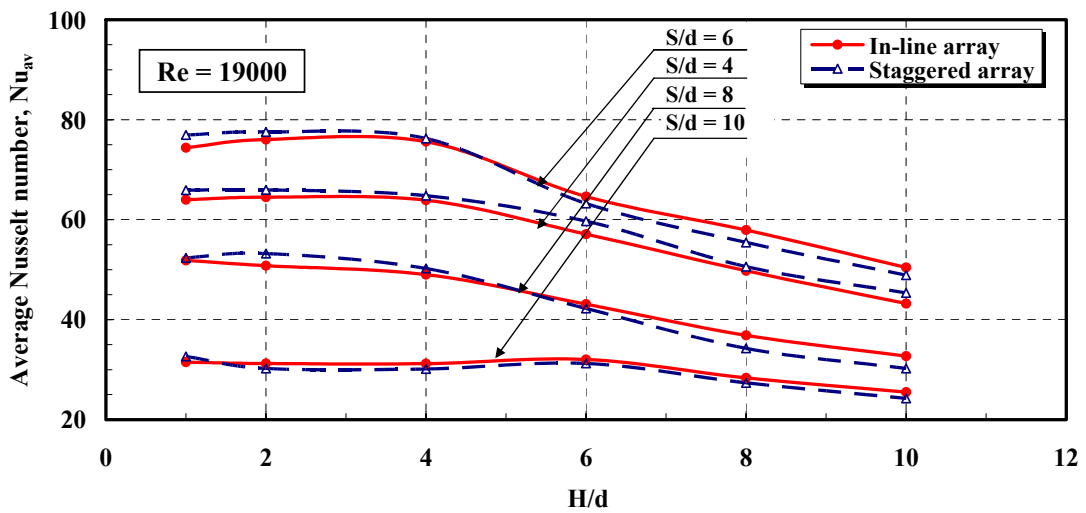


Fig. 4.14d Average Nusselt Number Versus H/d for the Staggered Array, Re = 19000

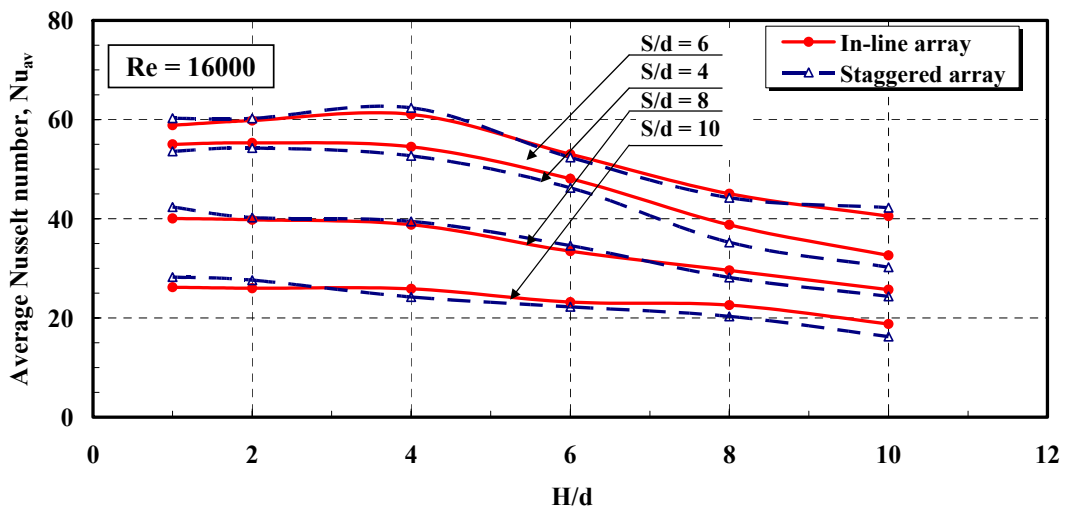


Fig. 4.14e Average Nusselt Number Versus H/d for the Staggered Array, Re = 16000

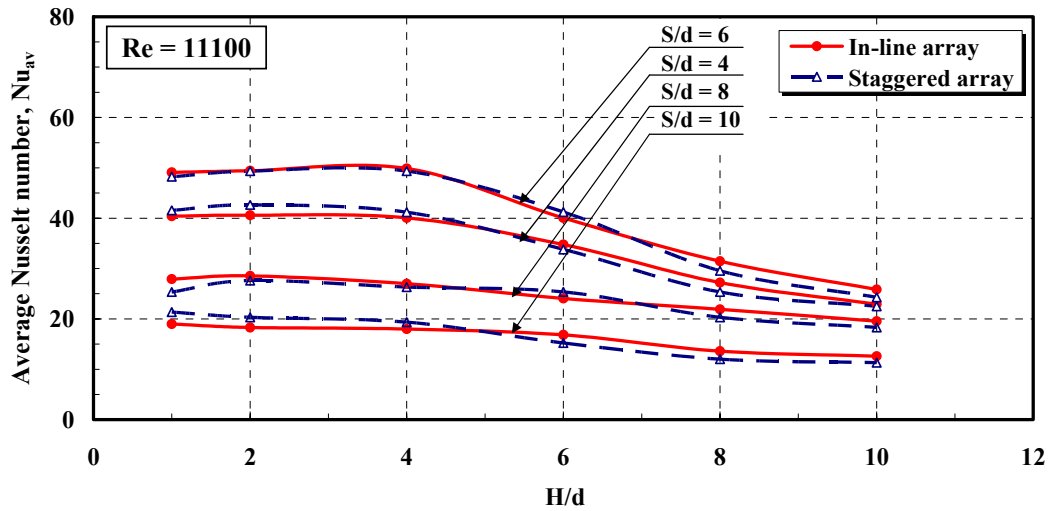


Fig. 4.14f Average Nusselt Number Versus H/d for the Staggered Array, Re = 11100

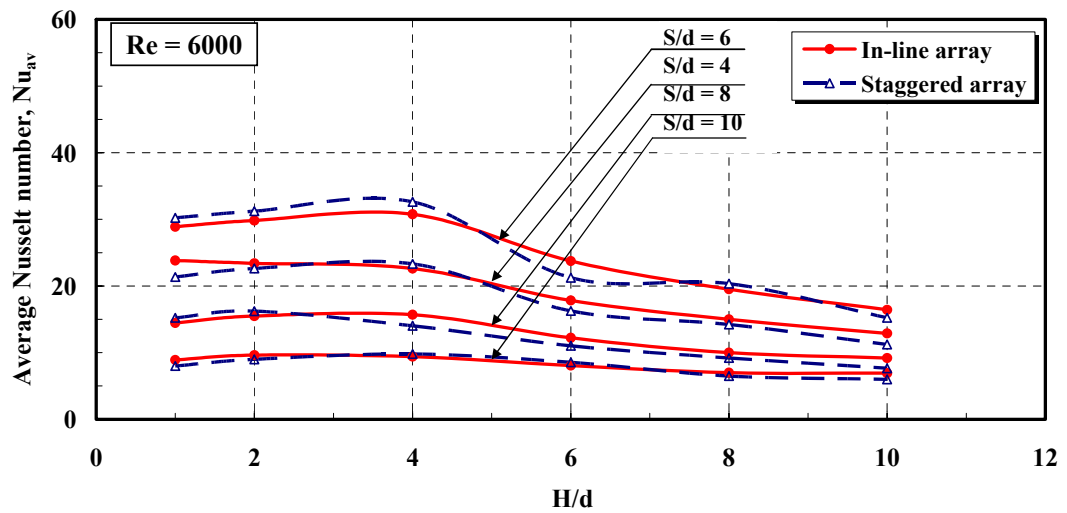


Fig. 4.14g Average Nusselt Number Versus H/d for the Staggered Array, Re = 6000

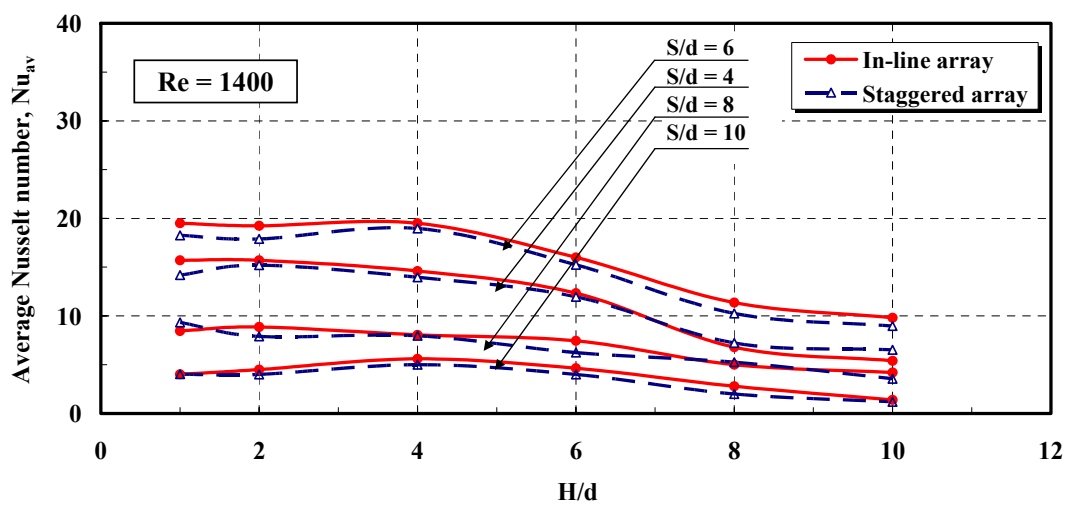


Fig. 4.14h Average Nusselt Number Versus H/d for the Staggered Array, Re = 14000

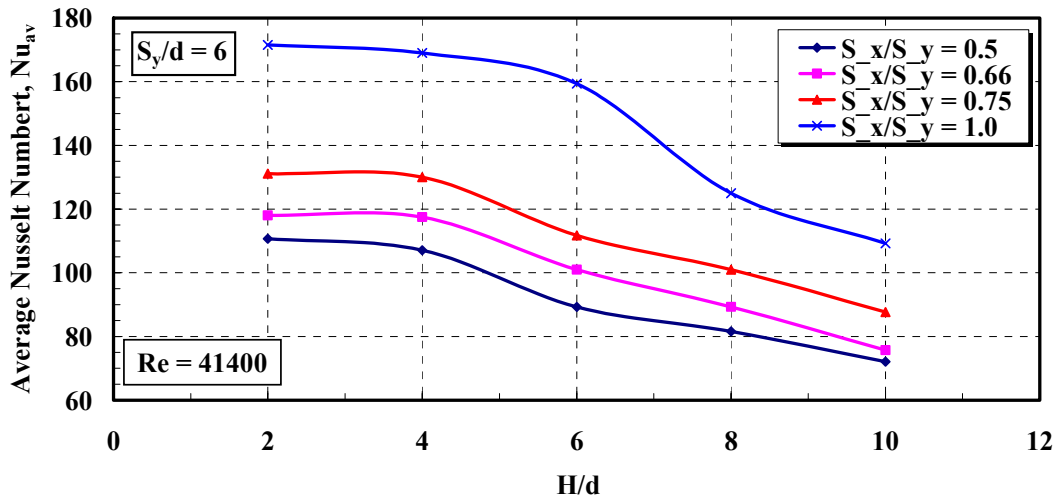


Fig. 4.15a Average Nusselt Number Distribution for Un-equal Spacing Distance,  $Re = 41400$

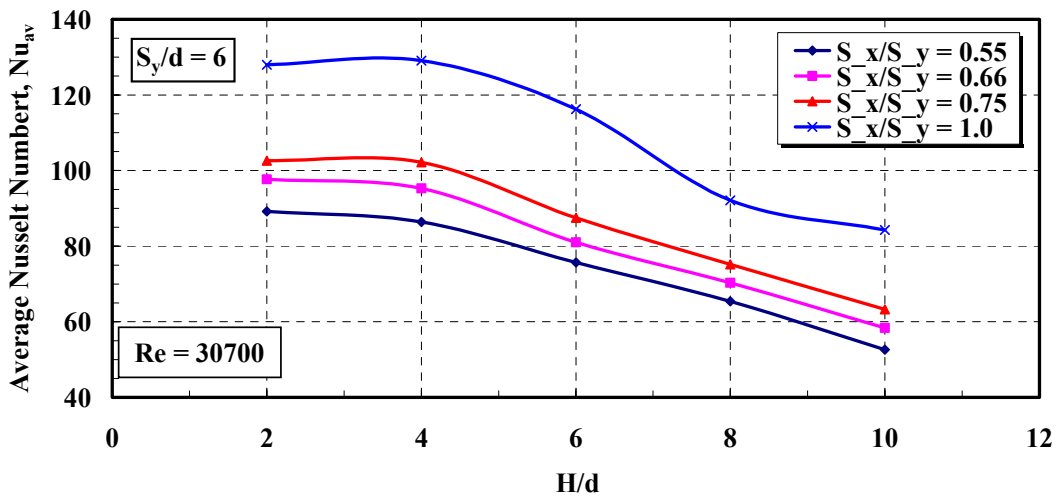


Fig. 4.15b Average Nusselt Number Distribution for Un-equal Spacing Distance,  $Re = 30700$

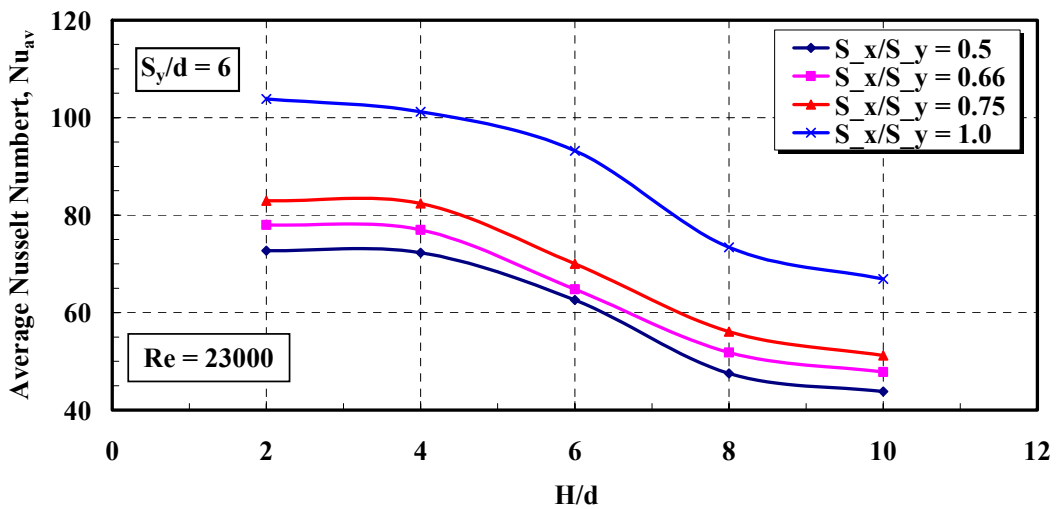


Fig. 4.15c Average Nusselt Number Distribution for Un-equal Spacing Distance,  $Re = 23000$

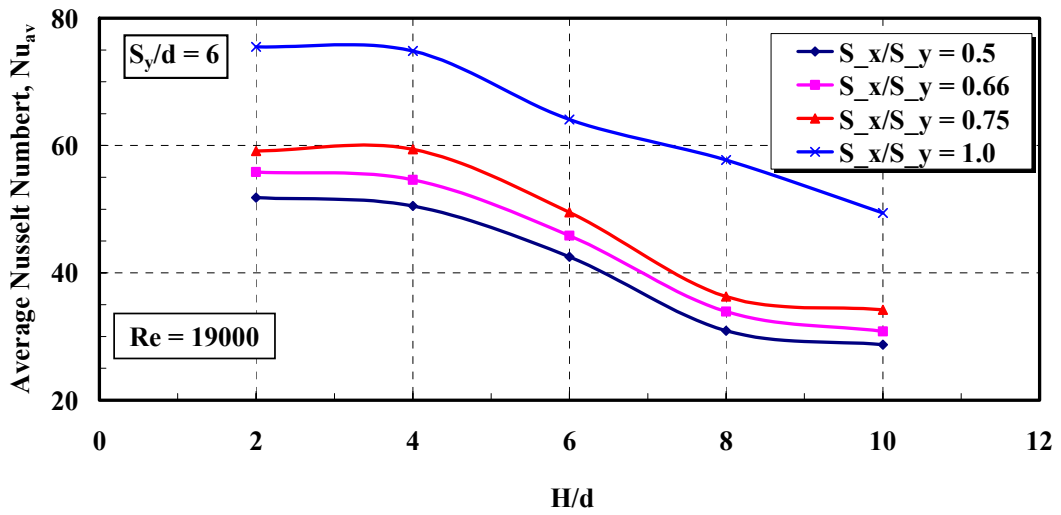


Fig. 4.15d Average Nusselt Number Distribution for Un-equal Spacing Distance,  $Re = 19000$

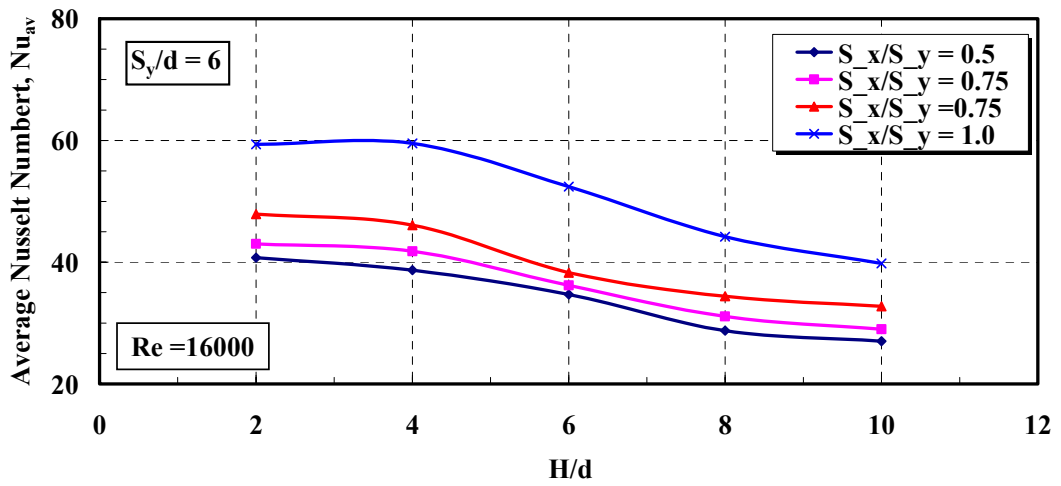


Fig. 4.15e Average Nusselt Number Distribution for Un-equal Spacing Distance,  $Re = 1600$

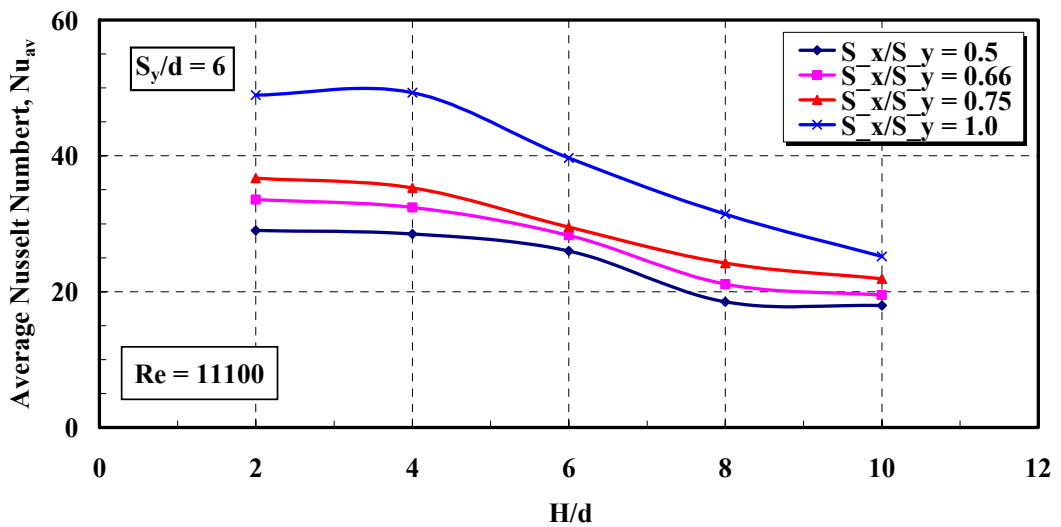


Fig. 4.15f Average Nusselt Number Distribution for Un-equal Spacing Distance,  $Re = 11100$

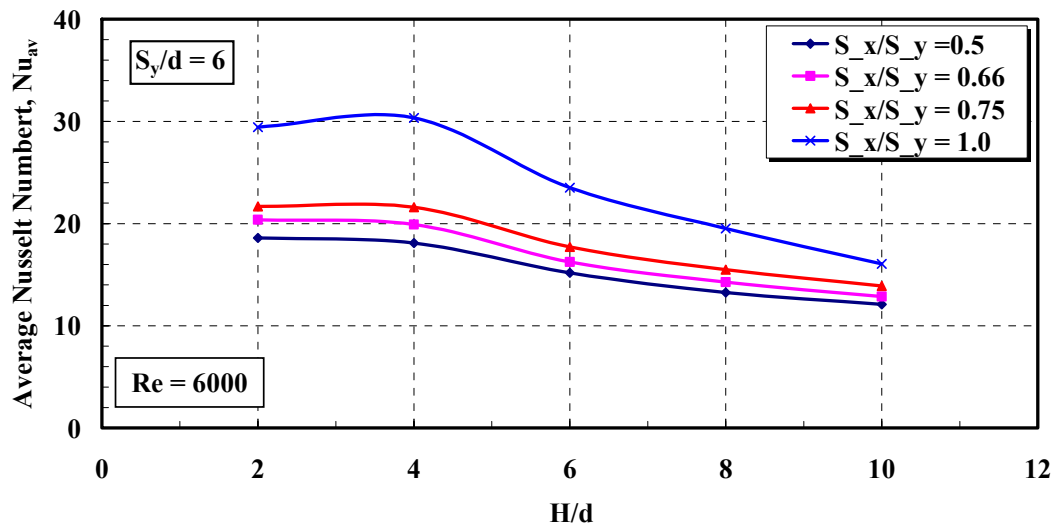


Fig. 4.15g Average Nusselt Number Distribution for Un-equal Spacing Distance,  $Re = 6000$

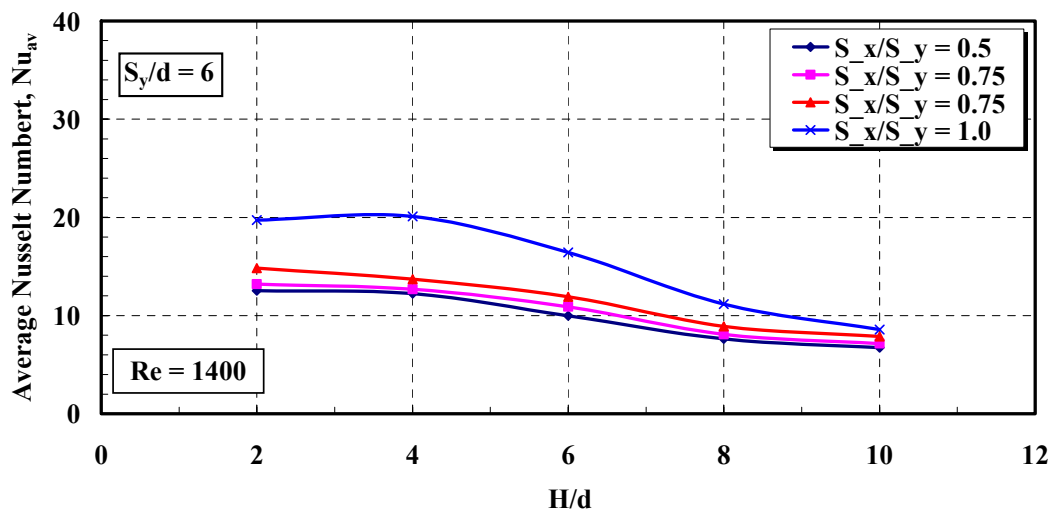


Fig. 4.15h Average Nusselt Number Distribution for Un-equal Spacing Distance,  $Re = 1400$

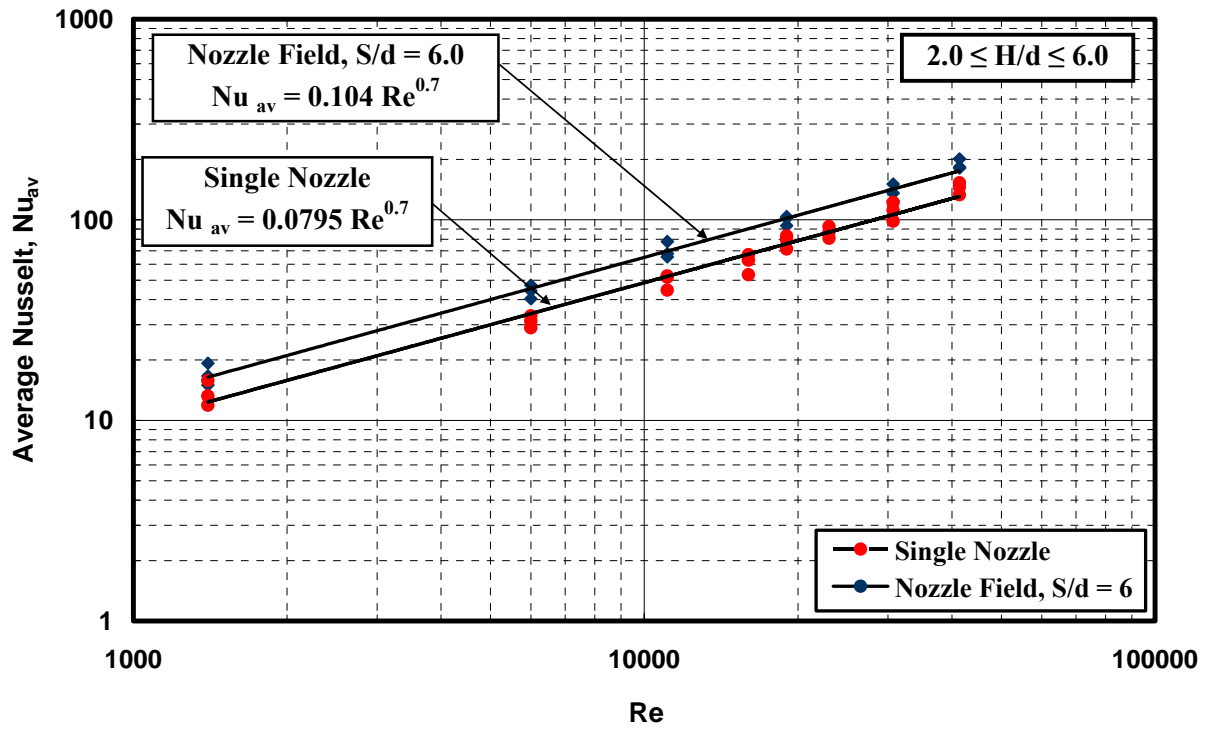


Fig 4.16 Average Nusselt Number Variation with Jet Reynolds Number

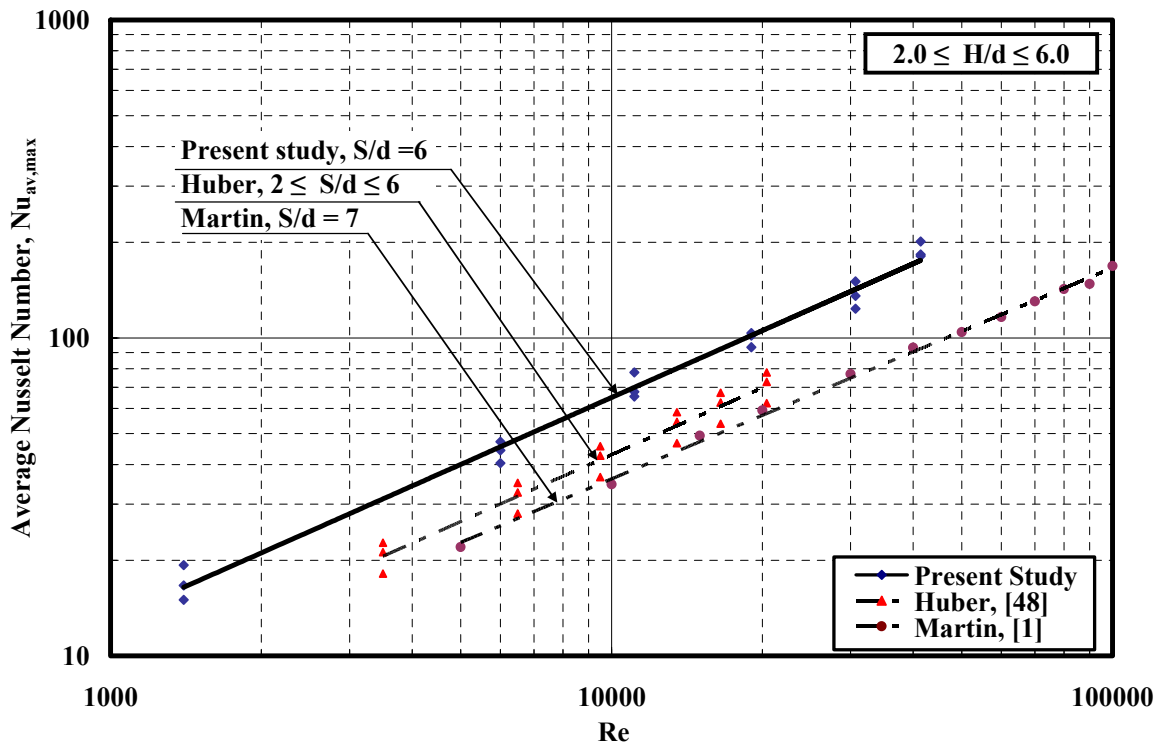


Fig. 4.17 Comparison of Average Nusselt Number with Previous Studies

## Heat Transfer for Hole Channels

### 5-1 Introduction

The hole channel impinging jets are used in a wide variety of applications such as cooling of combustion chamber and turbine blades. This chapter discussed the heat transfer characteristics for the hole channel impinging jet. The experimental measurements were made of the local heat transfer coefficients associated with a three rows of channels normal to a plan. Each channel has three holes with inner diameter is 5.8 mm, the spacing distance,  $S/d = \{4, 6, \text{and } 8\}$ . The three channels was arranged in-line array. These channel produced by perforated plates which are fixed in free tube as shown in Fig. 5.1. The width of these perforated plates is two hole diameter. The local heat transfer coefficients were integrated to obtain the average heat transfer coefficients which are reported here. In this chapter, the comparison are made for the average heat transfer of the hole channel impinging jet with the multiple jets system.

### 5-2 Local Nusselt Number Distribution:

Figs. 5.2a-e, 5.3a-e, and 5.4a-e show detailed local Nusselt number distribution for the hole channel as the function of non-dimensional location  $X/d$  on the impingement surface for three spacing distances of  $S/d = 4, 6, \text{ and } 8$  respectively. These figures based on the five Reynolds numbers for separation distance that is  $H/d = 2, 4, 6, 8, \text{ and } 10$ . From these figures it can be seen that, the major differences between the profiles are in the magnitudes and locations of the secondary peaks. As mentioned before, the secondary peaks exhibit a strong dependence on the Reynolds number, separation distance, and spacing distance. At the low Reynolds number  $Re = 1400$  and higher separation distance  $H/d \geq 6$ , there is no evidence of the secondary peaks, and the profiles is very similar to those obtained at  $H/d = 8, \text{ and } 10$  for all examined spacing distances. As the Reynolds number is increased to  $Re = 11100$ , the Nusselt

number profile shapes have not changed significantly but there is a faint indication of a secondary peak. At higher Reynolds number ( $Re = 19000$ ) the secondary peaks are clearly discernible but still not pronounced. But, when the Reynolds number is increased to  $Re = 23000$  these peaks are now clearly evident. As the Reynolds number is further increased of ( $Re = 41400$ ) and the spacing distance increases, the secondary peaks become more pronounced. These results are due to the increase of turbulent intensity with higher Reynolds number, where the turbulent boundary layer is more pronounced. In addition the increase of spacing distance,  $S/d$ , causes a reduction in the interference between adjacent jets.

The secondary peaks occur in the range of  $1.35 \leq X/d \leq 2.2$  for all spacing distances tested in the case of hole channel array. With increasing of Reynolds number and decreasing of separation distance, the location of these peaks moves outward in the radial direction and the local Nusselt number at these peaks is increased. This because the boundary layer transition occurs earlier at the lower separation distance. Martin [1] suggested that the secondary peaks could exceed the stagnation point Nusselt number for higher Reynolds numbers. But in the present study the stagnation point heat transfer rates are always larger than the secondary peaks approximately 15-20 % for all parameters tested in this work.

### **5-3 Influence of Spacing and Separation Distances:**

#### **5-3-1 Stagnation Nusselt Number $Nu_{st}$ :**

The stagnation Nusselt number  $Nu_{st}$  variations with the spacing distance  $S/d$  for different separation distance  $H/d$  is shown in Figs. 5.5a-h. All these results of stagnation Nusselt number are dependent of the Reynolds number  $1400 \leq Re \leq 41400$ . As a consequence, the maximum stagnation Nusselt number is obtained for spacing distance of  $S/d = 6$  within the range of distances tested for all Reynolds numbers. The effect of the separation distance  $H/d$  on the

stagnation Nusselt number is presented in Figs. 5.6a-h. From these figures, it can be seen that, the stagnation Nusselt number is nearly constant in the separation potential range of  $2 \leq H/d \leq 4$ . In the separation distance range of  $4 \leq H/d \leq 6$ , the stagnation Nusselt number is reduce rapidly for all three spacing distances. Then the stagnation Nusselt number is decreases monotonically with increase the separation distance,  $H/d \geq 6$ . For low Reynolds number  $1400 \leq Re \leq 6000$ , the values of stagnation Nusselt number for separation distance  $8 \leq H/d \leq 10$  are nearly constant for the three spacing distance.

The influence of the jet Reynolds number on the stagnation Nusselt number for the hole channel array will be discussed in the following figure. Fig 5.7 shows the optimum value of the stagnation Nusselt number at spacing distance  $S/d = 6$  in dependence on the Reynolds number. The parameter is the separation distance in the range of  $2 \leq H/d \leq 4$ . From this figure it can be seen that the stagnation Nusselt number varies according to  $Nu_{st} \approx Re^{0.5}$ . Fig. 5.7 also shows the values of stagnation Nusselt number for the jet array. This values obtained at optimum spacing distance  $S/d = 6$ . The separation distance  $H/d$  is ranged for  $2 \leq H/d \leq 6$ . This stagnation Nusselt number for jet array is 25% higher than for the hole channel.

### **5-3-2 Average Nusselt Number $Nu_{av}$ :**

The average Nusselt Number  $Nu_{av}$  deserves more concern in many practical applications. The surface averaged heat fluxes were obtained by integrating the local values of the Nusselt number as explained before in chapter three. The main purpose is to compute the heating capabilities of the centre jets under different spacing and separation distances,  $S/d$ , and  $H/d$ , respectively. The integrating areas were both square with a side length of  $S$  as shown in Fig. 4.11, which was the same to that selected by Dong et al. [55] in his study of a row of three butane/air flame impinging jets.

The average Nusselt number as a function of the spacing distance  $S/d$  has been interpolated from the measurements for different separation distances,  $H/d$ , in Figs. 5.8a-h. Every figure is based on one exit jet Reynolds number. From these figures, it can be seen that at the all values of separation distances, the average Nusselt number at the spacing distances of  $S/d = 4$  is the maximum value for all Reynolds numbers. But the average Nusselt number at spacing distance  $S/d$  of 6 is extremely closed to that at spacing distance  $S/d$  of 4. In case of higher spacing distance ( $S/d = 8$ ), the interference between adjacent jets is very weak and the impinging area is increased. Therefore the average Nusselt number in this case is lower value.

The average Nusselt number in dependence on the separation distance  $H/d$  was plotted in Figs. 5.9a-h. The spacing distance  $S/d$  is a parameter in all figures. Every figure is based on one exit jet Reynolds number. One can see that the separation distance in the range of  $2 \leq H/d \leq 4$  has no effect on the average Nusselt number for all spacing distances and Reynolds numbers. As the separation distance increase ( $H/d > 4$ ), the value of average Nusselt number decreases gradually.

The following Figs. 5.10a-b describe the effect of the spacing distance  $S/d$  on the average Nusselt number with differences Reynolds numbers  $41400 \leq Re \leq 6000$ . Each figure is based on the one separation distance ( $H/d = 4$  or 6). From these figures it can be noted that the exit jet Reynolds number has no effect on the maximum average Nusselt number position ( $S/d = 6$ ) for the two separation distances,  $H/d$ . In addition the value of the average Nusselt number is nearly constant in the range of spacing distance of  $4 \leq S/d \leq 6$ .

Fig. 5.11 shows the average Nusselt number against the Reynolds number at the optimum spacing distance of  $S/d = 4$  for the separation distances of  $2 \leq H/d \leq 4$ . For Reynolds number ranged from 1400 to 41400, the least square curve fitting gives the following correlation;

$$\text{Nu}_{\text{av}} = 0.0864 \cdot \text{Re}^{0.66} \quad \begin{cases} 1400 \leq \text{Re} \leq 41400 \\ 2 \leq H/d \leq 4 \\ 4 \leq S/d \leq 6 \end{cases} \quad (5-1)$$

Equation (5-1) represents the average Nusselt data for hole channel impinging jet with a standard deviation of 2.6%. For air the Prandtl number can be included in the above equation similar to References 34 and 48. Thus this equation can be rewritten as the following,

$$\text{Nu}_{\text{av}} = 0.0998 \cdot \text{Re}^{0.66} \cdot \text{Pr}^{0.42} \quad (5-2)$$

The average Nusselt numbers for the hole channel impinging jet reported in this chapter are compared to the average Nusselt numbers for free tube impinging jet which reported in chapter four also in Fig. 5.11. It was observed from this figure that the average Nusselt number for free tube impinging jet is greater than that of the hole channel impinging jet. In addition, the hole channel correlation has a Reynolds number exponent of 0.66, while the free tube impinging jet has an exponent of about 0.7. The hole channels arranged can be considered as mixture of perforated plate and free tube jet, therefore the exponent is decreased of 0.66.

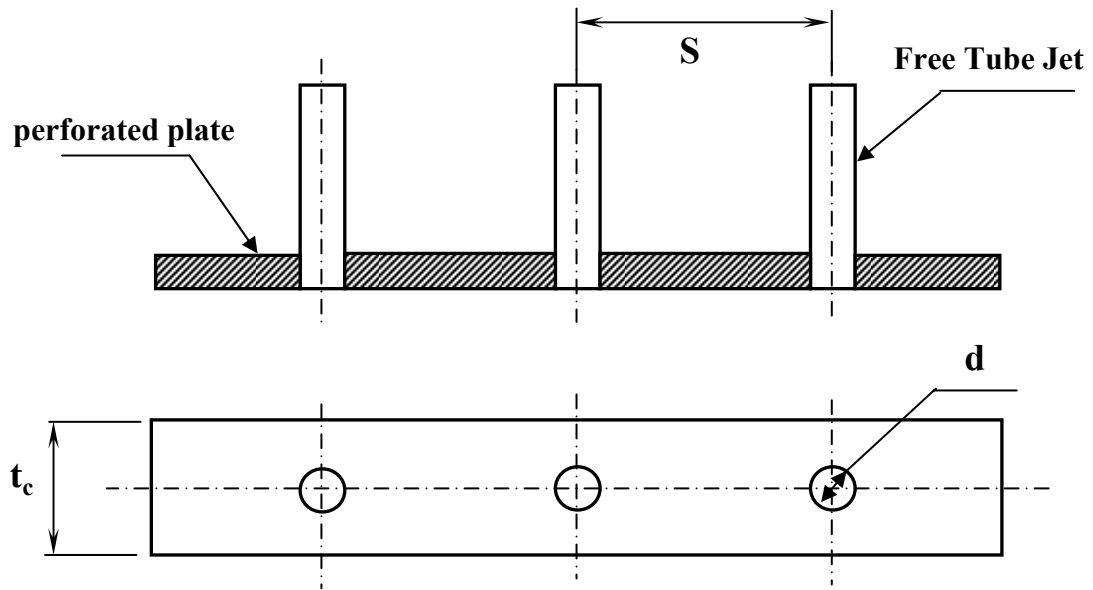


Fig. 5.1 Hole Channel Form,  $t_c = 2d$

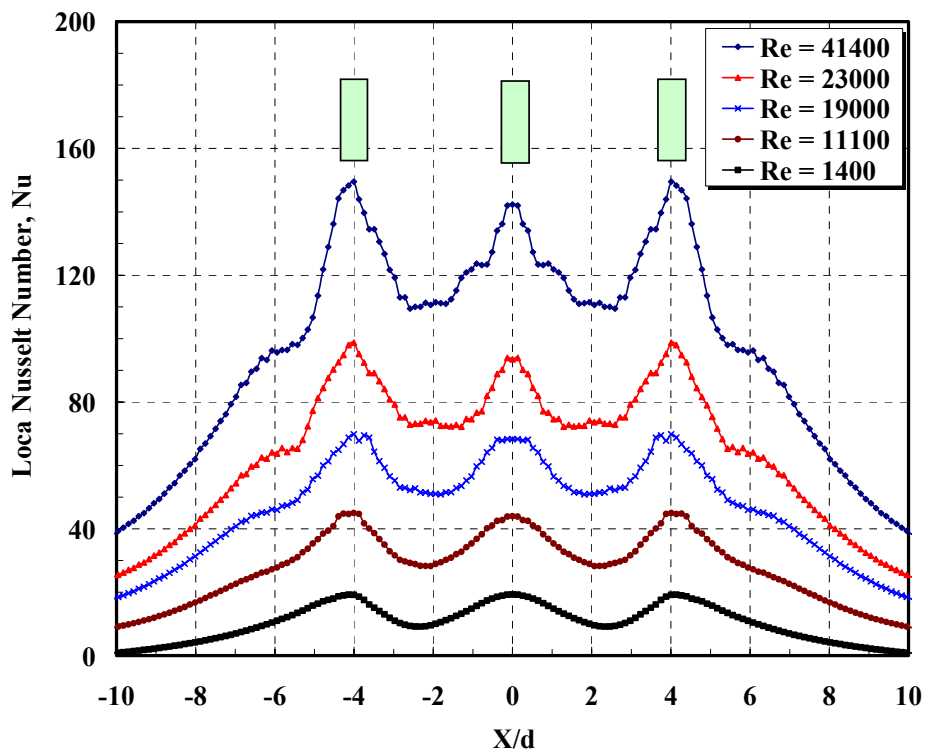


Fig. 5.2a Local Nu Distribution for Hole Channel,  
 $H/d = 2$ ,  $S/d = 4$ , and  $t_c/d = 2$

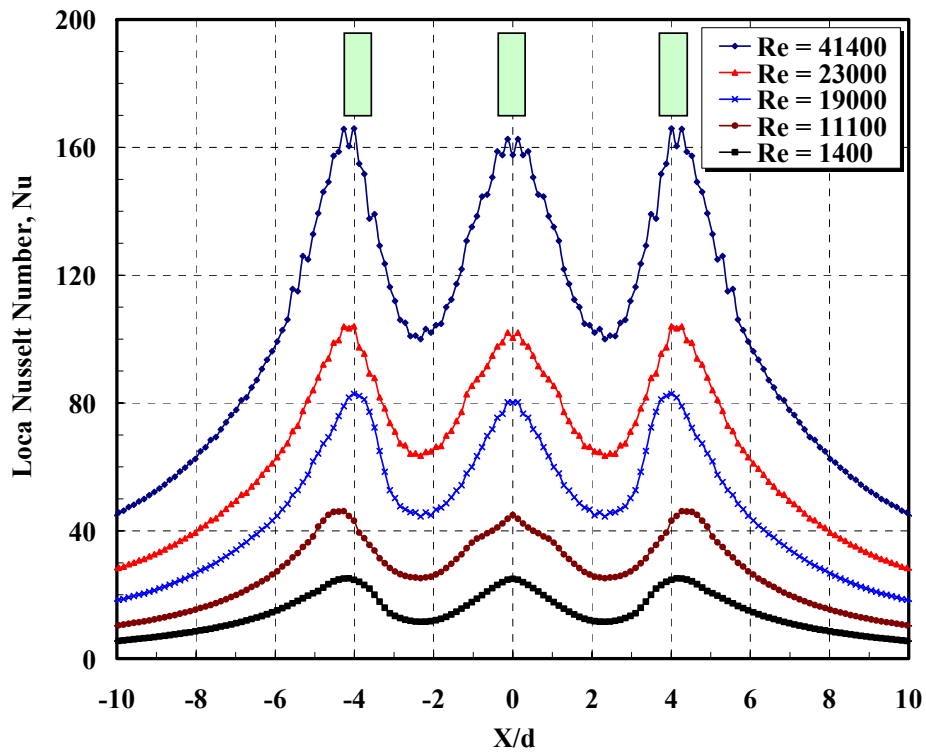


Fig. 5.2b Local Nu Distribution for Hole Channel,  
 $H/d = 4$ ,  $S/d = 4$ , and  $t_c/d = 2$

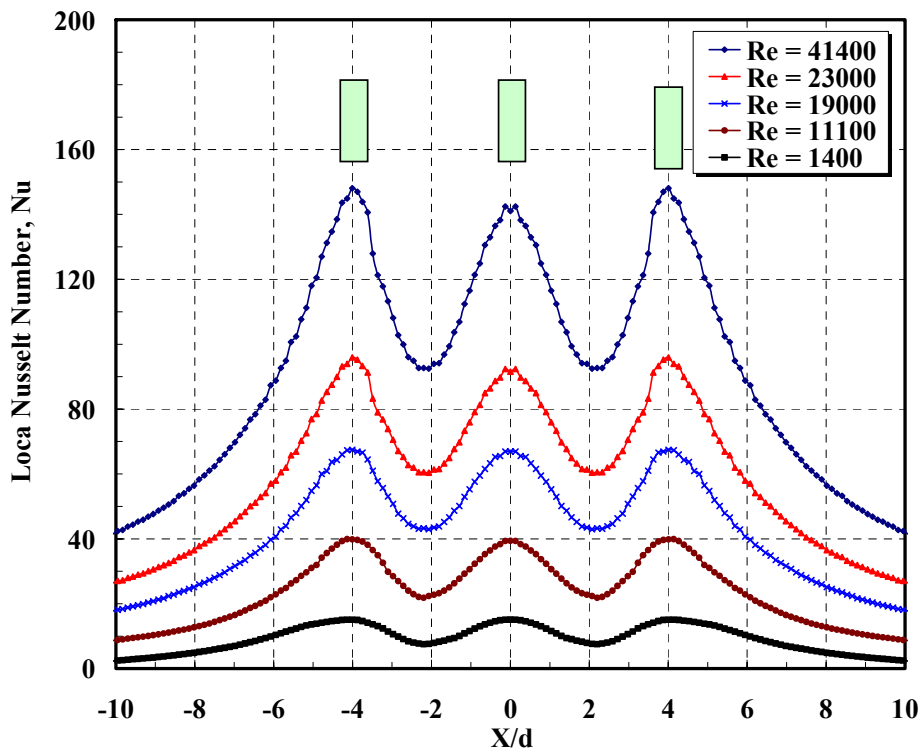


Fig. 5.2c Local Nu Distribution for Hole Channel,  
 $H/d = 6$ ,  $S/d = 4$ , and  $t_c/d = 2$

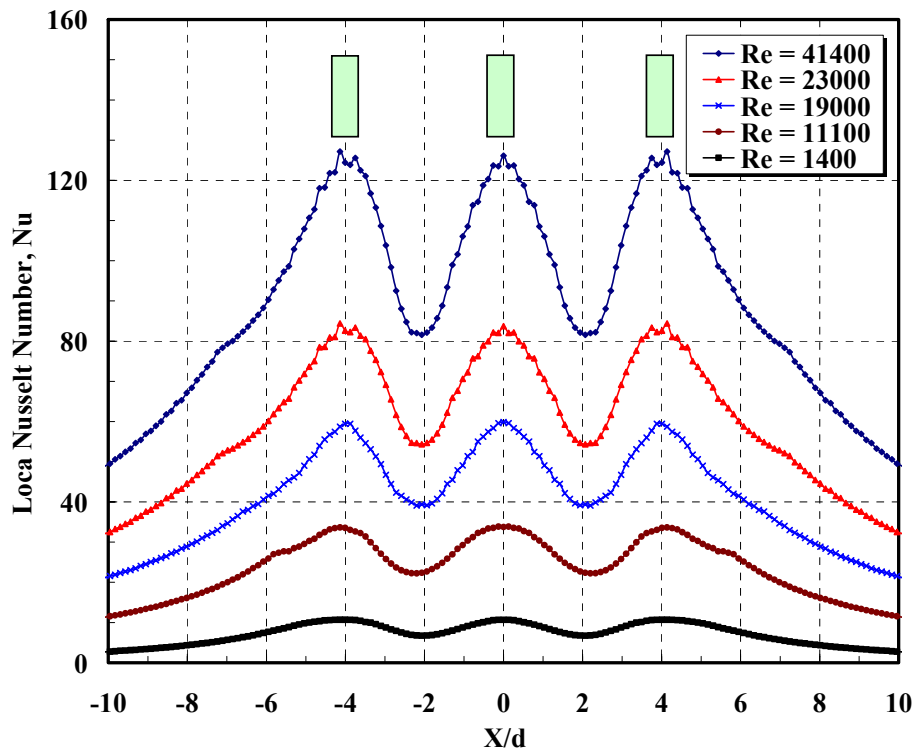


Fig. 5.2d Local Nu Distribution for Hole Channel,  
 $H/d = 8$ ,  $S/d = 4$ , and  $t_c/d = 2$

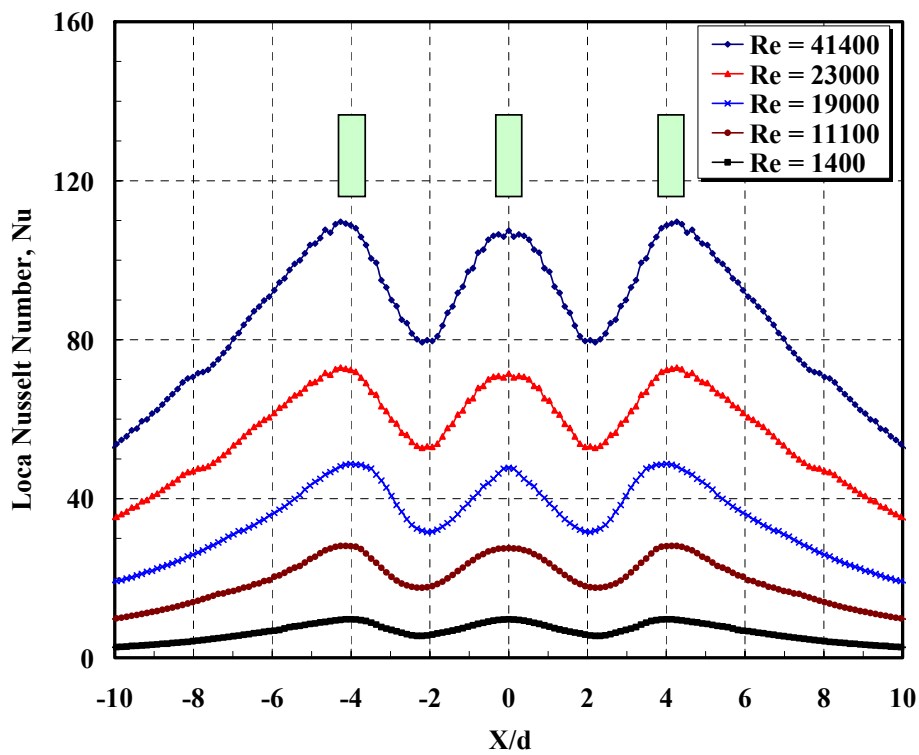


Fig. 5.2e Local Nu Distribution for Hole Channel,  
 $H/d = 10$ ,  $S/d = 4$ , and  $t_c/d = 2$

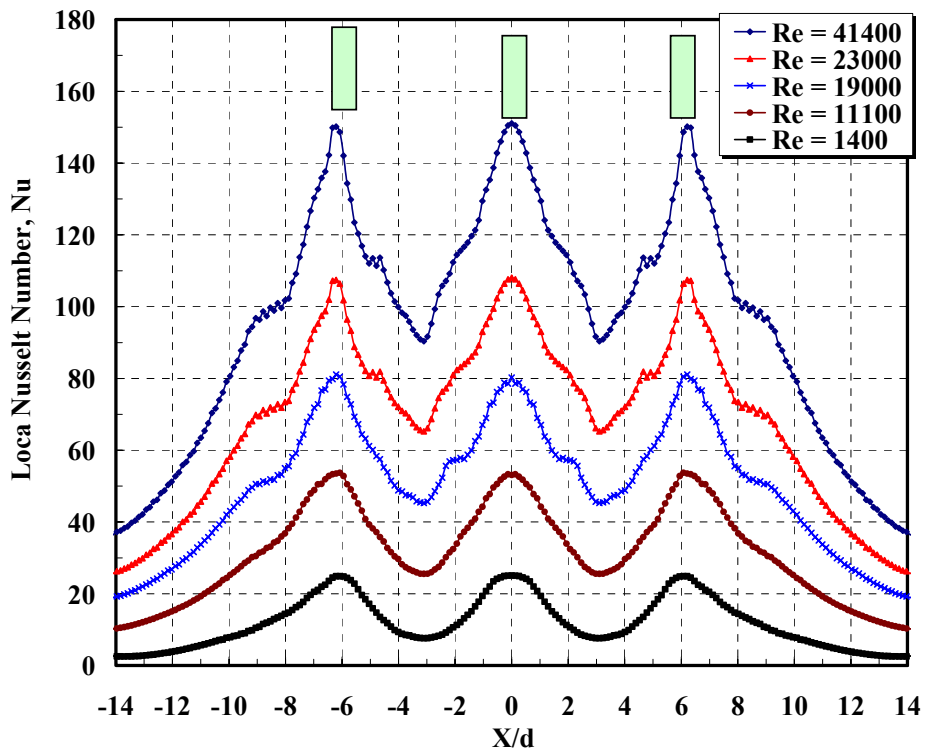


Fig. 5.3a Local Nu Distribution for Hole Channel,  
 $H/d = 2$ ,  $S/d = 6$ , and  $t_c/d = 2$

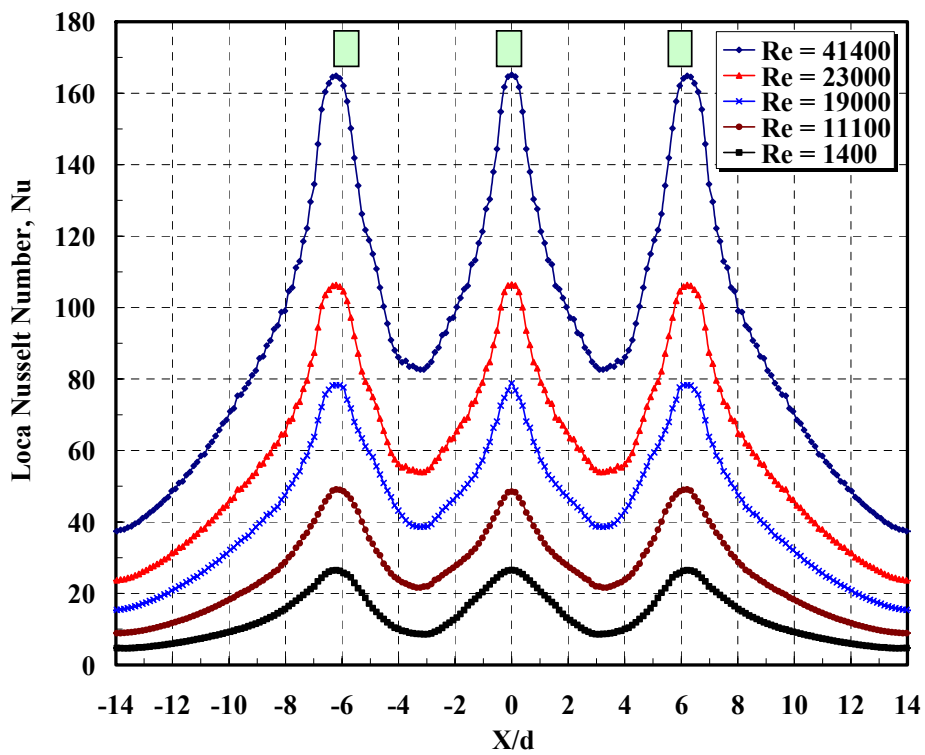


Fig. 5.3b Local Nu Distribution for Hole Channel,  
 $H/d = 4$ ,  $S/d = 6$ , and  $t_c/d = 2$

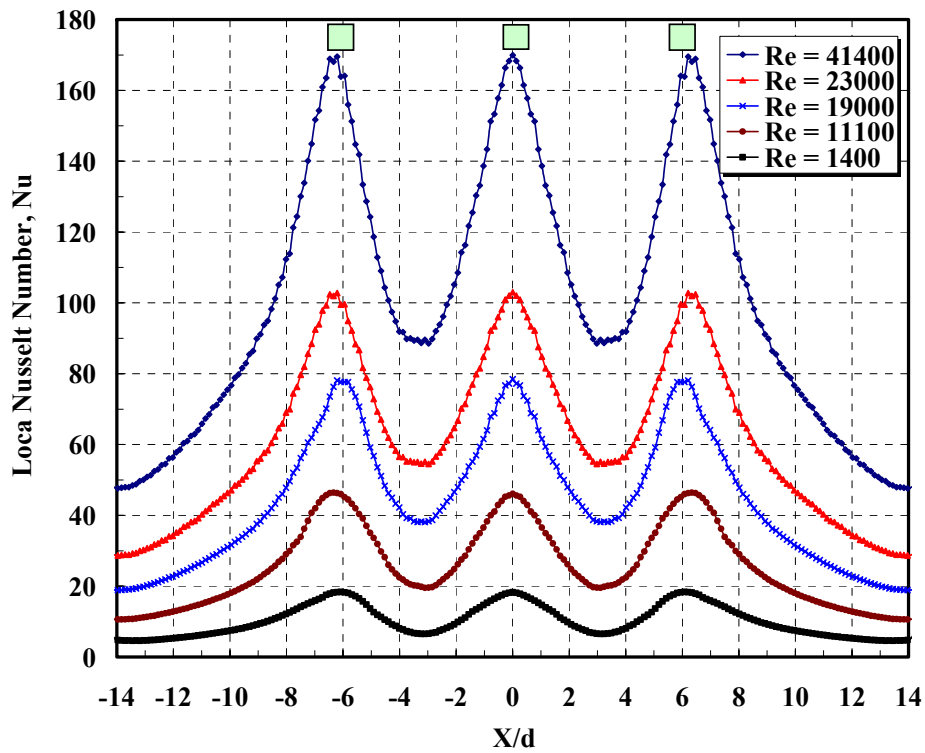


Fig. 5.3c Local Nu Distribution for Hole Channel,  
 $H/d = 6$ ,  $S/d = 6$ , and  $t_c/d = 2$

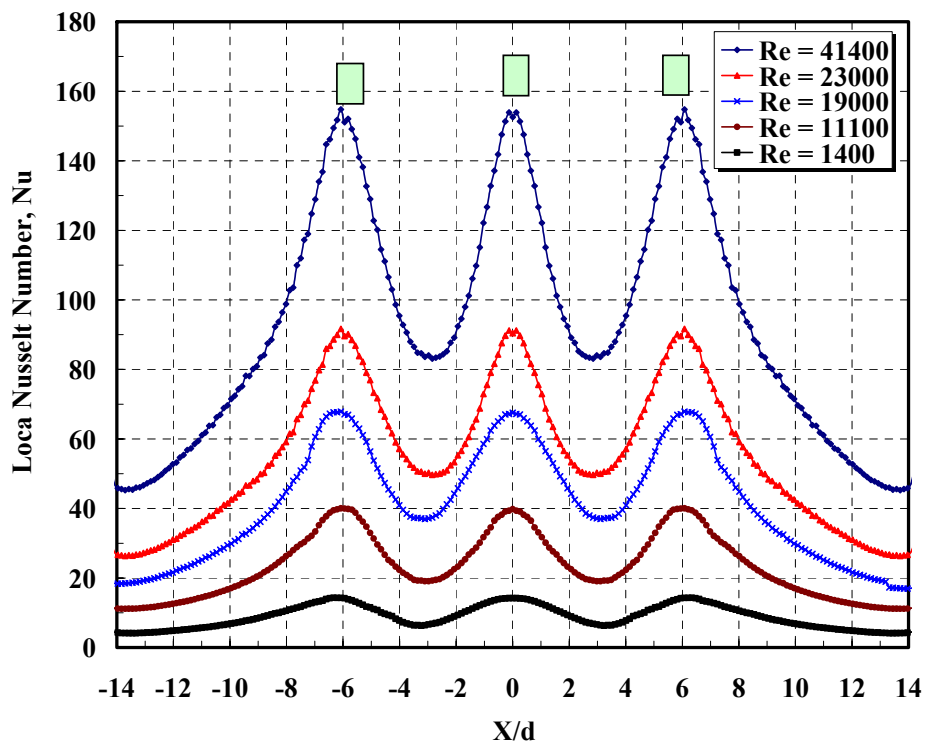


Fig. 5.3d Local Nu Distribution for Hole Channel,  
 $H/d = 8$ ,  $S/d = 6$ , and  $t_c/d = 2$

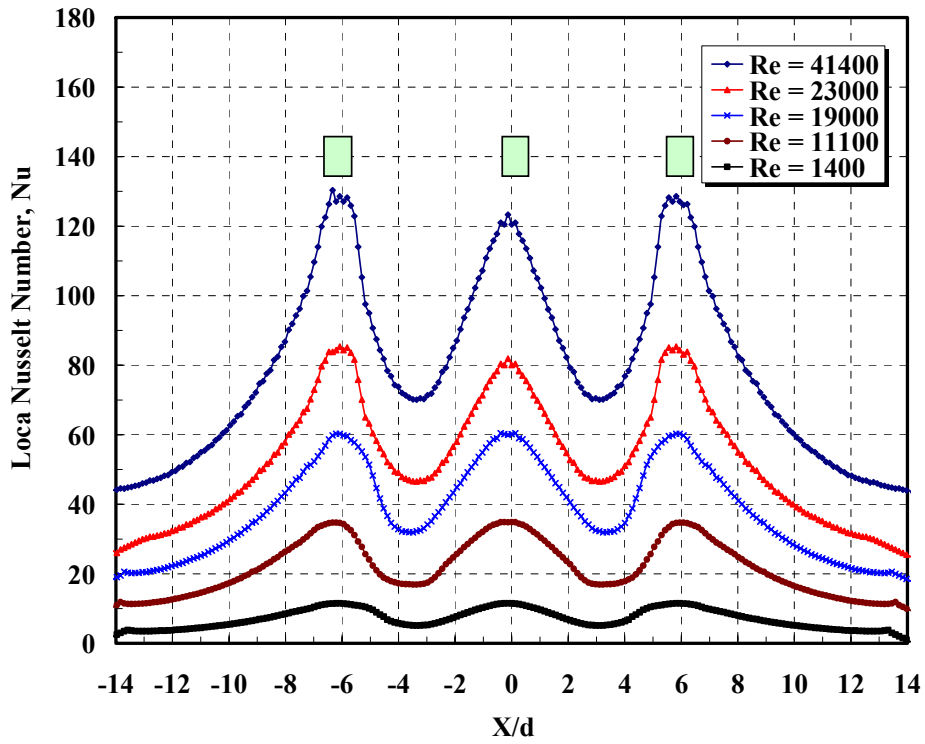


Fig. 5.3e Local Nu Distribution for Hole Channel,  
 $H/d = 10$ ,  $S/d = 6$ , and  $t_c/d = 2$

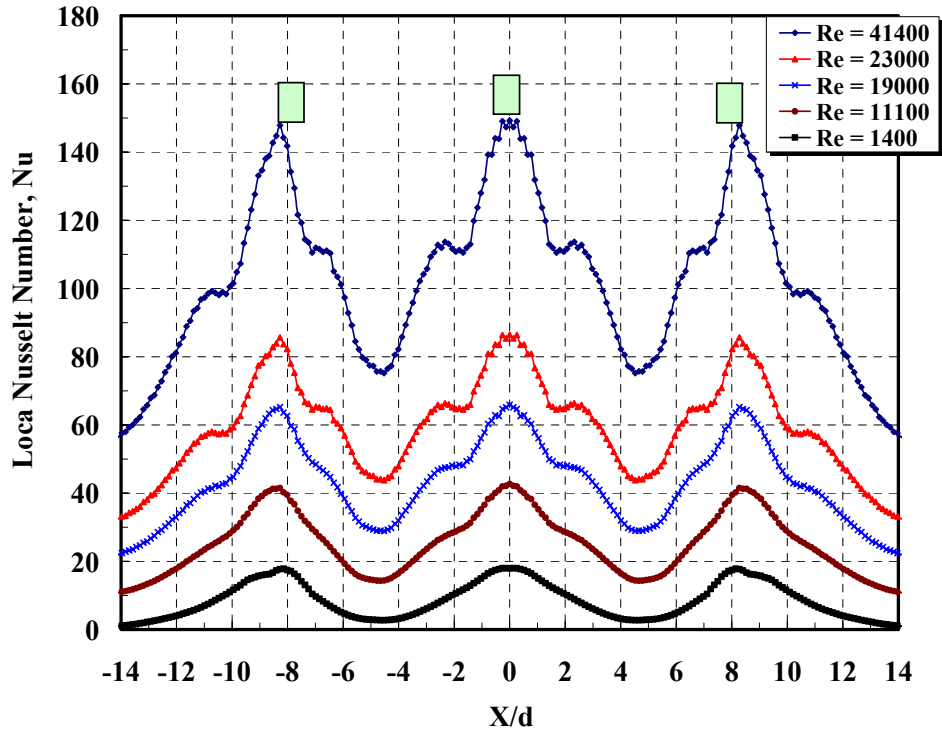


Fig. 5.4a Local Nu Distribution for Hole Channel,  
 $H/d = 2$ ,  $S/d = 8$ , and  $t_c/d = 2$

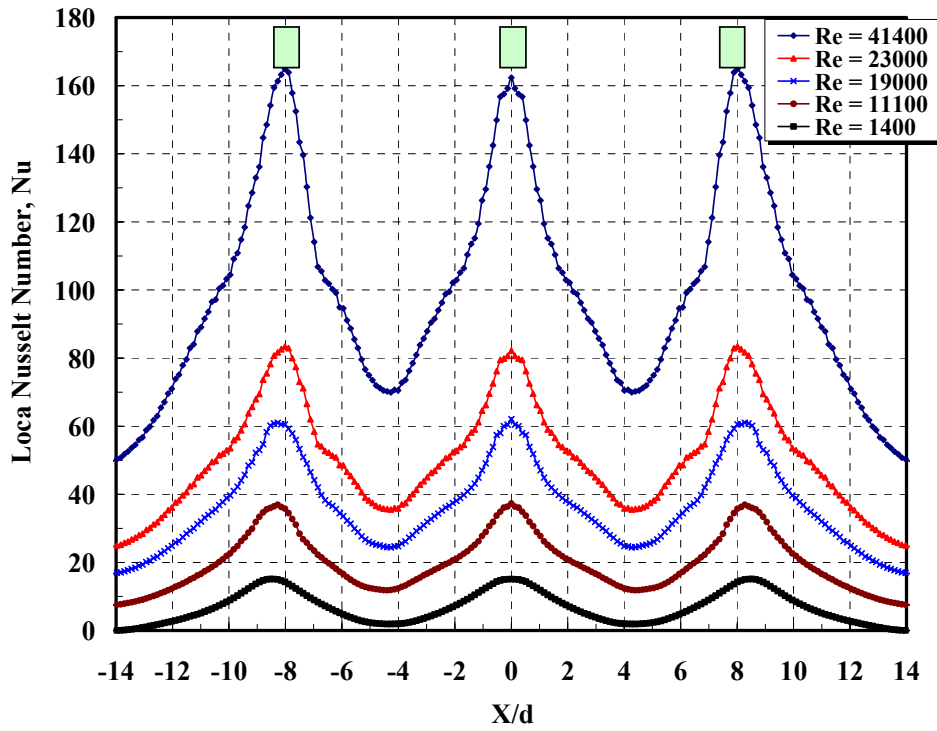


Fig. 5.4b Local Nu Distribution for Hole Channel,  
 $H/d = 4$ ,  $S/d = 8$ , and  $t_c/d = 2$

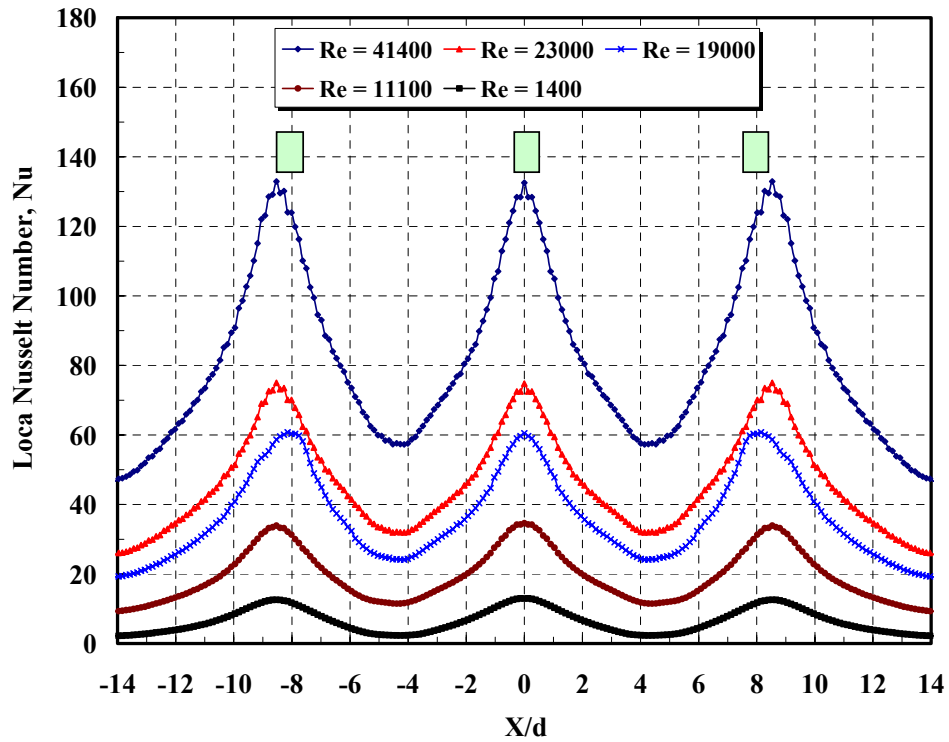


Fig. 5.4c Local Nu Distribution for Hole Channel,  
 $H/d = 6$ ,  $S/d = 8$ , and  $t_c/d = 2$

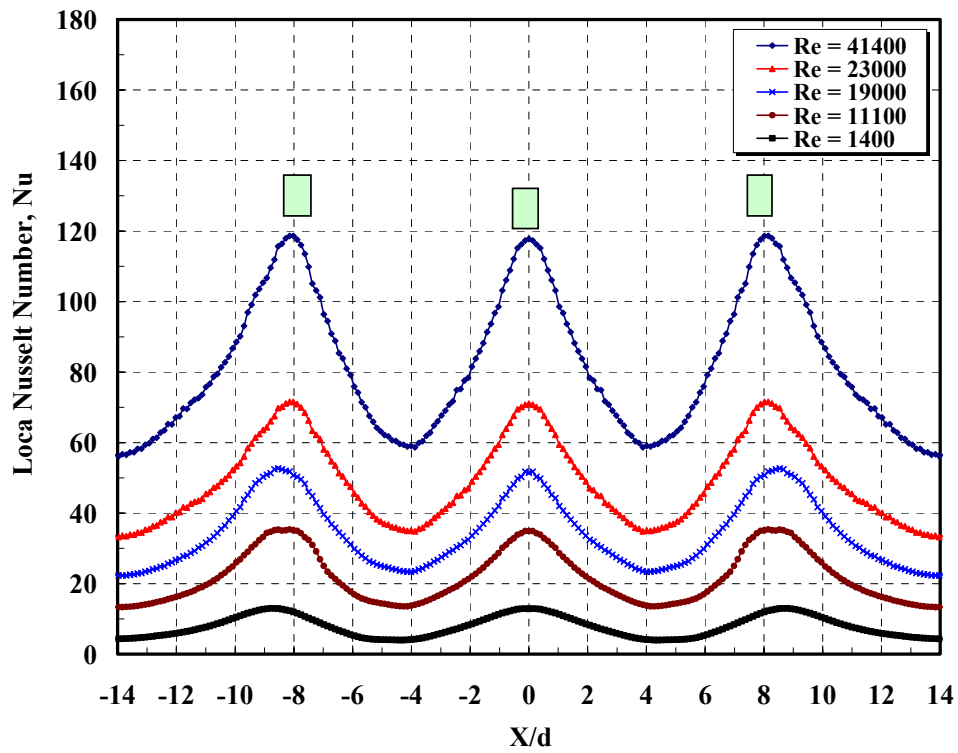


Fig. 5.4d Local Nu Distribution for Hole Channel,  
 $H/d = 8$ ,  $S/d = 8$ , and  $t_c/d = 2$

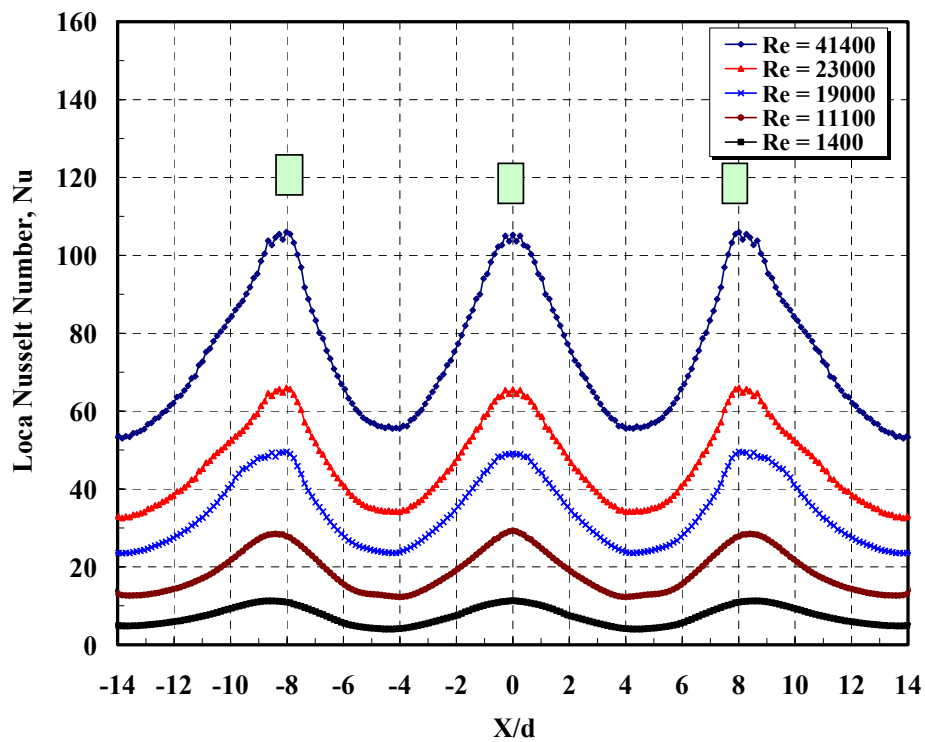


Fig. 5.4e Local Nu Distribution for Hole Channel,  
 $H/d = 10$ ,  $S/d = 8$ , and  $t_c/d = 2$

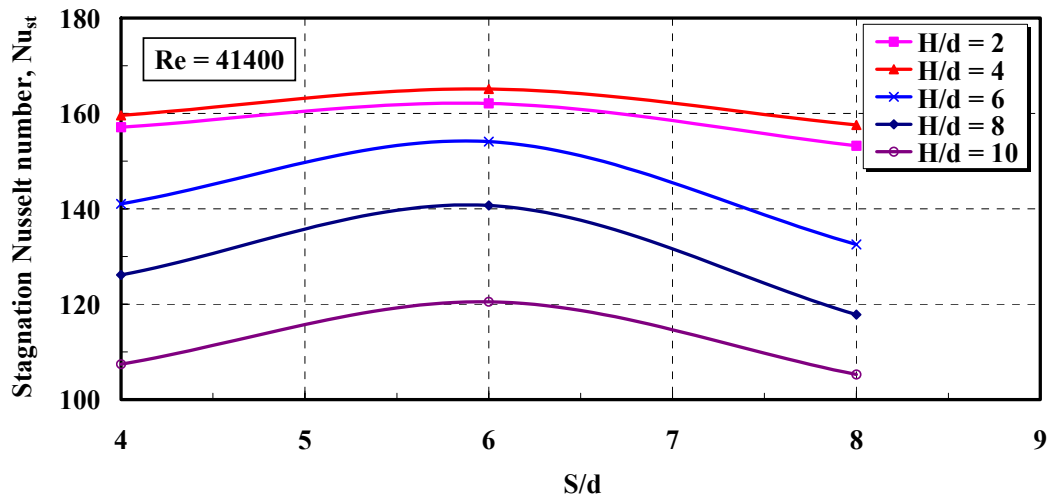


Fig. 5.5a Stagnation Nusselt Number Distribution, Re = 41400

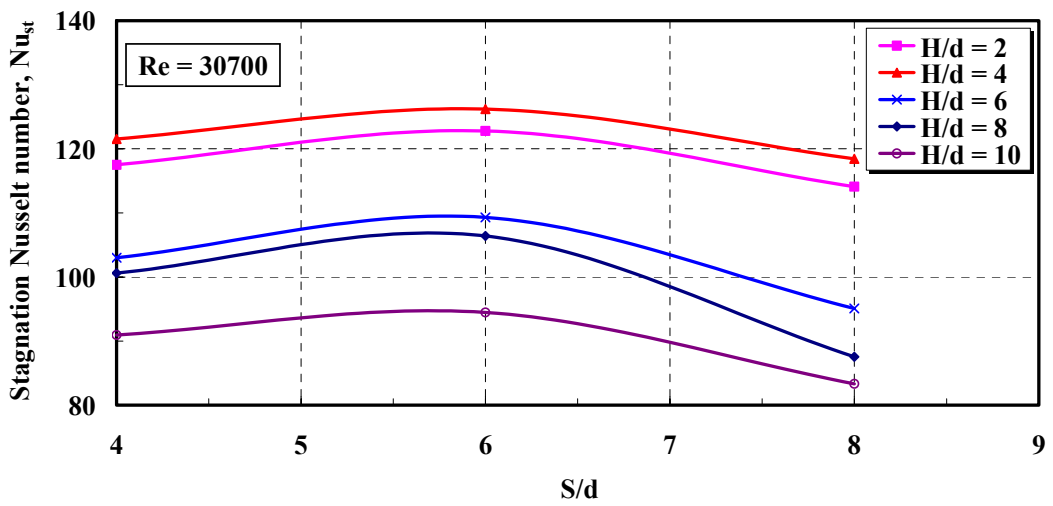


Fig. 5.5b Stagnation Nusselt Number Distribution, Re = 30700

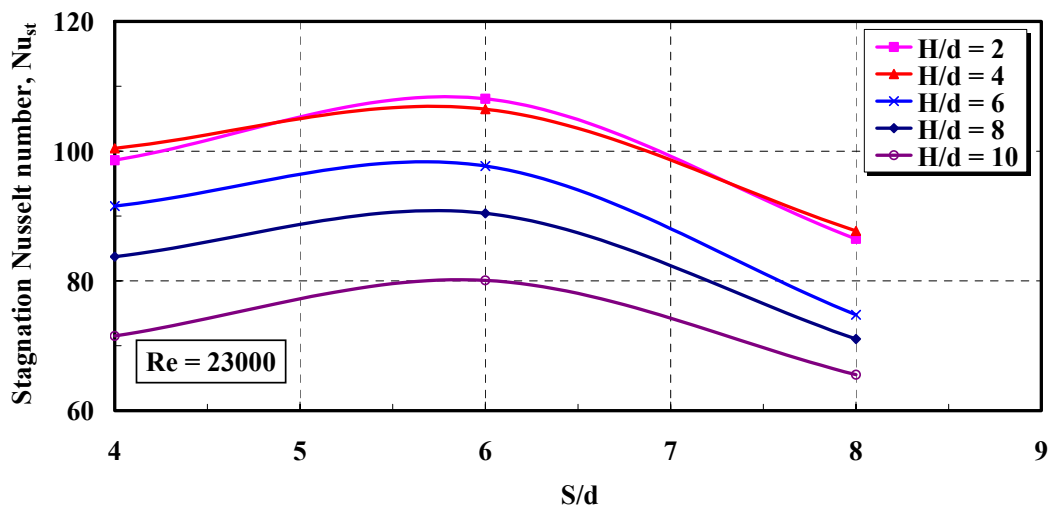


Fig. 5.5c Stagnation Nusselt Number Distribution, Re = 23000

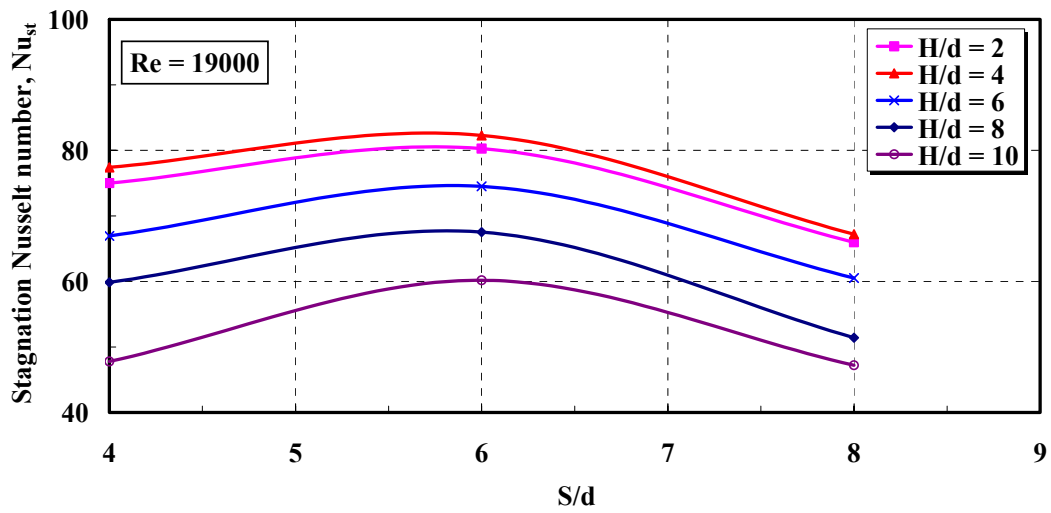


Fig. 5.5d Stagnation Nusselt Number Distribution, Re = 19000

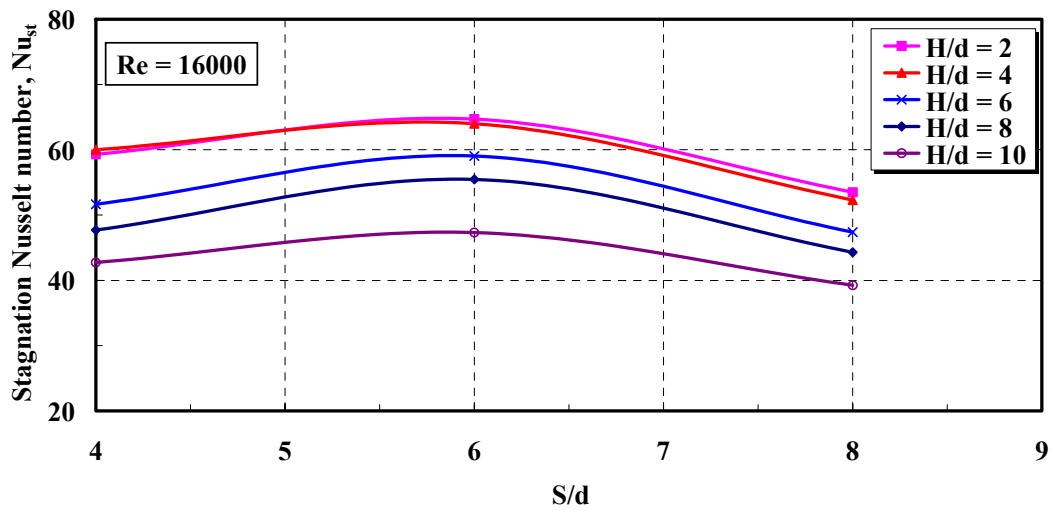


Fig. 5.5e Stagnation Nusselt Number Distribution, Re = 16000

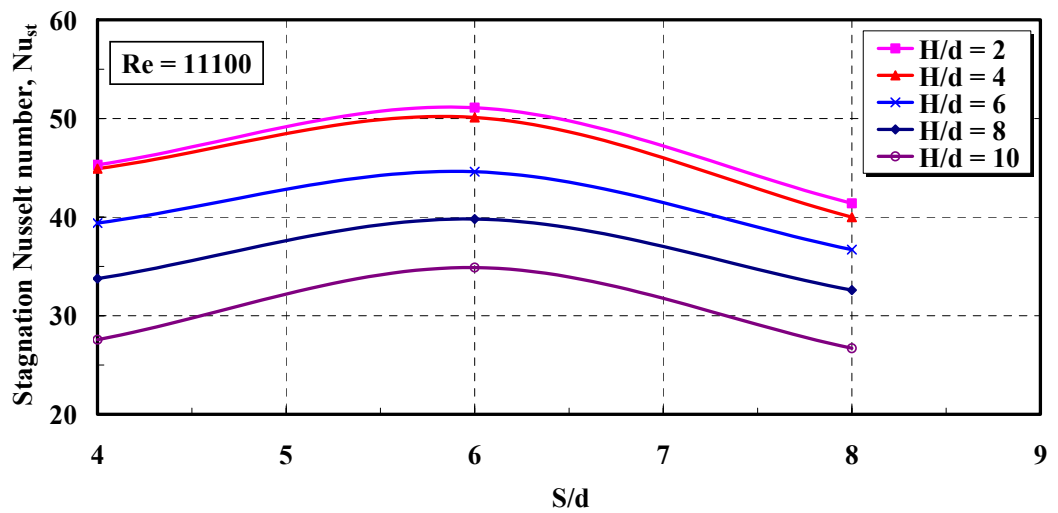


Fig. 5.5f Stagnation Nusselt Number Distribution, Re = 11100

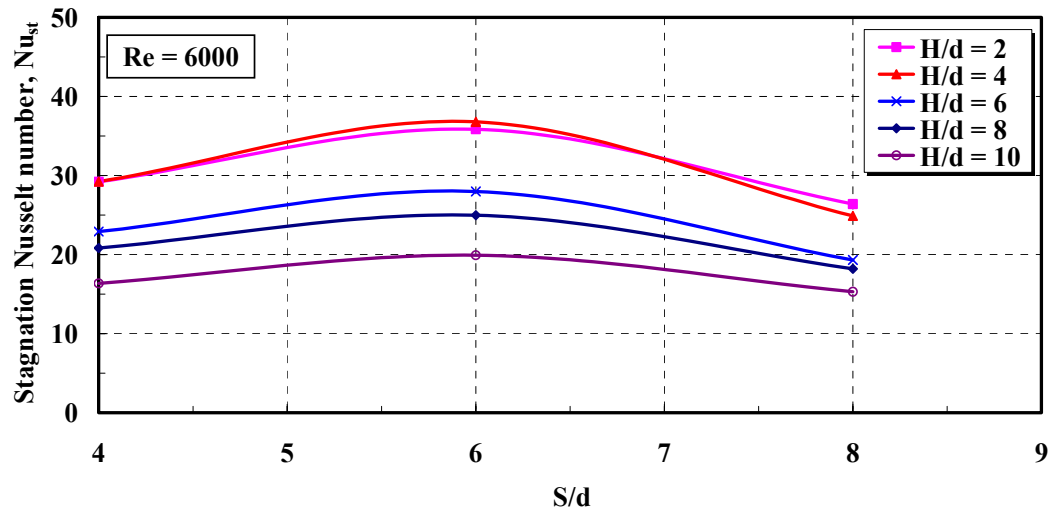


Fig. 5.5g Stagnation Nusselt Number Distribution, Re = 6000

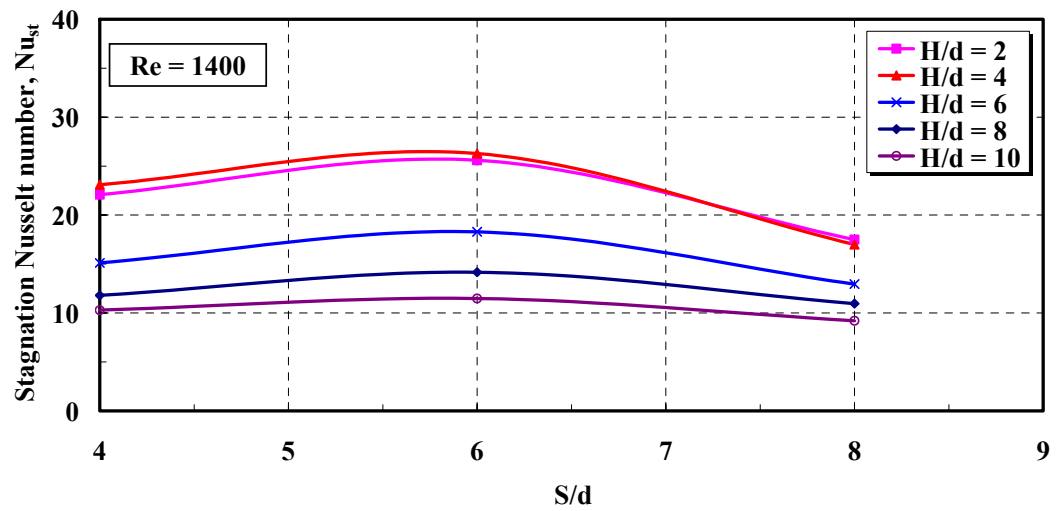


Fig. 5.5h Stagnation Nusselt Number Distribution, Re = 1400

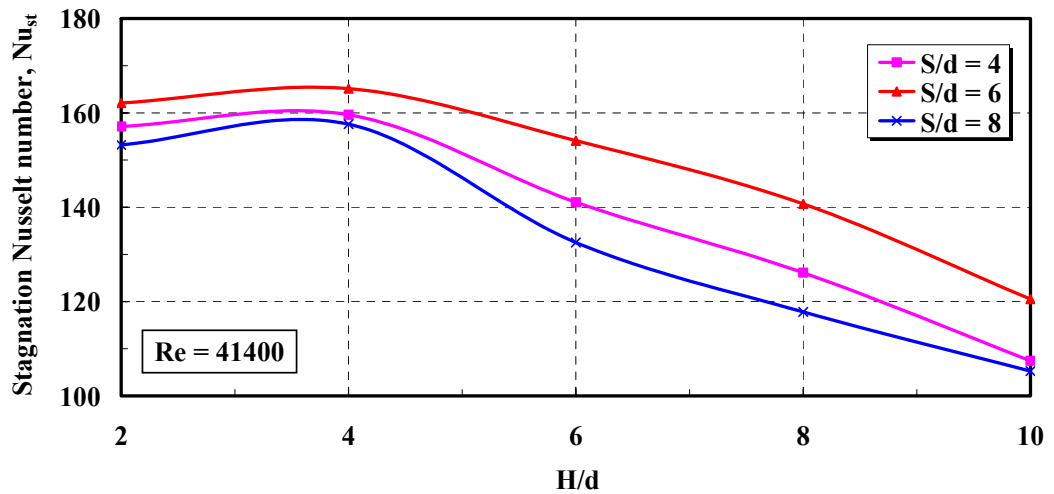


Fig. 5.6a Stagnation Nusselt Number Distribution, Re = 41400

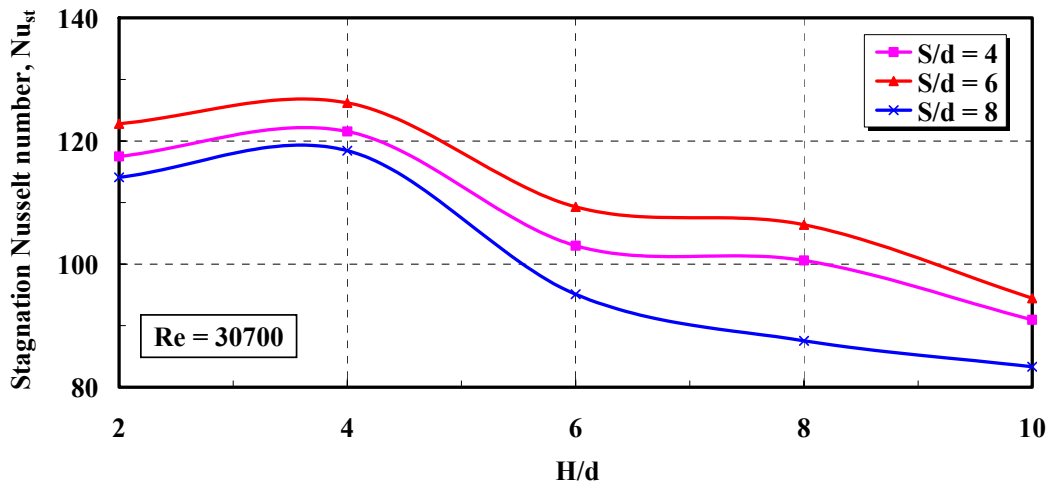


Fig. 5.6b Stagnation Nusselt Number Distribution, Re = 30700

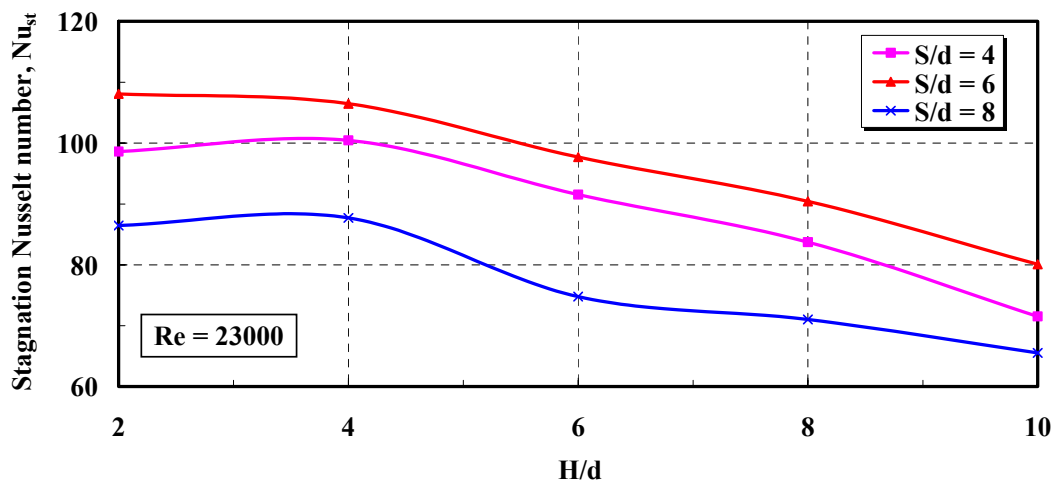


Fig. 5.6c Stagnation Nusselt Number Distribution, Re = 23000

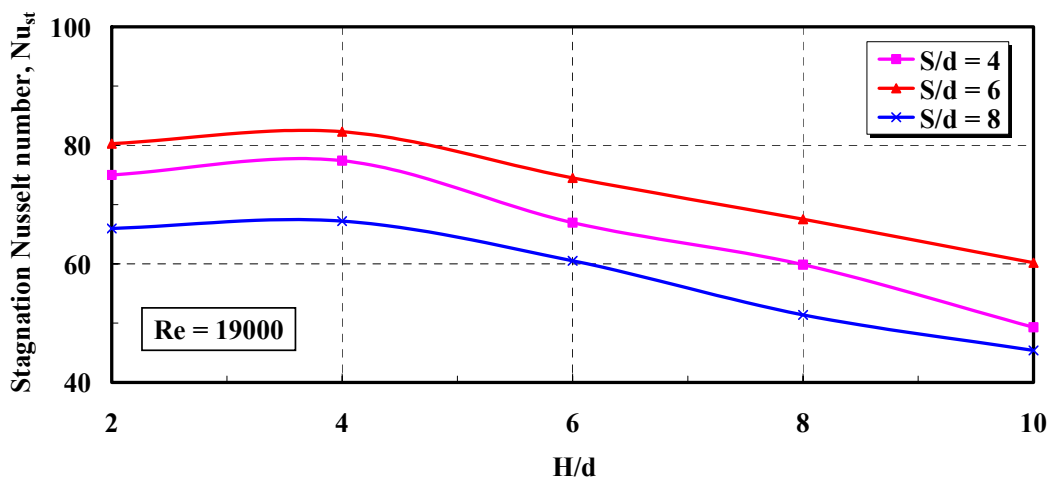


Fig. 5.6d Stagnation Nusselt Number Distribution, Re = 19000

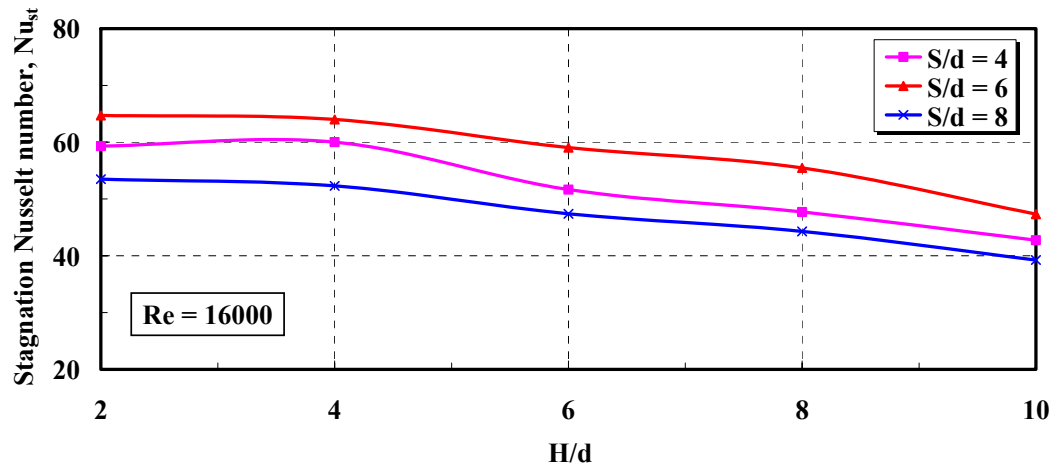


Fig. 5.6e Stagnation Nusselt Number Distribution, Re = 16000

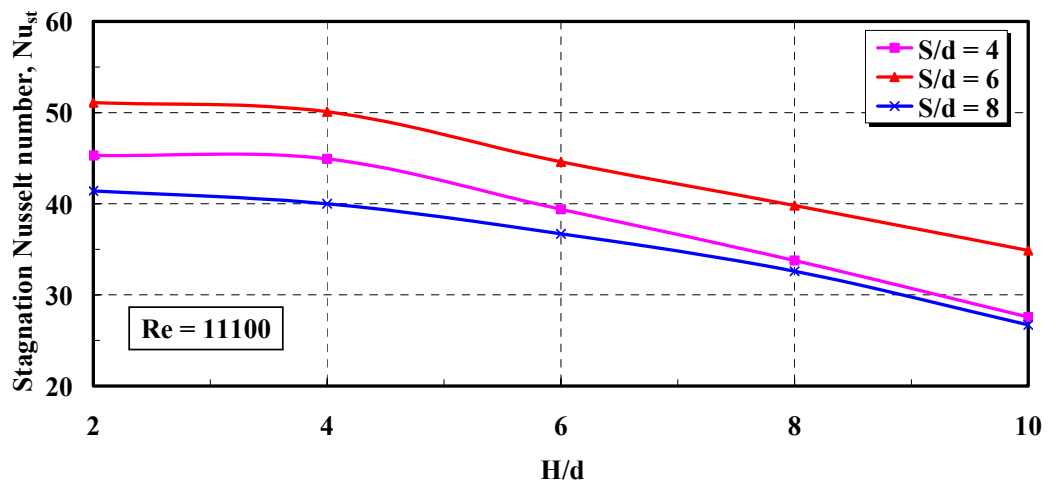


Fig. 5.6f Stagnation Nusselt Number Distribution, Re = 11100

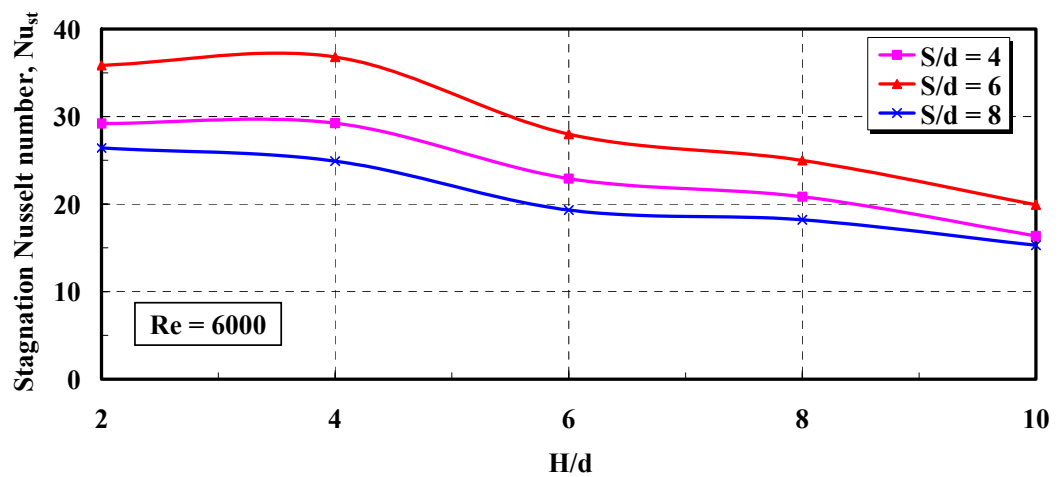


Fig. 5.6g Stagnation Nusselt Number Distribution, Re = 6000

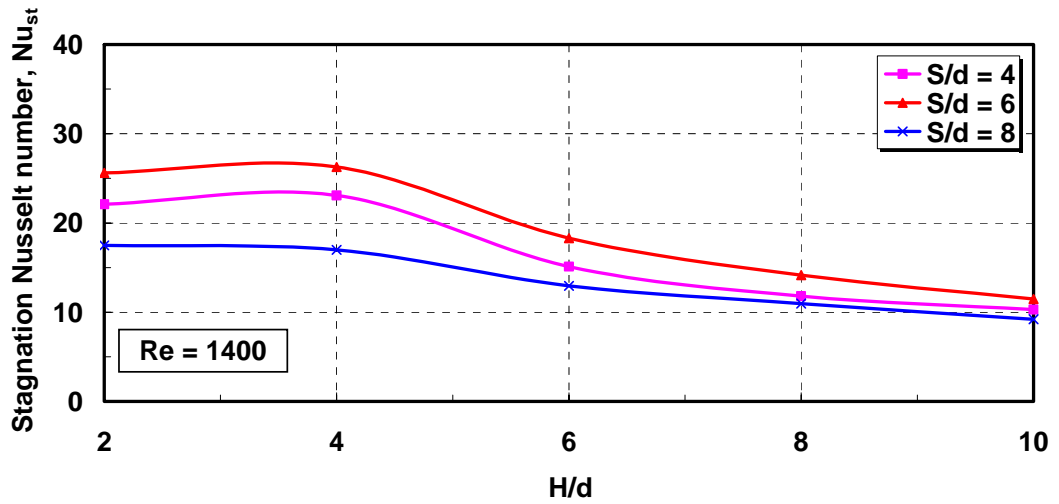


Fig. 5.6h Stagnation Nusselt Number Distribution, Re = 1400

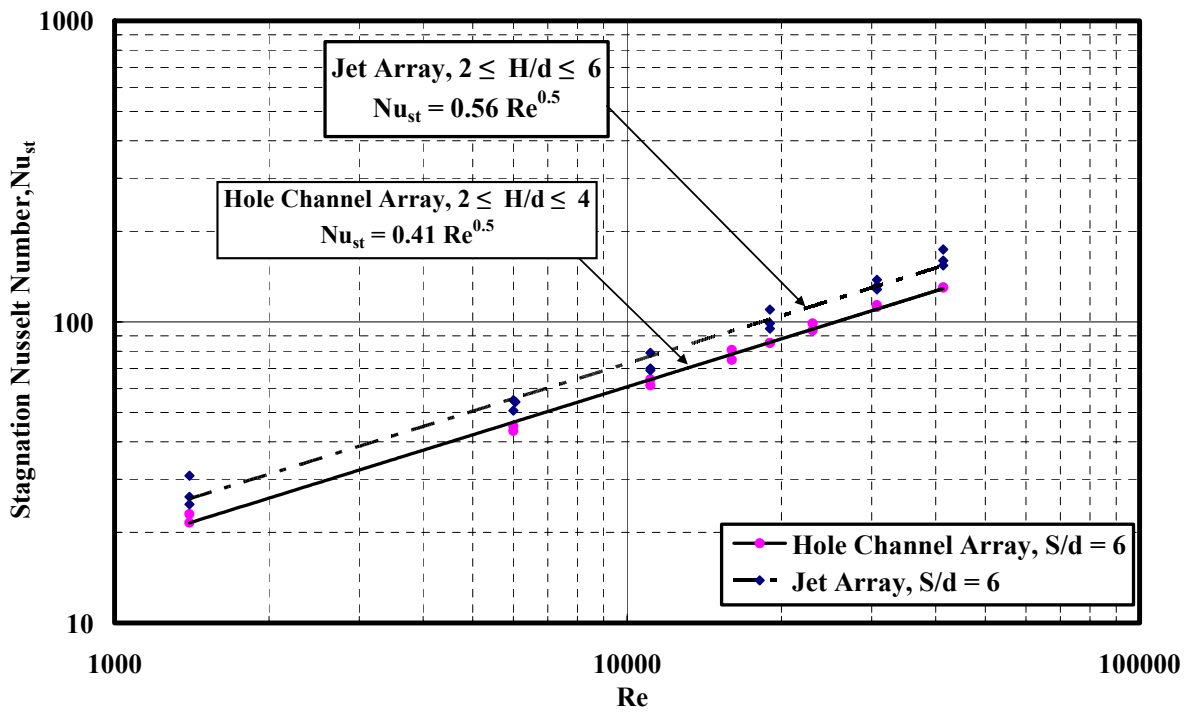


Fig. 5.7 Stagnation Nusselt Number Variation with Jet Reynolds Number

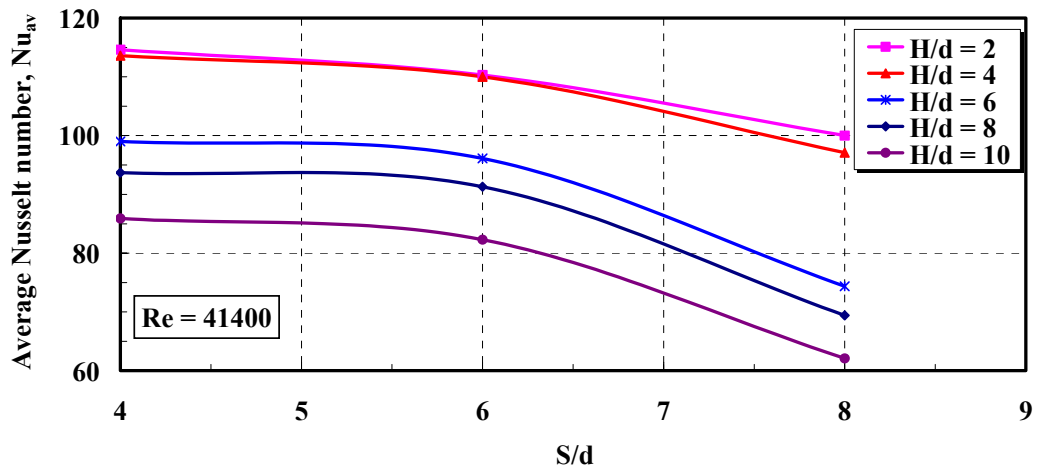


Fig. 5.8a Average Nusselt Number Distribution,  $Re = 41400$

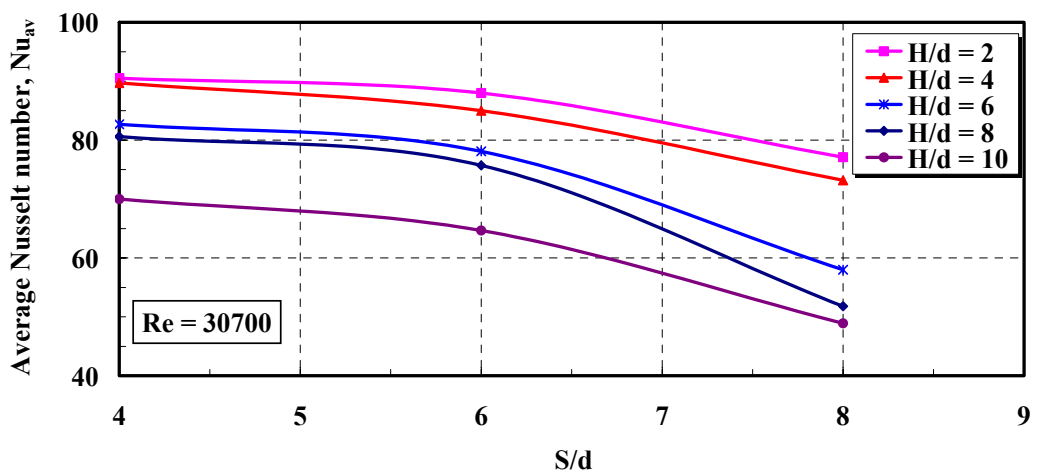


Fig. 5.8b Average Nusselt Number Distribution,  $Re = 30700$

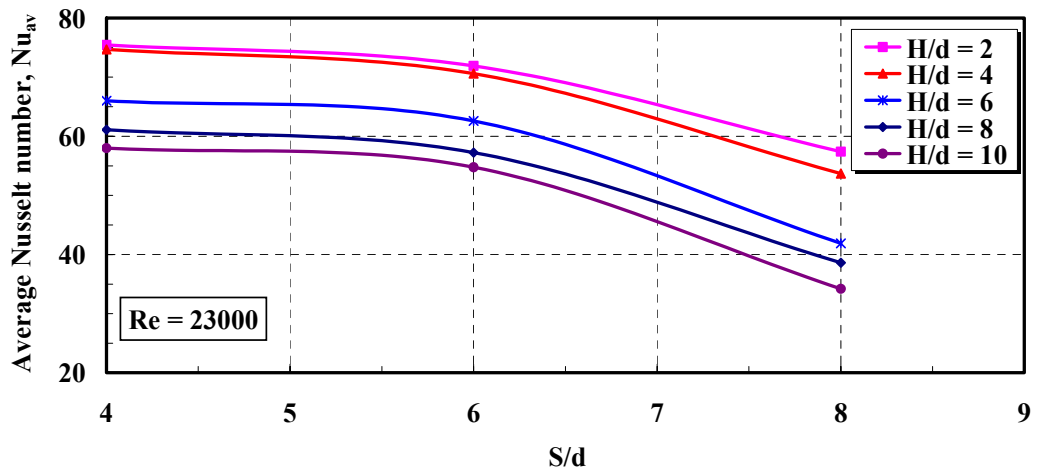


Fig. 5.8c Average Nusselt Number Distribution,  $Re = 23000$

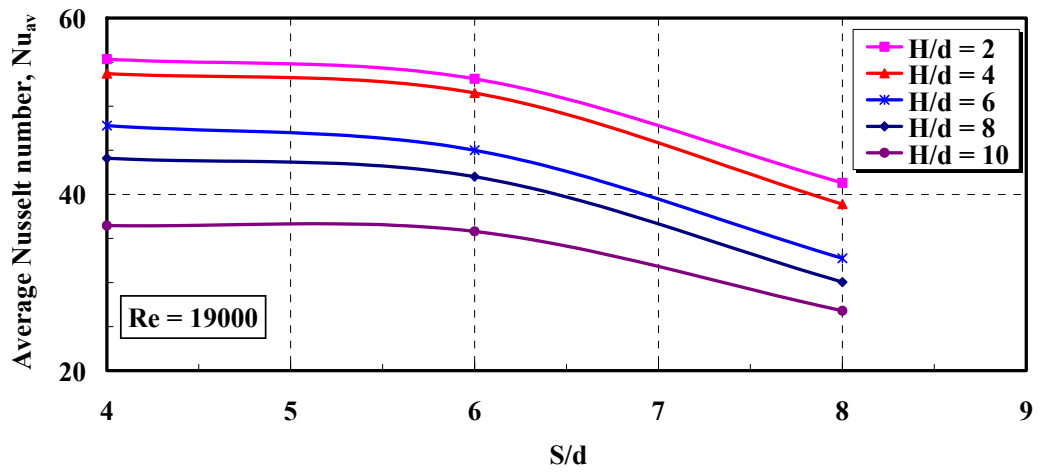


Fig. 5.8d Average Nusselt Number Distribution,  $Re = 19000$

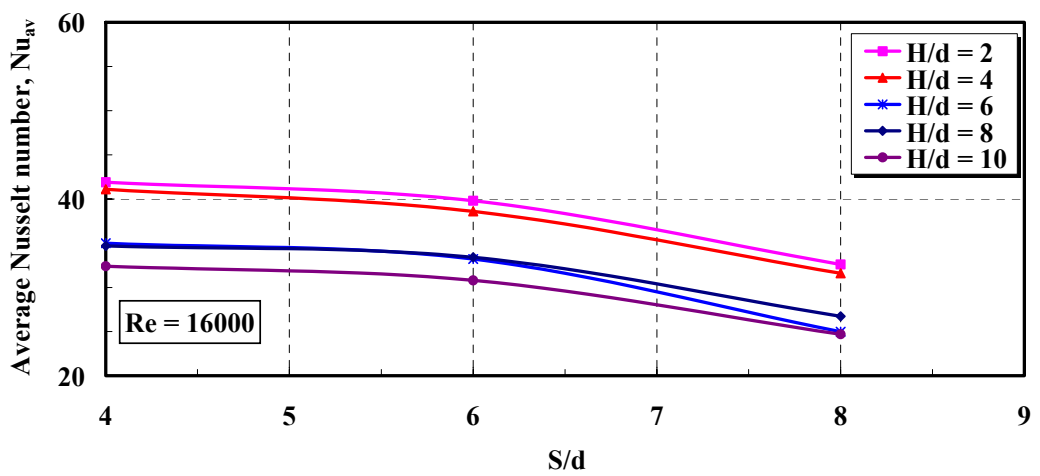


Fig. 5.8e Average Nusselt Number Distribution,  $Re = 16000$

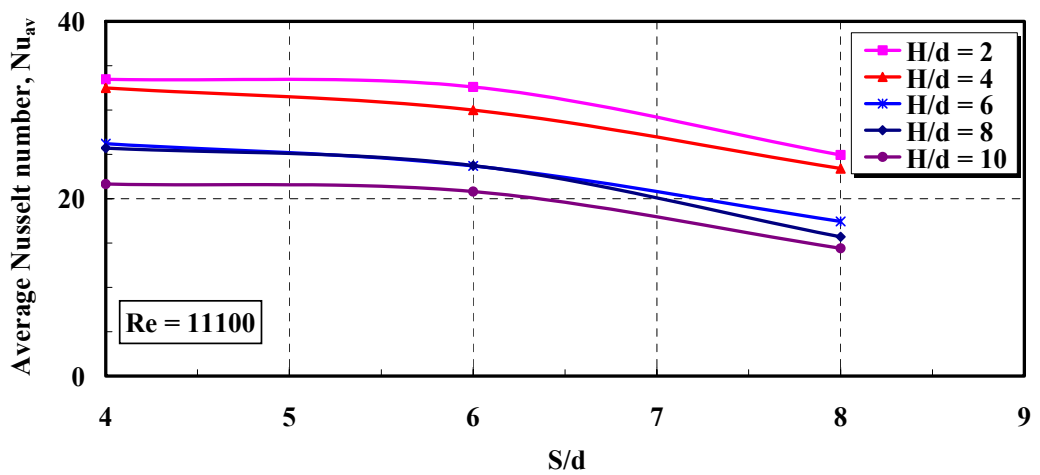


Fig. 5.8f Average Nusselt Number Distribution,  $Re = 11100$

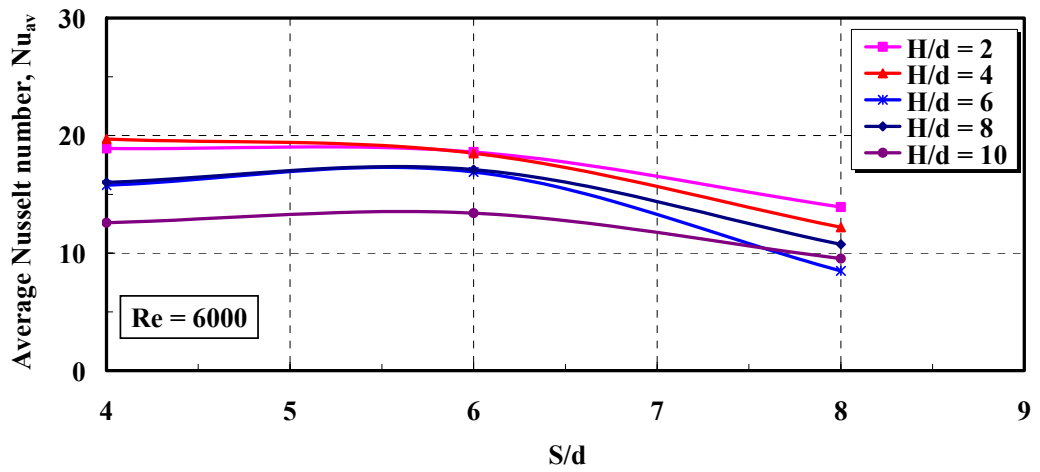


Fig. 5.8g Average Nusselt Number Distribution,  $Re = 6000$

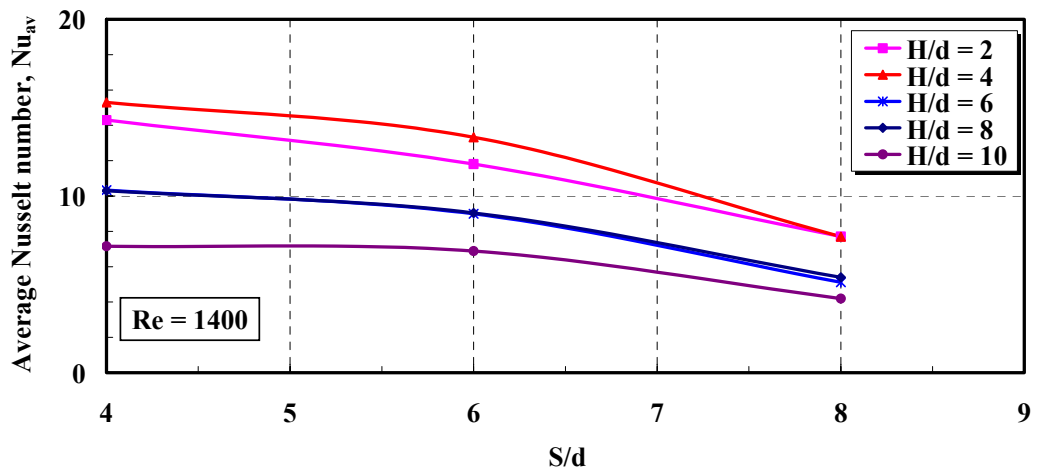


Fig. 5.8h Average Nusselt Number Distribution,  $Re = 1400$

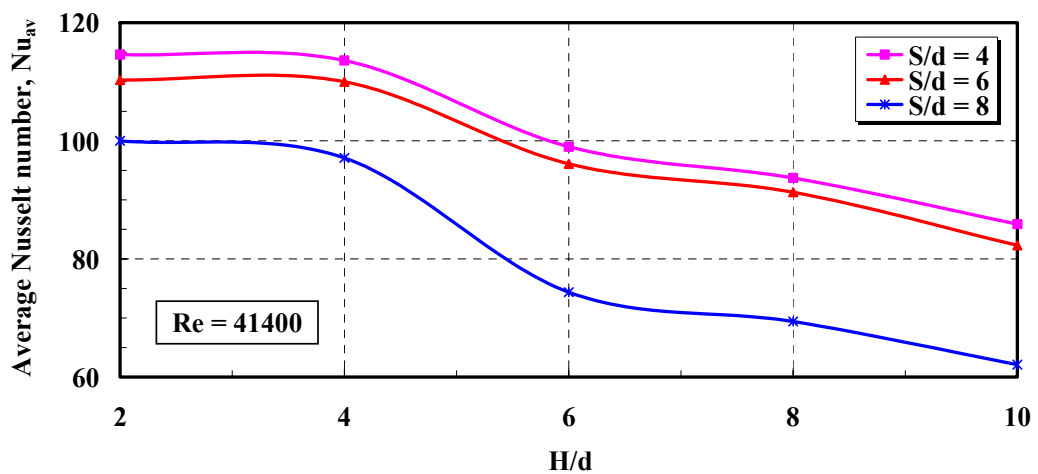


Fig. 5.9a Average Nusselt Number Distribution,  $Re = 41400$

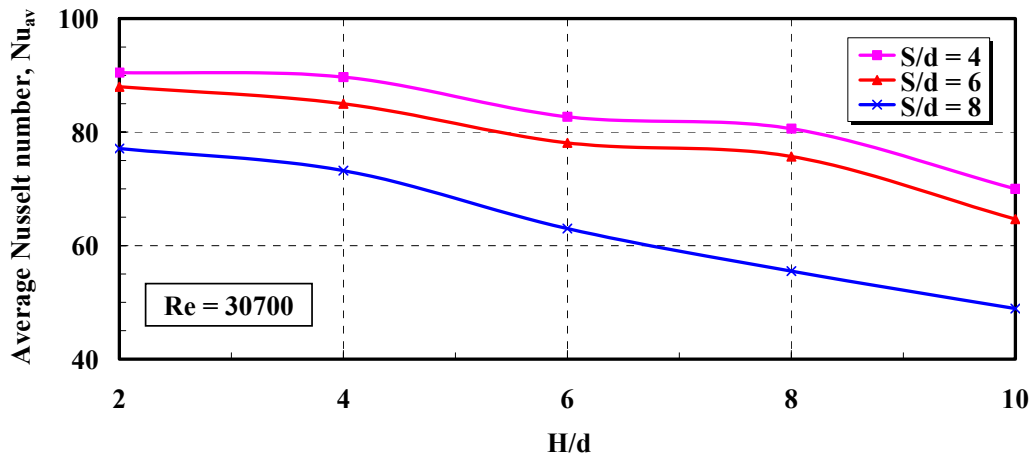


Fig. 5.9b Average Nusselt Number Distribution, Re = 30700

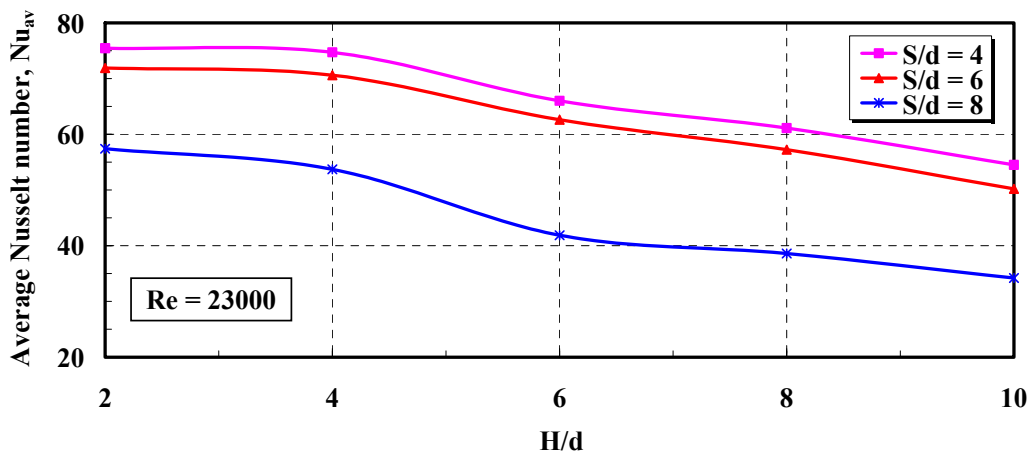


Fig. 5.9c Average Nusselt Number Distribution, Re = 23000

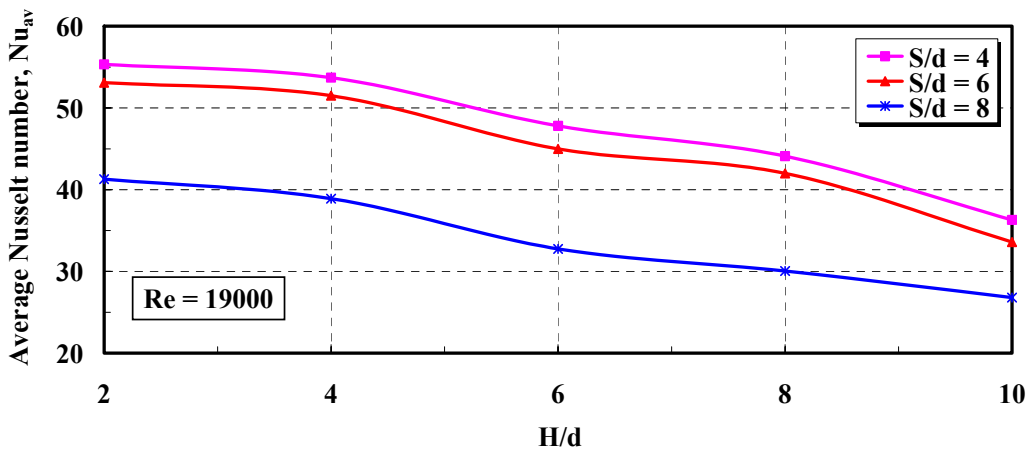


Fig. 5.9d Average Nusselt Number Distribution, Re = 19000

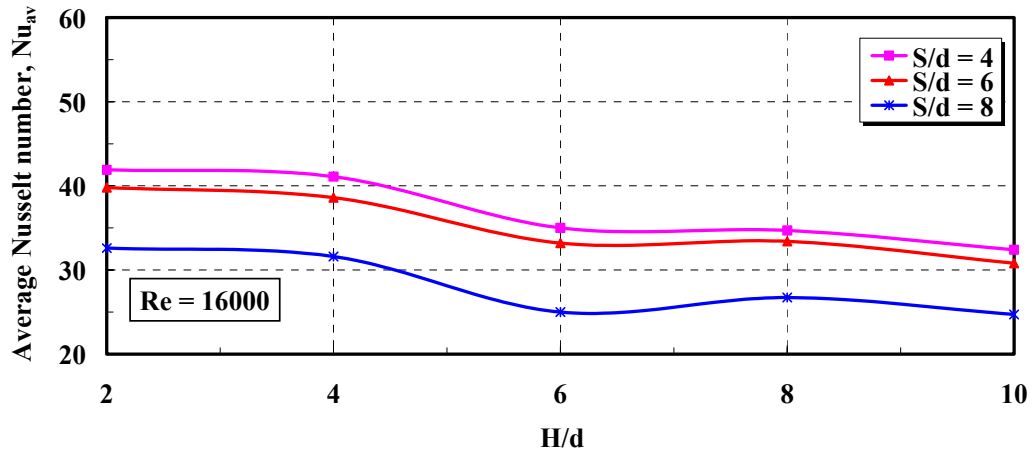


Fig. 5.9e Average Nusselt Number Distribution,  $Re = 16000$

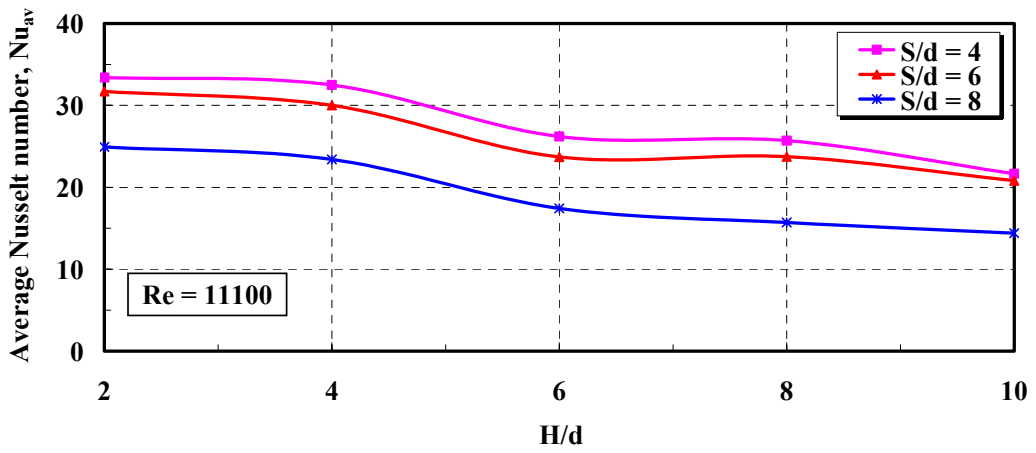


Fig. 5.9f Average Nusselt Number Distribution,  $Re = 11100$

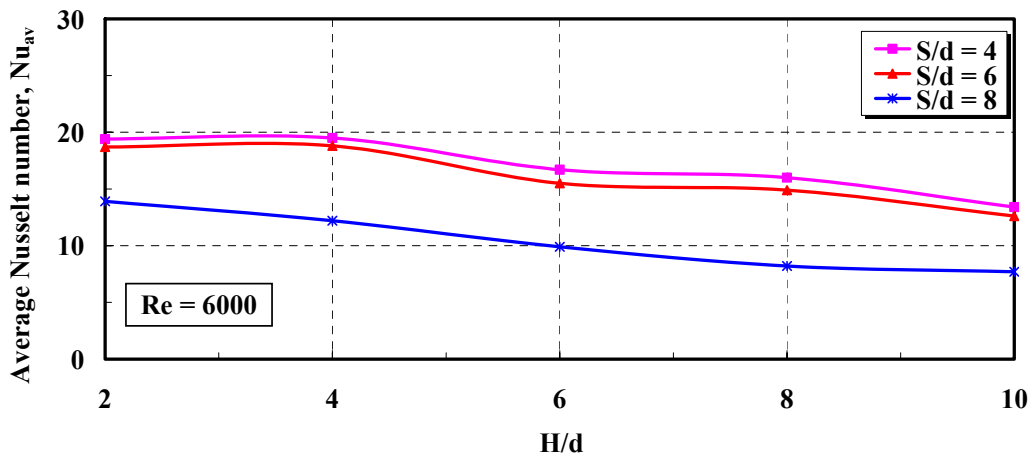


Fig. 5.9g Average Nusselt Number Distribution,  $Re = 6000$

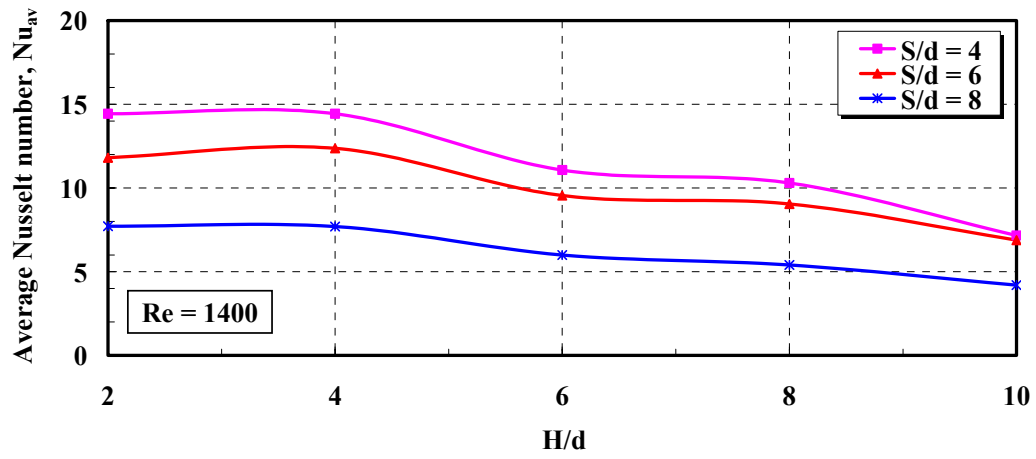


Fig. 5.9h Average Nusselt Number Distribution, Re = 1400

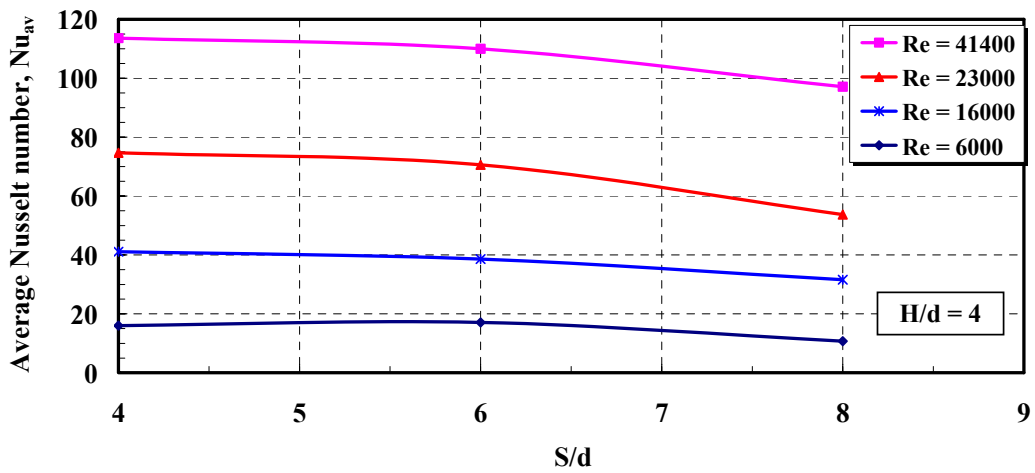


Fig. 5.10a Average Nusselt Number Distribution, H/d = 4

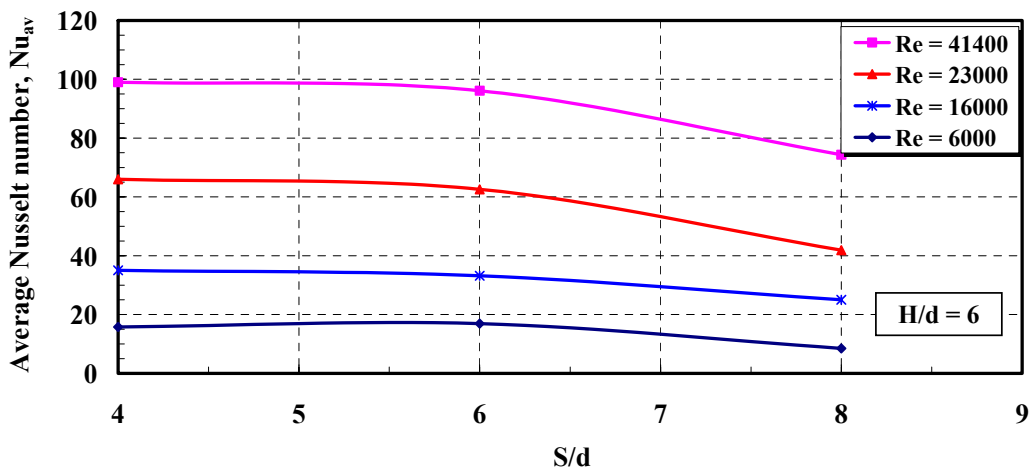


Fig. 5.10b Average Nusselt Number Distribution, H/d = 6

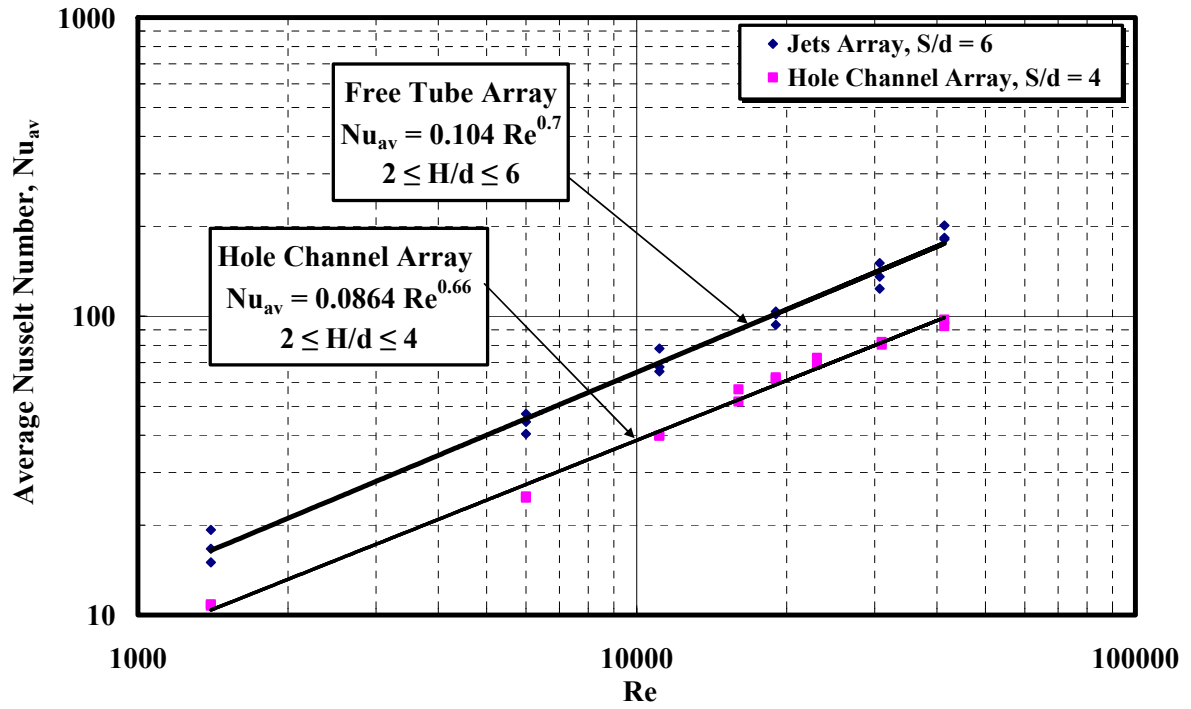


Fig. 5.11 Average Nusselt Number Variation with Jet Reynolds Number

## Uniformity of Heat Transfer for Multiple Free Jets

### 6-1 Introduction:

The need for a uniformity heat transfer over impingement plate is very important in many industrial processes such as drying of textile and paper industry, the tempering of glass sheets and the cooling of moving metal strips [8]. The last application has been illustrated through the paper presented at the QIRT2000 conference in which experimental study of array of slot nozzles are discussed [9]. The aim of this chapter is to compute the heat transfer uniformity over the impingement surface for in-line and staggered arrays and hole channels. The uniformity degree,  $U_n$ , is given from the following relation;

$$U_n = \frac{(\text{Nu}_{\text{avl}})_{\text{min}}}{(\text{Nu}_{\text{avl}})_{\text{max}}} \quad (6-1)$$

To estimate the uniformity over the impingement plate, the average heat transfer over the minimum and maximum lines must to be computed as explained in chapter three.

### 6-2 Uniformity of Heat Transfer:

#### 6-2-1 Uniformity of Heat Transfer for In-line Array:

This section explains the uniformity of heat transfer for in-line array. The maximum heat transfer line is placed through the stagnation points, while the minimum heat transfer line is located in the midway between adjacent jets for in-line array as shown in Fig. 6.1a-b. Figs. 6.2a-e illustrate the effect of the separation distance  $H/d$  on the maximum and minimum average heat transfer of in-line arrays for the following spacing distances,  $S/d = 2, 4, 6, 8,$  and  $10$ . They are based on two Reynolds numbers of 41400 and 19000. It was found that at small spacing distance of  $S/d = 2$  and with the increase of separation

distance  $H/d \geq 6$ , the uniformity is pronounced. For spacing distances  $S/d \leq 8$ , the difference between the maximum and minimum heat transfer are large approximately 67-73%. In addition, the separation distance has no effect on the average heat transfer in the range of  $1 \leq H/d \leq 5$  for two Reynolds numbers. Fig. 6.3 shows the influence of spacing distance  $S/d$  on the maximum and minimum average line Nusselt number. This figure is based on the same two Reynolds numbers and separation distance of  $H/d = 4$ . From this figure it can be seen that the maximum value for both maximum and minimum average line Nusselt number is corresponding to the spacing distance of  $S/d = 6$ . For high Reynolds number ( $Re = 41400$ ) the maximum value is more obviously than that at the low Reynolds numbers. In addition the values of maximum and minimum average heat transfer are nearly constant in the range of spacing distance of  $2 \leq S/d \leq 4$ . The ratio between the maximum and minimum average heat transfer are plotted with spacing distance  $S/d$  for two Reynolds number in Fig. 6.4. This figure is based on separation distance  $H/d$  is 4, and shows that the change in uniformity degree is small in the range of spacing distance of  $2 \leq S/d \leq 8$ . At higher spacing distance  $S/d > 8$  there is a higher rate of decrease in this degree.

Figures 6.5a-e presents the maximum, average, and minimum values of the Nusselt number as a function of Reynolds number for in-line array. The uniformity degree,  $Un$ , calculated based on the data in the above figures. The higher value of  $Un$  was from 86 to 80% for spacing distance  $S/d = 2$ , this is because the interference between adjacent jets is occurred before the flow impinging with the surface. In this case, the multiple jets are considered as one jet [2, 3]. For spacing distance  $S/d = 10$ , the interference between jets occurs after impinging with the surface and in the same time, the cross flow is strong in wall jet region. As a result of the above, the heat transfer rate decreases and the uniformity degree over the impinging surface is reduced to 50% and 45% for low and high Reynolds numbers respectively. In general the Nusselt number for in-line array can be represented as follows;

$$\text{Nu}_{\text{avl}} = c \cdot \text{Re}^m \quad (6-2)$$

where the value of the exponent  $m$  is 0.7, and the value of constant  $c$  is from 0.015 to 0.1107 for average line Nusselt number. While this value for average Nusselt number is from 0.03 to 0.104. The value of constant  $c$  is depended on the Reynolds number, separation distance, and spacing distance.

To estimate the uniformity heat transfer over impingement surface, the heat transfer should measured for in-line array with un-equal spacing distance. In this case, the jets arranged in in-line array with fixed spacing distance in the Y direction  $S_y/d = 6$ , and the spacing distance in the X direction  $S_x/d = \{3, 4, \text{ and } 4.5\}$ . Figs. 6.6 a-c show the effect of the separation distance on the maximum and minimum heat transfer for in-line array with different spacing distances  $S_x/S_y = 0.5, 0.67, \text{ and } 0.75$ . They are based on the same two Reynolds numbers. The maximum and minimum heat transfer are nearly constants in the separation distance range  $2 \leq H/d \leq 4$ , for the two Reynolds numbers. From these figures it can be noted that, the uniformity degree is nearly constant for three cases of  $S_x/S_y$ , and it equal about 80%.

### **6-2-2 Uniformity of Heat Transfer for Staggered Array:**

The uniformity degree of the heat for the staggered array will be illustrated in this section. The maximum heat transfer line is placed through the stagnation points, while the minimum heat transfer line located in the midway between adjacent jets for staggered as shown in Fig. 6.8a. Fig. 6.8b shows the maximum and minimum heat transfer distribution for staggered array. This figure is based on spacing distance of  $S/d = 8$  and separation distance of  $H/d = 2$  for Reynolds number of 30700. It can be noted that the value of average heat transfer over line A is the higher in the radial distance range of  $0 \leq X/d \leq 3$ . But in the radial distance range of  $3 \leq X/d \leq 10$ , the line B provides the maximum value of heat transfer. Figs. 6.9 a-e show the average heat transfer for maximum and minimum positions as function of separation distance for all spacing distances

$S/d$ . In these figures it's found that, the maximum and minimum heat transfers are nearly constant for the separation distance from 2 to 5. This is because of the impingement plate is located within the potential core length. Fig. 6.10 shows the effect of spacing distance on the maximum and minimum average Nusselt number. This figure was plotted at Separation distance equal to 4 and for two Reynolds numbers. Also the maximum position of the heat transfer is occurring at spacing distance equal 6 again for two Reynolds numbers. Fig. 6.11 presents the ratio between the maximum and minimum average heat transfer for staggered array at separation distance of  $S/d = 4$ , for the same different Reynolds numbers in Fig. 6.4. It can be seen that the uniformity degree is nearly constant and equal to 0.97 in the spacing distance range of  $2 \leq S/d \leq 8$  for both Reynolds numbers. This indicates that the different between the maximum and minimum average heat transfer is very small. Therefore the uniformity degree for heat transfer is very high in the case of staggered array.

In Figs. 6.12 a-e, the maximum, minimum, and average heat transfers are plotted with Reynolds number. The uniformity degree of the heat transfer is calculated from the above figures, the value of this uniformity degree is to be 97% for high and low Reynolds numbers for small spacing distance of ( $S/d = 2$ ). This value is about 86% and 65% for high and low Reynolds number respectively at spacing distance increase to  $S/d = 10$ . From these figures, it can be noted that the value of the constant  $c$  in equation (6-2) is from 0.028 to 0.1097, while the exponent of Reynolds number  $m$  is 0.7 as that for in-line array.

### **6-2-3 Uniformity of Heat Transfer for Hole Channel Array:**

Figures 6.13 a-c show the effect of the separation distance on the maximum and minimum heat transfer. For the separation distance range of  $2 \leq H/d \leq 4$ , both the maximum and minimum heat transfer are nearly constant value, for the two Reynolds numbers. Then the values of both maximum and minimum tend to be decreased. Fig. 6.14 presents the average line Nusselt number in

dependence on the spacing distance at separation distance,  $H/d = 4$ . This figure is based on the two Reynolds numbers of 41400 and 19000. It is clear that the spacing distance of  $S/d = 4$  provide the maximum value of heat transfer for both two Reynolds numbers. The uniformity degree of the heat transfer is presented in Fig. 6.15. It can be noted that the uniformity degree decreases with the increases of spacing distance. So the heat transfer in this case, hole channel array, has low uniformity degree than that in the cases of staggered and in-line arrays. Figs. 6.16 a-c show the average and average line Nusselt numbers as a function of Reynolds number for the hole channel array. From these figures, the average line Nusselt number can represent by the above equation (6-2), with Reynolds number exponent is about 0.66 and range of constant  $c$  from 0.0489 to 0.0825.

**6-4 Summary:**

From the previous results it is found that, the uniformity degree of the heat transfer is higher for staggered array and is low for hole channel array. This due to the interaction between jets before impinging with surface is more homogenous and the multiple jets can be considered as one jet for staggered array [1, 2]. Table 1 gives summery for the heat transfer uniformity for in-line, staggered, and hole channel arrays.

**Table-1 Uniformity Degree of Heat Transfer, ( $2 \leq H/d \leq 4$ ,  $Re = 41400$ ):**

Array	Spacing Distance, $S/d$				
	2	4	6	8	10
<b>In-line</b>	86%	81%	80%	73%	50%
<b>Staggered</b>	97%	97%	97%	95%	86%
<b>Hole Channel</b>		80%	64%	58%	
<b>In-line (<math>S_x \neq S_y</math>)</b>	Spacing Distance, $S_x/S_y$				
		<b>0.5</b>	<b>0.67</b>	<b>0.75</b>	<b>1.0</b>
		80%	80.5	78.8%	80%

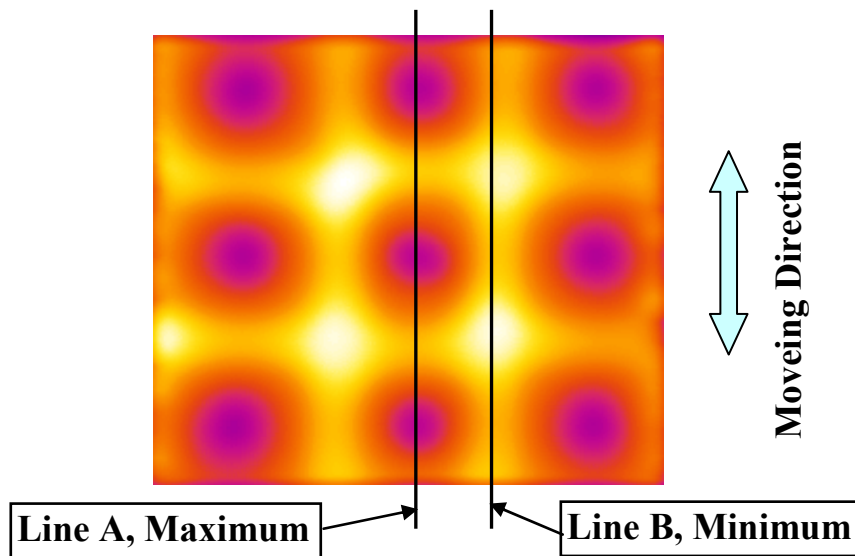


Fig. 6.1a Maximum and Minimum Heat Transfer Positions, for In-line Array

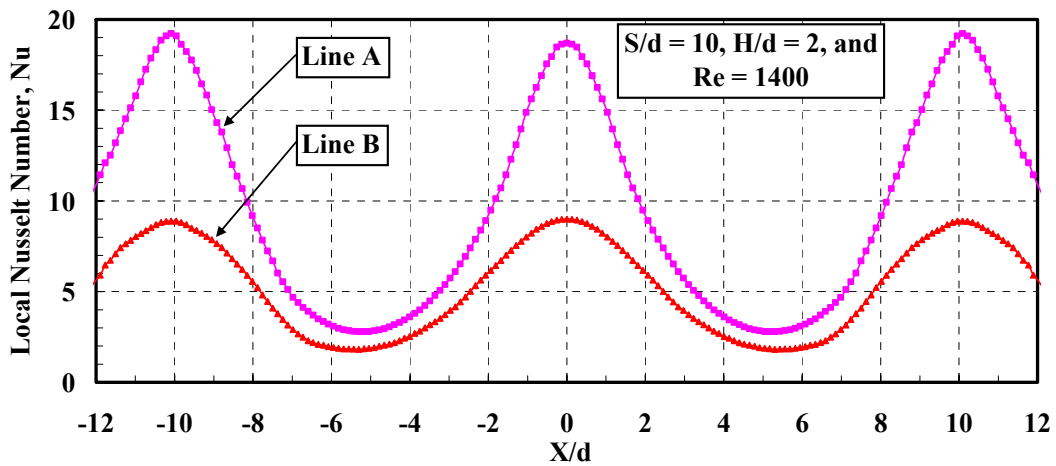


Fig. 6.1b Maximum and Minimum Heat Transfer Distribution, for In-line Array

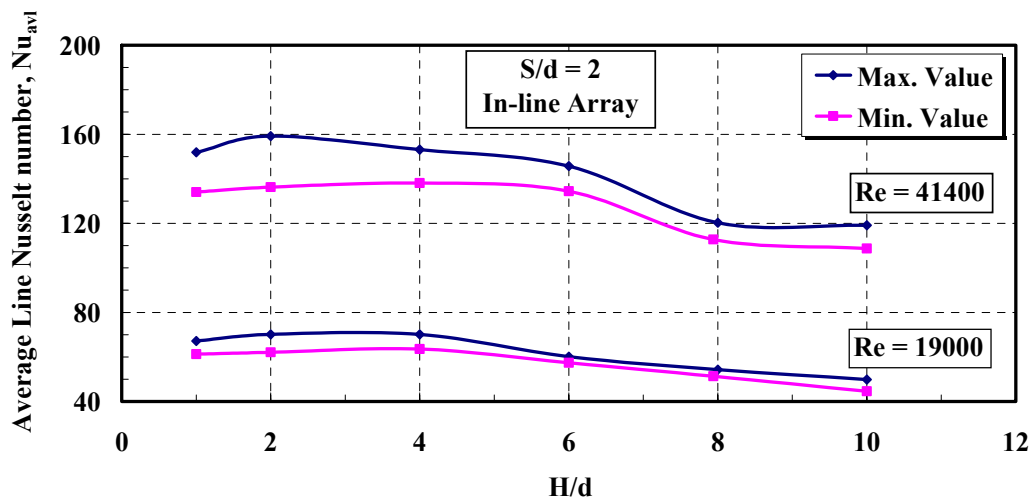


Fig. 6.2a Maximum and Minimum Average Line Nusselt Number for In-line Array,  $S/d = 2$

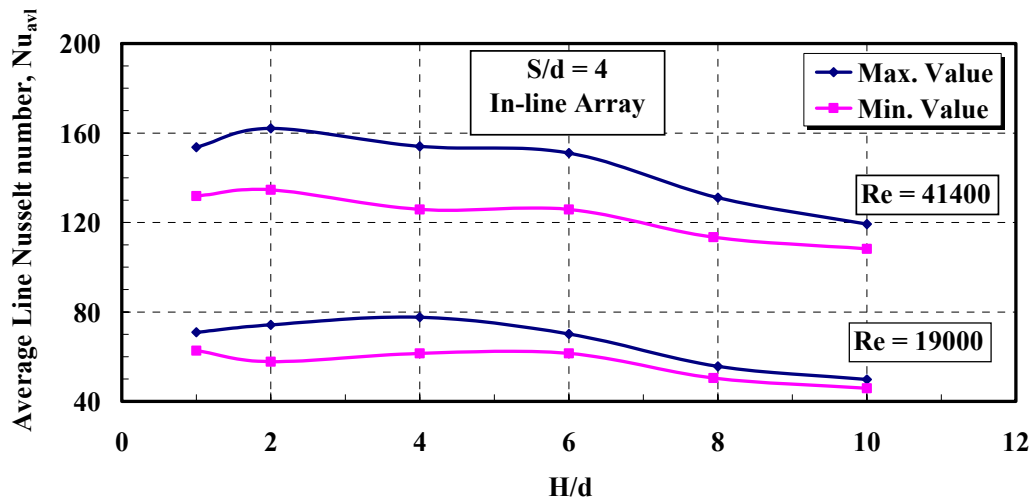


Fig. 6.2d Maximum and Minimum Average Line Nusselt Number for In-line Array,  $S/d = 4$

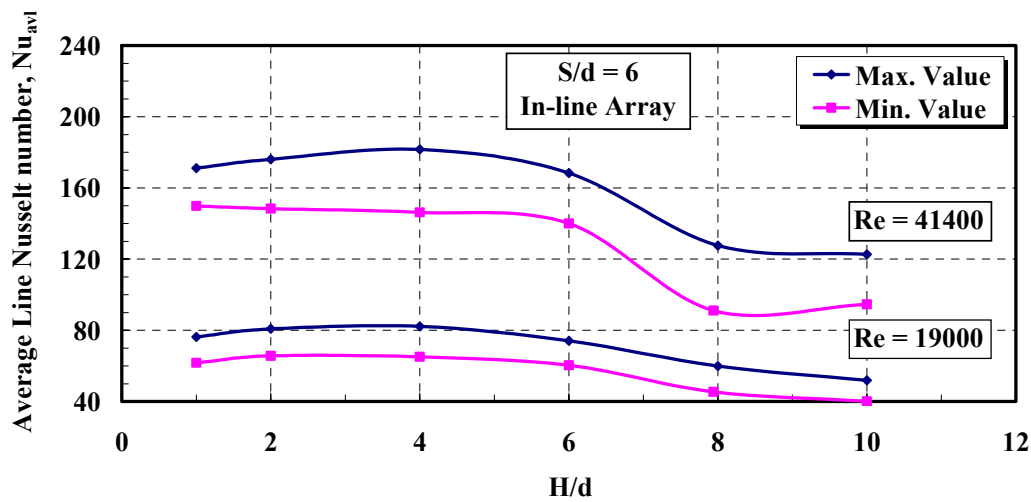


Fig. 6.2c Maximum and Minimum Average Line Nusselt Number for In-line Array,  $S/d = 6$

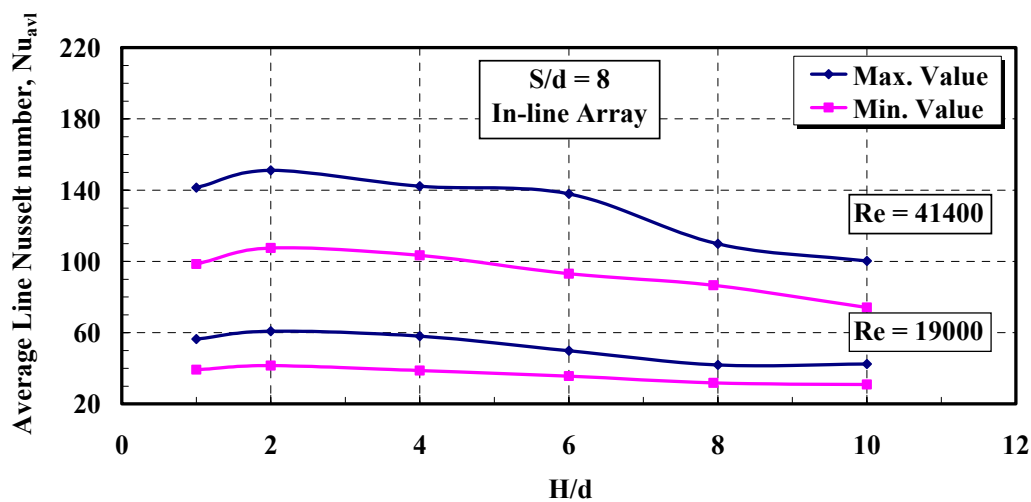


Fig. 6.2d Maximum and Minimum Average Line Nusselt Number for In-line Array,  $S/d = 8$

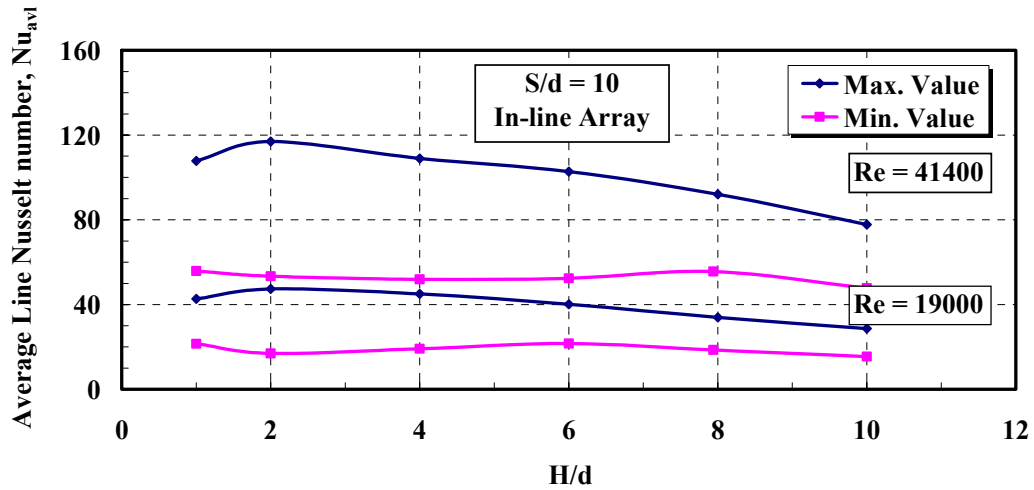


Fig. 6.2e Maximum and Minimum Average Line Nusselt Number for In-line Array,  $S/d = 10$

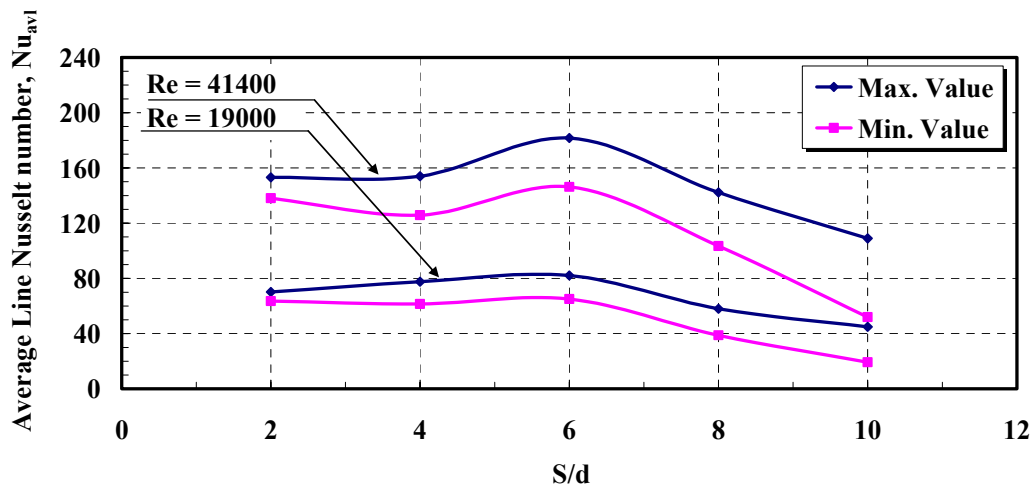


Fig. 6.3 Maximum and Minimum Average Line Nusselt Number for In-line Array,  $H/d = 4$

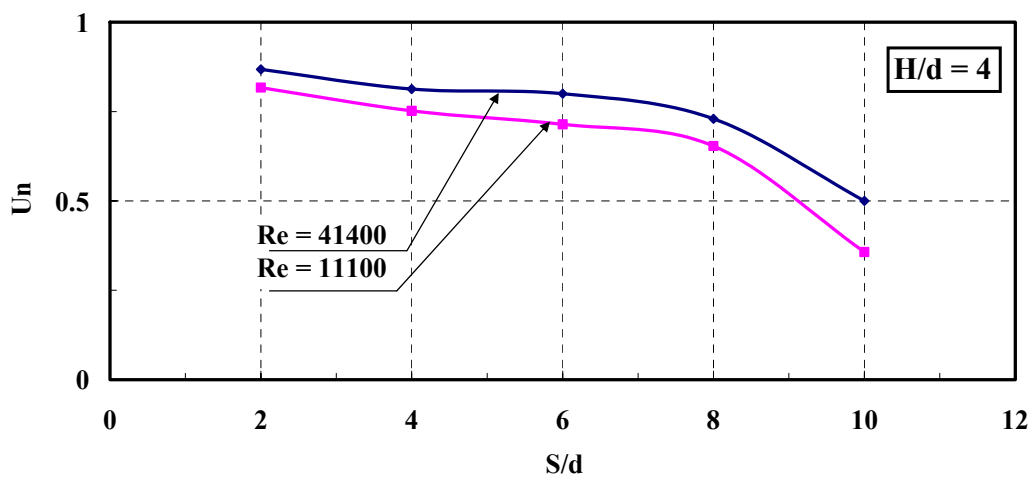


Fig. 6.4 Variation of the Uniformity Degree with the Spacing Distance for In-line Array

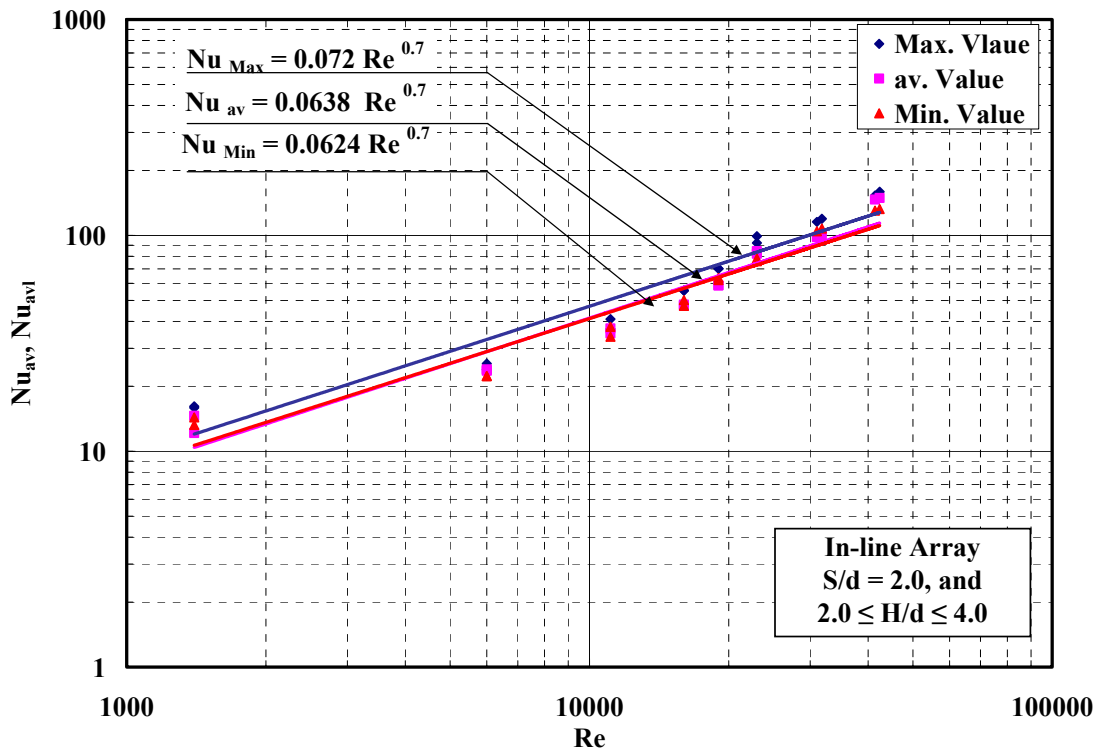


Fig. 6.5a Nusselt Number Variation with Jet Reynolds Number for In-line Array,  $S/d = 2$

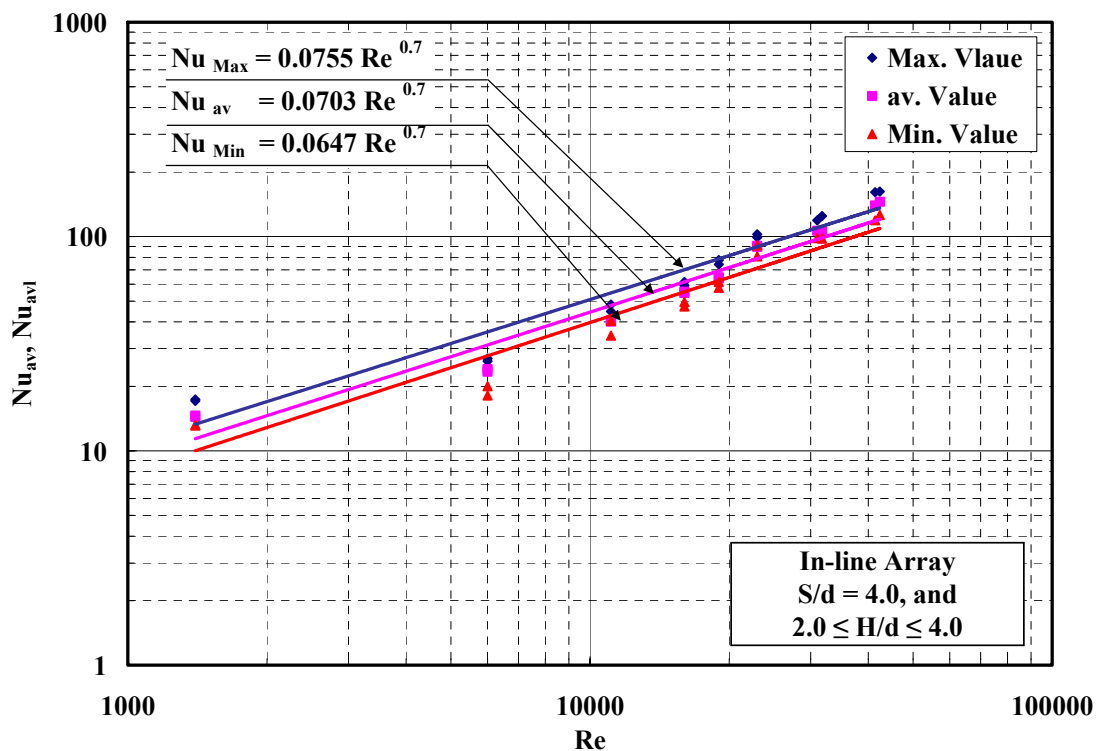


Fig. 6.5b Nusselt Number Variation with Jet Reynolds Number for In-line Array,  $S/d = 4$

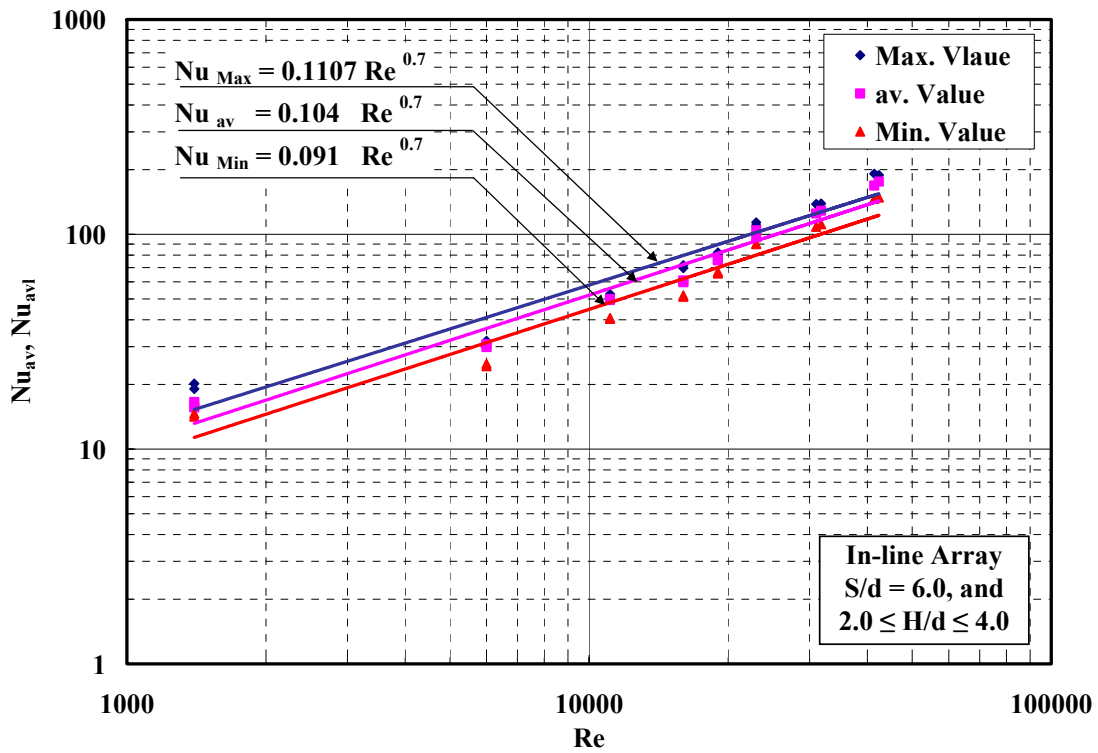


Fig. 6.5c Nusselt Number Variation with Jet Reynolds Number for In-line Array,  $S/d = 6$

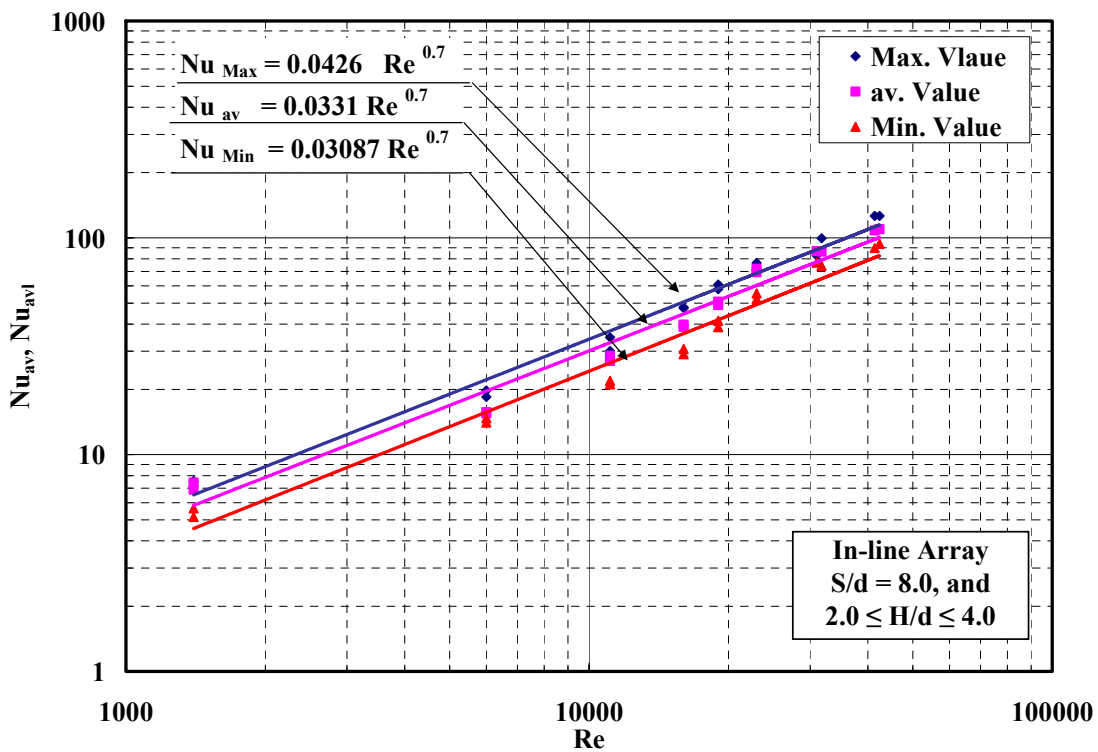


Fig. 6.5d Nusselt Number Variation with Jet Reynolds Number for In-line Array,  $S/d = 8$

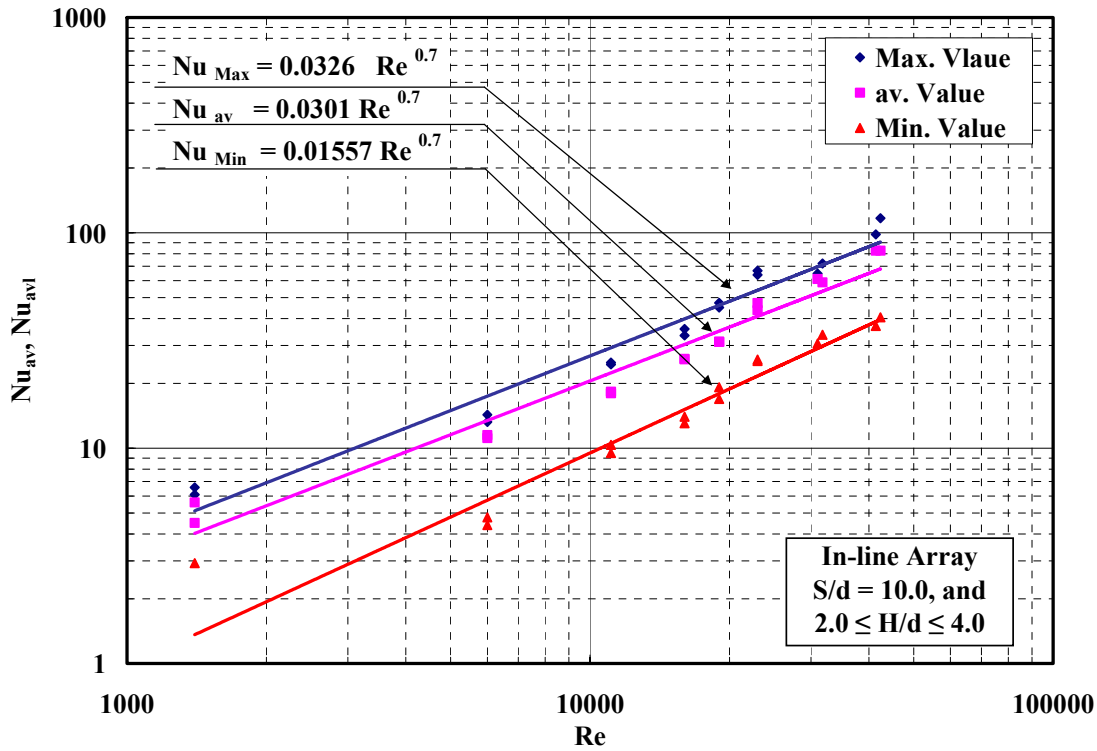


Fig. 6.5e Nusselt Number Variation with Jet Reynolds Number for In-line Array,  $S/d = 10$

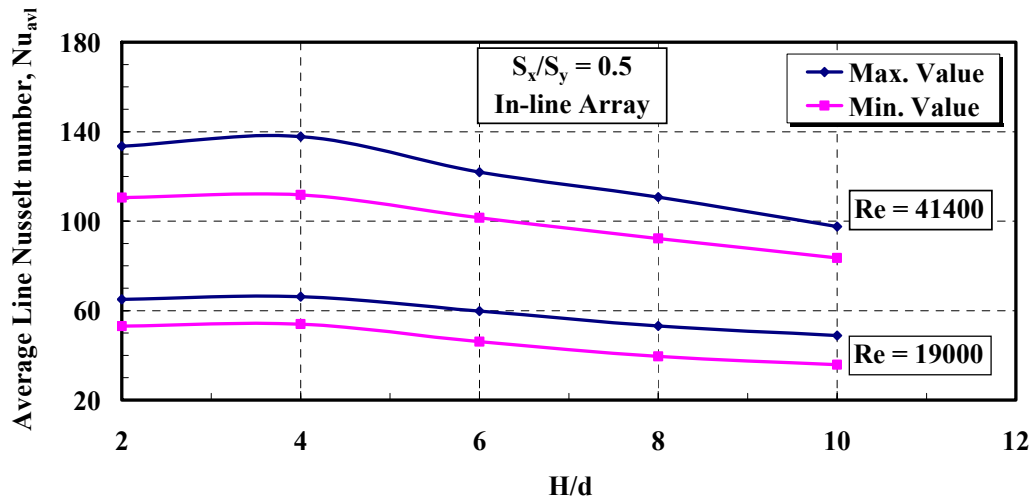


Fig. 6.6a Maximum and Minimum Average Line Nusselt Number for In-line Array,  $S_x/S_y = 0.5$

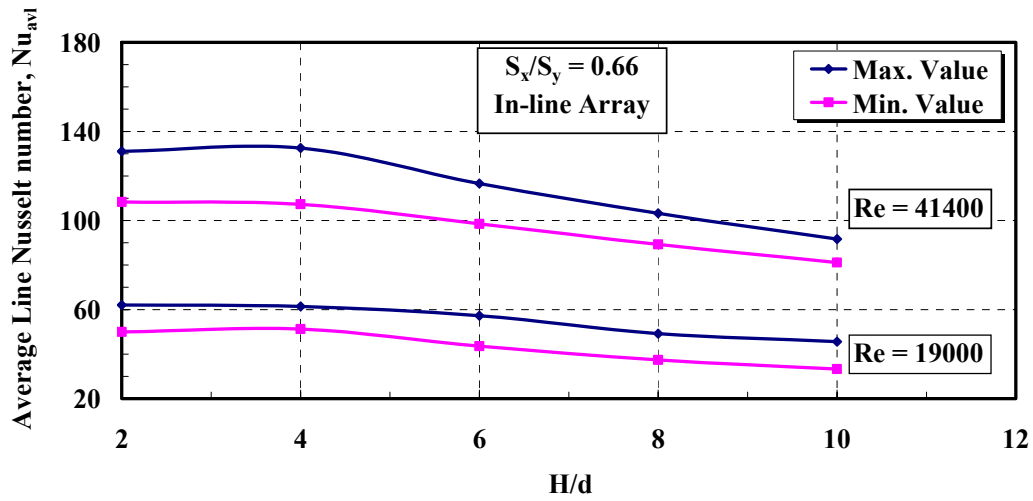


Fig. 6.6b Maximum and Minimum Average Line Nusselt Number for In-line Array,  $S_x/S_y = 0.66$

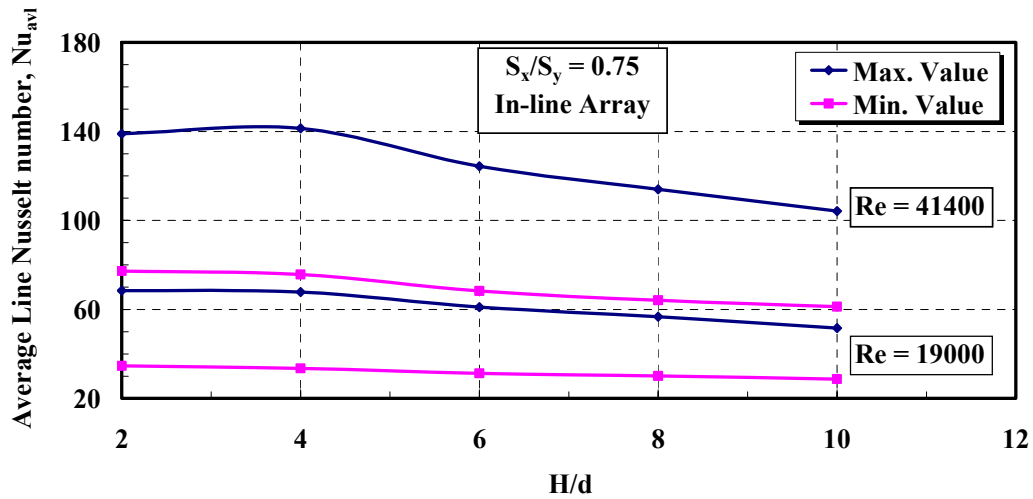


Fig. 6.6c Maximum and Minimum Average Line Nusselt Number for In-line Array,  $S_x/S_y = 0.75$

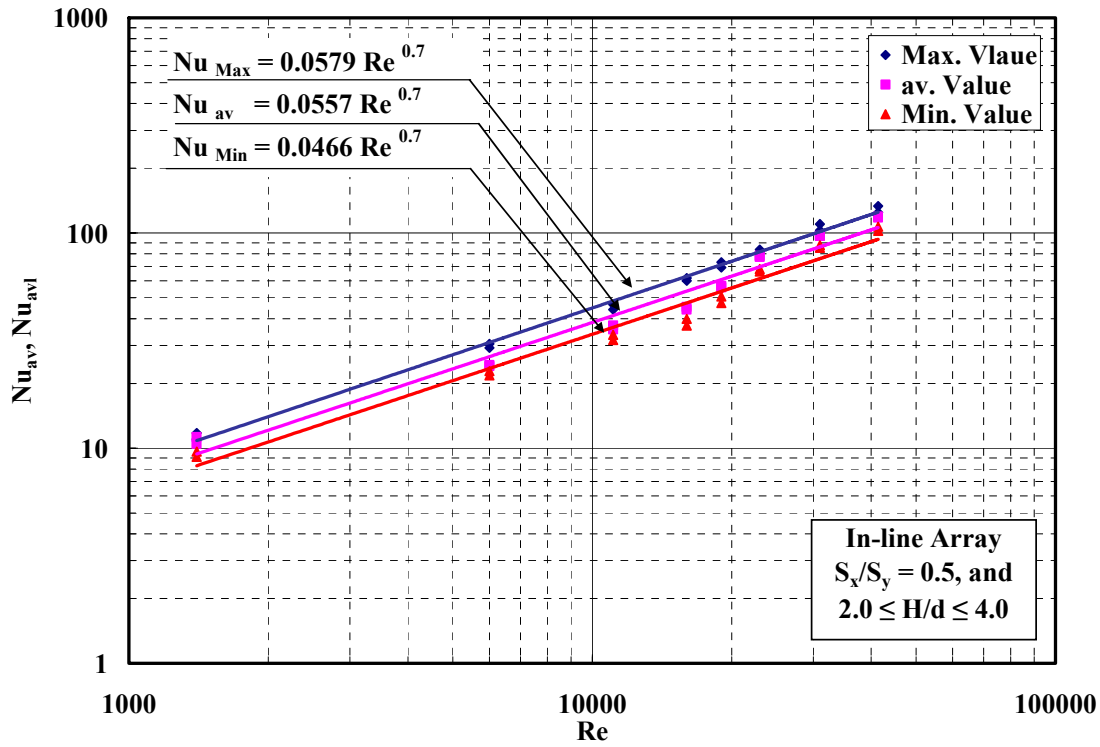


Fig. 6.7a Nusselt Number Variation with Jet Reynolds Number for In-line Array,  $S_x/S_y = 0.5$

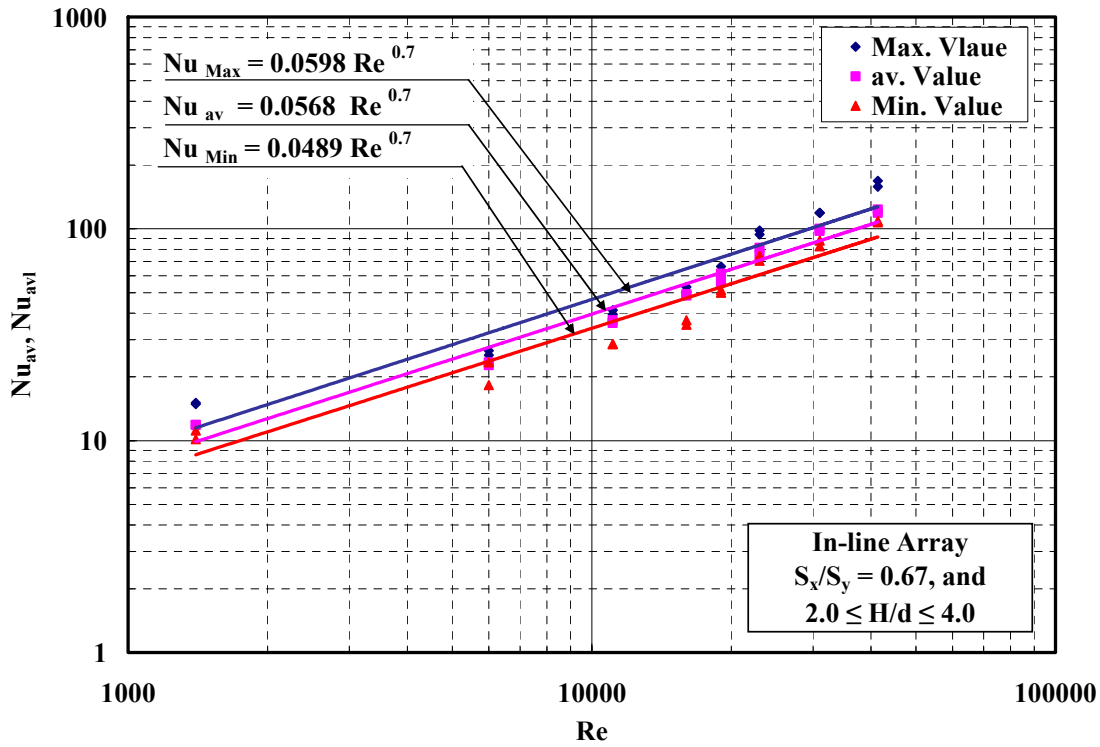


Fig. 6.7b Nusselt Number Variation with Jet Reynolds Number for In-line Array,  $S_x/S_y = 0.67$

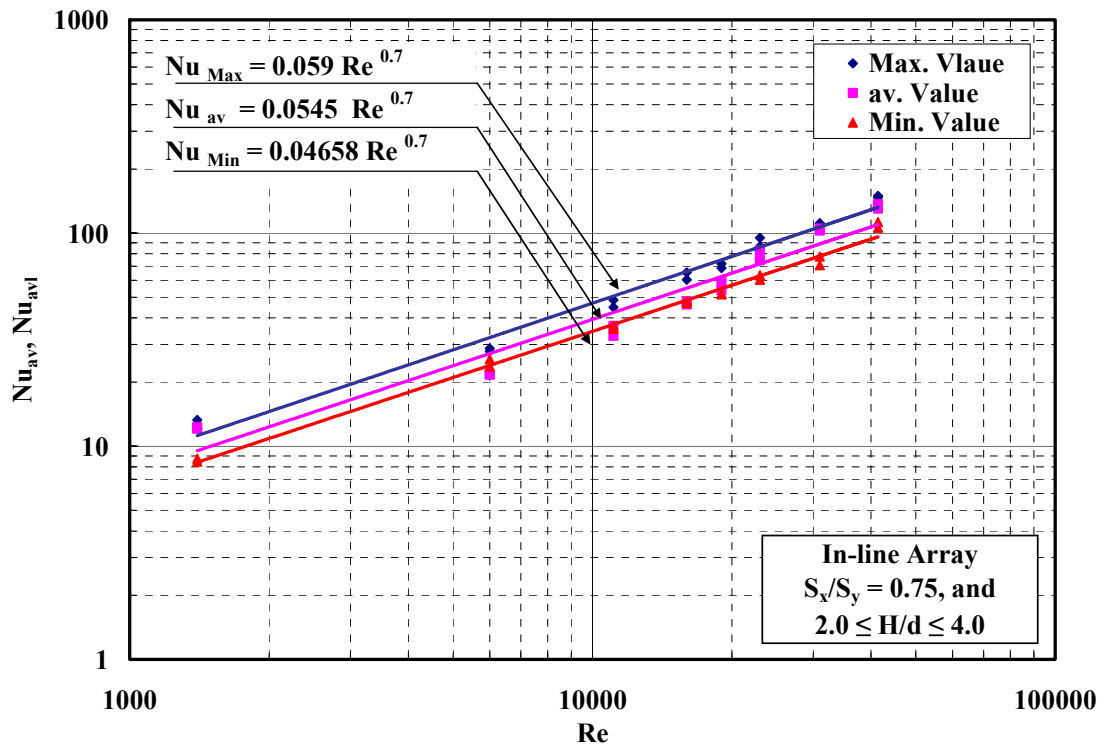


Fig. 6.7c Nusselt Number Variation with Jet Reynolds Number for In-line Array,  $S_x/S_y = 0.75$

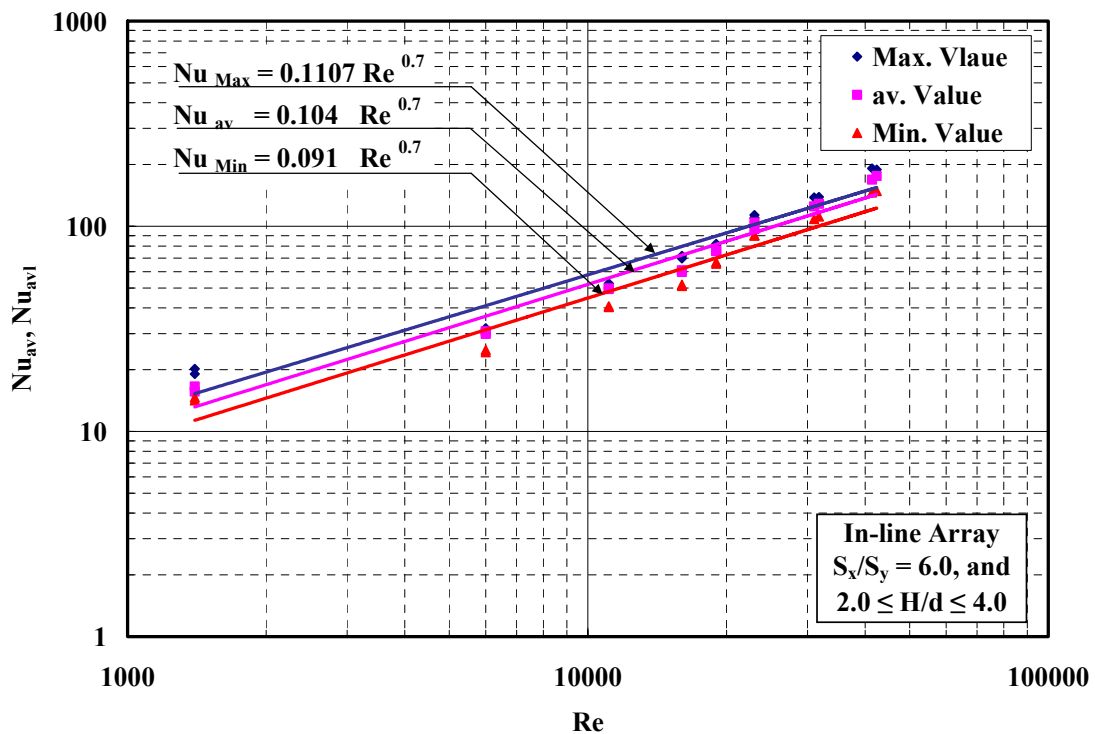


Fig. 6.7d Nusselt Number Variation with Jet Reynolds Number for In-line Array,  $S_x/S_y = 1.0$

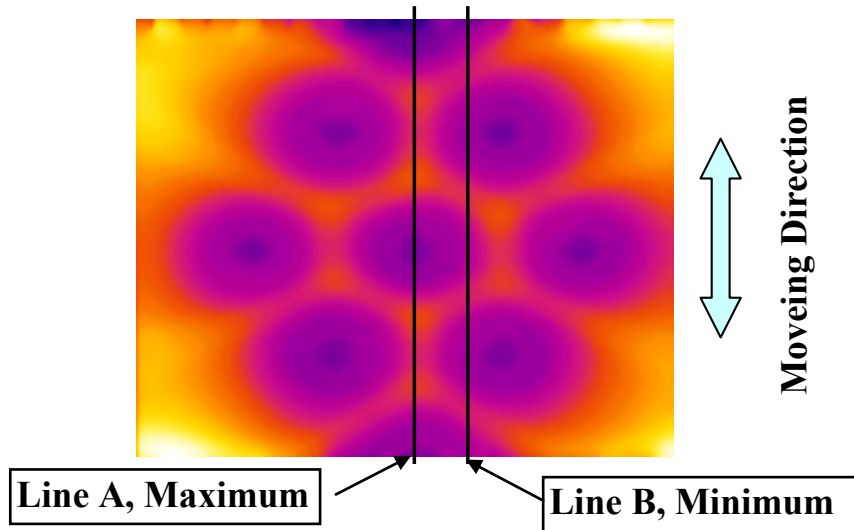


Fig. 6.8a Maximum and Minimum Heat Transfer Positions, for Staggered Array

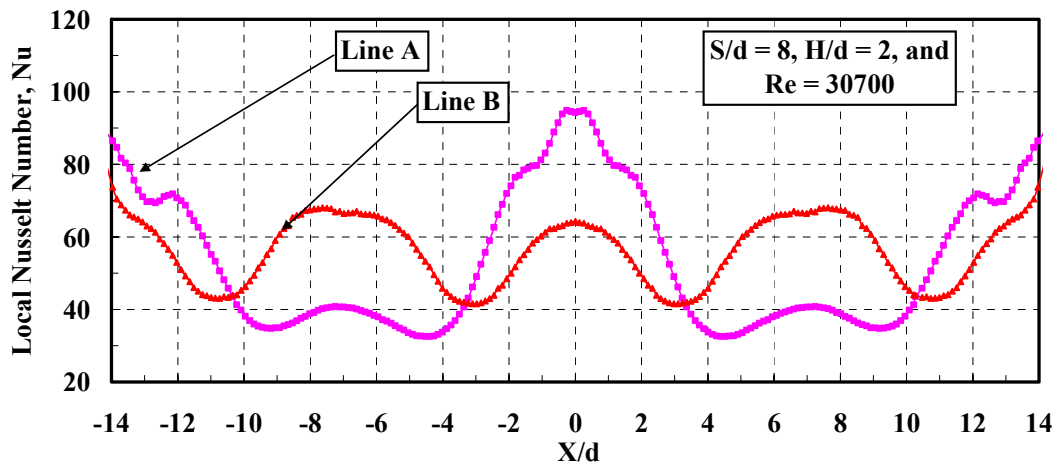


Fig. 6.8b Maximum and Minimum Heat Transfer Distribution, for Staggered Array

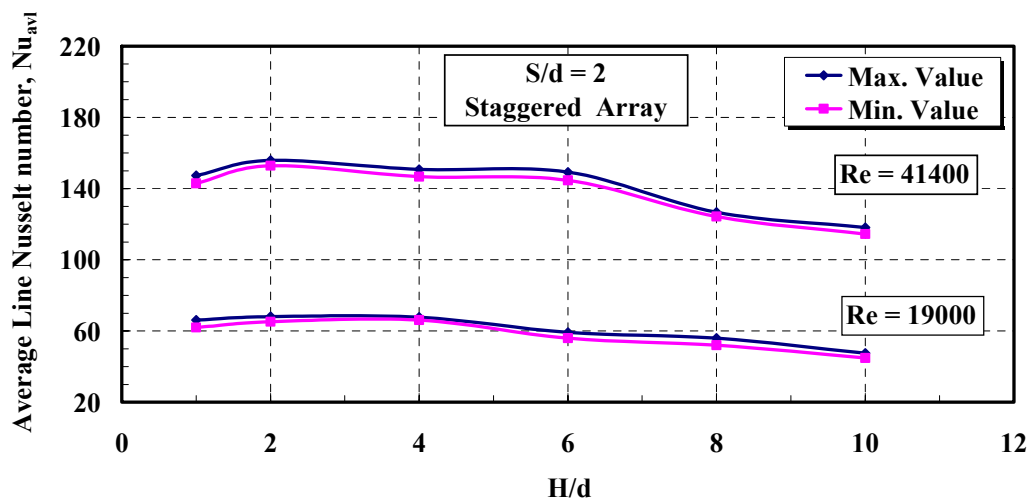


Fig. 6.9a Maximum and Minimum Average Line Nusselt Number

for Staggered Array,  $S/d = 2$

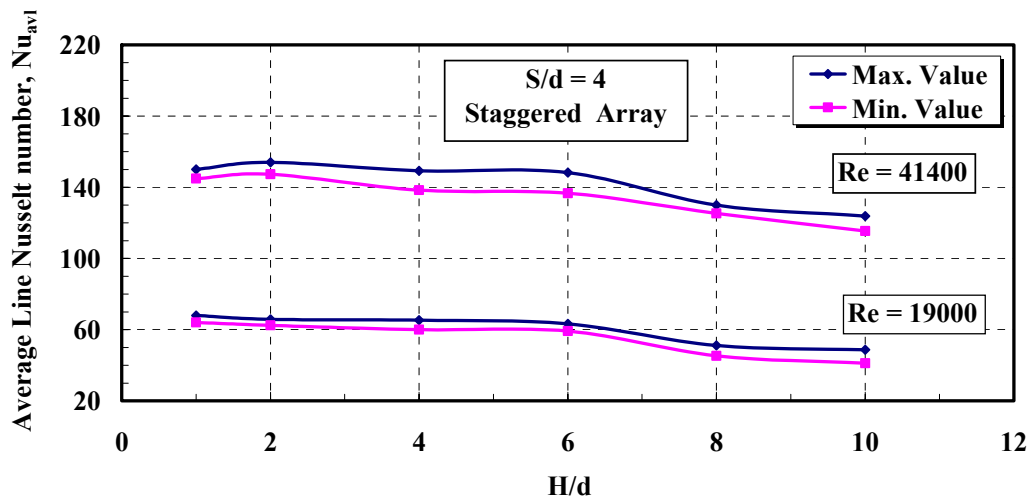


Fig. 6.9b Maximum and Minimum Average Line Nusselt Number for Staggered Array,  $S/d = 4$

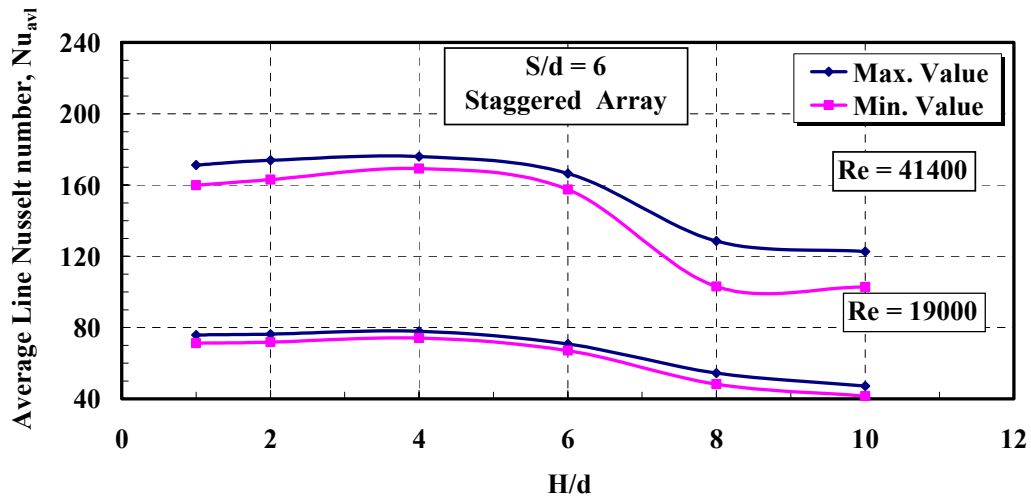


Fig. 6.9c Maximum and Minimum Average Line Nusselt Number for Staggered Array,  $S/d = 6$

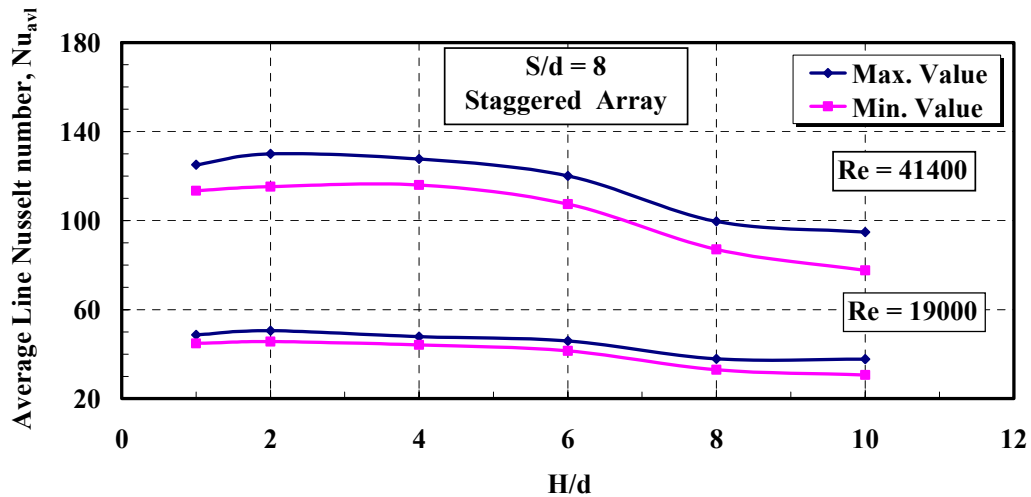


Fig. 6.9d Maximum and Minimum Average Line Nusselt Number for Staggered Array,  $S/d = 8$

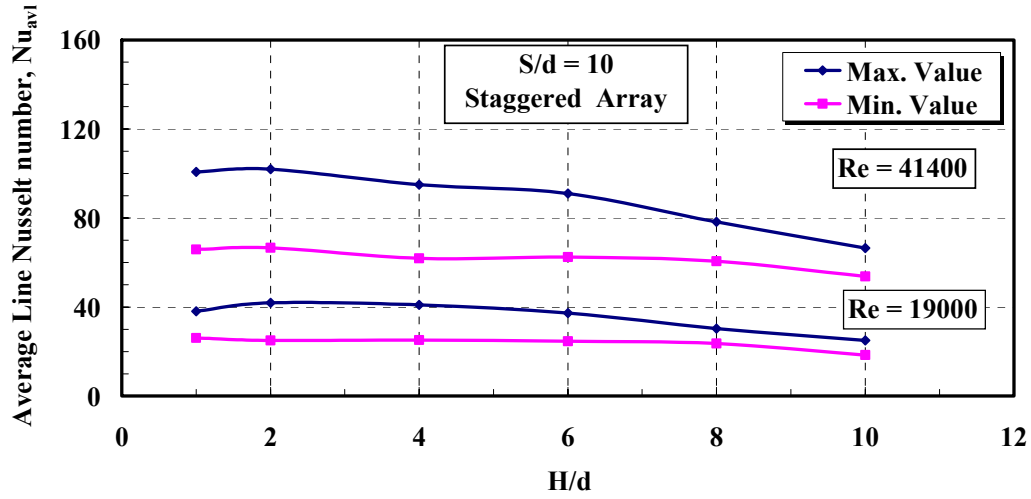


Fig. 6.9e Maximum and Minimum Average Line Nusselt Number for Staggered Array,  $S/d = 10$

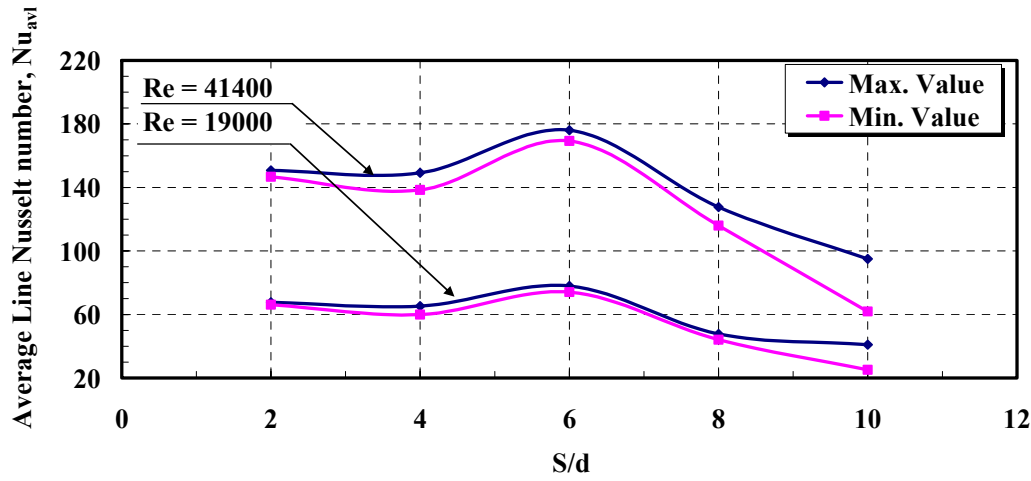


Fig. 6.10 Maximum and Minimum Average Line Nusselt Number for Staggered Array,  $H/d = 4$

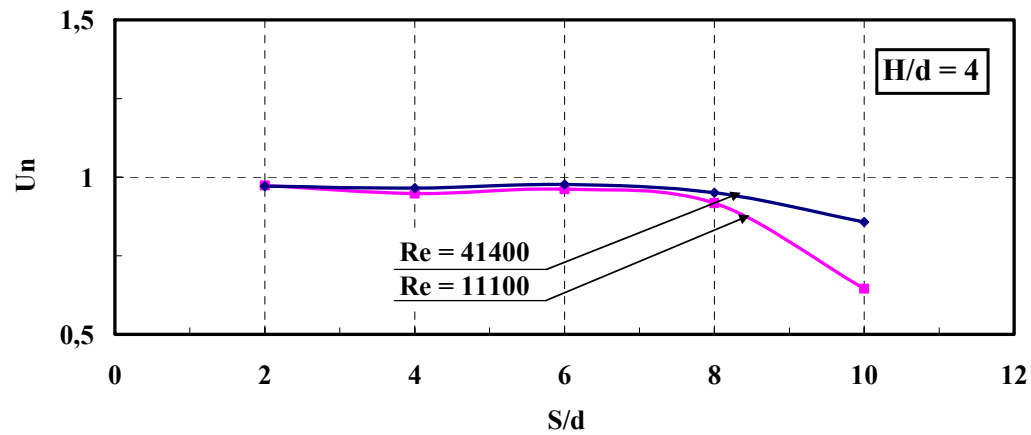


Fig. 6.11 Variation of the Uniformity Degree with the Spacing Distance for Staggered Array

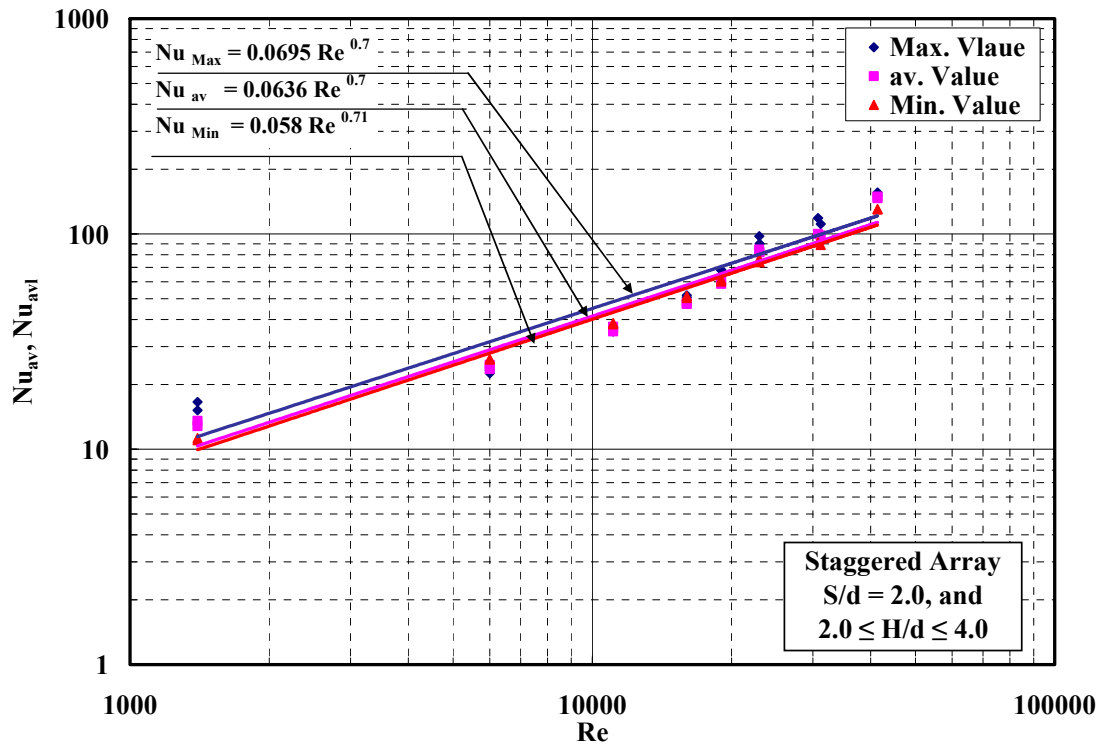


Fig. 6.12a Nusselt Number Variation with Jet Reynolds Number for Staggered Array,  $S/d = 2$

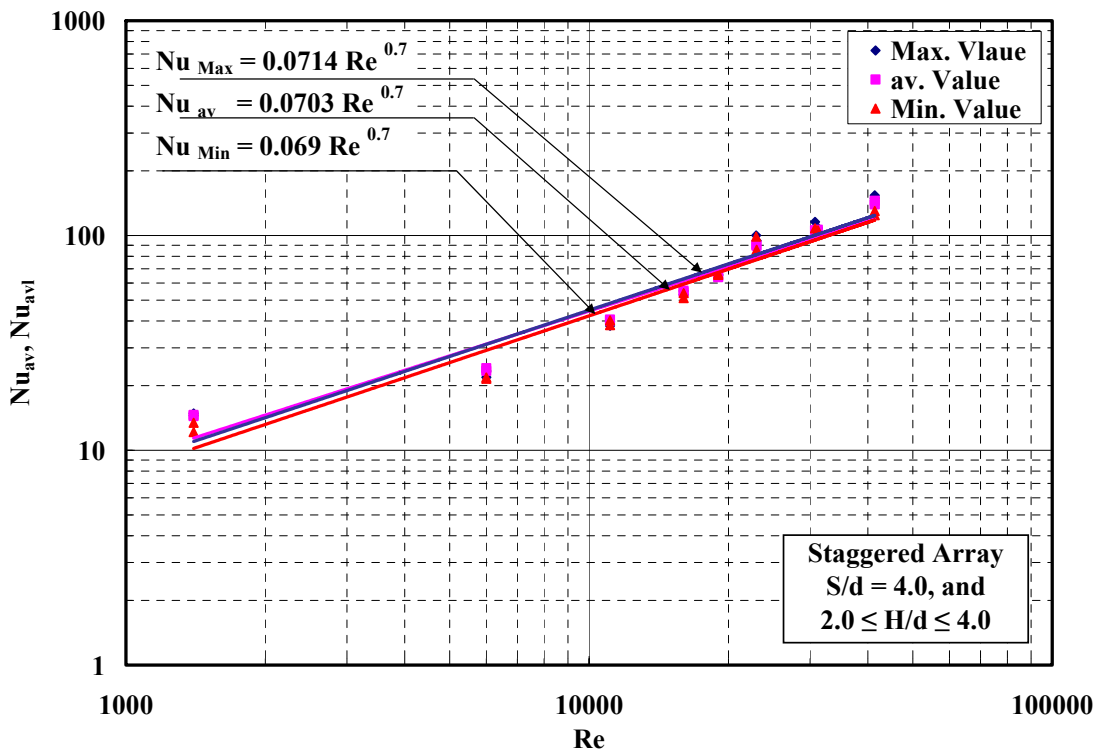


Fig. 6.12b Nusselt Number Variation with Jet Reynolds Number for Staggered Array,  $S/d = 4$

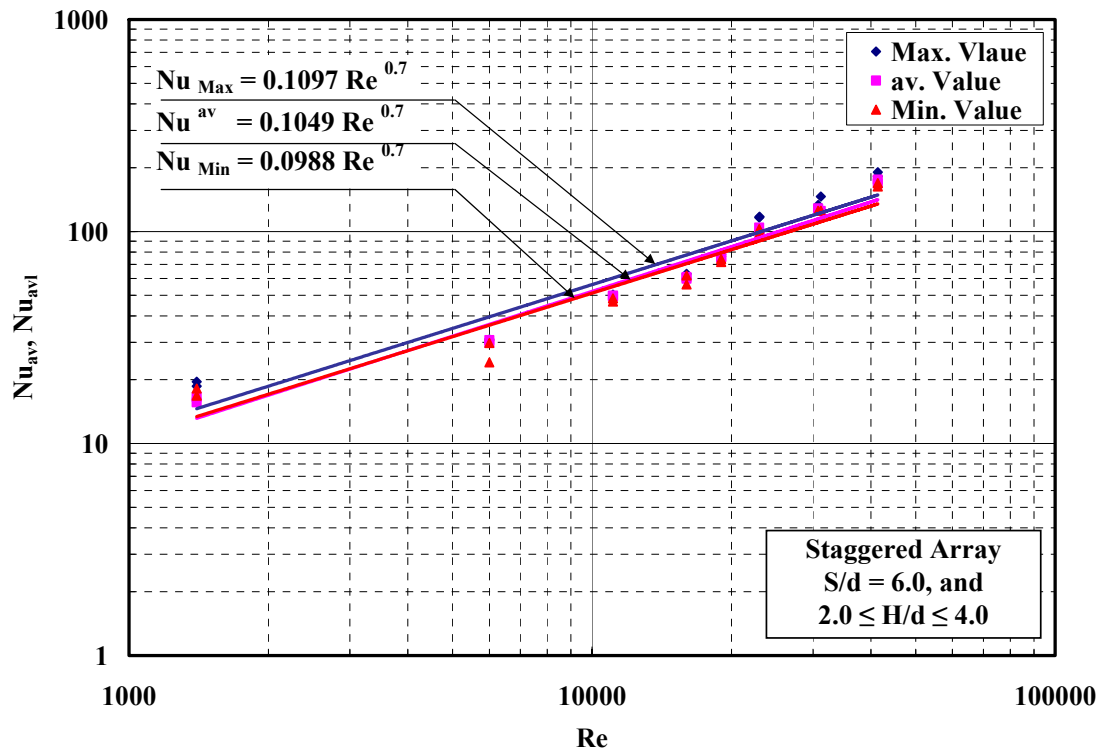


Fig. 6.12c Nusselt Number Variation with Jet Reynolds Number for Staggered Array,  $S/d = 6$

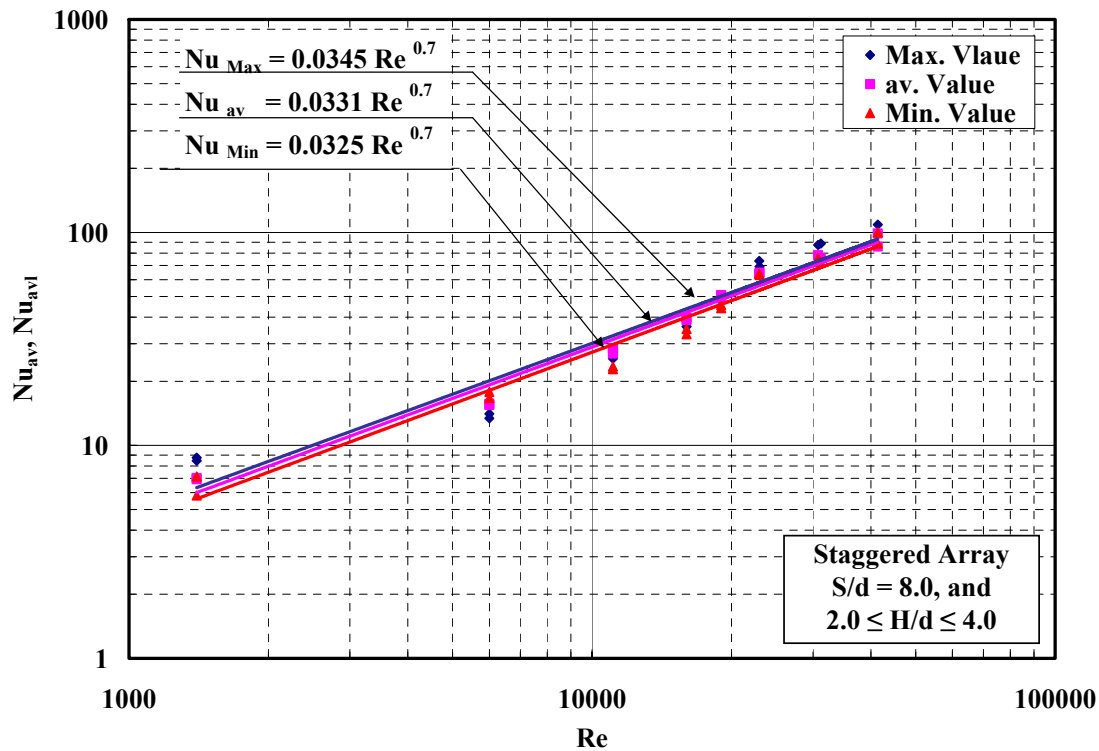


Fig. 6.12d Nusselt Number Variation with Jet Reynolds Number for Staggered Array,  $S/d = 8$

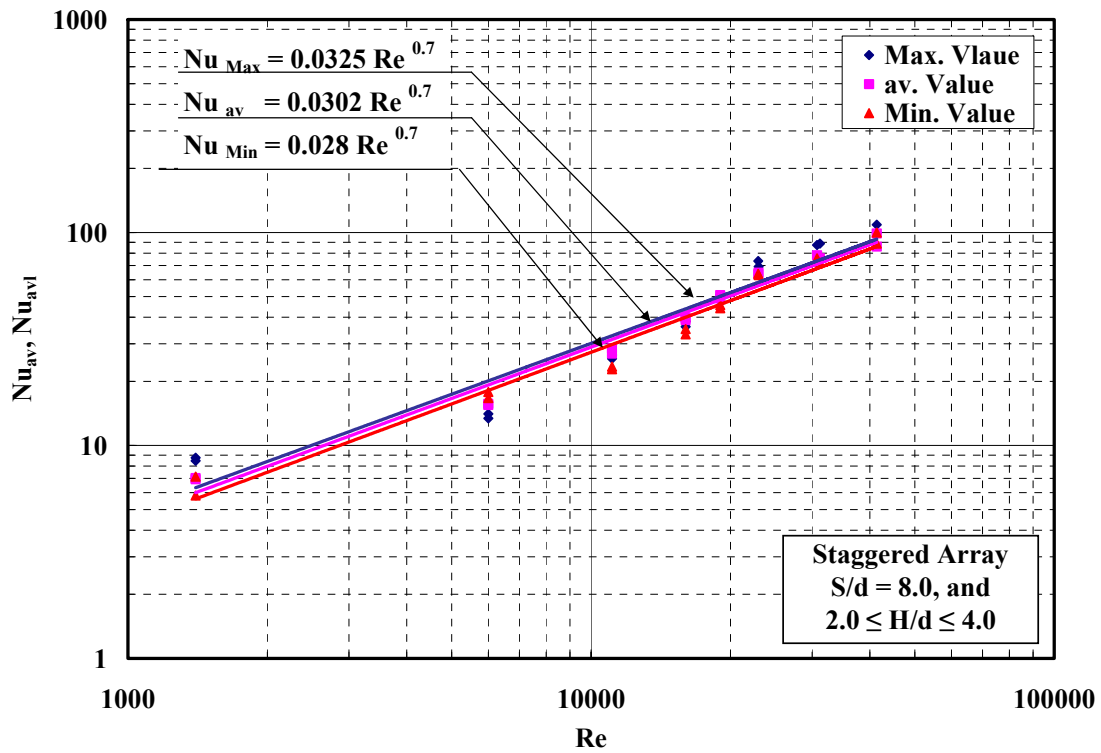


Fig. 6.12e Nusselt Number Variation with Jet Reynolds Number for Staggered Array,  $S/d = 10$

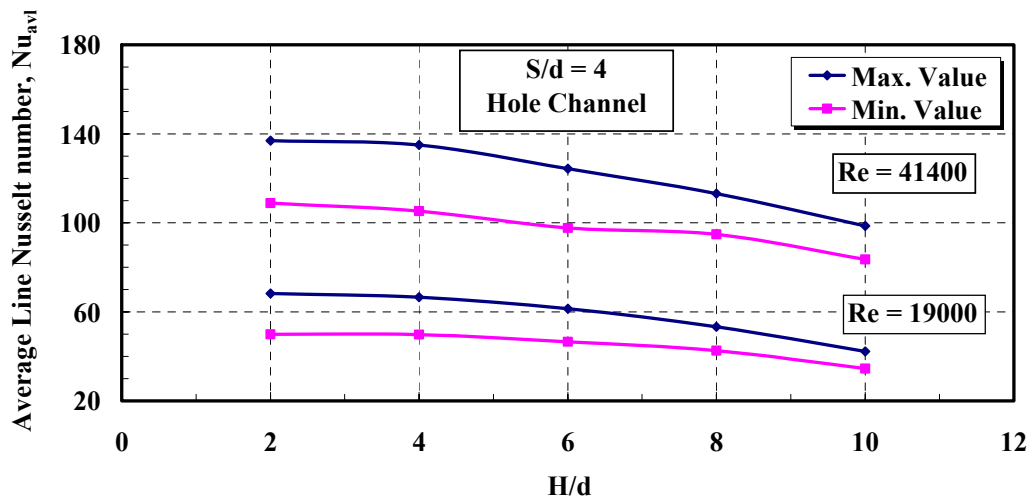


Fig. 6.13a Maximum and Minimum Average Line Nusselt Number for Hole Channel Array,  $S/d = 4$

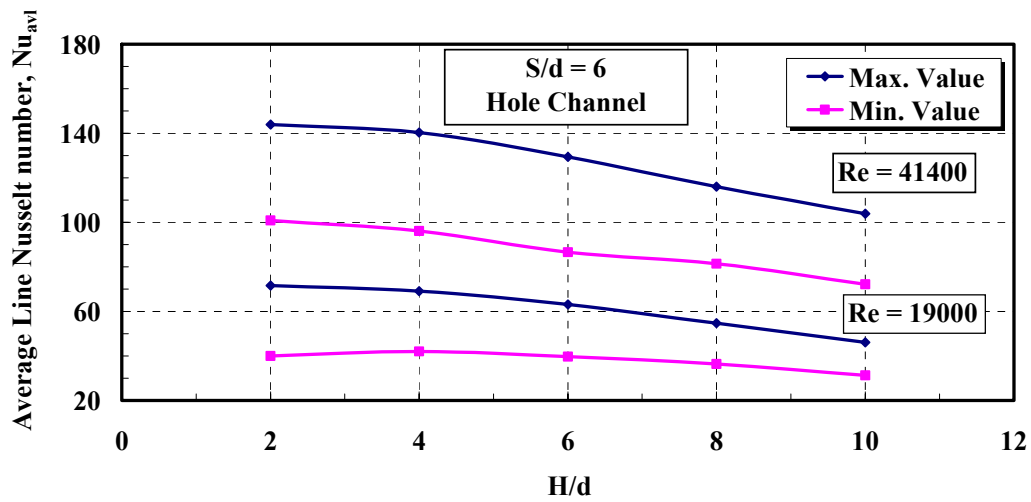


Fig. 6.13b Maximum and Minimum Average Line Nusselt Number for Hole Channel Array,  $S/d = 6$

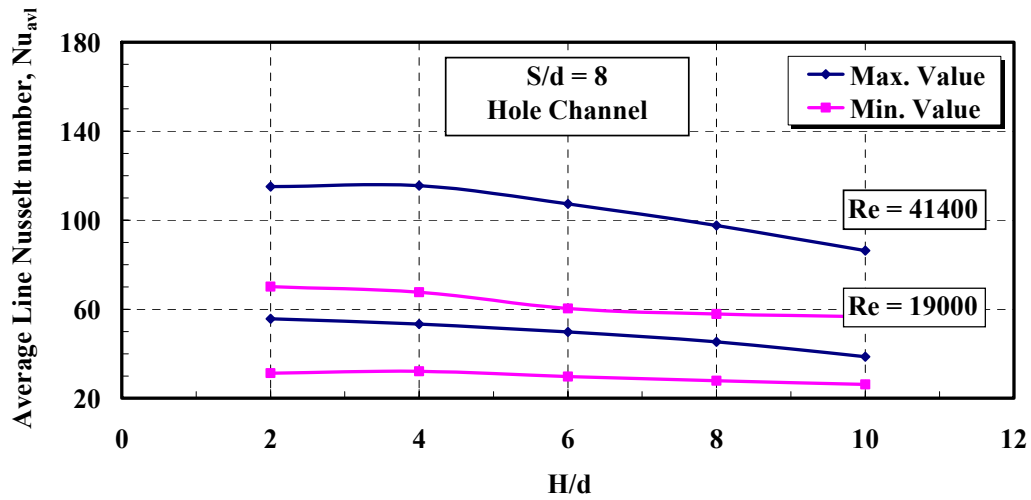


Fig. 6.13c Maximum and Minimum Average Line Nusselt Number for Hole Channel Array,  $S/d = 8$

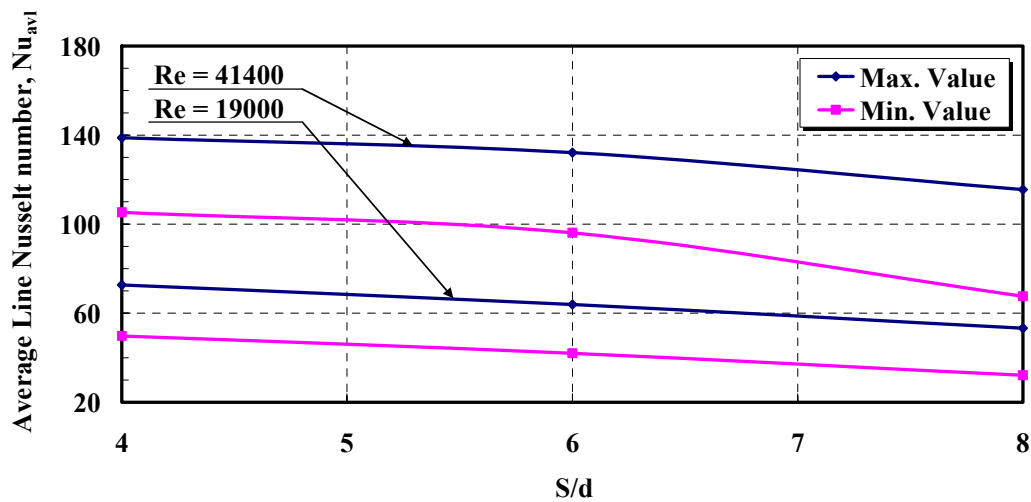


Fig. 6.14 Maximum and Minimum Average Line Nusselt Number for Hole Channel Array,  $H/d = 4$

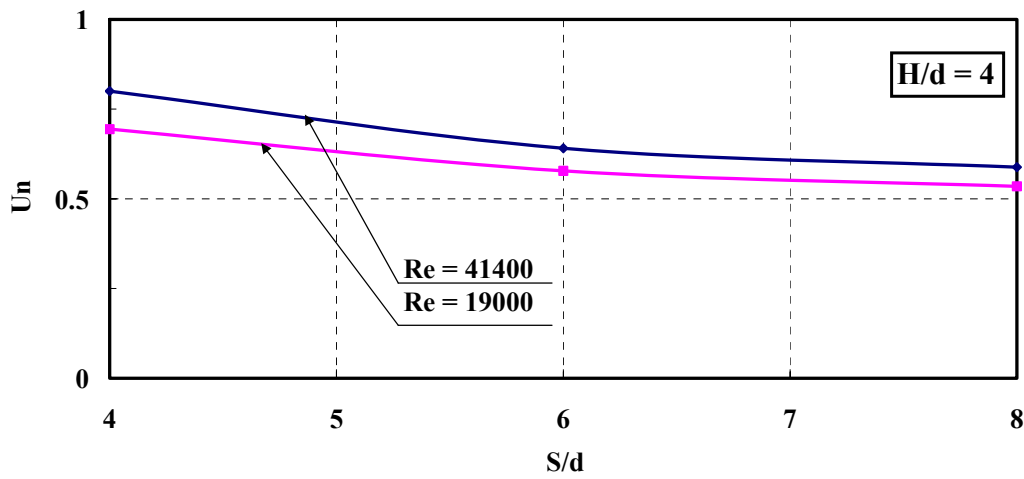


Fig. 6.15 Variation of the Uniformity Degree with the Spacing Distance for Hole Channel Array

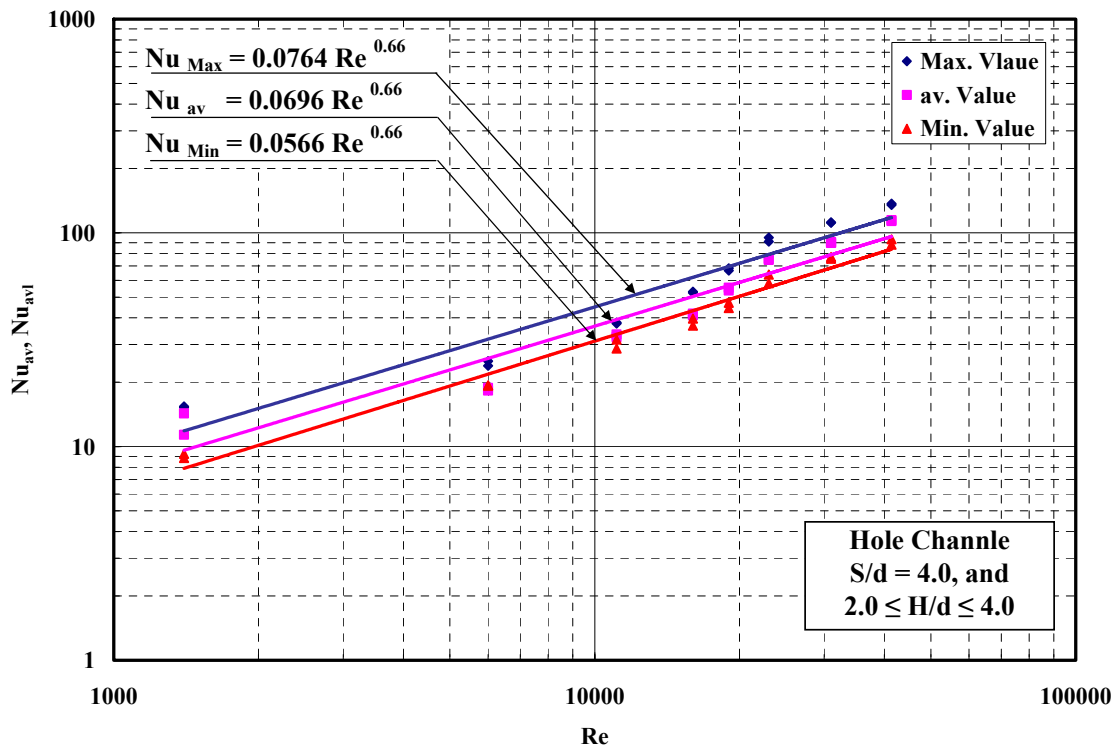


Fig. 6.16a Nusselt Number Variation with Jet Reynolds Number for Hole Channel Array,  $S/d = 4$

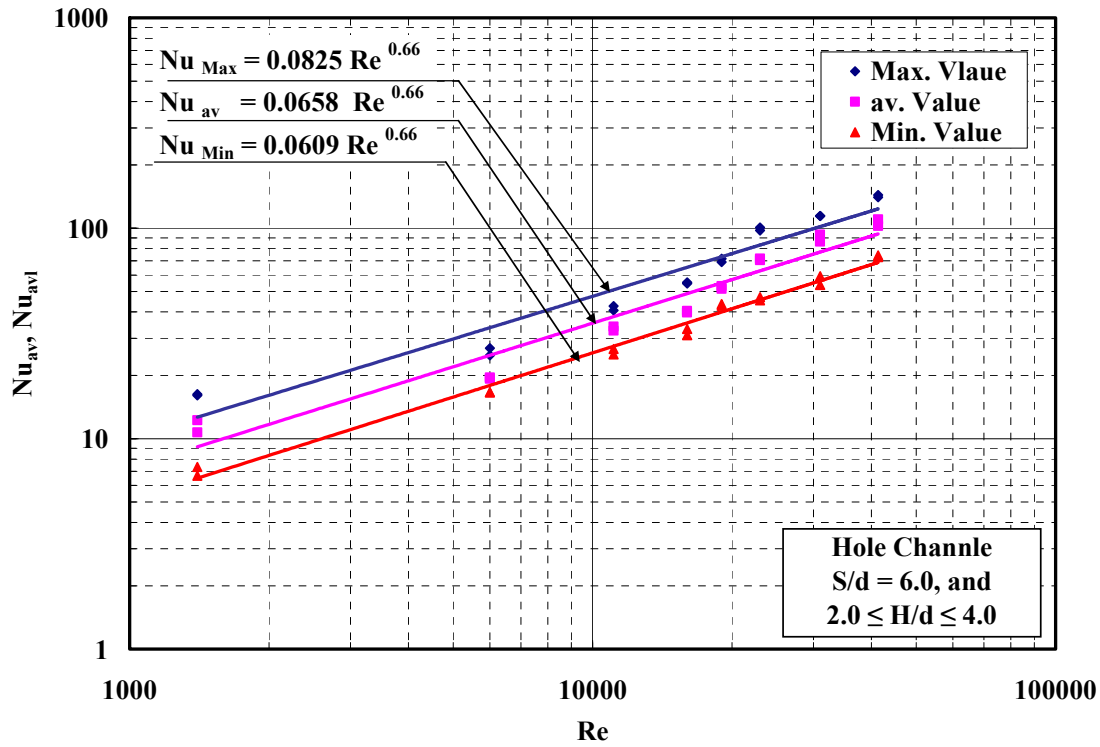


Fig. 6.16b Nusselt Number Variation with Jet Reynolds Number for Hole Channel Array,  $S/d = 6$

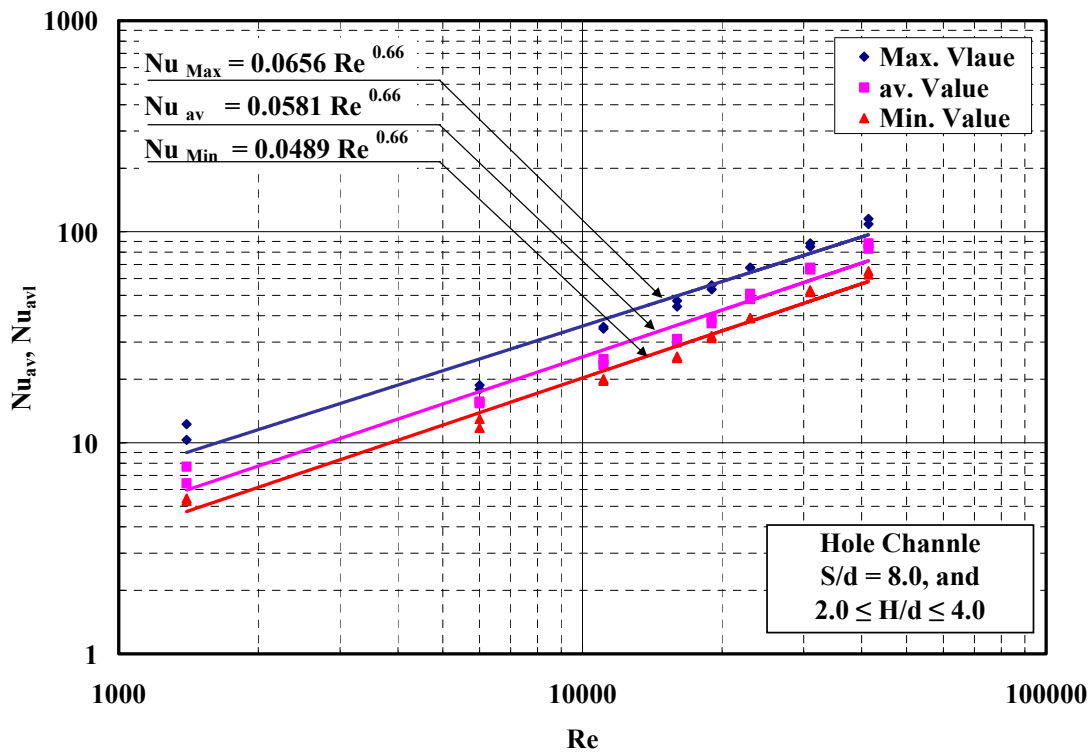


Fig. 6.16c Nusselt Number Variation with Jet Reynolds Number for Hole Channel Array,  $S/d = 8$

## Conclusions and Further Work

### 7-1 Conclusions

The heat transfer characteristics were investigated experimentally for multiple jets arrays and hole channel impinging to heated flat plate. For in-line and staggered arrays, the jets are considered as free tube jet. The cross flow which generated by interference between adjacent jets is reduced by using free tube jet. The effect of separation distance  $H/d$ , spacing distance  $S/d$ , and Reynolds number were investigated in this study. The temperature variations on the impinging surface were measured using an IR-thermography technique to get better spatial resolution. The local and averaged Nusselt numbers were discussed and compared with those of a single jet. In addition, the heat transfer uniformity over the impinging surface was calculated.

The general conclusions of this research accomplished are outlined below:

- (1) There are several differences between single and multiple impingement jet systems. While the multiple jet systems enhance the heat transfer more than a single nozzle by approximately 75% for optimum spacing distance  $S/d = 6$ . Also, the interaction between adjacent jets both before and after impingement is an important consideration in the design and characterization of multiple jet systems.
- (2) The highest stagnation point heat transfer is attained at the range of separation distance  $2 \leq H/d \leq 4$ , which corresponds approximately to the length of the jet potential core in the free jet zone. This result is the similar to the results for a single nozzle. Also, the stagnation point Nusselt number has a maximum value at spacing distance of  $S/d = 6$  for both in-line and staggered arrays, and hole channel.
- (3) The type of array (in-line or staggered) for multiple free tube jet systems has no effect on the average heat transfer. This is due to the variation of

the temperature distribution for the in-line array is equivalent with the same variation of the impinging area for the staggered array, Figs.4.14a-h

- (4) The spacing distance equal to 6 provide the maximum value of the average heat transfer over impinging surface for the in-line and staggered arrays. Also, the different of the inner jet diameter has no effect on the position of the maximum value of the average heat transfer. For hole channel array, the maximum value of the average heat transfer is occur at the spacing distance equal to 4.
- (5) The separation distance  $H/d$  has nearly no effect on the average heat transfer for in-line and staggered arrays, and hole channel in the range  $2 \leq H/d \leq 4$ .
- (6) At optimum spacing distance  $S/d = 6$ , the average heat transfer can be correlated as a function of Reynolds number ( $Nu_{av} \propto Re^{0.7}$ ) for in-line and staggered arrays. For hole channel, the maximum average Nusselt number occurs at spacing distance equal to 4 and it can be best fitted with  $Nu_{av} = 0.0882Re^{0.66}Pr^{0.42}$ . Also, the maximum average heat transfer for in-line and staggered arrays is greater than those of the hole channel at optimum spacing distance with the same experimental conditions.
- (7) The uniformity degree of heat transfer decreases with increase of both the spacing and separation distances. While this degree increases with increase of Reynolds number. For staggered array showed higher uniformity degree than in-line array. The hole channel array provided the lower values of this degree comparing with the other arrays. The unequal spacing distance ( $S_x/S_y$ ) has a negligible effect on the uniformity degree for an in-line array at spacing distance of  $S_y/d = 6$ .

## **7-2 Recommendations for Further Work:**

The following suggestions are highly recommended for future study in this area.

- In the present study, the smooth flat plate used as an impingement surface is made from inconel alloy 600. So, the local and averaged heat transfer will be determined for a rough impingement surface.

- The effect of curvature ratio ( $d_c/d$ ) on the local and averaged heat transfer from multiple jet systems impinging normal to heated concave and convex surfaces should be studied considering the location of maximum heat transfer.

- In this work the air is used as a fluid, therefore another fluid with high heat transfer coefficient as water or nitrogen liquid will be applied to determine the local and average heat transfer.

- The characteristics of the heat transfer from multiple jet systems were investigated experimentally in this study. In the future, a theoretical study using the numerical method for jet flow and heat transfer will be considered comparing with the experimental results.

## References

- [1] Martin H., "Heat Mass Transfer Between Impinging Gas Jets and solid Surfaces" *Adv. Heat Transfer*, Vol. 13, pp. 1-60, 1977.
- [2] Gromoll B. "Experimentelle Untersuchungen des Wärmeübergangs an von Düsensystemen senkrecht angeströmten ebenen Flächen" Ph.D. Thesis, University of Aachen, 1978.
- [3] Viskanta R. "Heat Transfer to Impinging Isothermal Gas and Flame Jets" *Experimental Thermal and Fluid Science*, Vol.6, pp. 111-134, 1993.
- [4] Button D. L., and Wilcox D. "Impingement Heat Transfer - A bibliography 1890-1975" *Preview Heat Transfer*, Vol. 4, pp. 83-98, 1978.
- [5] Gaunter J. W., Livingwood J. N. B., Hrycak P. "Survey of Literature of Flow Characteristics of a Single Turbulent Jet Impinging on a Flat Surface" NASA,, TN, D-5652, 1970.
- [6] Jambunathon K., Lai E., Moss M. A., Button B. L. "A Review of Heat Transfer Data for Single Circular Jet Impingement" *Int. J. Heat and Fluid Flow*, Vol. 13/2, pp. 106-155, 1992.
- [7] Goldstein R. J., Cho H. H. "A Review of Mass Heat Transfer Measurements Using Naphthalene Sublimation" *Experimental Heat Transfer Fluid Mechanics and Thermodynamic*, pp. 21-40, 1993.
- [8] Buchlin J. M., Brossard J., Gouriet J. B. "Infrared Thermography Study of Heat Transfer in an array of Round Jets" 7<sup>th</sup> Int. Conf. on Quantitative Infrared Thermography, Vol. D-17, pp. 1-7, 2004.
- [9] Buchlin J. M., Gouriet J. b., Planquart P., von Beeck J. P. A. J., Renard M. "Infrared Thermography Study of Heat Transfer in an Array of Slot Jet" In *Quantitative Infrared Thermography QIRT 2000*, pp. 132-137, 2003.

## References

---

- [10] Lebedev V. I. Sokolov A. N. "Study of Convective component of Complex Heat Exchanger of a Direct-Heating Furnace" *Glass Ceram.*, Vol. 33, pp. 352-354, 1976.
- [11] Livigood J. N: b., Hrycak P. "Impingement Heat Transfer from Turbulent Air Jet to Flat Plates a Literature Survey" NASA Technical Memorandum Report, TM, X-2778, 1973.
- [12] Becko Y. "Impingement Cooling" A Review, von Karman Institut for Fluid Dynamic Lecture Series, Vol. 83, 1976.
- [13] Hrycak P. "Heat Transfer from Impinging Jets" A lilerature Review, AWAL-TR-81-3054, 1981.
- [14] Jugho I., Sang-Joon I. "Stagnation Region Heat Transfer of a Turbulent Axisymmetric Jet Impingement" *Experimental Heat Transfer*, Vol. 12, pp. 137-156, 1999.
- [15] Goldstein R. J., Seol W. S. "Heat Transfer to a Row of Impinging Circular Air Jets Including the Effect of Entrainment" *Int. J. Heat and Mass Transfer* , Vol. 34, pp. 2133-2147, 1991.
- [16] Sparrow E. M., Lee L. "Analysis of Flow Field and Impingement Heat Mass Transfer Due to Non-uniform Slot Jet" *J. of Heat Transfer*, Vol., May1975, pp. 191-197, 1975.
- [17] Saad N. R., Douglas W. J. M., Mujumdar A. S. "Prediction of Heat Transfer Under an Axisymmetric Laminar Impinging Jet" *Industrial and Engineering Chemistry Fundamentals*, Vol. 1611, pp. 148-154, 1977.
- [18] Polat S., Hung B., Majumdar A. S., Dauglas W. J. M. "Numerical Flow and Heat Transfer Under Impinging Jet" A review, *Ann. Rev. Num. Fluid Mech. Heat Transfer*, Vol. 2, pp. 157-197, 1989.
- [19] Popiel C. O., Van der Meer T. H., Hoogendoorn C. J. "Convective Heat Transfer on a Plate in an Impinging Round Hot Gas Jet of Low Reynolds Number" *Int. J. Heat and Mass Transfer*, Vol. 23, pp. 1055-1068, 1980.

## References

---

- [20] Failla G., Bishop E.H., Liburdy J. A. “Enhanced Jet Impingement Heat Transfer with Cross flow at Low Reynolds Number” *J. of Electronics manufacturing*, Vol. 912, pp. 167-178, 1999.
- [21] Baydar E. “Confined Impinging Air Jet at Low Reynolds Number” *Experimental Thermal and Fluid Sciences*, Vol.19, pp. 27-33, 1999.
- [22] Gardon R., Cobonpue J. “Heat Transfer Between a Flat Plate and Jet of Air Impinging on It” *Int. Development in Heat Transfer, Second Int. Conf.*, pp. 454-460, ASME, New York, 1962.
- [23] Huang G. C. “Investigations of Heat Transfer Coefficient for Air Flow Through Round Jets Impinging Normal to a Heat Transfer Surface” *J. Heat Transfer*, Vol. 85, pp. 237-245, 1963.
- [24] den Oucen C., Hoogendoorn C. J. “Local Convective Heat Transfer Coefficient for Jets on a Plate: Experiments Using Liquid Crystal Technique” *Heat Transfer*, Vol. 5, pp. 293-297, 1974.
- [25] Hoogendoorn C. J. “The Effect of Turbulence on Heat Transfer at a Stagnation Point” *Int. J. of Heat and Mass Transfer*, Vol. 20, pp. 1333-1338, 1977.
- [26] Goldstein R. J., Behbahn A. J “Impingement of a Circular Jet with and without Crossflow” *Int. J. of Heat and Mass Transfer*, Vol. 25., pp. 1377-1383, 1982.
- [27] Gardon R., Arfirat J. C. “The Role of Turbulence Determining the Heat Transfer Characteristics of Impinging Jets” *Int. J. of Heat and Mass Transfer*, Vol.8, pp. 1261-1272, 1965.
- [28] Donaldson C. D., Snedeker R. S., Margolis D. D. “A Study of Free Jets Turbulence Structure and Impingement Heat Transfer” *J. Fluid Mech.*, Vol. 45, pp. 477-512, 1971.
- [29] Hollworth B. R., Wilson S. J. “Entrainment Effect on Impingement Heat Transfer: Part I Measurement of Heated Jet Velocity on Temperature

## References

---

- Distribution and Recovery Temperature on Target Surface” J. Heat Transfer, Vol. 106, pp. 797-803, 1984.
- [30] Hollworth B. R., Gero L. R. “Entrainment Effect on Impinging Heat Transfer: Part II, Local Heat Transfer Measurement” J. Heat Transfer, Vol. 107, pp. 910-919, 1989.
- [31] Streight S. A., Diller T. E. “The Effect of Thermal Entrainment on Jet Impingement Heat Transfer” J. Heat Transfer, Vol.106, pp. 27-33, 1984.
- [32] Streigt S. A., Diller T. G. “A Analysis of the Effect of Entrainment Temperature on Jet Impingement Heat Transfer” J. Heat Transfer, Vol. 106, pp. 804-810, 1984.
- [33] Obat N. T., Majumdar A. S., Douglas W. S. “The Effect of Nozzle Geometry on Impingement Heat Transfer Under Round Turbulent Jet” ASME Paper WA/HT-53, ASME New York,1979.
- [34] Adler W. “Experimentelle Bestimmung des Wärmeübergangs bei der Prallströmung über einen hohen Reynoldszahlenbereich mittels Infrarot-Thermografie“ Ph. D. Thesis, Otto-von-Guericke Universität Magdeburg, Germany, 2002.
- [35] Lytle D., Webb B. W. “Secondary Heat Transfer Maxima for Air Jet Impingement at Low Nozzle-to Plate Spacing” Experimental Heat Transfer, Fluid Mechanics and Thermodynamics, pp. 776-783, 1991.
- [36] Angioletti M., Di Tommaso R. M., Nino E., Ruocco G. “Simultaneous Visualization of Flow Field and Evaluation of Local Heat Transfer by Transitional Impinging Jets” Int. J. of Heat and Mass Transfer, Vol. 46, pp. 1703-1713, 2003.
- [37] Hollworth B. R., Berry R. D. “Heat Transfer from Arrays of Impinging Jets with Large Jet-to-Jet Spacing” J. Heat Transfer, Vol. 100, pp. 352-357, 1978.
- [38] Hilgeroth E. “Wärmeübergang bei Düsenströmung senkrecht zur Austauschfläche“ Chemie-Ing.-Techn. Vol. 37, pp. 1264-1272, 1965.

- [39] Kercher D. M., Tabakopp W. "Heat Transfer by a Square Array of Round Air Jets Impinging Perpendicular to a Flat Surface Including the Effect of Spent Air" *J. of Engineering for Power*, ASME, pp. 73-82, 1970.
- [40] Koopman R. N., Sparrow E. M. "Local and Average Transfer Coefficient Due to an impinging Row of Jets" *Int. J. Heat and Mass Transfer*, Vol. 19, pp. 673-683, 1976.
- [41] Florschuetz L. W., Berry R. A., Metzger D. E. "Periodic Streamwise Variations of Heat Transfer Coefficients for Inline and Staggered Arrays of Circular with Cross Flow of Spent Air" *J. Heat Transfer*, Vol. 102, pp. 132-137, 1980.
- [42] Dyban E. P., Mazur A. I., Golovanov V. P. "Heat Transfer and Hydrodynamics of an Array of Round Impinging Jets with One-Side Exhaust of the Spent Air" *Int. J. of Heat and Mass Transfer*, Vol. 23, pp. 667-676, 1980.
- [43] Florschuetz L. W., Truman C. R., Metzger D. E. "Streamwise Flow and Heat Transfer Distributions for Jet Array Impingement with Cross Flow" *J. Heat Transfer*, Vol. 103, pp. 337-342, 1981.
- [44] Godstein R. J., Timmers J. F. "Visualization of Heat Transfer from Arrays of Impinging Jets" *Int. J. of Heat and Mass Transfer*, Vol. 25, pp. 1857-1868, 1982.
- [45] Pan Y., Webb B. W. "Heat Transfer Characteristics of Arrays of Free Surface Liquid Jets and Jet Arrays" in *Proc. 6<sup>th</sup> AIAA/ASME Thermophys, Heat Transfer Conf.* ASME, New York, 1994.
- [46] Florschuetz L. W., Isoda Y. "Flow Distributions and Discharge Coefficient Effects for Array Impingement with Initial Cross Flow" *J. of Engineering for Power*, Vol. 105, pp. 296-304, 1983.
- [47] Florschuetz L. W., Metzger D. E., Su C. C. "Heat Transfer Characteristics for Jet Array Impingement with Initial Cross Flow" *J. Heat Transfer*, Vol. 106, pp. 34-41, 1984.

- [48] Huber A. M., Viskanta R. “Effect of Jet-to-Jet Spacing on Convective Heat Transfer to Confined, Impinging Arrays of Axisymmetric Air Jets” *Int. J. Heat and Mass Transfer*, Vol. 37, pp. 2859-2869, 1994.
- [49] Huber A. M., Viskanta R. “Comparison of Convective Heat Transfer to Perimeter and Centre Jets in a Confined, Impinging Array of Axisymmetric Air Jets” *Int. J. Heat and Mass Transfer*, Vol. 37, pp. 3025-3030, 1994.
- [50] Huber A. M., Viskanta R. “Convective Heat Transfer to a Confined Impinging Arrays of Air Jets with Spent Air Exits” *J. Heat Transfer*, Vol. 116, pp. 570-576, 1994.
- [51] Xiaojun Y., Nader S. “Measurements of Local Heat Transfer Coefficients from a Flat Plate to a Pair of Circular Air Impinging Jets” *Experimental Heat Transfer*, Vol. 9, pp. 29-47, 1996.
- [52] Jung-Yang S., Mao-De L. “Optimum Jet-to-Jet Spacing of Heat Transfer of Staggered Arrays of Impinging Air Jets” *Int. J. Heat and Mass Transfer*, Vol. 44, pp. 3997-4007, 2001.
- [53] Brevet P., Dejeu C., Jolly M., Vullierme J. J. “Heat Transfer to a Row of Impinging Jets in Consideration of Optimization” *Int. J. Heat and Mass Transfer*, Vol. 45, pp. 4191-4200, 2002.
- [54] Lo May Su, Chang W. S. “Detailed Heat Transfer Measurements of Impinging Jet Arrays Issued from Grooved Surfaces” *Int. J. of Heat and Mass Transfer*, Vol. 41, pp. 823-841, 2002.
- [55] Dong L. L., Cheung C. S., Leung C. W. “Heat Transfer Characteristics of an Impinging Butane/Air Flame Jet of Low Reynolds number” *Experimental Heat Transfer*, Vol. 14, pp. 265-282, 2001.
- [56] Dong-Ho R., PilHyun Y., Hyung H. C. “Local Heat/Mass Transfer and Flow Characteristics of Array Impinging Jets with Effusion Holes Ejecting Spent Air” *Int. J. Heat and Mass Transfer*, Vol. 46, pp. 1049-1061, 2003.

## References

---

- [57] Arjocu S. C., Liburdy J. A. "Identification of Dominant Heat Transfer Modes Associated with the Impingement of an Elliptical Jet Array" *J. Heat Transfer*, Vol. 122, pp. 240-247, 2000.
- [58] Hollworth B. R., Lehmann G., Rosiczkowski J. "Arrays of Impinging Jets with Spent Fluid Removal Through Vent Holes on the Target Surface, Part 2: Local Heat Transfer Jet" *J. of Engineering for Power*, Vol. 105, pp. 393-402, 1983.
- [59] Saad N. R., Polat S., Douglas W. J. "Confined Multiple Impinging Slot Jets Without Cross Flow Effects" *J. Heat and Fluid Flow*, Vol. 13, pp. 2-14, 1992.
- [60] Gao L., "Effect of Jet Hole arrays Arrangement on Impingement Heat Transfer" M. Sc. Thesis Faculty of Agricultural and Mechanical, Louisiana University, 2003.
- [61] Koopman R. N. "Local and Average Heat Transfer Coefficients for Multiple Impinging Jets" Ph.D. Thesis, Department of Mech. Eng., University of Minnesota, 1975.
- [62] Behbahani A. J. "Heat Transfer to Staggered Arrays of Impinging Circular Jets" Ph.D. Thesis, Department of Mech. Eng., University of Minnesota, 1979.
- [63] Obot N. T., Trabold T. A. "Impingement Heat Transfer Within Arrays of Circular Jets, Part 1 Effect of Minimum, Intermediate and Complete Cross Flow for Small and Large Spacing" *J. Heat Transfer*, Vol. 107, pp. 872-879, 1987.
- [64] Dong. L.L., Leung C. W., Cheung C. S. "Heat Transfer of a Row of Three Butane/Air Flame Jets Impinging on a Flat Plate" *Int. J. Heat and Mass Transfer*, Vol. 46, pp. 113-125, 2003.
- [65] Metzger D. E., Yamashita T., Jenkins C. W. "Improvement Cooling of Concave Surfaces with Lines of Circular Air Jets" *J. of Eng. Power*, Vol. 91, pp. 149-158, 1969.

## References

---

- [66] Hollworth B. R., Dagan L. “Arrays of Impinging Jets with Spent Fluid Removal Through Vent Holes on the Target Surface, Part 1: Average Heat Transfer” *J. of Eng. Power*, Vol. 102, pp. 994-999, 1980.
- [67] Sheriff H. S., Zumbrennen D. A. “Local and Instantaneous Heat Transfer Characteristics of Arrays of Pulsating Jets” *J. Heat Transfer*, Vol. 121, pp. 341-348, 1999.
- [68] Chang Y. K., Hammand G. D., Macaskill C., Ward J. “An Experimental Study of Two-Dimensional Jet Impingement Heat Transfer in a Confined Cross Flow” *J. Heat Transfer*, Vol. 3, pp. 1205-1230, 1986.
- [69] Baliley J. C., Bunker R. S. “Local Heat Transfer and Flow Distributions for impinging Jet Arrays of Dense and Sparse Extent” *Proc. of 2002 IGTI, Int. Conf. of Gas Turbine and Exposition*, pp. 1-10, 2002.
- [70] Yan W. M., Mei S. C., Liu H. C., Soong C. Y., Yang W. J. “Measurement of Detailed Heat Transfer on a Surface Under Arrays of Impinging Elliptic Jets by a Transient Liquid Crystal Technique” *Int. J. Heat and Transfer*, Vol. 47, pp. 5235-5245, 2004.
- [71] Metzger D. E., Florschütz L. W., Tagueuchi D. I., Behee R. D. “Heat Transfer Characteristics for In-line and Staggered Arrays of Circular Jets with Cross Flow of Spent Air” *J. Heat Transfer*, Vol. 101, pp. 587-593, 1979.
- [72] Freidman S. J., Mueller A. C. “Heat Transfer to Fat Surface” *Proc. General Discussion on Heat Transfer Institution of Heat Transfer Eng. London*, pp. 138-142, 1951.
- [73] Ichimiya K., Okuyama K. “Characteristic of Impingement Heat Transfer Caused by Circular Jets With Confined Wall” *23<sup>rd</sup> Int. Cold Region Heat Transfer Conf.*, pp. 523-532, University of Alaska, Fairbanks, 1991.
- [74] Narayanan V., Seyed-Yagoobi J., Page R. H. “An Experimental Study of Fluid Mechanics and Heat Transfer in an Impinging Slot Jet Flow” *Int. J. Heat and Mass Transfer*, Vol. 47, pp. 1827-1845, 2004.

- [75] Slayzak, Viskanta R., Incropera F.P “Effects of Interaction Between Adjacent Free Surface Planar Jets on Local Heat Transfer from the Impingement Surface” *Int. J. Heat and Mass Transfer*, Vol. 37, pp. 269-282, 1994.
- [76] Seyad-Yaggobi J., Narayanan V., Page R. H. “Comparison of Heat Transfer Characteristics of Radial Jet Reattachment Nozzle to In-line Impinging Jet Nozzle” *J. Heat Transfer*, Vol. 120/2, pp. 335-341, 1998.
- [77] Hakenesch P. R. “Thin Layer Thermography a new Heat Transfer Measurements Technique” *Experimental in Fluids*, pp. 257-265, 1999.
- [78] Rajaratnan N. “Turbulent Jets” Elsevier, New York, 1976.
- [79] Abromovich G., N. “The Theory of Turbulent Jets” MIT Press, Cambridge, Mass, 1963.
- [80] Massaud K. “Principle of Convective Heat Transfer” 2<sup>nd</sup> Springer, Verlary, New York, 1994.
- [81] Sarghini F., Ruocco G. “Enhancement and Reversal Heat Transfer by Computing Models in Jet Impingement” *Int. J. Heat and Mass Transfer*, Vol. 47, pp. 1711-1718, 2004.
- [82] Tiaushe L., Sullivan J. P: “Heat Transfer Flow Structures in an Excited Circular Impinging Jets” *Int. J. Heat and Mass Transfer*, Vol. 39, pp. 3695-3706, 1996.
- [83] Glauert M. B. “The Wall Jet” *J. of Fluid Mechanics*, Vol. 6, pp. 625-634, 1956.
- [84] Lohe H. “Wärme- und Stofftransport beim Aufblasen von Gasstrahlen auf Flüssigkeiten” *Fortschritt Berichte VDI, Zeitschrift*, 1967.
- [85] Reichardt H. “Gesetzmäßigkeiten der freien Turbulenz“ *VDI, Forschungsheft*, Vol. 414, 1942.

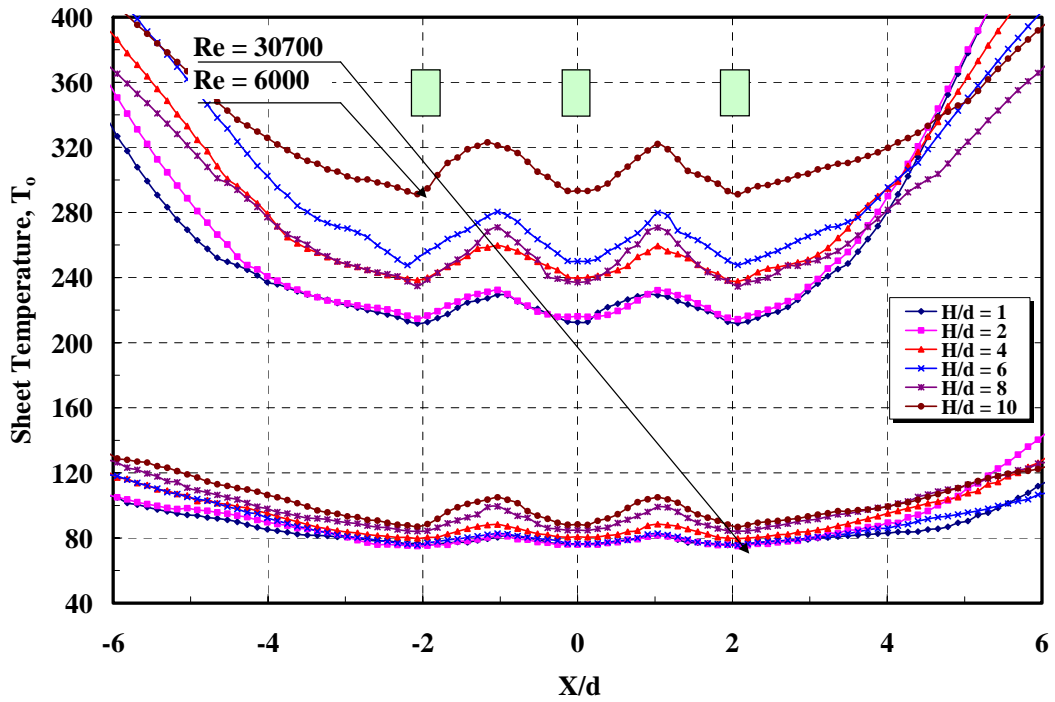
- [86] Garimella S. V., Rice R. A. "Heat Transfer Submerged and Confined Jets Impingement Heat Transfer in High Heat Flux Systems" ASME, HTD, Vol. 301, pp. 59-68, 1994.
- [87] Azer K., Benson J. R., Manno V. P. "An Experimental Investigation of Micro jet Impingement Cooling" J. Heat Transfer In Electronic Equipment, Eds., HTD, Vol. 171, pp. 1-10, 1991.
- [88] Giralt F., Chia C. J., Trass O. "Characterization of the Impingement Region in an Axisymmetric Turbulent Jet" Int. Chem. Fundamental, Vol. 16, pp. 21-28, 1977.
- [89] Brahma R. K. "Predication of Stagnation Point Heat Transfer for a Slot Jet Impinging on a Flat Surface" Wärme- und Stoffübertragung, Vol. 27/2, pp. 61-66, 1992.
- [90] Puschmann F., Specht E. "Transient Measurement of Heat Transfer In Metal Quenching with Atomized Sprays" Experimental Thermal and Fluid Science, Vol. 28, pp. 607-615, 2004.
- [91] Puschmann F., Specht E., Schmidt J. "Measurement of Spray cooling Heat Transfer Using an Infrared-Technique in Compination with the Phase-Doppler Technique and a Paternoster" Int. J. Heat and Techology, Vol. 19, pp. 51-56, 2001.
- [92] Runa S. "Experimentelle Untersuchung der Kritischen Wärmestromdichte von aufwärts und abwärts strömenden Wasser in einem senkrechten Kreisrohr bei niedrigen Drücken und niedrigen Massenstromdichten" Fortschritt-Berichte VDI: Verfahrenstechnik 351, 1994.
- [93] Tawfek A. A. "Heat Transfer and Pressure Distributions of an Impinging Jet on a Flat Surface" Heat and Mass Transfer, Vol. 32, pp. 49-54, 1996.
- [94] Aihara T., Kim J. K., Marayama S. "Effects of Temperature Depended on Fluid Properties on Heat Transfer Due to an Axisymmetric Impinging Gas Jet Normal to a Flat Surface" Wärme- und Stoffübertragung, Vol. 25, pp. 145-153, 1990.

- [95] Van der Meer T. H. "Stagnation Point Heat Transfer from Turbulent Low Reynolds Number Jets and Flame Jets" *Experimental Thermal and Fluid science*, Vol. 4, pp. 115-126, 1991.
- [96] Rahimi M., Owen I., Mistry J. "Impingement Heat Transfer in an Under-Explained Axisymmetric Air Jet" *Int. J. Heat and Mass Transfer*, Vol. 46, pp. 263-272, 2003.
- [97] Rajesh P. K., Das M. K. "Conjugate Forced Convection Heat Transfer from a Flat Plate by Laminar Plane Wall Jet Flow" *Int. J. Heat and Mass Transfer*, Vol. 48, pp. 1896-2910, 2005.
- [98] Peper E. "Strömungsstruktur, Wärmeübergang, Strahlkraft und Druckerlust radialer Prallstrahlfelder" *Fortschritt Berichte VDI, Reihe 3*, Vol. 481, 1997.
- [99] Howorth L. "On the Calculation of the Steady Flow in the Boundary Layer Near the Surface of a Cylinder in a Stream" *ARC-RM*, 1632, 1935.
- [100] Akiyama T., Yamamoto k., Squires K. D., Hishida K. "Simulation and Measurement of Flow and Heat Transfer in Two Planar Impinging Jets" *Int. J. Heat and Fluid Flow*, Vol. 26, pp. 244-255, 2005.
- [101] Park T. H., Choi H. G., Yoo J. Y., Kim S. J. "Streamline Upwind Numerical Simulation of Two-Dimensional Confined Impinging Slot Jets" *Int. J. Heat and Mass Transfer*, Vol. 46, pp. 251-262, 2003.
- [102] Scholtz M. T., Trass O. "Mass Transfer in a Non-uniform Impinging Jet" *AICHE J.*, Vol. 16/1, pp. 82-96, 1970.

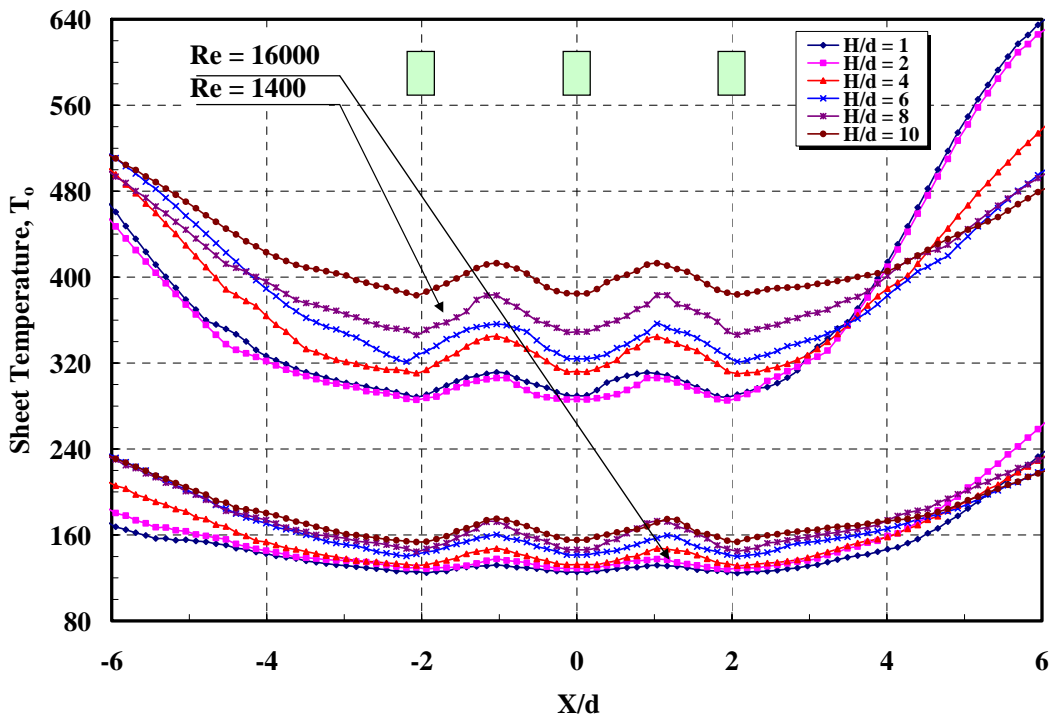
## Appendices

### A- Distribution of Surface Temperature:

#### A-1 In-line Array:

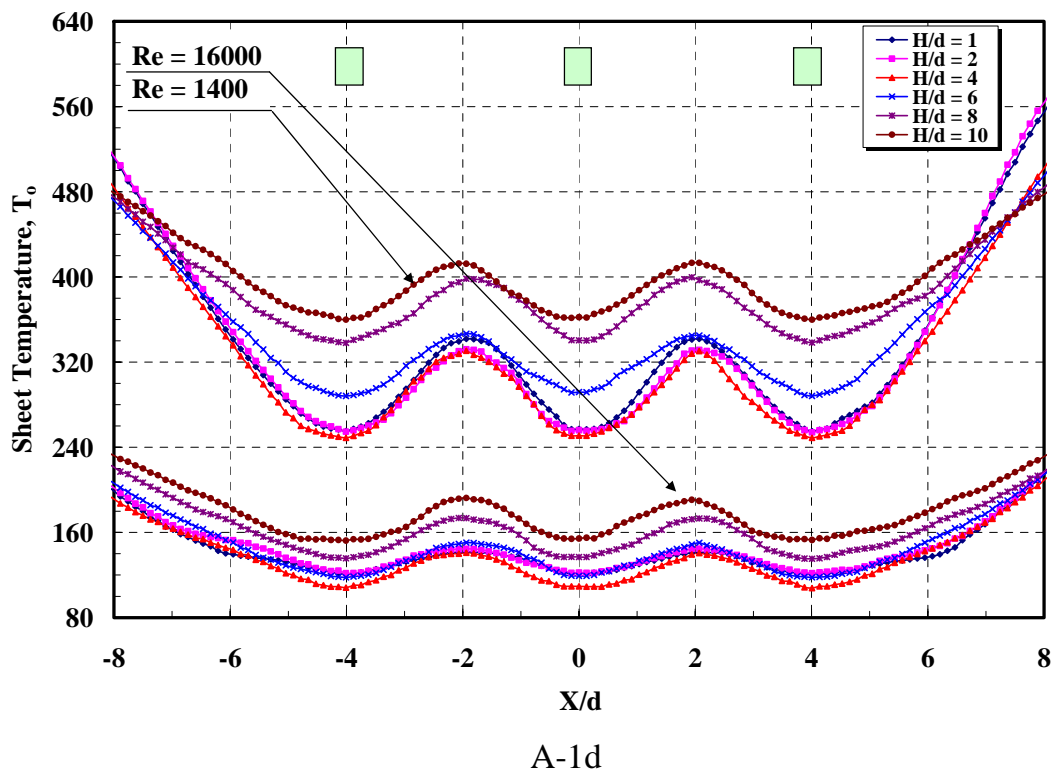
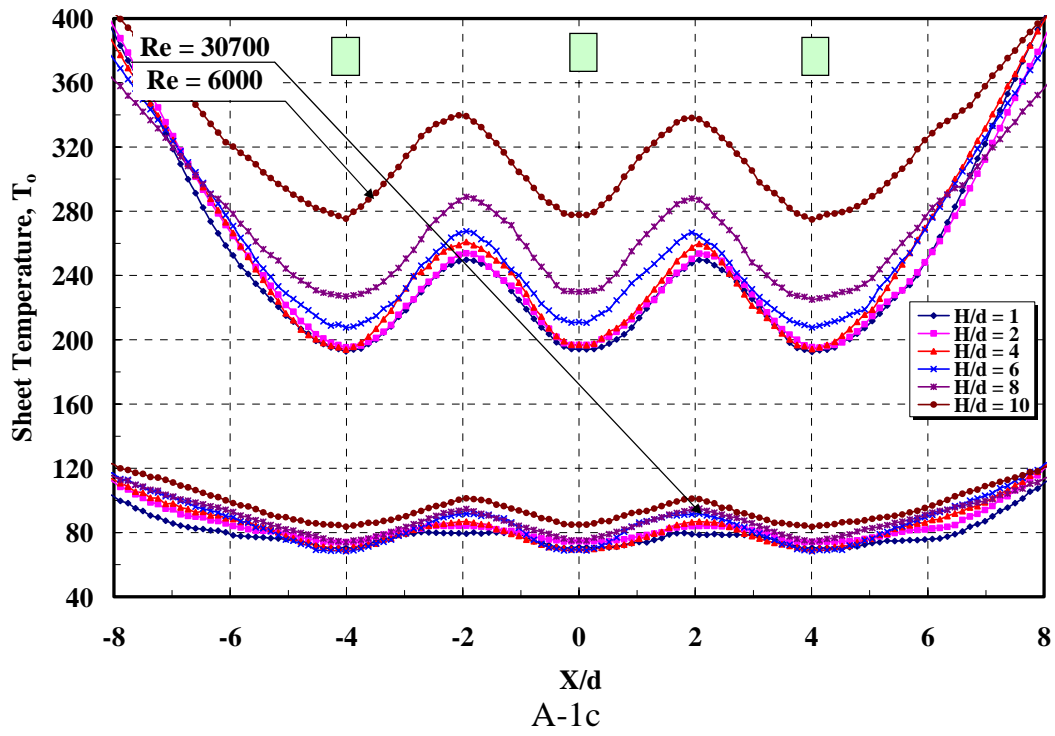


A-1a

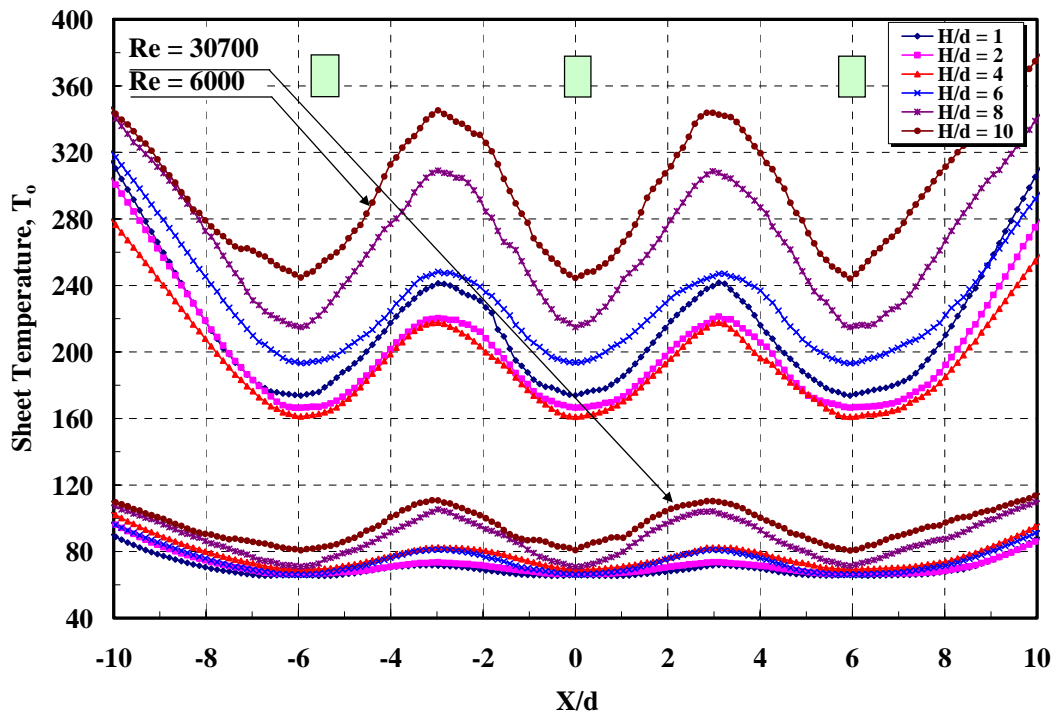


A-1b

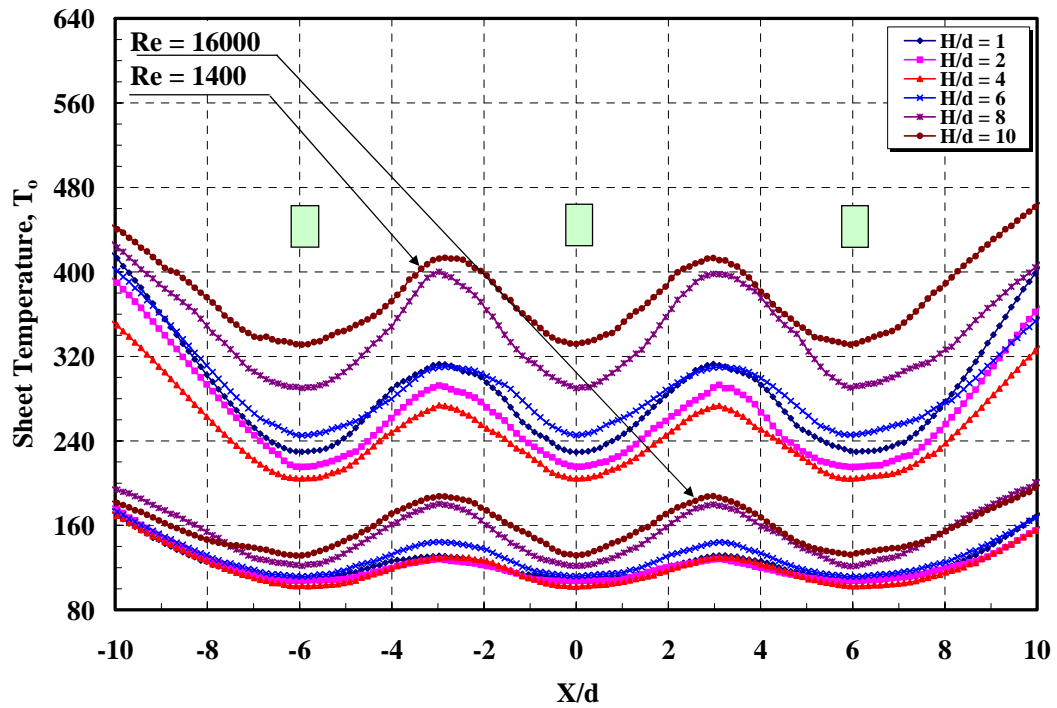
Figs. A-1a-b Temperature Distribution for In-line Array at  $S/d = 2$



Figs. A-1c-d Temperature Distribution for In-line Array at  $S/d = 4$

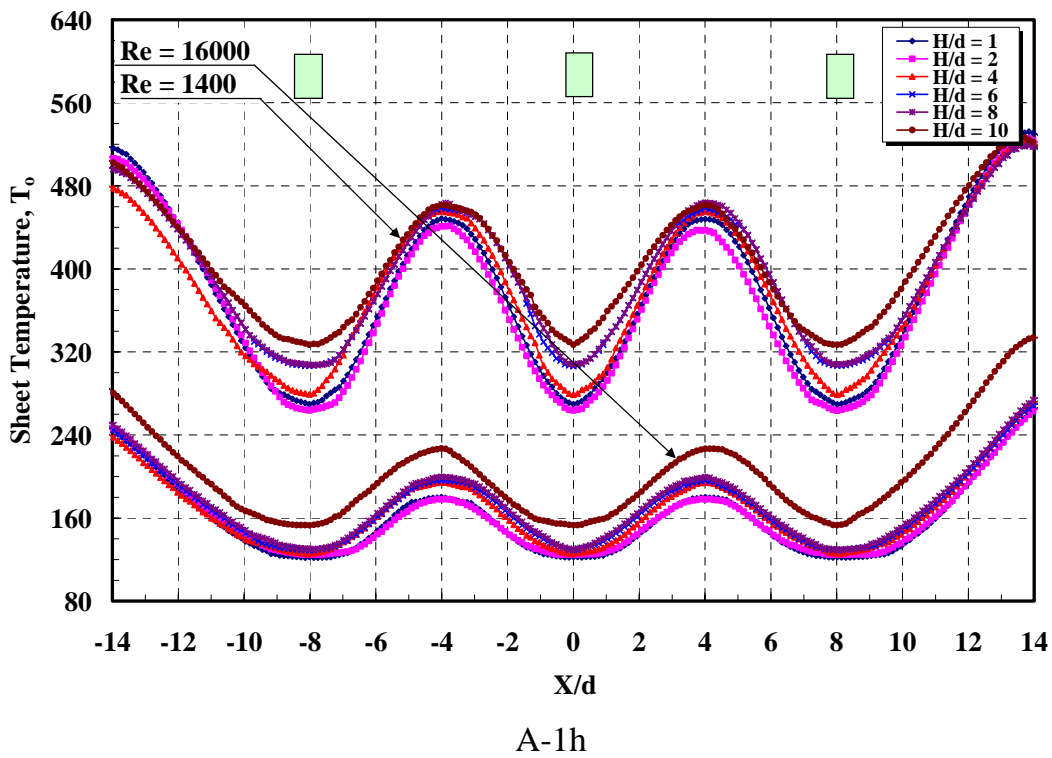
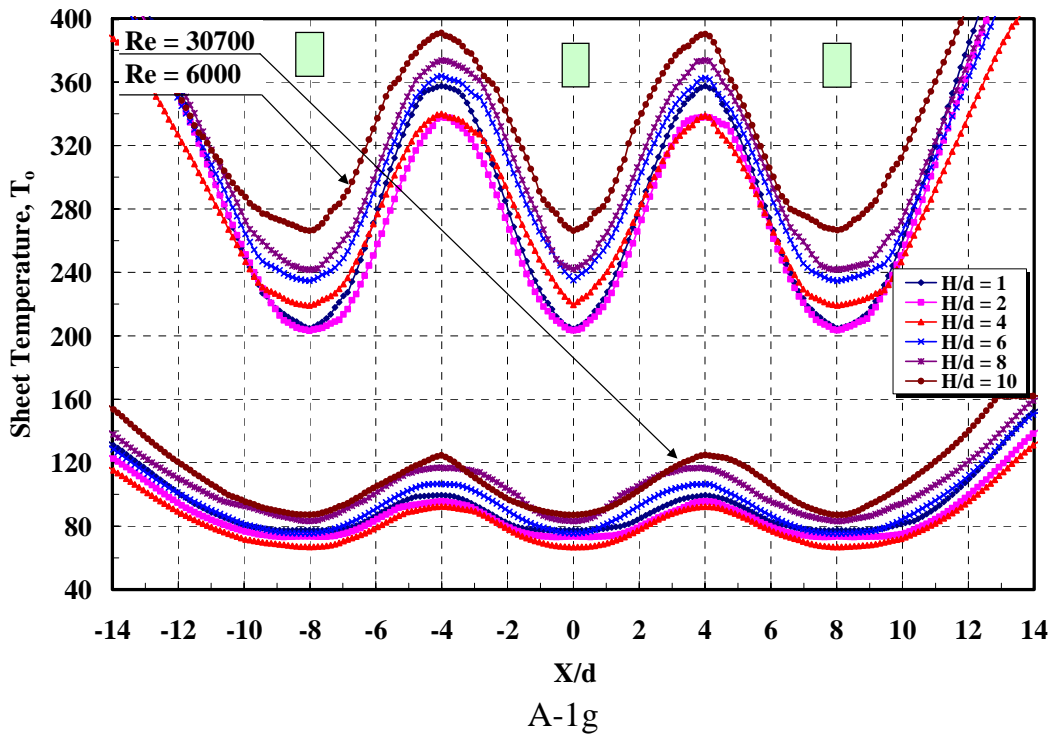


A-1e

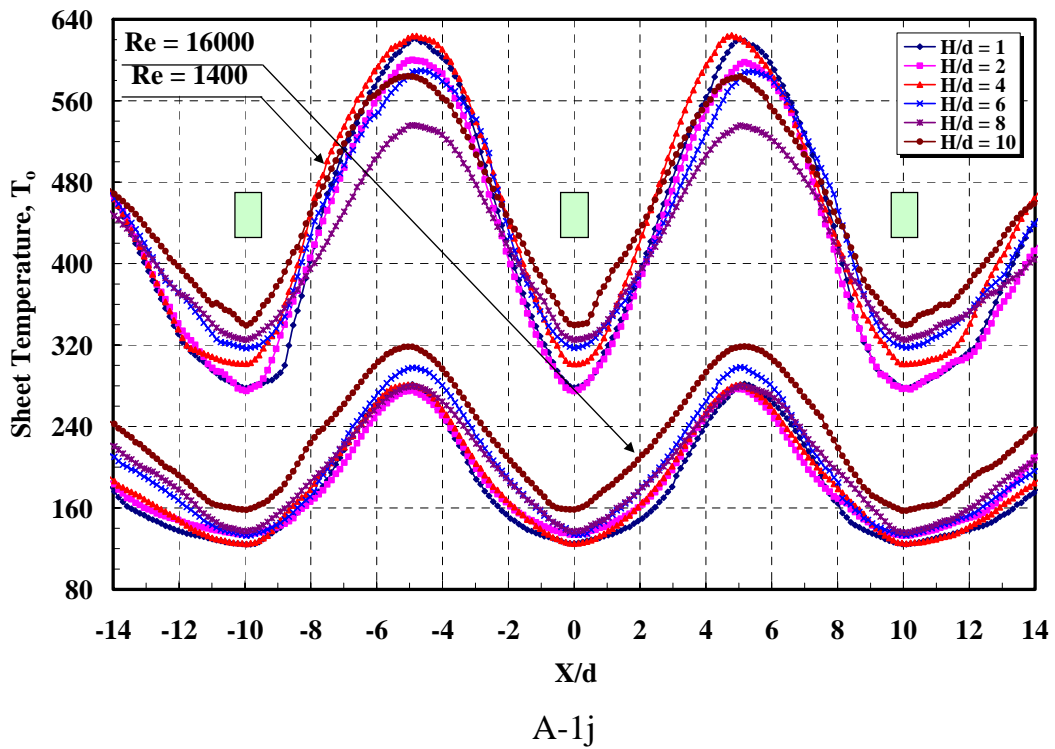
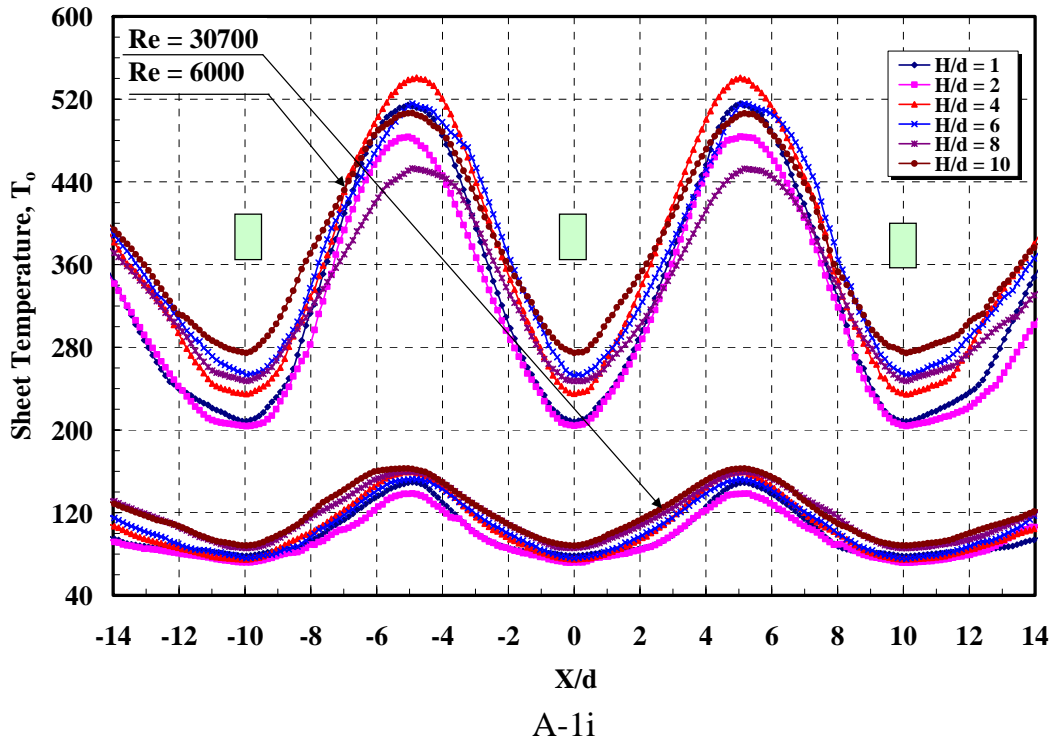


A-1f

Figs. A-1e-f Temperature Distribution for In-line Array at  $S/d = 6$

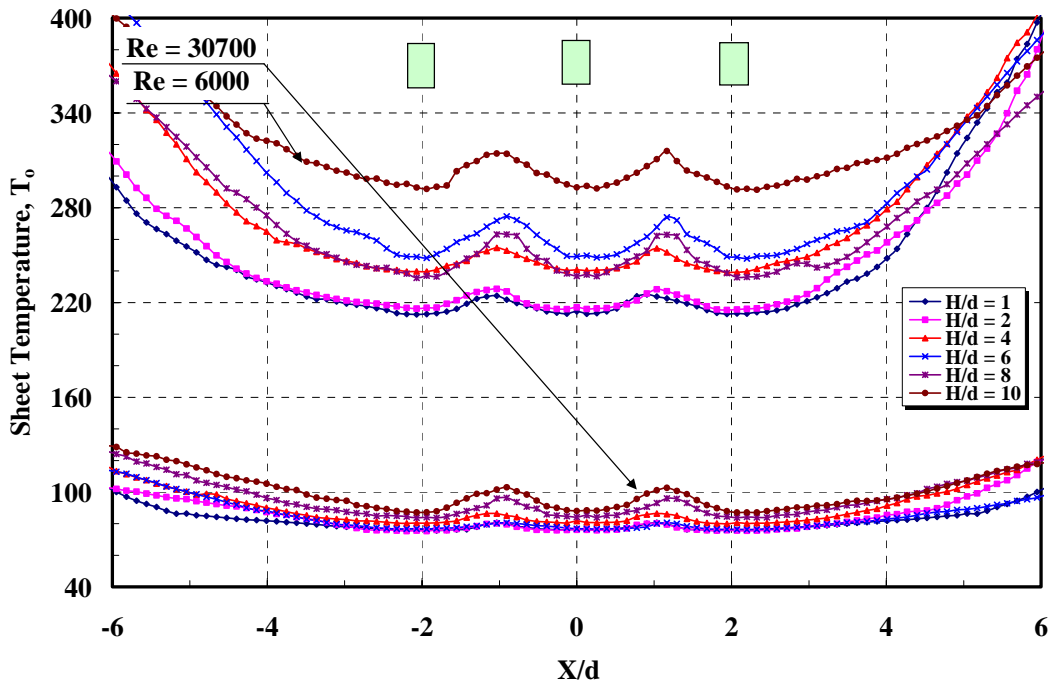


Figs. A-1g-h Temperature Distribution for In-line Array at  $S/d = 8$

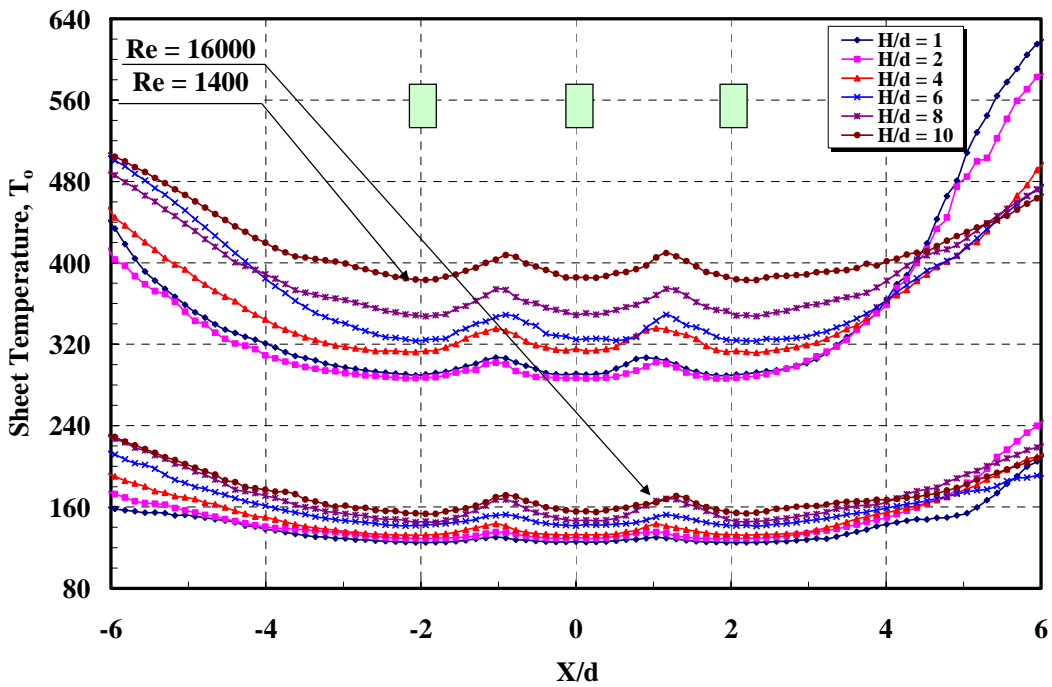


Figs. A-1i-j Temperature Distribution for In-line Array at  $S/d = 10$

**A-2 Staggered Array:**

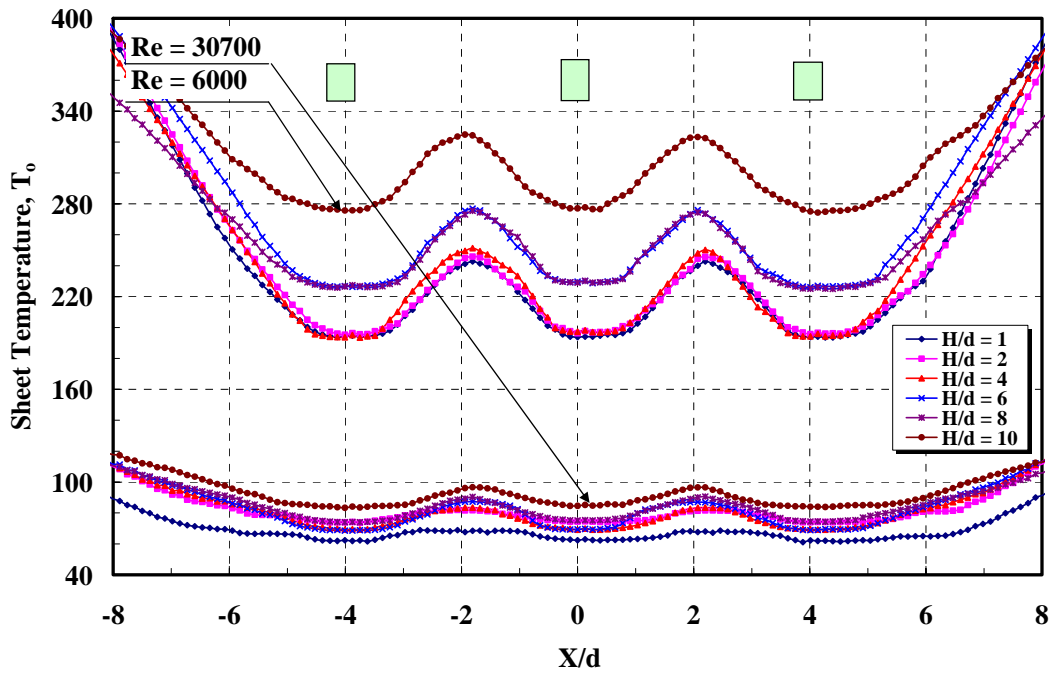


A-2a

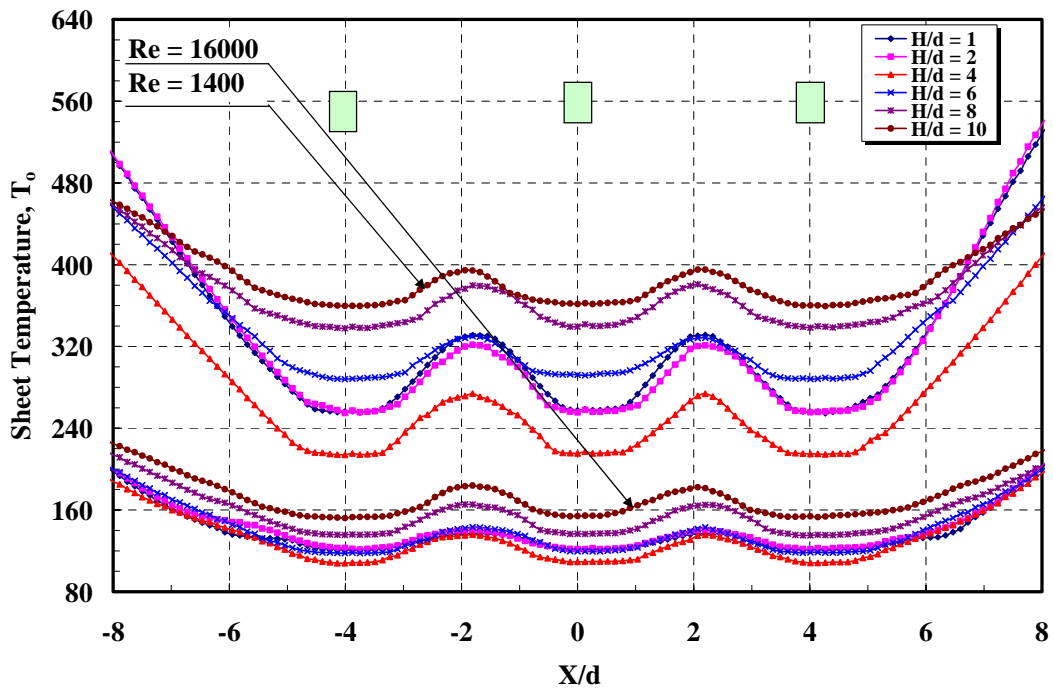


A-2b

Figs. A-2a-b Temperature Distribution for Staggered Array at  $S/d = 2$

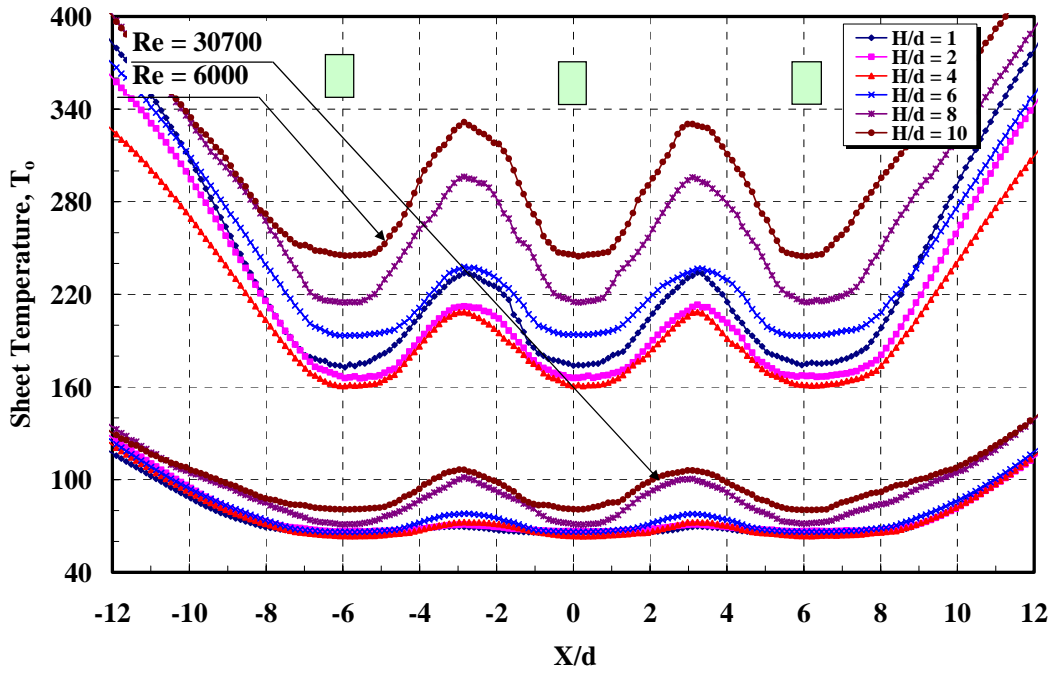


A-2c

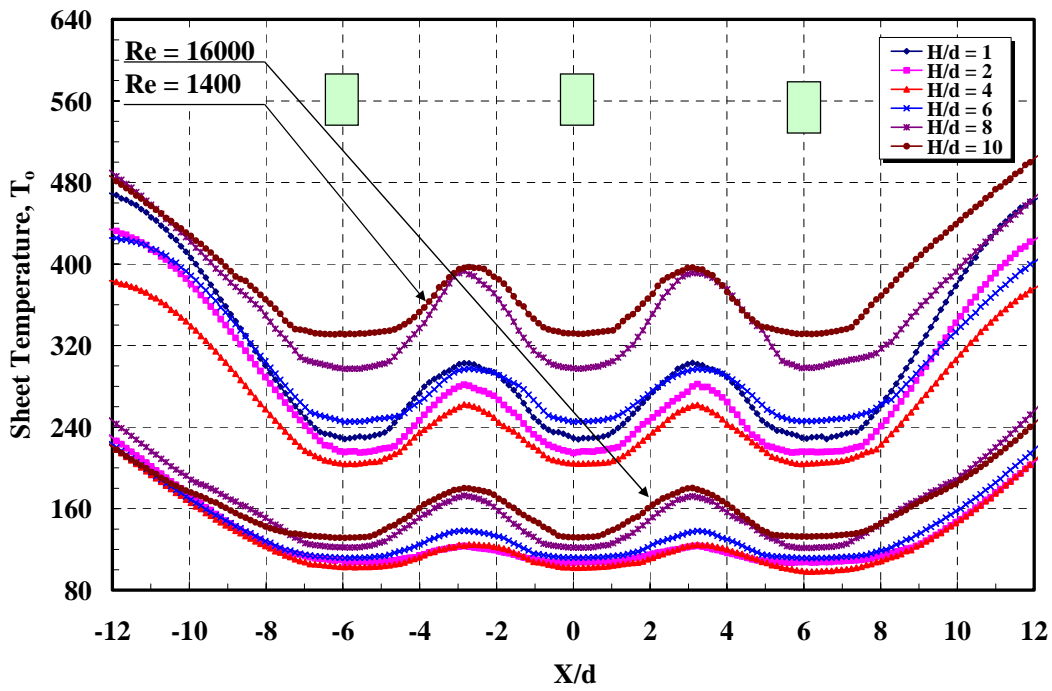


A-2d

Figs. A-2c-d Temperature Distribution for Staggered Array at  $S/d = 4$

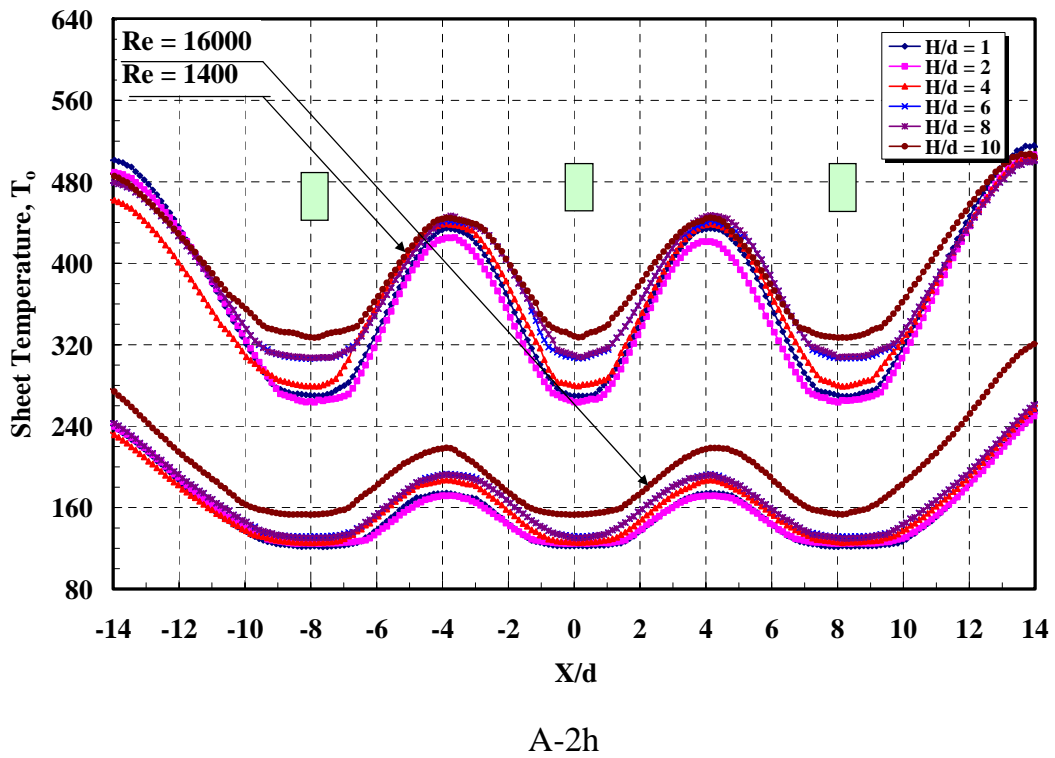
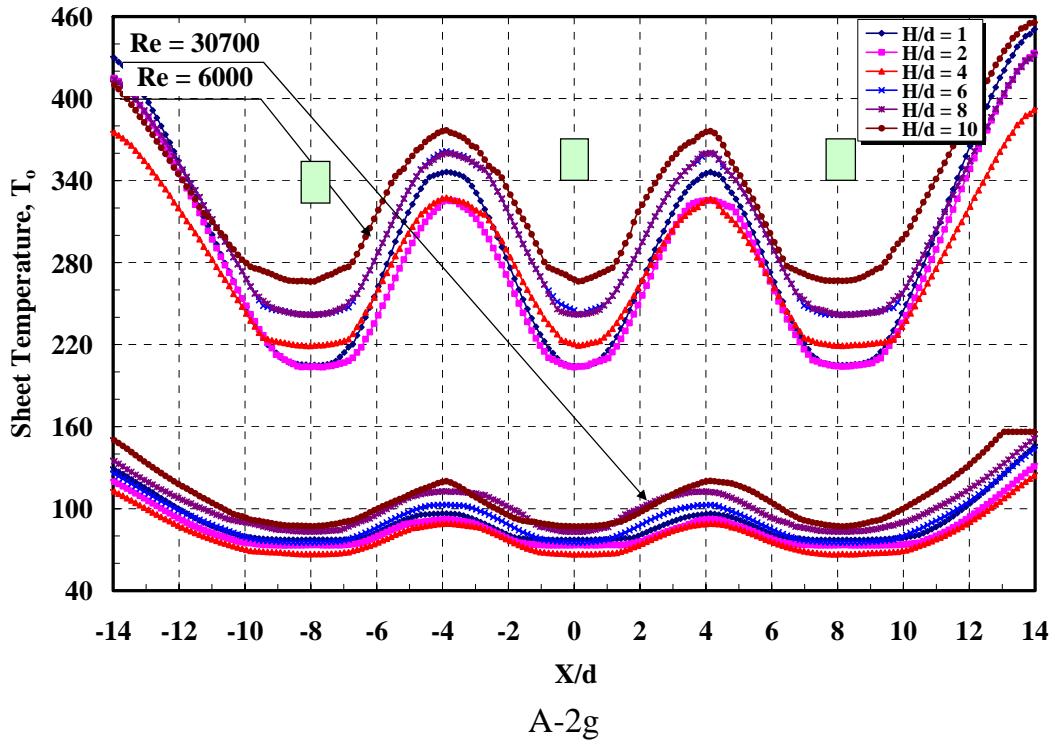


A-2e

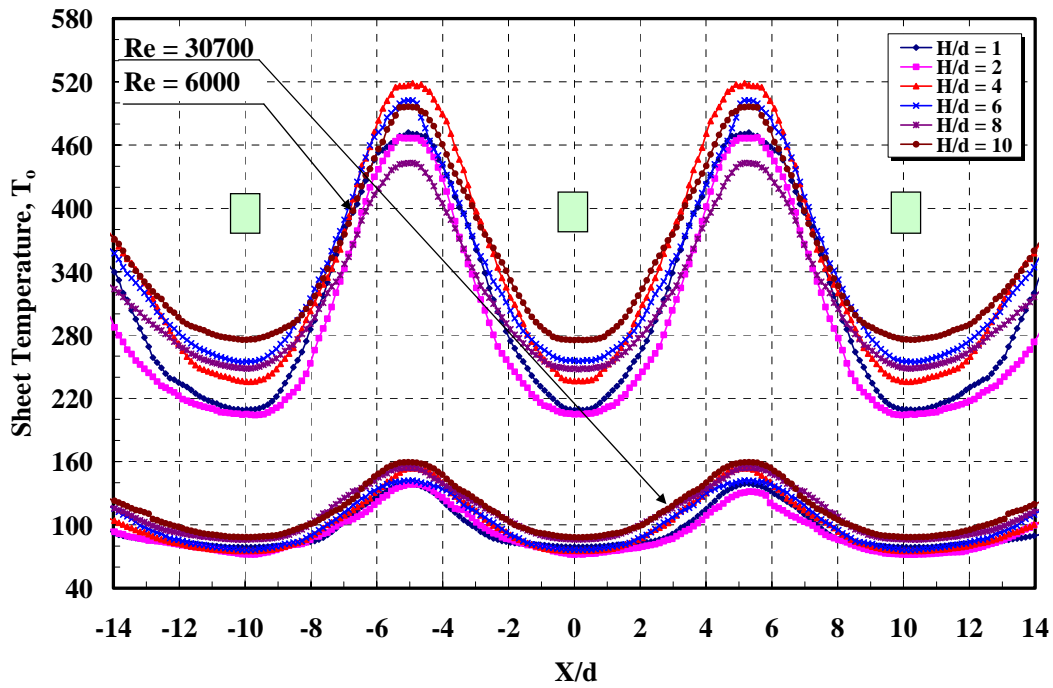


A-2f

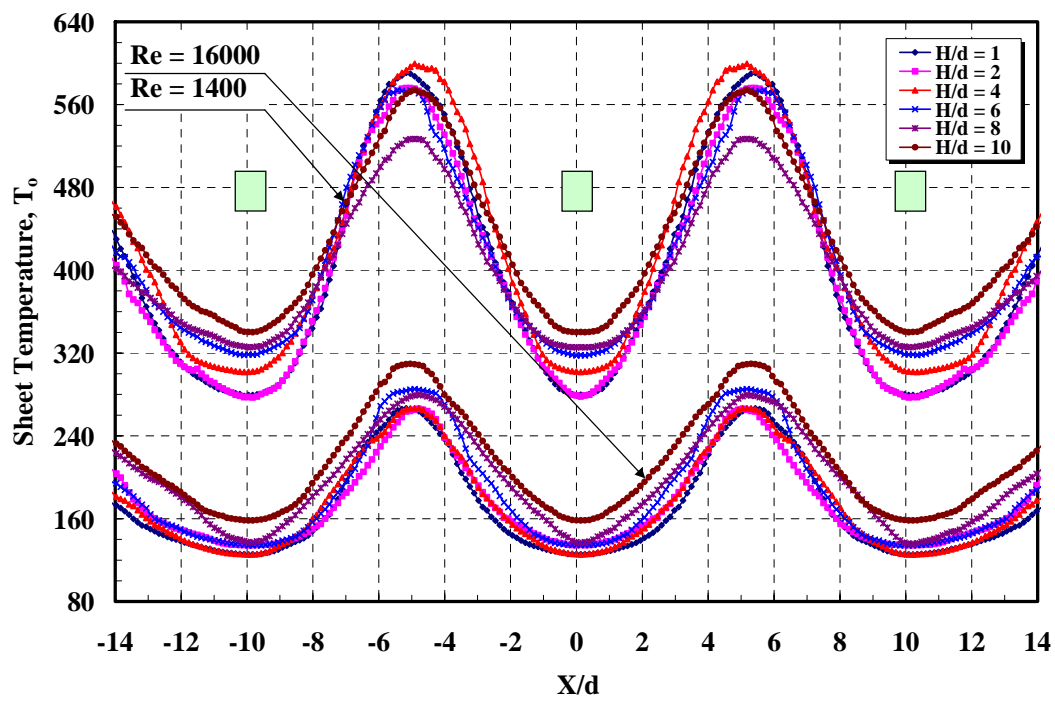
Figs. A-2e-f Temperature Distribution for Staggered Array at  $S/d = 6$



Figs. A-2g-h Temperature Distribution for Staggered Array at  $S/d = 8$



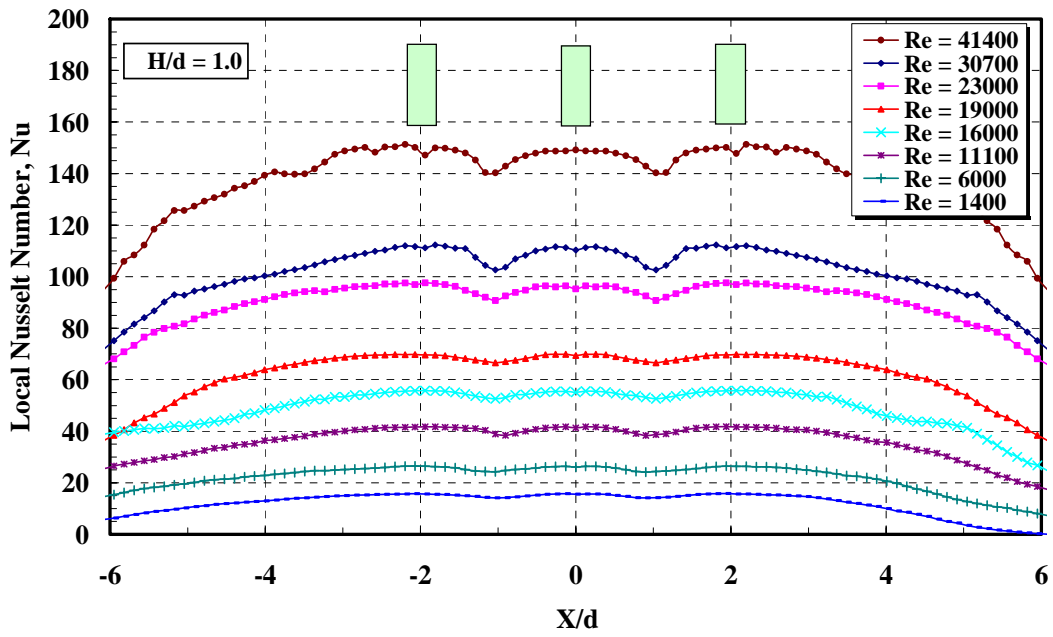
A-2-i



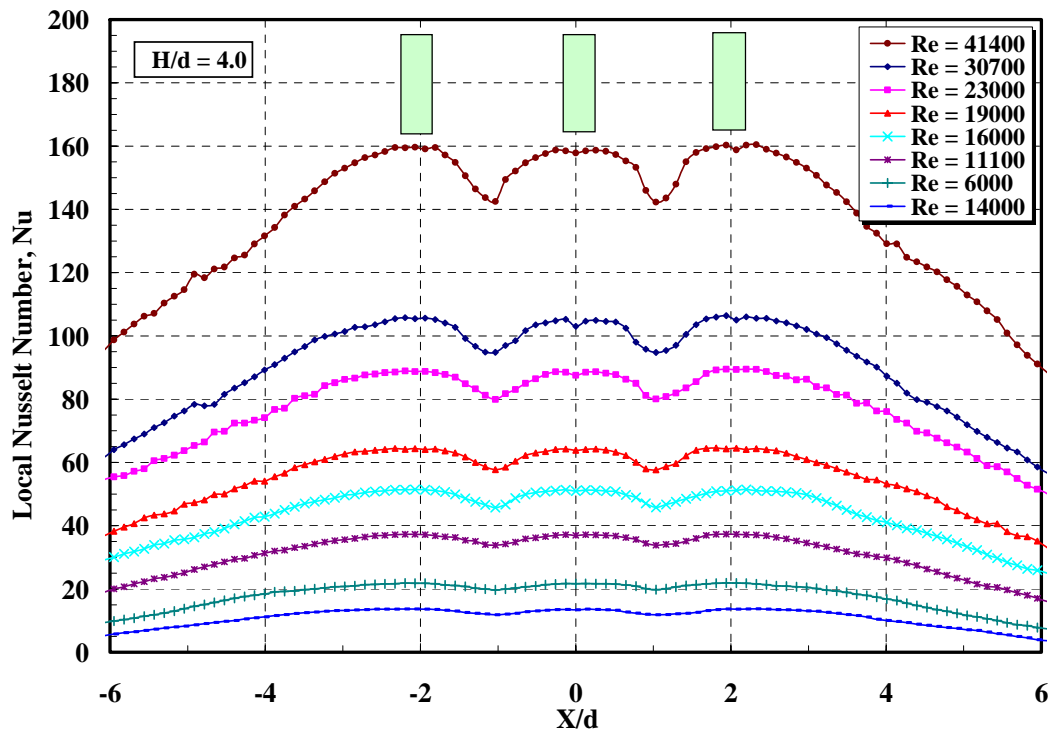
A-2j

Figs. A-2i-j Temperature Distribution for Staggered Array at  $S/d = 10$

**B- Local Nusselt Number Distribution for Staggered Array:**

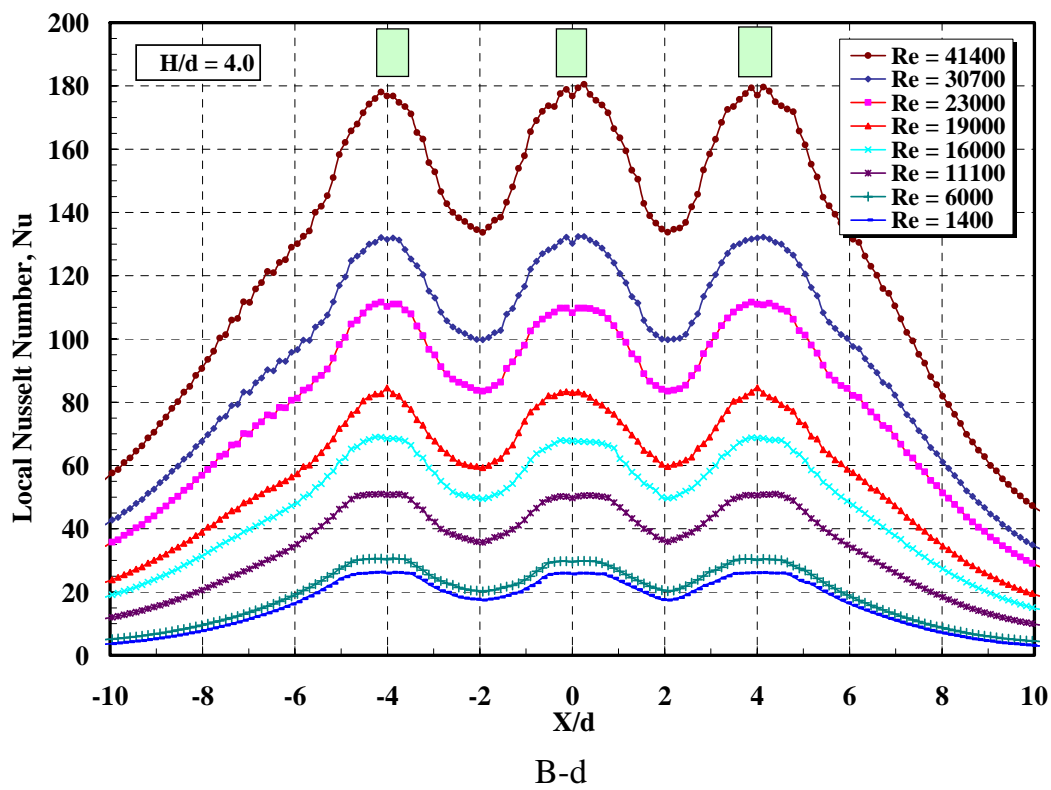
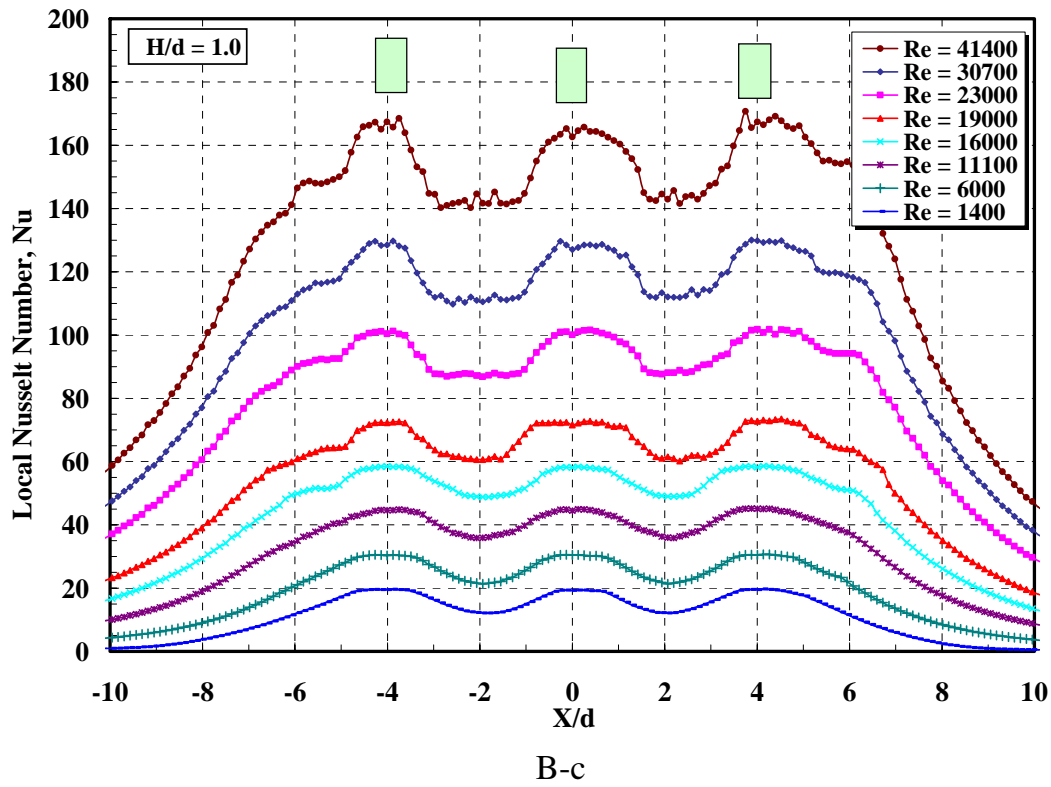


B-a

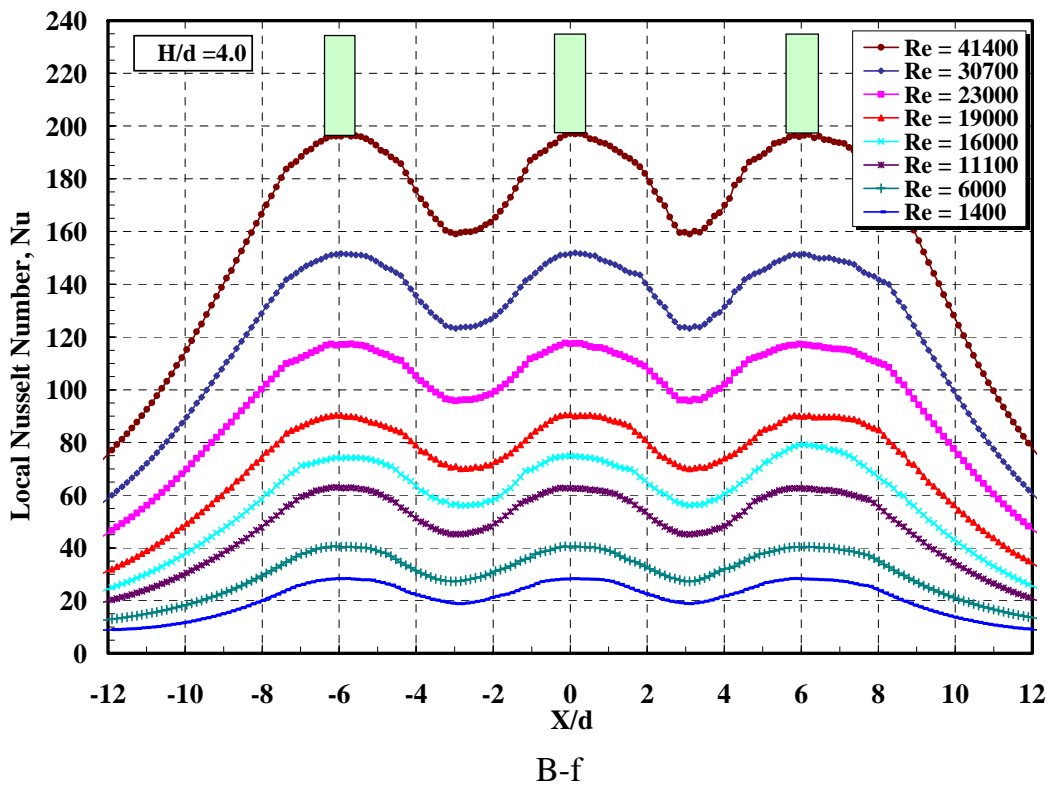
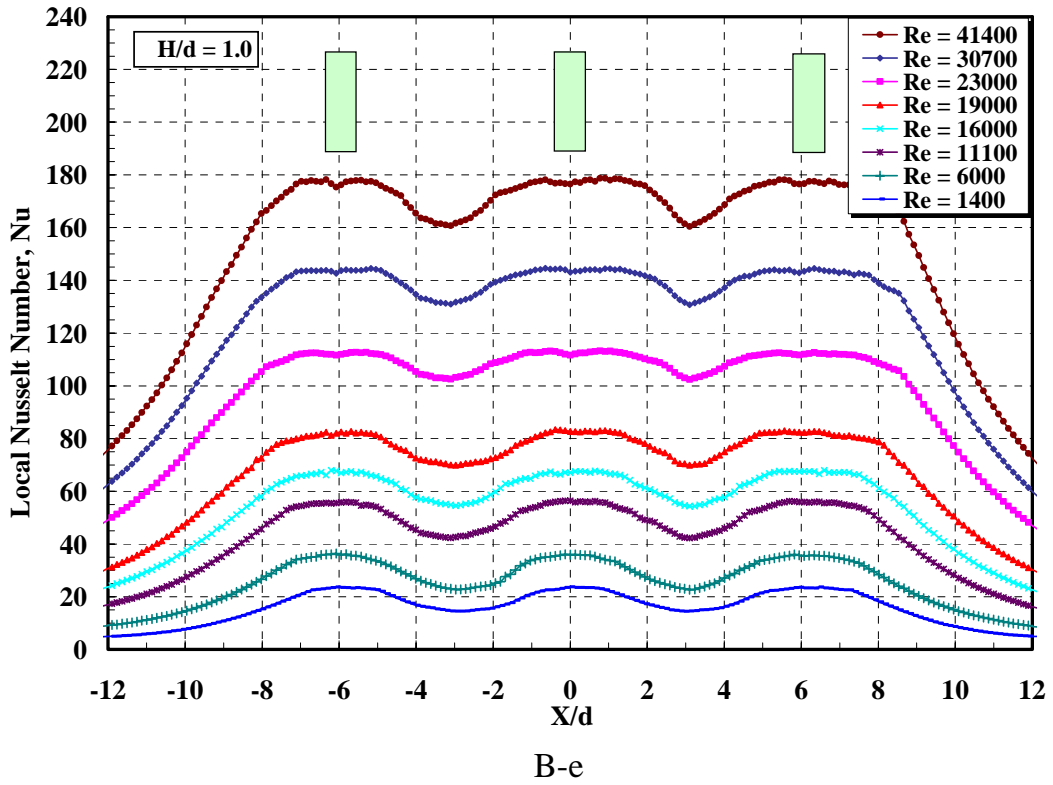


B-b

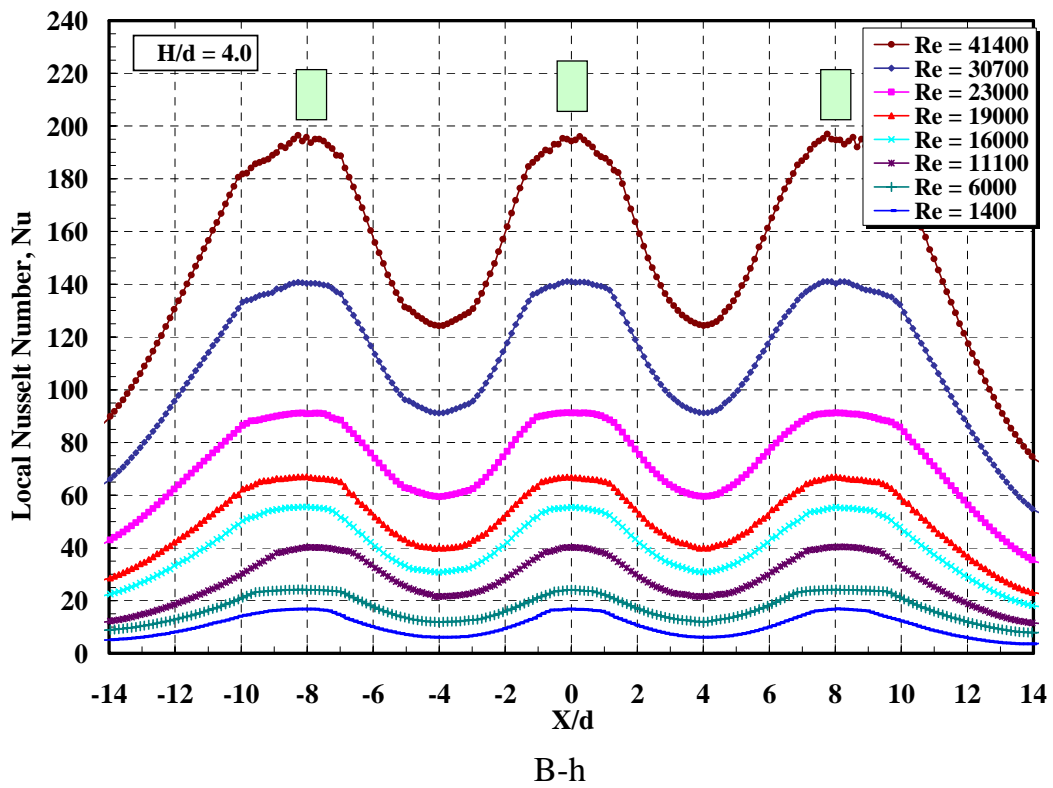
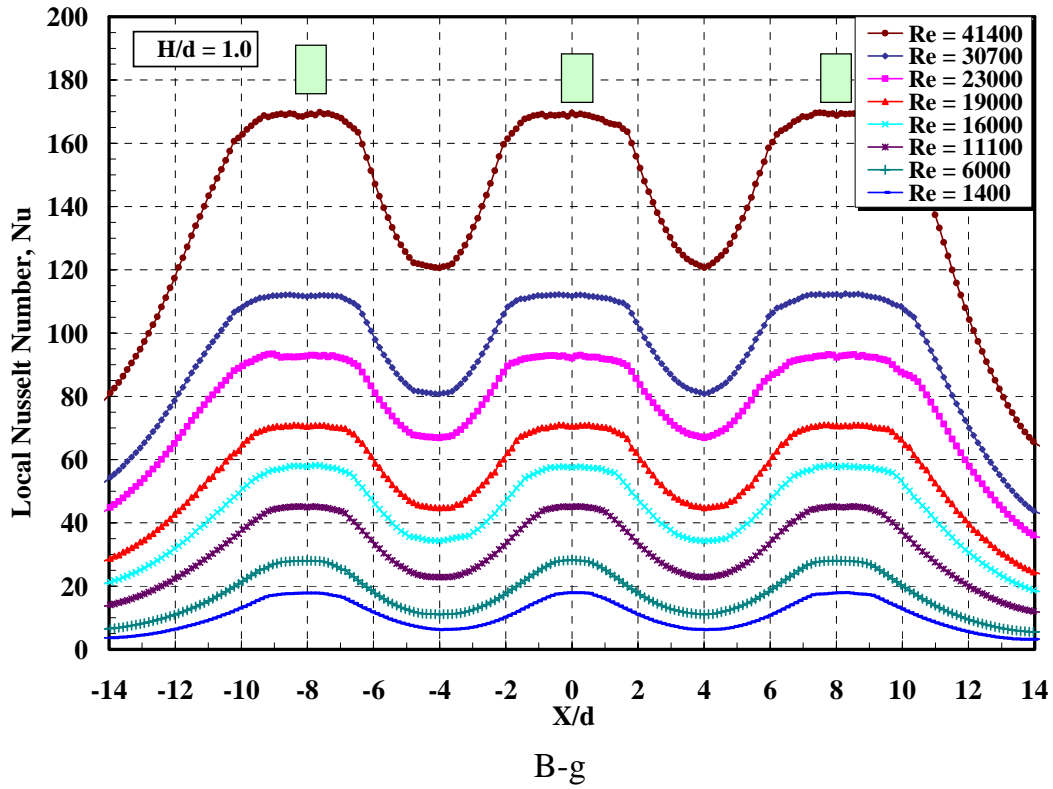
Figs. B-1a-b Local Nusselt Number Distribution for Staggered Array,  
 $S/d = 2$



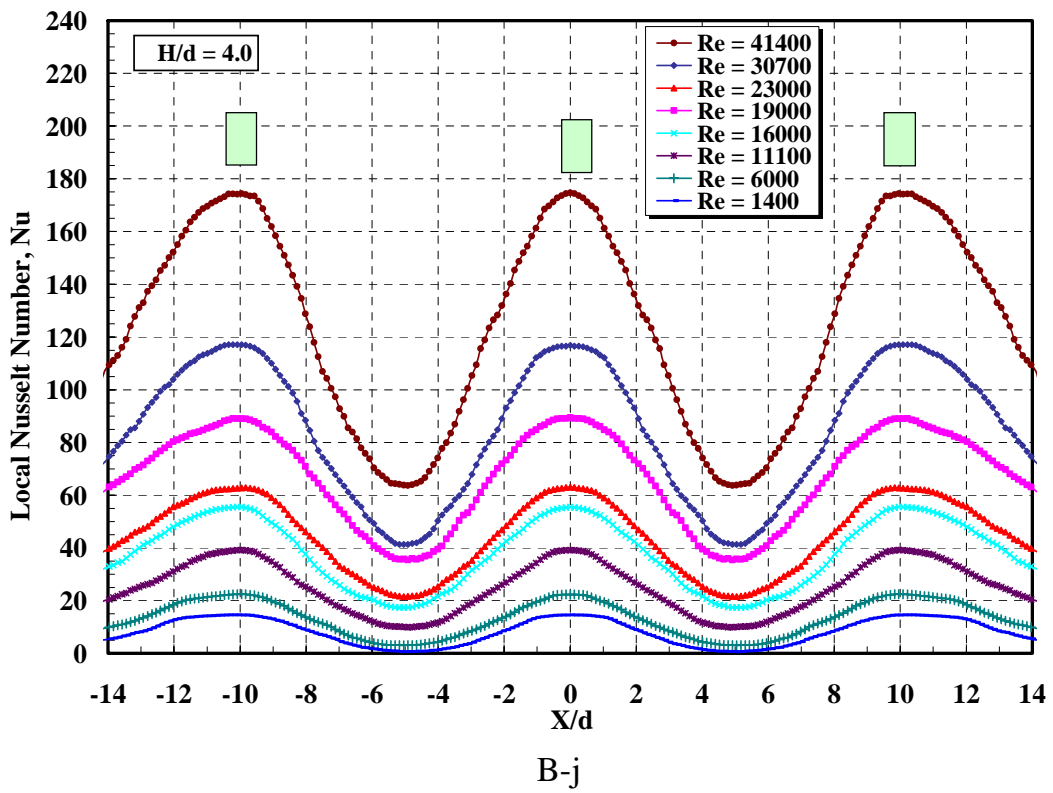
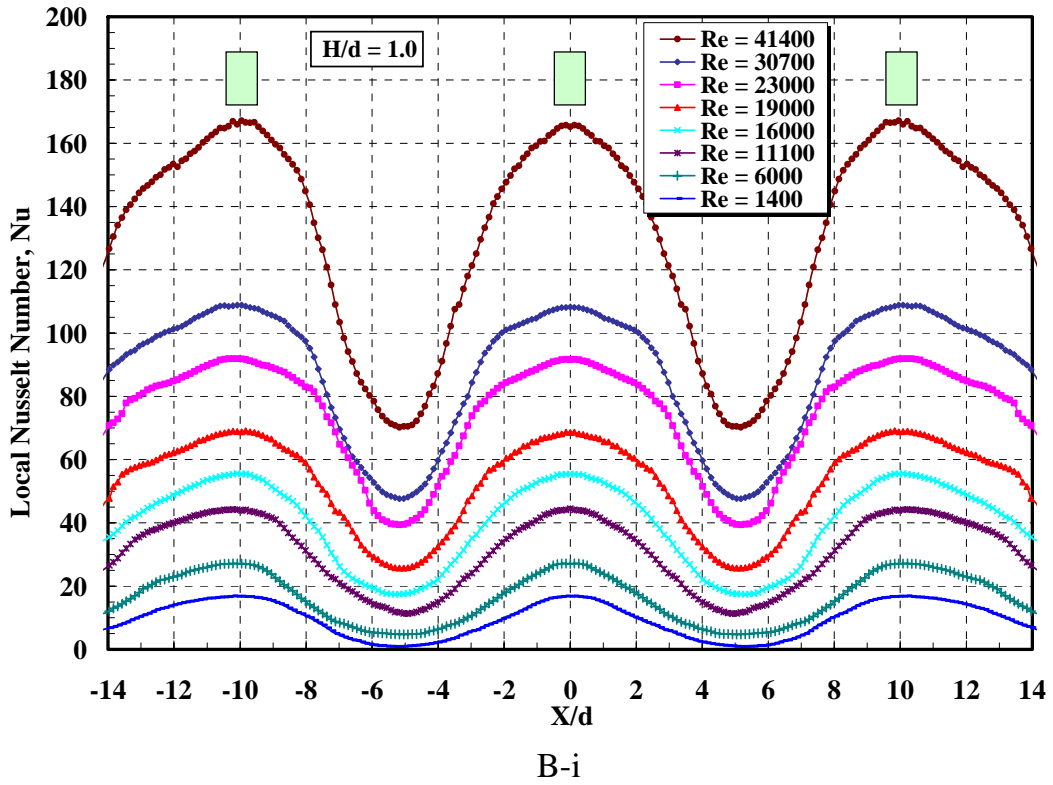
Figs. B-1c-d Local Nusselt Number Distribution for Staggered Array,  $S/d = 4$



Figs. B-1e-f Local Nusselt Number Distribution for Staggered Array,  $S/d = 6$



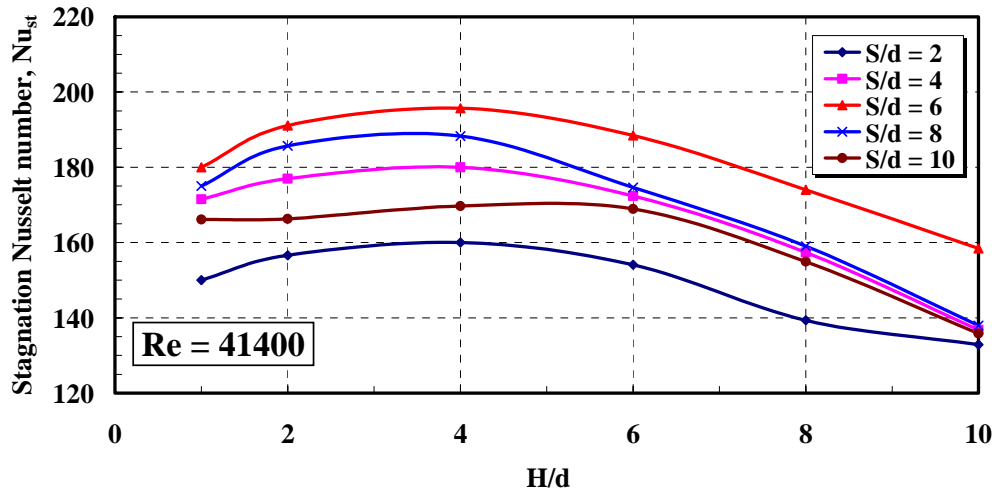
Figs. B-1g-h Local Nusselt Number Distribution for Staggered Array,  $S/d = 8$



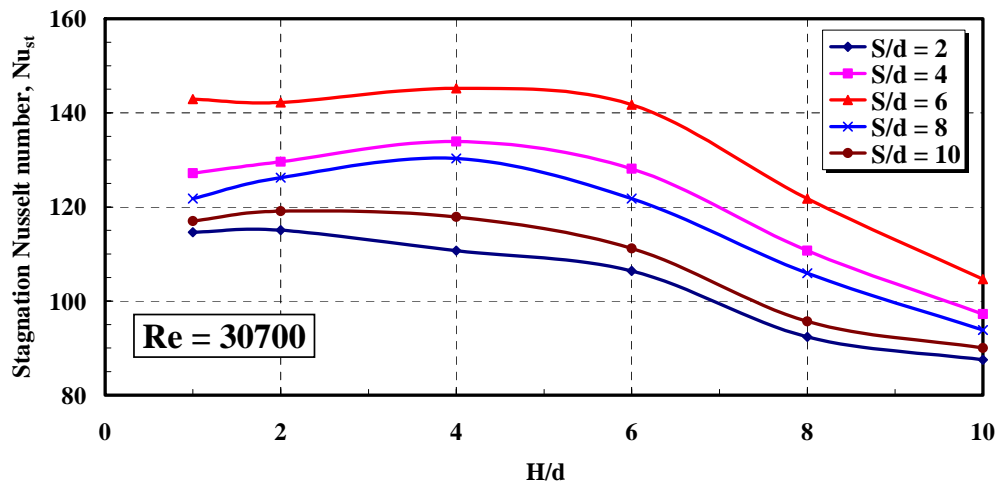
Figs. B-1i-j Local Nusselt Number Distribution for Staggered Array,  $S/d = 10$

**C- Effect of Separation Distance at Stagnation Point:**

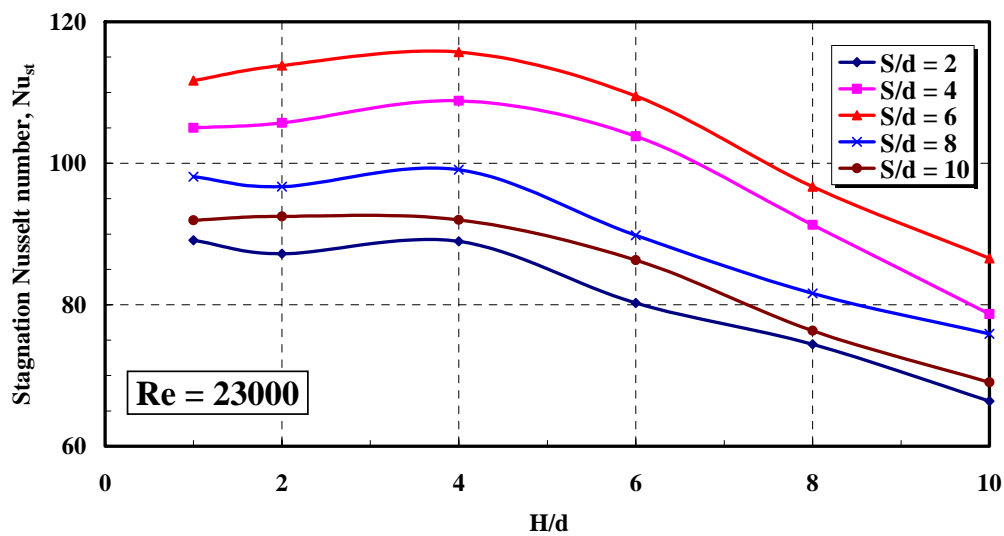
**C-1 In-line Array:**



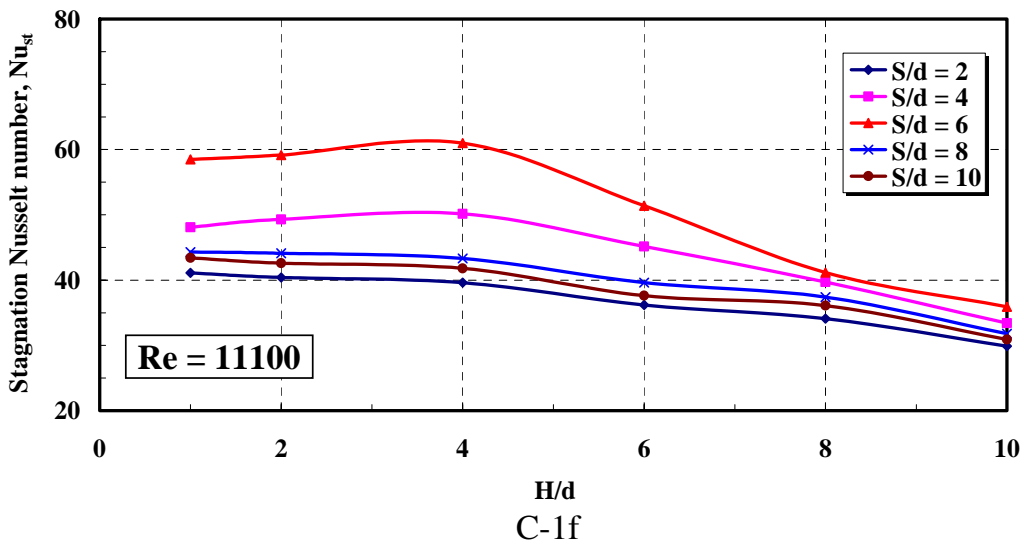
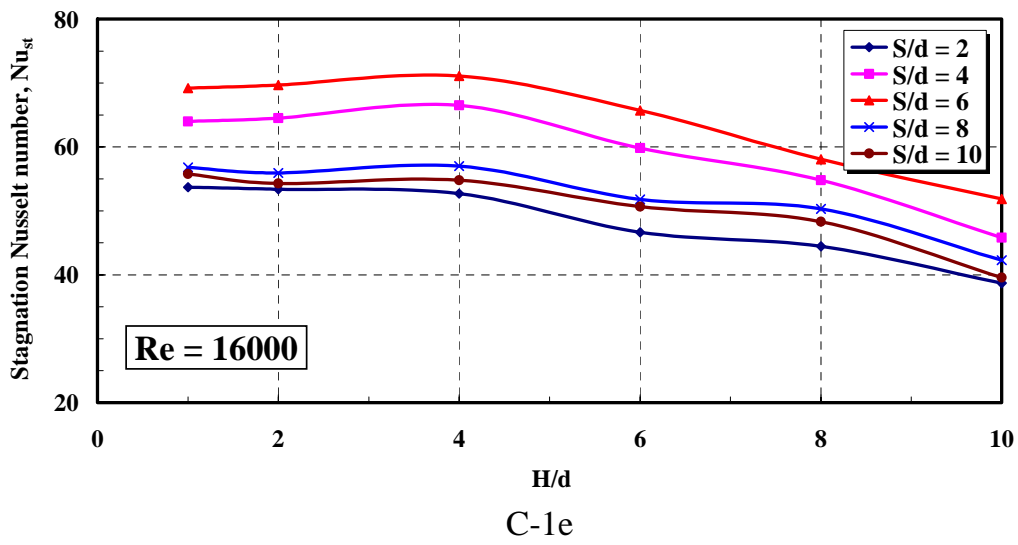
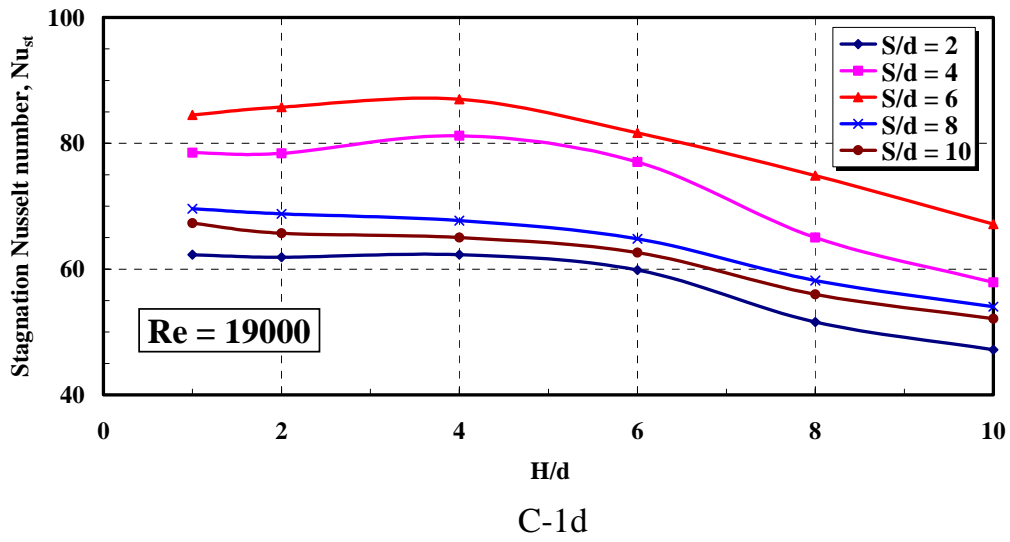
C-1a

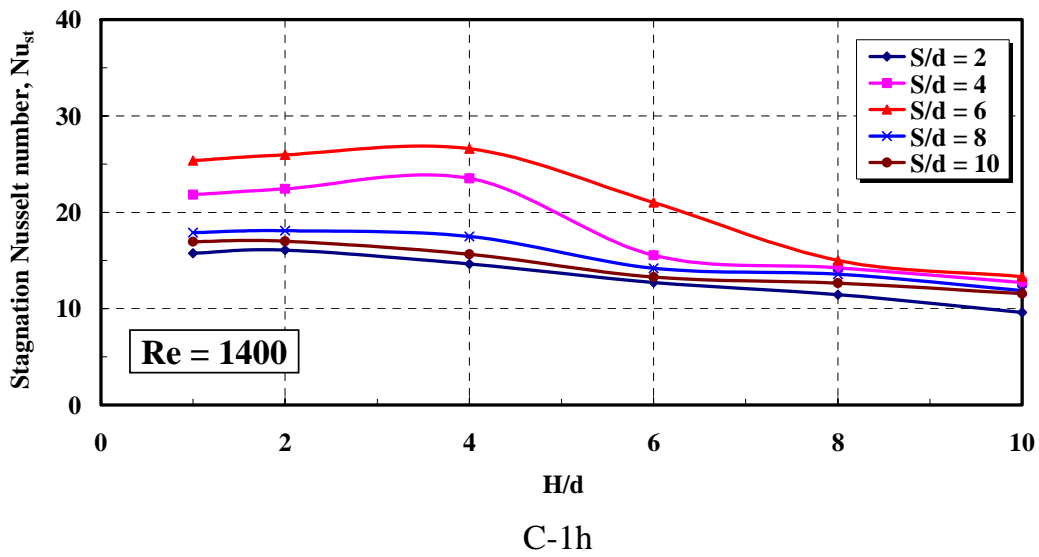
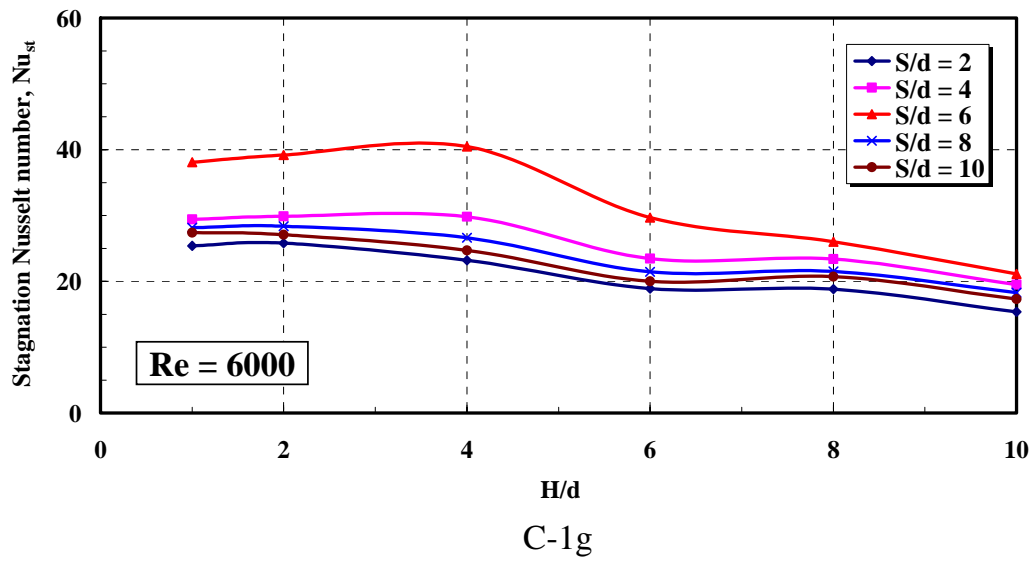


C-1b



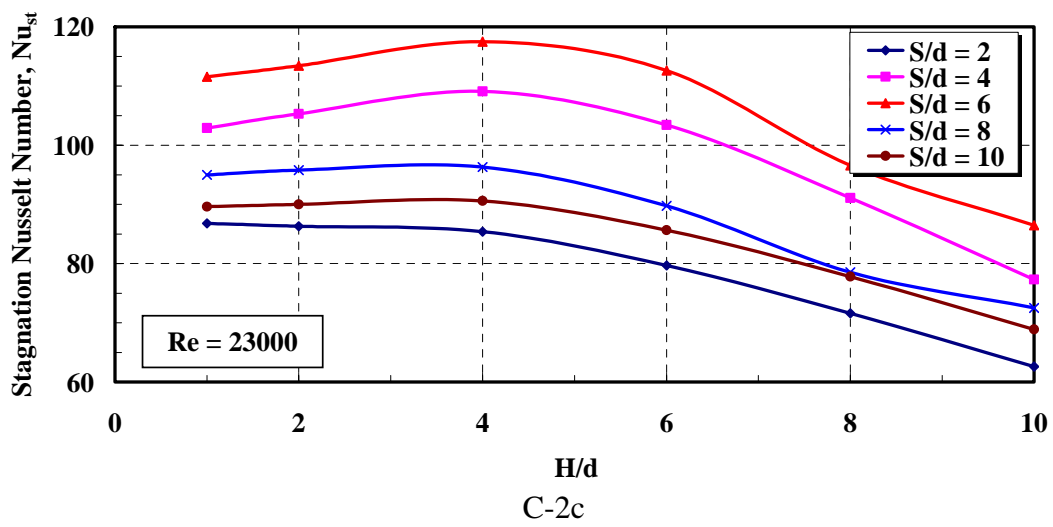
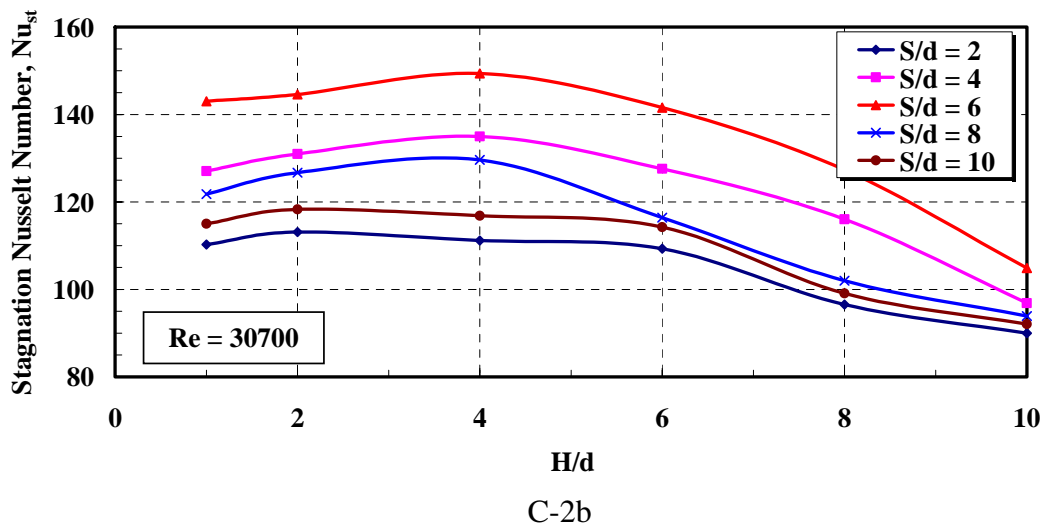
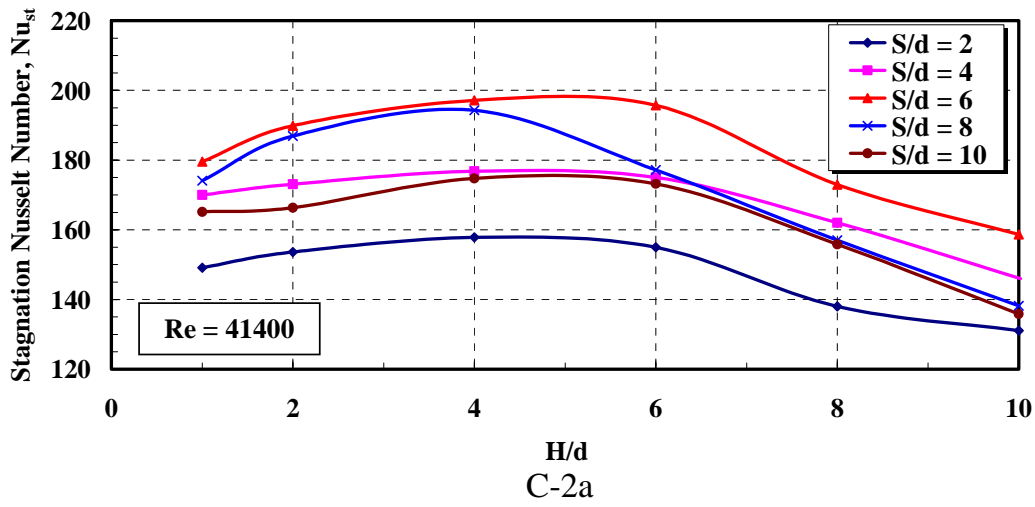
C-1c

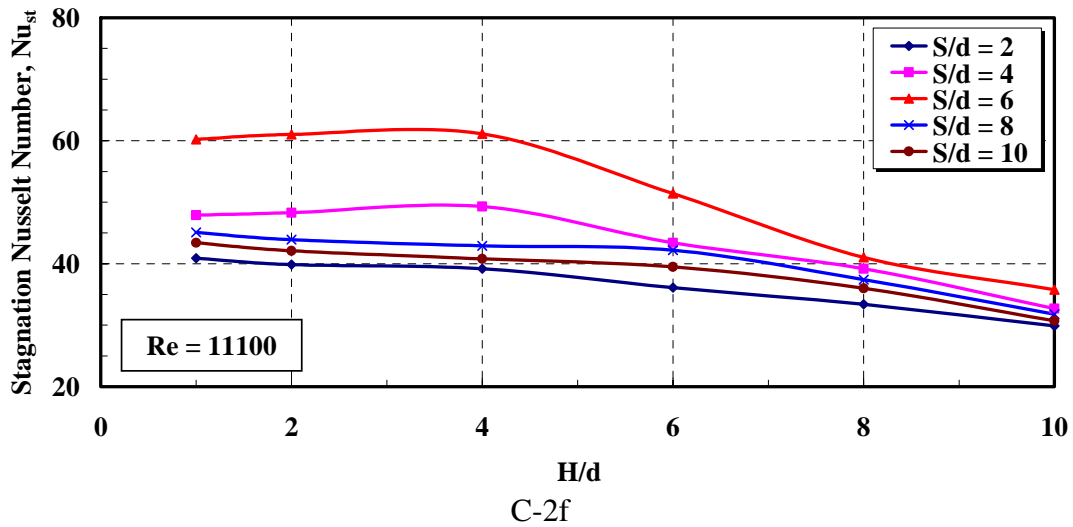
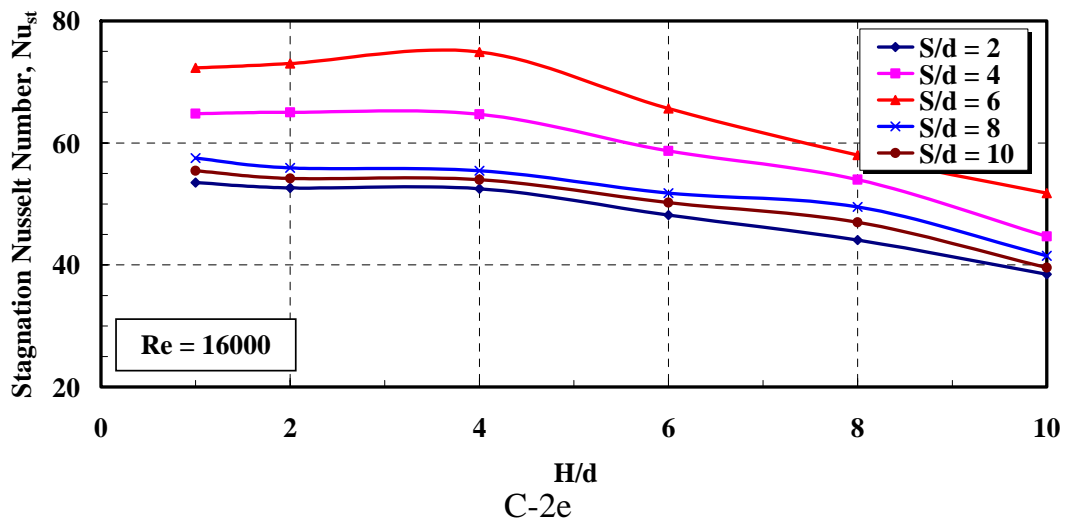
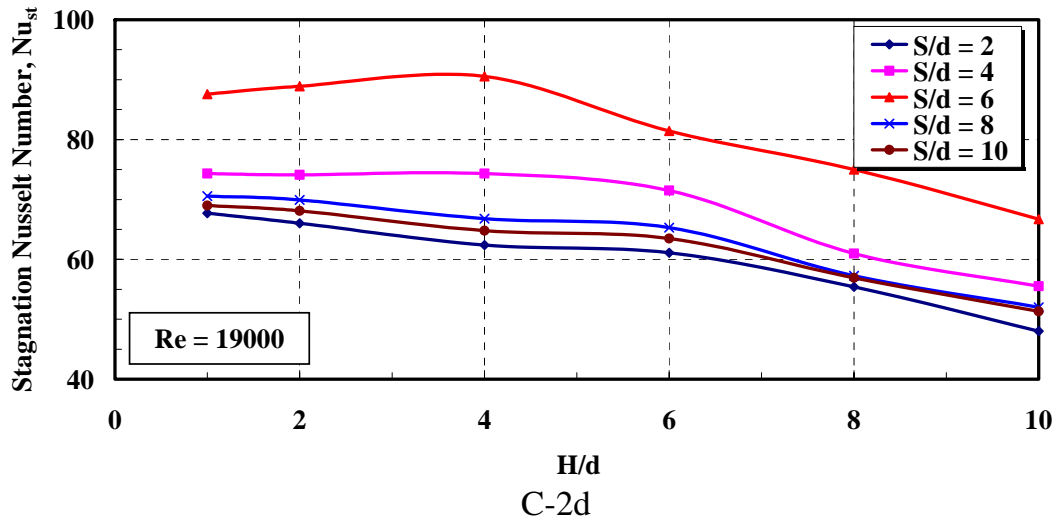


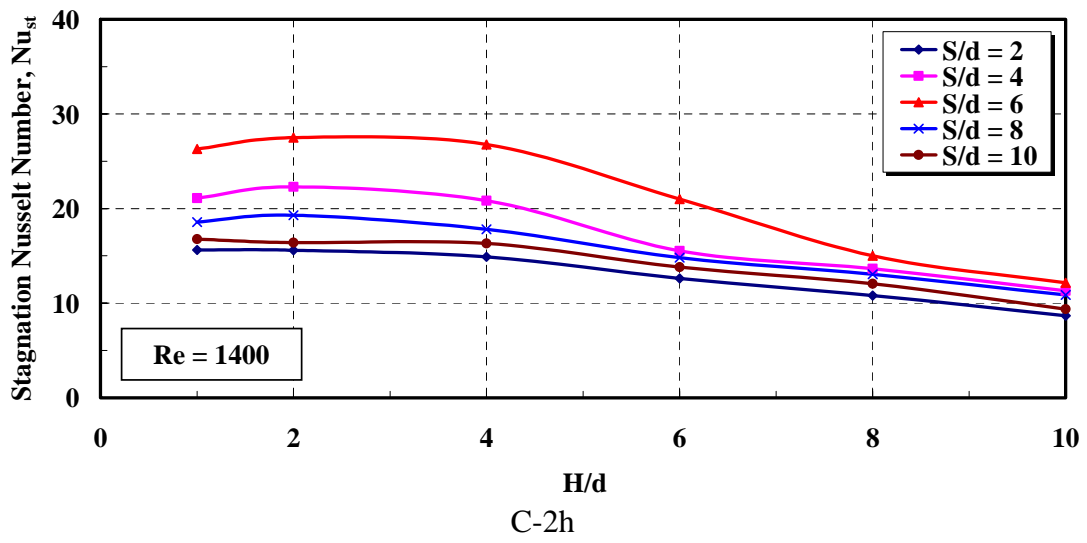
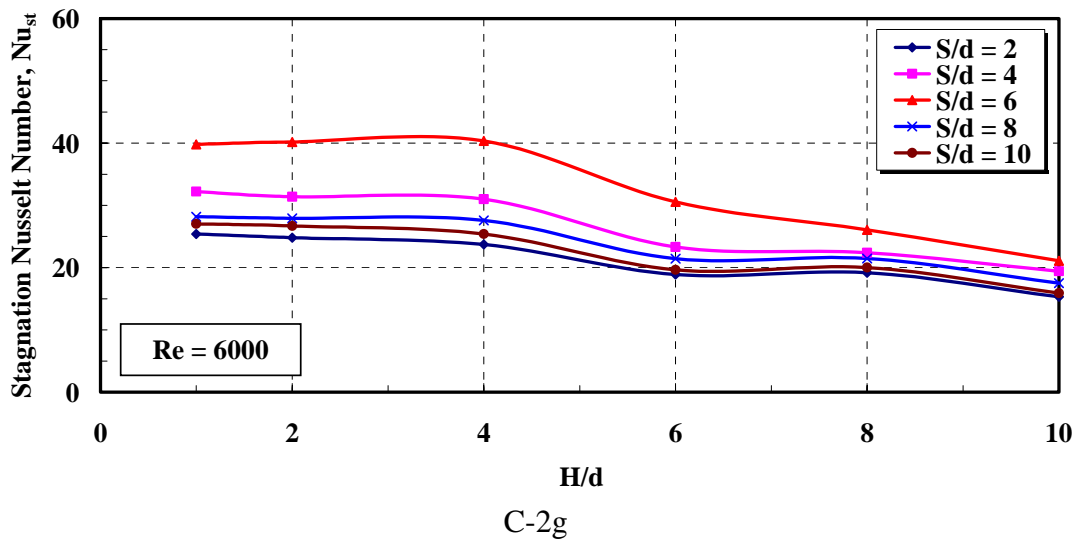


Figs. C-1a-h Stagnation Nusselt Number Distribution for In-line Array

**C-2 Staggered Array:**







Figs. C-2a-h Stagnation Nusselt Number Distribution for Staggered Array

**Nomenclature**

<b><u>Symbol</u></b>		<b><u>Explanation</u></b>
A	[m <sup>2</sup> ]	Plate area
C <sub>1,2</sub>	[-]	Integration constant
c	[-]	Constant
c <sub>p</sub>	[kJ/(kg.K)]	Specific heat
d	[m]	Inner nozzle diameter
d <sub>c</sub>	[m]	Curved surface diameter
d <sub>h</sub>	[m]	Hydraulic diameter
H	[-]	Separation distance
I	[A]	Direct current
k	[W/(m.K)]	Thermal conductivity
l	[m]	Metal sheet length
m	[-]	Exponent
Nu	[-]	Local Nusselt number
n	[-]	Exponent
n <sub>p</sub>	[Pixel]	Number of pixel
Pr	[-]	Prandtl number
p	[Pa]	Pressure
Q	[W]	Heat transfer rate
q̇	[W/m <sup>2</sup> ]	Heat flux
R	[Ω]	Resistance
Re	[-]	Jet Reynolds number
RF	[-]	Recovery factor
r	[m]	Radius
S	[m]	Spacing distance
t	[m]	Metal sheet thickness
t <sub>c</sub>	[m]	Hole channel width
T	[°C]	Temperature
U	[m/sec.]	Mean velocity at jet exit
Un	[-]	Degree of uniformity

## Nomenclature

---

u	[m/sec.]	Flow velocity
V	[m <sup>3</sup> ]	Volume
w	[m]	Metal sheet width
X	[m]	Streamwise coordinate
Y	[m]	Coordinate perpendicular to streamwise direction

### *Greek symbols*

$\alpha$	[W/(m <sup>2</sup> .K)]	Convective heat transfer coefficient
$\beta$	[Pa/m]	Pressure gradient in the radial direction
$\delta$	[m]	Boundary layer thickness
$\Delta X_p$	[mm]	Length of pixel
$\varepsilon$	[-]	Emissivity
$\theta$	[-]	Dimensionless temperature
$\nu$	[m <sup>2</sup> /sec.]	Kinematic viscosity
$\rho$	[kg/m <sup>3</sup> ]	Fluid density
$\rho_{el}$	[ $\Omega$ .m]	Specific electrical resistance
$\sigma$	[W/(m <sup>2</sup> .K <sup>4</sup> )]	Stefan-Boltzmann constant

### *Subscripts*

1, 2	Number
$\alpha$	Convective heat transfer
$\varepsilon$	Radiation heat transfer
a	Air
ad	Adiabatic
av	Average over area
avl	Average over line
c	IR-Camera
co	Correct
I	Electrical
j	Jet
k	Conduction heat transfer
m	Metal

## Nomenclature

---

Max.	Maximum
Min.	Minimum
o	Surface
p	Pixel
r	Radial distance
s	Static
st	Stagnation

# Lebenslauf

**Name:** Mohamed Attalla

**Geburtstag:** 28.12.1968

**Geburtsort:** Kena - Ägypten

**Familienstand:** verheiratet

**Schulbildung:**  
1973-1983: Grundschule  
1983-1987 Mittelschule

**Stdium:**  
Sep. 1987- Mai. 1992 Maschinenbauwesen (Energie Abteilung)  
Mai. 1992- Feb.1994 Military  
Feb. 1994-Dez. 1998 Master

**Berufliche Tätigkeiten**  
Dez. 1998- Juli. 2002 Wissenschaftliche Mitarbeite, Hoch Institut für Energy  
– Aswan - Ägypten

**Promotion**  
Juli. 2002-Okt. 2005 Institut für Strömungstechnik und Thermodynamik  
Fakultät für Verfahrens- und Systemtechnik  
Otto-von-Guerike-Universtät Magdeburg,  
Magdeburg - Deutschland